Evaluation of Novel Gallium Doped Bioactive Glass for the Management of Osteosarcoma

Shirin Bagheri Hanaei

Doctor of Philosophy

Aston University

April 2025

Abstract

Development and characterisation of gallium-doped bioactive glasses for osteosarcoma treatment

Shirin Bagheri Hanaei

Doctor of Philosophy

April 2025

Department of Engineering and Physical Science

Aston University

Osteosarcoma is the most common primary malignant bone tumour in adolescents and young adults, often requiring aggressive treatment that includes surgery and chemotherapy. Despite advances in clinical management, challenges such as chemoresistance, tumour recurrence, and implant-associated infections persist. This research focuses on the development and characterisation of gallium-doped bioactive glasses (Ga-BGs) as a multifunctional material capable of both anticancer and antimicrobial activity, while supporting bone regeneration.

A series of Ga-BGs were synthesised by incorporating varying molar percentages of Ga_2O_3 into the 45S5 bioactive glass system (0-5 mol% Ga). The glasses were evaluated for their physicochemical properties, ion release profiles, and biological performance. The cytotoxic effects of Ga-BG conditioned media were investigated using osteosarcoma (OS) cell lines (Saos-2, HOS and U2-OS) and normal human osteoblast as well as healthy human mesenchymal stem cells. Results from MTT and Live/Dead assays revealed a selective cytotoxic effect on OS cells, with minimal impact on healthy cells. Flow cytometry confirmed elevated transferrin receptor (TfR) expression in OS cells, supporting gallium's targeted action through iron-mimicking mechanisms. Caspase-3/7 activation assays further demonstrated the induction of apoptosis in cancer cells following exposure to Ga-doped media.

In parallel, the antibacterial activity of Ga-BGs was investigated against *E. coli* and *S. aureus* using viability assays, time-kill studies, and fluorescence microscopy. The materials exhibited dose-dependent bactericidal activity, in particular against *E. coli*, highlighting their potential in preventing implant-associated infections.

Overall, this study represents Ga-BGs as a promising dual-function biomaterial, offering targeted anticancer effects alongside antimicrobial properties. The findings provide a

foundation for the future development of therapeutic strategies for OS that integrate tumour suppression, infection control, and bone regeneration.

Keywords: gallium, bioglass, bone cancer, osteoblast, cytotoxicity, osteosarcoma

تقدیم به پسر عزیزم، کیان

که خنده‌ها و کنجکاوی‌هایش هر روز الهام‌بخش من است. این اثر را با تمام عشق به تو هدیه می‌کنم

To my dearest son Kian, whose laughter and curiosity inspire me daily. This work is for you, with all my love.

Acknowledgements

First and foremost, I would like to express my deepest gratitude to my supervisor, Professor Richard Martin, for their invaluable guidance, encouragement, and support throughout the course of this research. Their insightful advice, patience, and dedication were instrumental in shaping this work.

I would also like to extend my sincere thanks to the co-supervisors and specifically to Dr. Ewan Ross for their technical expertise and constructive feedback, which significantly enriched this project. My appreciation also goes to Dr. Yvonne Reinwald, Dr. Patricia Esteban, as well as the staff and colleagues, especially at the EPS and HLS department/Labs 334 and 343, whose support, collaboration, and motivation made this journey both productive and enjoyable.

A special thanks to Sarcoma UK, whose financial support made this research possible.

To my friends and fellow PhD candidates, thank you for your companionship, encouragement, and humour—it has been a privilege to grow and learn alongside you.

I would like to extend my deepest gratitude to my family. I am especially thankful to my mother, Mrs Homa Hanaei, and my father, Mr Jalal Hanaei, for their unwavering love, constant support, and the countless sacrifices they have made for me throughout this journey. To my sister, Neda and my brother-in-law, Shafa, for their unwavering encouragement, emotional support, and constant belief in me throughout this journey.

Finally, my heartfelt thanks go to the most supportive person throughout this journey- my husband, Sam. Thank you for being my constant source of strength, patience, and unconditional love. Your support has been the foundation that has carried me through every challenge.

I am deeply grateful to God, whose countless blessings have shaped me and guided me to where I am today.

COVID-19 Impact Statement

This doctoral research commenced in October 2019 and was significantly affected by the COVID-19 pandemic during its early experimental phase. In March 2020, Aston University closed all campus facilities in line with national lockdown measures, resulting in the suspension of laboratory access until July 2020. Following the partial reopening, access remained restricted, with no weekend entry permitted for an additional two months due to security limitations.

Given that many of the planned experiments, particularly long-term cell culture assays, required continuous monitoring and specific time-point sampling required weekend access to the laboratory facilities and these restrictions delayed the start of laboratory-based research. During this period, the focus of the project was temporarily redirected toward literature review, research planning, data organisation, and refinement of experimental protocols to ensure efficient use of laboratory time upon reopening.

Although the pandemic caused unavoidable delays to the experimental schedule, most of the research objectives were subsequently completed. The integrity and validity of the data presented in this thesis remain uncompromised, and the overall outcomes accurately reflect the intended scope and aims of the PhD project.

List of Contents

Chapter 2 - Fabrication and Characterisation of Gallium-Doped Bioactive Glass and the Analysis of Dissolution Behaviour

Chapter 3 – *In Vitro* Cellular Response to Gallium Doped Bioactive Glass

List of Abbreviations

Degrees Celsius	°C
Microlitre	µL
Micrometer	µm
Amorphous Calcium Phosphate	ACP
Analysis of Variance	ANOVA
American Type Culture Collection	ATCC
bi-phasic Calcium Phosphate	BCP
Calcium Phosphate Cement	CPC
Colony Forming Units	CFU
Coefficient Thermal Expansion	CTE
Deoxyribonucleic acid	DNA
Diffuse Histiocytic Lymphoma	DHL
Diffuse Poorly Differentiated Lymphocytic Lymphoma	DPDL
Dimethyl Sulfoxide	DMSO
Dose Limiting Toxicity	DLT
Dulbecco's Phosphate-Buffered Saline	D-PBS
Dulbecco's Modified Eagle Medium	DMEM
Eagle's Minimum Essential Medium	EMEM
Endosseous Ridge Maintenance Implant	ERMI
Energy dispersive X-ray Spectroscopy	EDS
Escherichia coli	E. coli
External Beam Radiotherapy	EBRT
Extracellular Matrix	ECM
Fetal Bovine Serum	FBS
Fourier Transform Infrared Spectroscopy	FTIR
Gallium	Ga
Gallium Maltolate	GaM
Gallium-Doped Bioactive Glass	Ga-BG
Glass Polyalkenoate Cements	GPC
Heme Oxygenase-1	HO-1
Human Mesenchymal Stem Cells	hMSC
Human Osteosarcoma	HOS
Hydroxycarbonate Apatite	HCA

Inductively Coupled Plasma Optical Emission Spectrometry	ICP-OES
Insulin-Like Growth Factor II	IGF-II
Limb-Salvage Surgery	LSS
Magnetic Resonance Imaging	MRI
Mammalian Target of Rapamycin	mTOR
Matrix Metalloproteinases	MMP
Metal Transcription Factor-1	MTF-1
Methyl Thiazolyl Tetrazolium	MTT
Minimum Essential Medium	MEM
Nodular Poorly Differentiated Lymphocytic Lymphoma	NPDL
Non-Bridging Oxygens	NBO
Normal Human Osteoblast	NHOst
Nutrient Agar	NA
Nutrient Broth	NB
Phosphate-Buffered Saline	PBS
Photodynamic Therapy	PDT
Polylactic Acid	PLA
Reactive Oxygen Species	ROS
Renal Cell Carcinoma (RCC)	RCC
Ribonucleic acid	RNA
Scanning Electron Microscopy	SEM
Simulated Body Fluid	SBF
Staphylococcus aureus	S. aureus
Surgical Site Infection	SSI
Trafsferrin	Tf
Transferrin Receptor	TfR
Tricalcium Phosphate	TCP
Vascular Endothelial Growth Factor	VEGF
Viable But Non-Culturable	VBNC
Wingless-related integration site	WNT
World Health Organisation	WHO

List of Tables

Chapter 1

Chapter 2

List of Figures

Chapter 1

Chapter 2

Chapter 3

Appendix

Chapter 1

Introduction and Aims

1.1 Overview

Osteosarcoma (OS), a severe primary cancerous disorder, is the most common bone cancer that affects primarily children and young adults and is often present in adults over 40 years of age, with males affected more than females. It is a rare tumour characterised by malignant mesenchymal cells and bone stroma development [1]. It occurs mainly in the long bones, specifically in the distal femur, proximal tibia and proximal humerus. The tumour is usually found in the metaphysis, called the growth plate of the long bones where the most proliferative cells are clustered [2]. The tumour is mostly identified by an appendicular primary tumour, and it is extremely aggressive in which the cells uncontrollably divide and ultimately destroy the tissues. Many patients with OS have metastases, mainly in the lungs, even after primary tumour resection [3]. OS cells arise from mesenchymal stem cells (MSCs) that follow the osteoblastic differentiation pathway. As a result, OS cells exhibit osteoblast-specific markers, such as alkaline phosphatase, osteocalcin, and bone sialoprotein. The tumours they form are distinguished by the production of a mineralised osteoid matrix, which is synthesised by the OS cells themselves. There are several subtypes of osteosarcoma, with the specific type being determined by the stage of differentiation at which the oncogenic transformation occurs [4]. The osteoblastic subtype of OS is observed in the most differentiated cells, where OS cells generate large amounts of osteoid matrix arranged in a complex trabecular structure. This formation often extends beyond the normal bone, creating a characteristic “sunburst” pattern on radiographic images due to tumour expansion, mineralisation, and the formation of periosteal spicules or “streamers”. In contrast, the chondroblasts subtype arises from mutations in less differentiated cells, leading to the production of a cartilaginous matrix alongside the osteoid matrix, resembling endochondral ossification. The final variant, fibroblastic OS, develops from the least differentiated OS cells, giving rise to a structure that closely resembles fibroblastic matrix tissue [5].

1.2 Aetiology and genomics

Aetiology of OS is extremely complicated and unclear, and it is believed that a combination of genetic and epigenetic are the main risk factors. One of the potential contributors of OS is mutation in *TP53* which encodes the p53 protein. P53 is an important regulator for cell

proliferation and apoptosis. *TP53* mutation compromises the gene tumour suppressor function and tumorigenic transformation [6]. Mutation in *the RB1 gene, which encodes Retinoblastoma protein (Rb),* causes hereditary retinoblastoma. Mutation in *RB1* causes the cells to lose the tumour suppression activity, which induces a different range of cancers. Rb interacts with E2F transcription factors to regulate the cell cycle and is also involved in normal differentiation processes. OS is very common in patients with RB1 mutations, apart from retinoblastoma itself. Compared to the general population, there is a 500-fold rise in the risk of acquiring OS in individuals with RB1 mutations [7, 8].

1.3 Symptoms, diagnosis and treatment

The most obvious symptoms of OS are pain, swelling/lumps and tenderness, limp and bone fractures and stiff joints [9]. Patients normally require medical help only after an incident like trauma or intense exercise, which means there is usually a delay in the diagnosis of OS, and the period of the symptoms is 3 months on average, while the patients might have experienced symptoms for many months or even years before diagnosis. The first line of diagnosis is achieved using an X-ray. Any symptoms such as osteoblastic, osteolytic or soft tissue swelling require immediate attention and diagnosis through MRI and CT scan [4]. For a definitive OS diagnosis, an invasive biopsy by a pathologist or oncologist is necessary. In addition, histology must be performed to investigate the stage of cancer. Besides using imaging for diagnosis, biochemical laboratory testing of urine and blood is essential [10].

The current therapeutic approaches for OS are primarily based on radiotherapy and chemotherapy with generic cytotoxic drugs, including cisplatin, doxorubicin, and methotrexate, continued with tumour resection and chemotherapy [11]. There are also other alternative therapies available, including laser medication, immunotherapy, phototherapy, nanoparticles or stem cell transplants, and many other less-used treatments. In almost all cases, surgery is a must with the aim of removing the primary tumour completely, with wide margins [12]. Limb salvage surgery is an advanced procedure that includes endoprosthetic replacement, biological restoration utilising allografts or autographs, or a mixture of both. Rotationality can be considered for tumours around the knee (in the proximal tibia or in the distal femur) [4]. Neoadjuvant chemotherapy (chemotherapy before surgery) is considered a standard treatment for OS patients as it not only reduces the tumour burden but also makes

it possible to histologically evaluate the tumour response to the treatment and tailored chemotherapy [13]. However, there are a lot of side effects with the chemotherapy drugs such as vomiting, hypersensitivity reactions, nausea, neurotoxicity, nephrotoxicity and cardiomyopathy [14]. In addition, OS metastasis also shows resistance to conventional chemotherapies that have been effective in treating the primary tumour and chemotherapy is not effective for >30% of metastatic OS patients [15, 16].

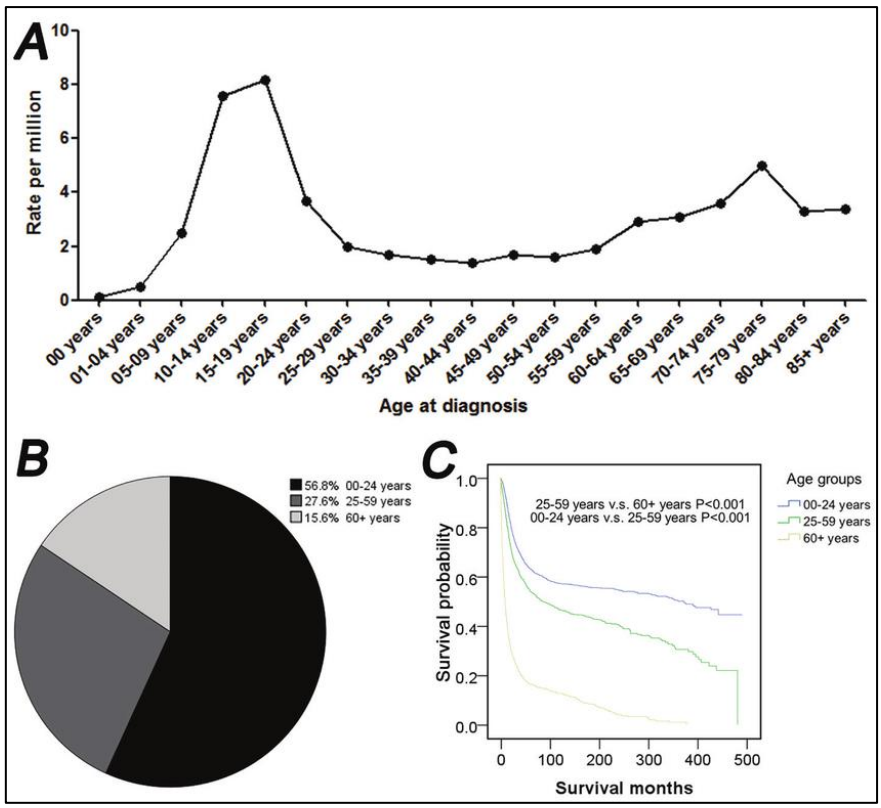

Figure 1.1. OS incidence, age distribution, and survival rates based on age at diagnosis from 1973 to 2012. (A) Osteosarcoma incidence rate categorised by age at diagnosis. (B) Pie chart illustrating the distribution of OS cases across three age groups: 0–24, 25–59, and ≥60 years. (C) Survival analysis curve comparing the survival outcomes of patients within the same age groups (0–24, 25–59, and ≥60 years) [17].

1.4 Current methods for OS treatment

The choice of cancer treatment is determined by several factors, including the type and stage of cancer, its severity, tumour size, location, and the patient's medical history and background [18]. This section discusses a concise overview of the current treatment approaches for OS.

1.4.1 Surgery

The primary treatment for OS is surgery, which involves the removal of abnormal tissue. Surgery is also utilised for diagnostic purposes, to determine the cancer stage, for reconstructive procedures to restore body function, or as a preventative measure. The most common surgical approach is Limb-Salvage Surgery (LSS), which aims to remove the cancerous tumour from a limb (e.g., arm or leg) while preserving as much of the limb as possible, thereby avoiding amputation. This procedure involves excising the affected bone and surrounding tissue, which is often replaced with a metal implant to maintain the function and appearance of the limb. However, when the tumour extensively infiltrates soft tissues or neurovascular structures, amputation is usually necessary [19, 20].

1.4.2 Chemotherapy

Chemotherapy involves the administration of cytotoxic antineoplastic drugs to target and destroy cancer cells by disrupting their growth and division. These drugs reach their target organs through the vascular system and serve multiple purposes beyond direct tumour eradication. They may be used to shrink tumours before surgery or radiotherapy (neoadjuvant chemotherapy), prevent metastasis, reduce the risk of recurrence, or as part of chemoradiation and palliative treatment [21, 22]. Chemotherapy is delivered in different phases depending on disease progression. Neoadjuvant chemotherapy, administered before surgery, aims to reduce tumour size, and improve surgical outcomes. Standard chemotherapeutic agents include high-dose methotrexate, doxorubicin (Adriamycin), cisplatin, and ifosfamide (for high-risk cases) [23]. Adjuvant chemotherapy, given post-surgery, is used to eliminate microscopic metastatic cells and follows the same drug regimen as neoadjuvant therapy to prevent recurrence. In cases of metastatic or recurrent osteosarcoma, more aggressive regimens, or experimental drugs, such as gemcitabine and docetaxel, are considered, for lung metastases, which are common in advanced disease [24]. A combination of chemotherapy drugs is often used to enhance efficacy, and chemotherapy in conjunction with surgery has been effective in treating various cancers, including leukaemia, colorectal cancer, breast cancer, pancreatic cancer, and ovarian cancer [25]. While chemotherapy is not a curative treatment on its own, it can reduce tumour size or alleviate pain, particularly in cases where surgery is not an option. However, chemotherapy affects not

only cancer cells but also healthy cells, including those in the bone marrow, gastrointestinal lining, and hair follicles, leading to side effects such as anaemia, immunosuppression, diarrhoea, mouth sores, nausea, and vomiting due to the suppression of red and white blood cell production [26].

1.4.3 Radiotherapy

Whilst widely used to treat many different cancers radiotherapy is a less common treatment approach for osteosarcoma (OS). It is not routinely used for osteosarcoma treatment due to the tumour's inherent radioresistance, meaning high doses of radiation are required to achieve therapeutic effects, often at the expense of damaging surrounding healthy tissue. This is particularly concerning in younger patients, where radiation can impair bone growth and development [27]. Radiotherapy is typically considered when surgical removal is not feasible, or the tumour is located in a challenging anatomical region. It involves the use of high-energy ionising radiation, primarily X-rays, to target and destroy cancer cells by damaging their DNA [23]. Unlike cancerous cells, which are unable to repair themselves, healthy cells can recover from radiation-induced damage, making the treatment selectively effective. To minimise harm to surrounding tissues, multiple radiation beams are directed from different angles, ensuring that the highest dose is delivered precisely to the tumour site while reducing exposure to healthy tissues [28]. Radiotherapy is administered through two main techniques: external beam radiotherapy (EBRT), where radiation is applied from outside the body, and internal radiotherapy, also known as brachytherapy or radioisotope therapy, where a radioactive source is placed in the body near the tumour. Some patients may undergo a combination of both techniques for more effective treatment. While radiotherapy is primarily used for the treatment of cancers, including head and neck cancers, it can also be combined with chemotherapy (chemoradiation) or surgery to enhance treatment efficacy. Additionally, it may be employed to decrease the risk of recurrence following surgery or as a palliative measure to alleviate cancer-related symptoms. In some cases, neoadjuvant radiotherapy is administered before surgery to shrink the tumour, making it easier to remove [29].

1.5 Bioactive glass: an overview

1.5.1 Nature of glasses

Glasses have been used by humans in different ways and applications for centuries. Whilst some applications are well-known, glasses can also be used for biomedical applications such as bone regeneration and dental hypersensitivity treatment [30].

Glass is a non-crystalline (amorphous) solid material typically formed by cooling a liquid melt rapidly enough to prevent the formation of a regular crystalline structure. In comparison to crystalline solids, glasses have no long-range order or major symmetry in their atomic structure [29]. Rather, the atoms that form the glass are amorphous without a defined atomic structure. In aqueous environments, the glass composition directly impacts many of its properties, like density, glass stability, solubility, thermal expansion coefficient (CTE), and ion release [31, 32].

Unlike the consistent and well-defined stoichiometry of crystalline compounds, glasses can be synthesised into a nearly infinite variety of formulations that can be tailored to a particular need [31]. In addition, the glass characteristics can be altered through doping, which is the addition of other oxides into the glass composition which resulting in the release of ionic dissolution for specific purposes and applications [33].

1.5.2 Glass structure

One of the earliest structures of glass was introduced by Zachariasen. Zachariasen's hypothesis says the atoms in both glass and crystal are connected through identical interactions and pulsate about their position in equilibrium with this structural difference that, unlike crystals, glass structure lacks regularity and symmetry [34].

The thermal behaviour of glass is commonly characterised by three key temperatures: the glass transition temperature (Tg), the crystallization temperature (Tc), and the melting temperature (Tm). T_g is an important aspect of the glass where the viscous liquid transitions into solid glass. It refers to the temperature range over which the glass transforms from a hard and brittle state to a more rubbery or viscous state upon heating. It marks the transition between the glassy and supercooled liquid states. T_g plays role in the conversion of the liquid into either a crystalline state or glass. Tm (melting temperature) represents the temperature

at which the crystalline phase completely melts into a homogeneous liquid. Cooling the liquid below the T_m slowly will produce crystalline materials, but if this cooling rate is fast enough, it will result in glass formation. Tc (crystallization temperature) is the temperature at which a glass begins to crystallize upon heating, leading to the formation of a crystalline phase within the amorphous matrix. The glass transition behaviour can be illustrated using a volume-temperature diagram (Fig. 1.2). When a liquid is cooled to a temperature below its T_m, the material undergoes a transition into a crystalline state, characterised by a long-range periodic atomic arrangement [35-37]. However, if the cooling process is sufficiently rapid, crystallisation is suppressed, leading to the formation of glass instead. The glass transition occurs over a range of temperatures (Tg) rather than at a distinct single temperature, making it a gradual transformation rather than a sharp phase change [38].

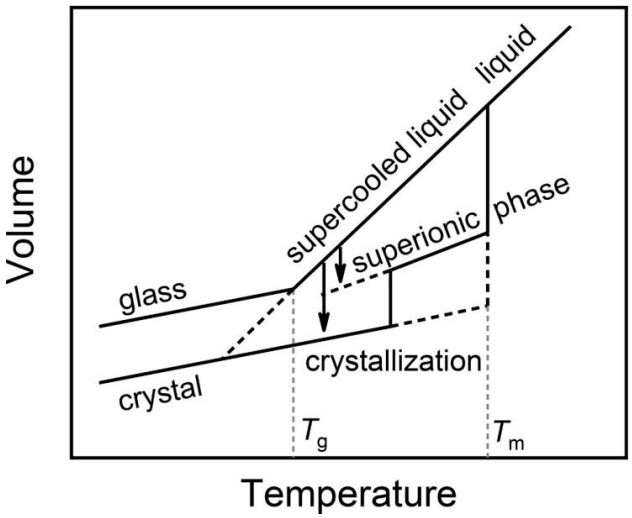

Figure 1.2: Schematic representation of Glass or crystal formation from liquid melt [38].

Zachariasen noticed in analysing the structure of vitreous silica that the glass network consists of silicon atoms which are surrounded by oxygen tetrahedra. The tetrahedra are linked via angle sharing so that each oxygen atom is connected to two silicon atoms. Figure 1.3 represents the 2-dimensional of this structure with tetrahedra shown as triangles. In a glass structure, atoms are covalently connected to oxygen. The components in the oxide glasses are categorized into three groups, depending on the type of structural function [39].

1) Network formers are the elements which create the glass network through the formation of oxygen tetrahedra, also known as structural units or network units. They are the glass key

components, capable of forming 3D structures. These units are linked by corner sharing building oxygen bridges, called bridging oxygen (Figure 1.3a). Network formers examples are SiO_2, P_2O_5, and B_2O_3.

2) Network modifiers are the elements which disrupt the glass network by developing terminal oxygen, also known as non-bridging oxygen (NBO) (Figure 1.3c). Alkaline and alkaline earth oxides are common examples.
3) Intermediate oxides are components that can play a role as either network formers or network modifiers, based on the composition of the glass, including Ga_2O_3, MgO and Al_2O_3 [40].

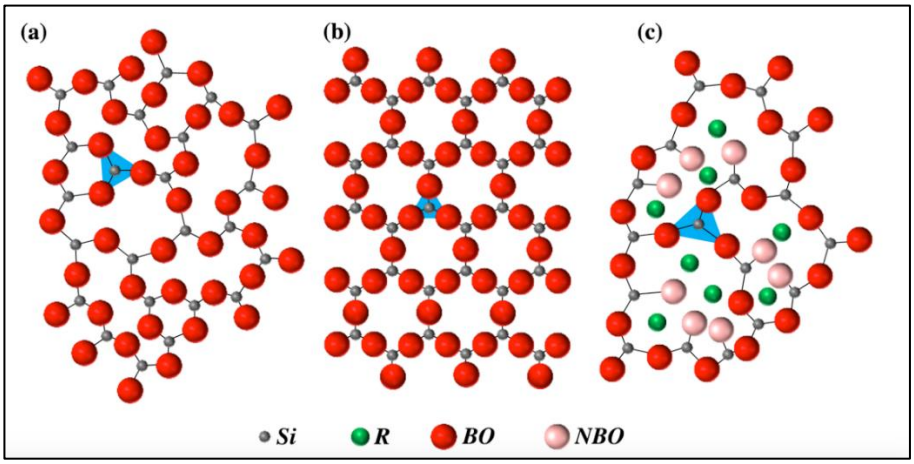

Figure 1.3. Two-dimensional representation of network structure of **(a)** vitreous and **(b)** crystalline silica; **(c)** vitreous silicate (R stands for a generic modifier cation, while BO and NBO stand for bridging oxygen and non-bridging oxygen, respectively) [39]**.**

The addition of oxides of divalent cations like CaO in glass formulation results in higher stability of the glass rather than monovalent oxides such as Na_2O or binary compositions of alkali silicate. The fundamental components of most bioactive glasses are SiO_2, P_2O_5, Na_2O, and CaO [41]. Depending on the composition of the glasses, the network former can consist of only one oxide, such as silicate, phosphate, or borate glasses, or more complex compositions involving the glass network former oxides, like boro-phosphate glasses and borosilicate [42].

1.5.3 Reaction with body fluids

Bioactive glasses induce biological responses after exposure to the aqueous environment *in vitro* or implantation in the human body, resulting in the formation of a hydroxyapatite (HA) layer on the surface of the glass (Figure 1.4). In fact, the biological activity of BG is via two mechanisms, (i). formation of HA layer on the interface of the BGs and the host tissue, (ii). ionic dissolution product and osteogenesis mechanism [37]. HA layer induces the integration of the BGs to the bone through interaction with collagen fibrils of bone defects. The mechanism behind the formation of the HA layer is quite well understood; however, how HA biologically interacts with the host tissue is not clear [33]. It is believed that bone integration with HA includes protein adsorptions, collagen fibrils corporations, bone progenitor cells attachment and differentiation, extracellular matrix (ECM) excretion and mineralisation, but the scientific proof for most of these stages is inadequate and limited. The glass dissolution products stimulate osteoprogenitor cells and induce the growth of new bone [36].

1.5.3.1 Mechanism of hydroxyapatite layer formation on bioactive glasses

The mechanism by which HA layer is formed is through the solution-mediated dissolution of the glass which is very similar to the traditional corrosion of glass [43]. The dissolution product aggregation induces alteration in both the pH and chemical contents of the solution, which results in providing the optimum pH and surface sites for the nucleation of HA. HA formation includes five stages *in vivo* and *in vitro* [40, 44].

1- Exchange of Na^+ and/or Ca^{2+} with H^+ and H_3O^+cations from the solution rapidly, which results in silanol bond (Si-OH) formation on the surface of the glass. The solution's pH rises, and regions rich in silica (cation-depleted) form on the surface of the glass. If the formulation of the glass contains phosphate it is also released from the glass.

$$Si - O^-Na^+ + H^+ + OH^- \longrightarrow Si{-}OH^+ + Na^+(aq) + OH \qquad (1.1)$$

2- Due to the high pH, the silica glass network undergoes disruption by OH^- which causes the breaking of Si–O–Si bonds. The silica is released in the form of silicic acid ($Si(OH)_4$) to the solution inducing more silanols production at the glass and solution interface.

$$Si{-}O{-}Si + H_2O^- \longrightarrow Si{-}OH + OH{-}Si \qquad (1.2)$$

3- Silanol groups condensation on the surface of the glass, creating a silica-rich matrix that repolymerises.
4- Due to the open structure of the silica gel the exchange of the ions between the fluid and the glass continues: Ca^{2+} and PO^{3-}_4 groups migrate to the surface via the silica layer and together with the Ca^{2+} and PO^{3-}_4 which exist in the fluid, amorphous $CaO–P_2O_5$ layer is formed on the surface of the silica layer.
5- Carbonate (CO_3^{2-}) and hydroxyl (OH^-) groups are incorporated from the solution, and finally the $CaO\text{-}P_2O_5$ crystallises into HA.

1.5.3.2 Ionic dissolution products and osteogenesis

After the formation of HA, the next stages are not well understood and what is known is the adsorption and deposition of biological growth factors to the HA layer for activation of stem cell differentiation. This is followed by macrophage activity for removing the debris and preparing the site for the cells to occupy the space. Then, the stem cells attach to the surface of the BG and proliferate and differentiate to form bone-growing cells like osteoblasts. Osteoblasts generate ECM to form bone. Inorganic calcium phosphate matrix crystallises in order to enclose bone cells in a living composite structure and finally proliferation and growth of bone tissue [45, 46].

The osteoproduction properties, which are simply the growth of new bone away from the bone-implant interface, are one of the most important aspects of BGs for bone regeneration, which other bioactive ceramics lack [47]. *In vitro* studies demonstrated that human osteoblast grows on the surface of BGs and produce collagenous ECM and mineralise, which results in bone nodule formation without the addition of any supplements into the cell culture to promote growth [48-50]. While other bioactive ceramic requires the addition of osteogenic supplements in the cell culture media for the formation of bone nodules such as b-glycerophosphate and dexamethasone. Calcium ions and soluble silica released from BGs promote the division of osteoblast cells, the development of growth factors, and ECM proteins. Based on *in vitro* studies human osteoblast showed an increase in the intracellular calcium level and upregulation of seven families of genes in 24 hours after being exposed to Bioglass 45S5 ionic dissolution products [51, 52]. Insulin-like growth factor II (IGF-II) is one of the genes which is upregulated 3-fold after treatment with conditioned media containing Bioglass®. This gene triggers the proliferation of osteoblasts *in vitro*. It suggests IGF-II may

mediate the stimulating impact of the Bioglass 45S5 dissolution ionic products on osteoblast proliferation. Dissolution product dose is an important matter to consider, as excessively high concentrations of the ions could generate toxicity. It also affects gene expression since the highest gene expression is seen at 60–90 μg/ml of calcium ions and 20 μg/ml of soluble silica [53]. The cell cycles of osteoblasts are also affected by the dissolution product of bioactive glass, as the osteoblast transition from the G0 phase to the G1 phase is mediated by transcription factors that were highly expressed due to the impact of the ionic dissolution products. Although there was an increase in the cells' apoptosis due to the presence of dissolution product, the surviving cells showed improved synthesis and mitosis [54].

1.5.4 Simulated body fluid (SBF) testing and calcium phosphate formation

SBF testing is a widely used *in vitro* method for evaluating the bioactivity of materials by assessing their ability to induce apatite formation under physiological-like conditions. Although SBF tests are valuable for screening bioactive materials, their results have historically lacked reproducibility due to variations in solution composition, surface-area-to-volume ratio, temperature control, and static versus agitated conditions. To address these inconsistencies, Kokubo *et al.* [55] proposed a more standardised methodology for SBF preparation and testing, establishing guidelines that closely resemble a universal reference for bioactivity assessment. Their protocol improved comparability between studies and clarified that SBF should be regarded as a comparative rather than a predictive tool for *in vivo* behaviour. During immersion, the formation of calcium phosphate (CaP) phases can proceed through several intermediate stages, including amorphous calcium phosphate (ACP), dicalcium phosphate dihydrate (DCPD, brushite), octacalcium phosphate (OCP), and tricalcium phosphate (TCP), ultimately leading to the precipitation of HA or carbonated hydroxyapatite (HCA). The nature and progression of these phases depend on factors such as solution supersaturation, pH, and ionic exchange between the glass and the surrounding medium, providing insights into the bioactivity potential of the tested material [55].

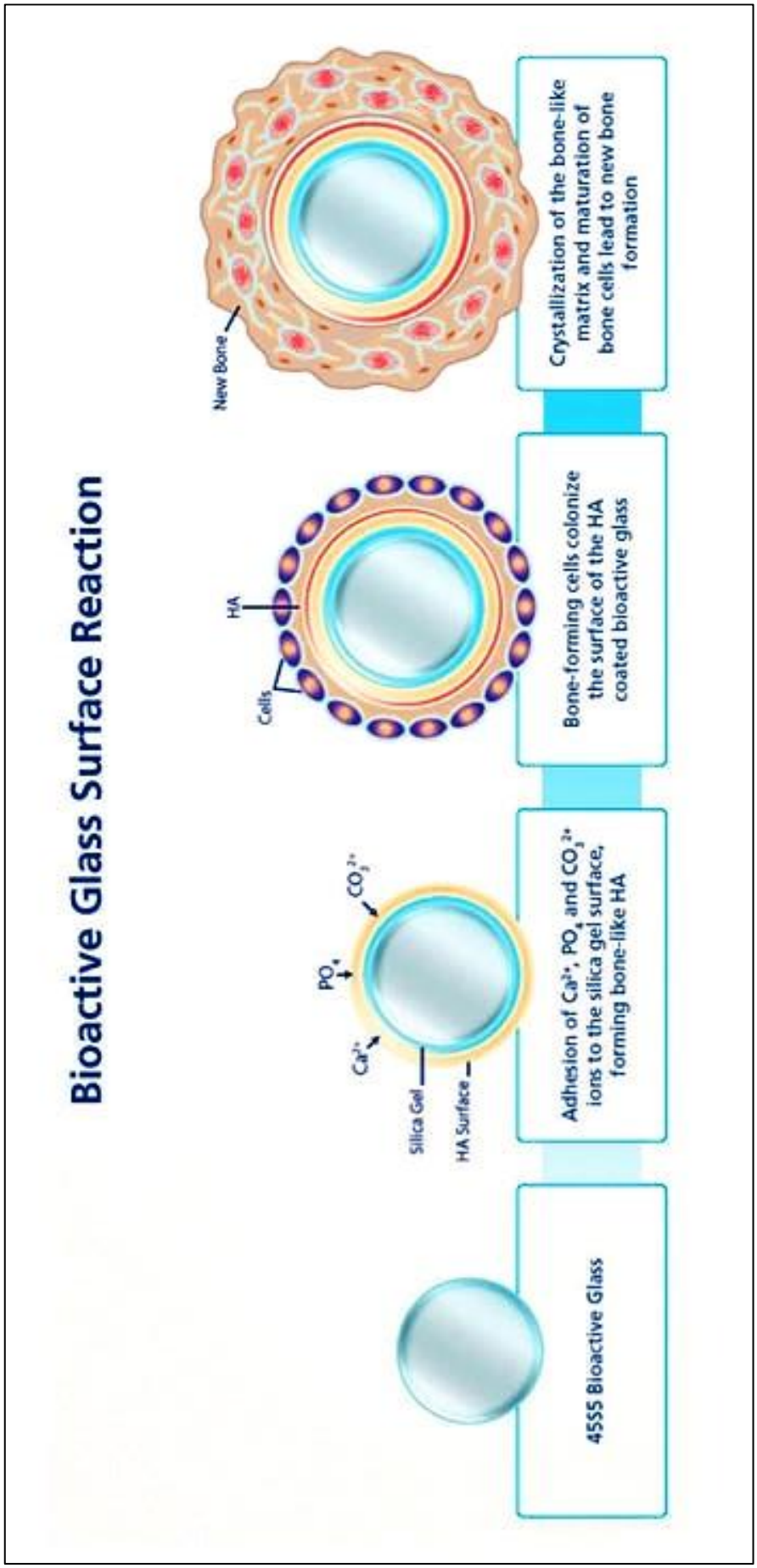

Figure 1.4. Integration of Bioglass with bone. The reaction with surrounding physiological fluid at the surface of Bioglass is shown in the first two steps, and the formation of new bone is shown in the last two stages [122].

1.6 Bioactive glass methods of fabrication

There are two different methods for the fabrication of BG: the traditional melt-quenching method and the sol-gel method. Bioglass 45S5 and other commercially available BG have been fabricated by melt-quenching. By this route, the oxide powders are mixed and melted together at a temperature above 1300˚C in platinum crucibles using electric furnaces. After melting, the molten liquid is quenched either by casting into graphite moulds or fritting into water. In the sol-gel route, the inorganic network of covalently bonded silica is formed at room temperature, and this inorganic gel forms silica nanoparticles which can be dried and heat-treated at around 600˚C to form the glass (Figure 1.5) [56, 57].

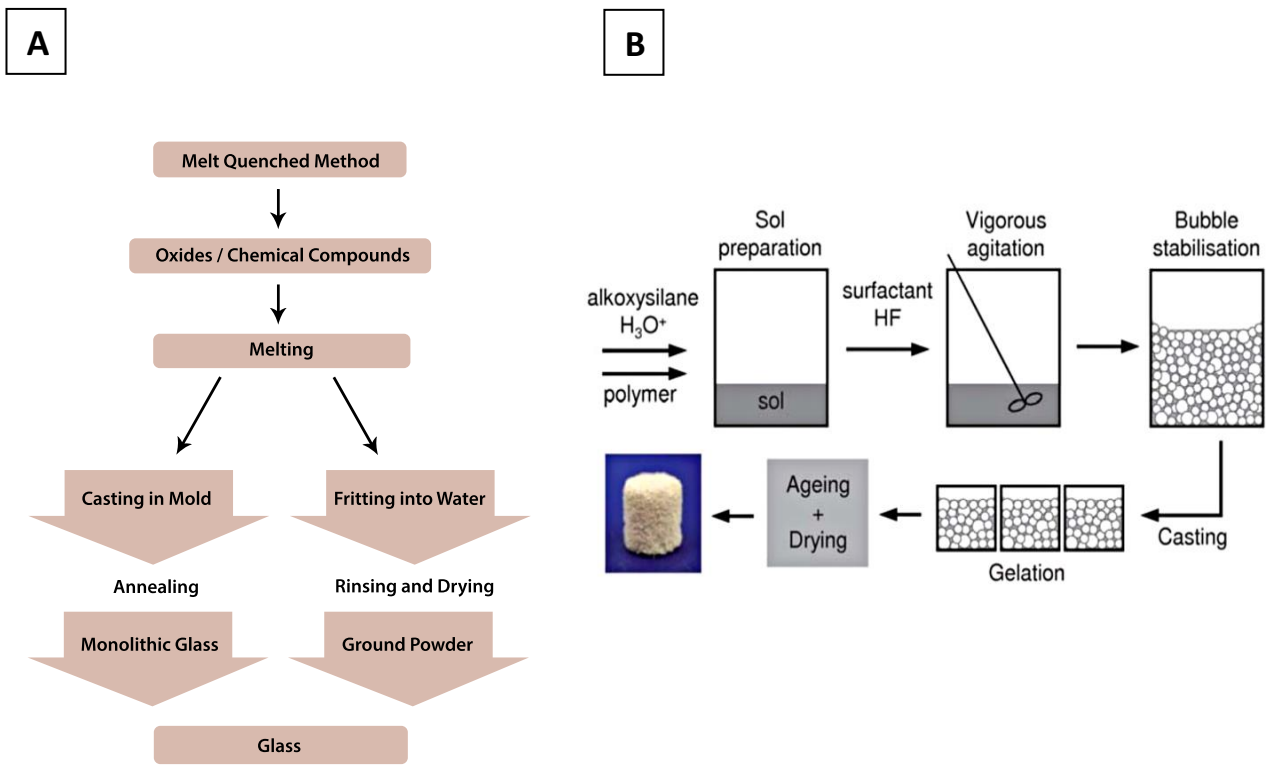

Figure 1.5. A) Schematic representation of melt quench method for the development of glass particles. **B)** Schematic of the sol-gel foaming process for scaffold synthesis [56].

1.7 Bioactive glass products and medical applications

Bioglass 45S5 has been used for the treatment of bone defects in orthopaedics and the jaw for over a million patients. Many new compositions and different kinds of bioactive glasses

have been introduced over the last forty years to optimise the response of the body according to the different clinical applications [29]. Table 1.1 represents the different biomedical applications of BGs and human tissue responses following their implantation.

The first surgical application of Bioglass® was in the treatment of ear infections caused by the degradation of middle ear bones, which results in deafness in patients. The Bioglass® 45S5 middle ear prosthesis implants were used to replace the bones and restore hearing via sound transmission from the eardrum to the cochlea. Application of Bioglass® for this purpose was very successful, as other available plastic or metal implants failed due to the formation of fibrous tissue around them and rejection of the implant [58].

Bioglass® has also been used in dental restoration in the form of cones for Endosseous Ridge Maintenance Implant (ERMIÒ). These cones were placed into tooth extraction sites, which help provide a stable ridge for dentures. Despite the successful application of these products, these are not in clinical use as surgeons prefer a scaffold with the ability to be shaped or cut and customised according to the patient's requirements [59].

The application of Bioglass® granules is preferred by orthopaedic surgeons, where they can mix the granules with blood from the patient and press the mixture into the defect. The blood makes it easier to handle the material and includes natural growth factors and cells capable of promoting bone regeneration. The first Bioglass® particulate (PerioGlas) was used as a synthetic bone graft for the treatment of periodontal diseases. The Bioglass® particles are applied to the root of healthy teeth to regenerate bone around the root in the jaw and produce a solid platform for anchoring titanium implants [60]. Also, S53P4 glass granules were investigated for bone defect post-removal of benign bone tumours caused in the tibia (shin), humerus (arm) and hands. The outcomes were compared between patients treated with autografts and those treated with S53P4 bioactive glass granules. The results showed that treatment with S53P4 led to a doubling in cortical bone thickness compared to the autograft group. Furthermore, the S53P4 granules began to gradually degrade, which is consistent with their bioactivity and contributed to stimulated bone remodelling at the implantation site [59].

Bioactive glass 45S5 (46.1 mol% SiO_2, 24.4 mol% Na_2O, 26.9 mol% CaO, and 2.6 mol% P_2O_5) and S53P4 (53 mol% SiO_2, 23 mol% Na_2O, 20 mol% CaO, and 4 mol% P_2O_5) are the two most extensively studied compositions within the bioactive glass family. The higher SiO_2 and lower CaO and Na_2O content of S53P4 results in a more polymerised glass network, leading to slower dissolution and ion release compared to 45S5. Consequently, 45S5 demonstrates

faster ion exchange and hydroxyapatite layer formation, which promotes strong bonding to bone but also contributes to reduced chemical durability and a higher tendency for crystallisation during thermal processing. In contrast, S53P4 exhibits enhanced structural stability, making it more suitable for clinical granule applications such as bone void fillers, and it possesses well-documented antibacterial properties due to its sustained ion release profile. However, its slower dissolution rate results in delayed bioactivity and longer *in vivo* resorption times compared with 45S5. Overall, 45S5 offers rapid bioactivity and bonding at the expense of stability, while S53P4 provides improved durability and antibacterial benefits, though with slower resorption kinetics [61, 62].

Treatment of tooth hypersensitivity is another application of 45S5 Bioglass®. Very fine glass particles called NovaMin® are incorporated into toothpaste to treat the hypersensitivity by up to 35%. According to clinical studies, particles of Bioglass® 45S5 bind to the dentine, which results in the formation of a layer of hydroxyapatite that is similar to tooth enamel that ultimately induces dentine tubule blockage. Tubules in dentine are connected to the pulp chamber that holds nerve endings. Glass dissolution products induce mineralisation by the deposition of calcium phosphate on the dentine tubules, which also causes an increase in the pH. Human saliva contains mineralisation inhibitor factors; therefore, the rise in pH and burst of phosphate and calcium help to boost mineralisation [63].

Bioactive glasses can be used for coating metallic implants. Metallic implants are usually bioinert, meaning they can be isolated from the host tissue by encapsulation of fibrous tissue post-implantation. Using bioactive glass for coating the implants increases their stability after implantation and bonds to the host tissue. However, there is a limitation with this strategy as bioactive glasses are biodegradable by nature, which can result in the degradation of the implant coating over time [64]. The key to achieving this limitation is tailoring the glass composition so the glass can provide a good coating on the implants and produce a layer of hydroxyapatite; different layers of a composition may be required for optimal dissolution and integration into the host tissue [65].

Table 1.1. Therapeutic applications of bioactive glass and tissue responses.

Medical Field	Therapeutic/Medial Device	Example of implant/material	Cellular response	Implant type	Ref
Orthopaedic applications	• Arthroplasty • Orthopaedic fixation devices for, *Arthrodesis* *spinal fusion*	Alumina, Yettrium-stabilized zirconia Silicon nitride bioceramic-based bone grafts	Fibrous tissue	Inert	[66-68]
Coatings for chemical bonding	Hydroxyapatite surface coatings Diamond-like carbon coatings Calcium phosphate coatings Nitride coatings	calcium phosphate-based bioceramic diamond-like carbon film HA /TCP coating Titanium nitride coatings	Interfacial bond formation	Bioactive	[69-71]
Bone tissue engineering	Bioceramic bone fillers Tissue-engineered bone constructs	hydroxyapatite/collagen nanocomposite scaffold, Bioglass 3D porous graphene/nano-bioglass58S composite scaffold	Implant replacement with the surrounding tissue	Bioactive/ Biodegradable	[72,73]
Dental applications	Dental prosthesis Laminate veneers Dental implants Restorative dentistry Preventive dentistry Endodontics	alumina, spinel, lithium disilicate reinforced ceramics, and zirconia porcelain veneers zirconia dental implant fluoroaluminosilicate glass powder β-TCP, amorphous calcium phosphate, and HA Calcium-enriched mixture cement	Fibrous tissue	Inert	[74-77]
Ocular prosthesis	Glass ocular implants Silicon ocular implants Porous hydroxyapatite ocular implants Aluminium oxide ocular implants	Mules implant Solid or porous silicon episcleral implants porous coralline HA sphere Bioceramic orbital implant	Implant replacement with the surrounding tissue	Bioactive/ Biodegradable	[78-80]

1.8 Clinical applications of bioactive glass for bone

The field of bioactive glasses (BGs) for cancer therapy is rapidly advancing, with numerous clinical trials currently underway. Resources like Clinicaltrials.gov, ciscrp.org, and isrctn.com provide valuable information on the latest ongoing trials worldwide in this area. Figure 1.6 outlines the various stages involved, from the initial concept development to the fabrication and clinical implementation of the bioactive glass platform.

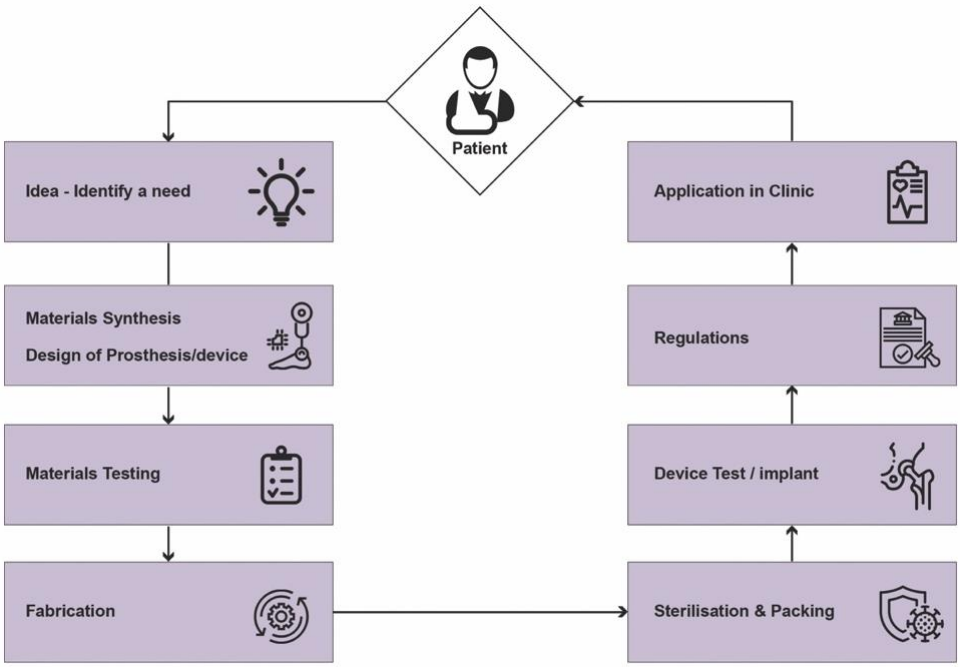

Figure 1.6. Schematic view of different stages to form the idea for a new bioactive glass to the point where said material can be used in human.

One of the most common uses of bioactive glasses (BGs) in clinical trials is for the treatment of benign tumours. Bone defects that arise following surgery for benign bone tumours are often addressed using allografts or autografts, as these materials offer essential properties required for effective bone grafting. However, these methods have notable limitations, including limited availability, donor site morbidity, and the risk of disease transmission. Synthetic bone grafts present a promising alternative to both autografts and allografts, effectively overcoming these drawbacks. Since these synthetic substitutes are composed of calcium phosphates, they closely resemble the structure and composition of natural bone minerals and exhibit osteoconductive properties that are crucial for bone remodelling and regeneration.

A clinical trial (NCT00841152) compared two synthetic ceramic bone graft substitutes: bioactive glass (BG), marketed as Bonalive®, and beta-tricalcium phosphate (TCP), known as ChronOs, for filling bone defects following the surgical removal of benign bone tumours. The trial began in March 2009 and concluded in December 2018. Based on preclinical research, BG was anticipated to outperform TCP in promoting defect repair and enhancing functional recovery post-surgery.

The study enrolled 120 participants (both male and female, aged 18 and older) who had either primary or recurring benign bone tumours requiring surgical removal and defect filling. The patients were divided into two groups. Stratum I focused on hand lesions, comparing BG and TCP with autologous bone grafts (harvested from the iliac crest) as the standard treatment. Stratum II examined large, long-bone lesions, comparing BG, TCP, and allogeneic bone grafts (frozen femoral heads) as the control.

Following treatment, various outcomes were assessed, including hand-grip strength (Stratum I), cortical bone window healing via CT scan (Stratum II), biomaterial integration observed through radiographs, pain levels, surgical wound healing, bone defect recovery, and soft tissue complications at the surgical site. The results of the trial had not been disclosed at the time of reporting [81].

The effectiveness of bioactive glass (BG)-S53P4 was assessed and compared with autogenous bone (AB) grafts in patients diagnosed with benign bone tumours between 1993 and 1997. This study involved 25 participants (both male and female, aged over 18) who had been identified with a primary tumour via X-ray, either due to pain or a pathological fracture. Before the trial commenced, all fractures were treated, and participants were then divided into two groups: one receiving BG treatment and the other receiving AB treatment.

In the BG group, BonAlive® Biomaterials was used as the bone graft, whereas in the AB group, bone harvested from the iliac crest was used to fill the cavity. The findings revealed a significant difference between the two groups. Bone remodelling in the BG group was notably slower compared to the AB group. However, 36 months post-implantation, no difference in cavity volume was observed between the two groups. A key advantage of using BonAlive® is that it eliminates the need for a second surgical procedure to harvest bone from the patient's

hip, an area with limited bone supply, which not only reduces patient morbidity but also shortens operative time and lowers the risk of donor site complications.

CT scans and X-ray results showed higher bone density in the BG group. MRI scans revealed predominantly or partially fatty bone marrow and residual BG granules were observed in patients with larger bone tumours. These findings demonstrate that BG-S53P4 is a promising material with favourable safety, osteoinductive properties, bone-bonding capabilities, and antimicrobial effects, making it a viable option for treating benign bone tumours [82].

In another clinical trial, the injectable bi-phasic calcium phosphate (BCP) ceramic bone substitute, CERAMENT™ | BONE VOID FILLER, was investigated in patients with benign bone tumours to assess its effectiveness in promoting bone remodelling and regeneration as a treatment option (NCT02567084). CERAMENT™ was also evaluated for its potential to convert bone cysts into healthy bone tissue and stimulate bone growth in cystic areas that were not directly filled with the substitute.

The study involved 14 participants with benign bone tumours and was conducted between February 2011 and December 2014. The tumours were treated using a minimally invasive procedure, involving small surgical incisions rather than a large opening. The resulting bone defects were filled with the bi-phasic, injectable CERAMENT™ BONE VOID FILLER. This bone substitute is composed of 60% (w/w) synthetic calcium sulfate (CaS) and 40% (w/w) HA. To enhance its visibility in radiological imaging, the mixture was combined with a water-soluble radio-contrast agent, iohexol (180 mg/mL), making it radiopaque.

The procedure included percutaneous injection into bone cysts or minimally invasive surgery for the removal of solid tumours, followed by defect filling with CERAMENT™. Participants were allowed to bear full weight immediately after the procedure and were monitored clinically and radiologically for one year. After 12 months, bone healing and remodelling were evaluated using CT scans and X-rays and assessed according to the Modified Neer classification of radiological outcomes. Additionally, the volumes of both cysts and new bone formation were measured [83].

1.9 Therapeutic potential of gallium

Gallium (Ga) is the most used metal for the treatment of cancer after platinum. Ga is anti-inflammatory and anti-bacterial, with application for treating osteoporosis and cancer-mediated hypercalcemia as it can prevent bone resorption by osteoclasts and stimulate bone mineralisation [84]. Incorporation of Ga ions can create anti-microbial properties of the glass, and it can prevent bacterial growth through the limitation of bacterial attachment and by damaging the bacterial Ribonucleic acid (RNA) and DNA [85, 86]. The anti-tumour properties of Ga were confirmed in 1971 by Hart *et al*. studies conducted on calf thymus DNA have demonstrated that Ga can bind to DNA and disrupt the helix DNA. It can induce apoptosis, which is believed to occur via triggering the condensation of chromatin. It also prevents DNA replication by forming complexes with TfR and blocking iron uptake, which results in cellular Iron deprivation [87, 88].

Ga compounds have vast applications from the electronic industry to the therapeutic and diagnostic agent in cancer treatment and anti-inflammatory (Figure 1.7). One of the earliest medical applications of Ga is the radiogallium as a tumour imaging agent. Early observations revealed that radioactive Ga (^{67}Ga) was localised in the malignant cells in animals with tumours. This discovery led to a ^{67}Ga scan to find cancerous tumours in patients. This discovery that tumours could take up ^{67}Ga raised the question whether non-radioactive Ga compounds could also accumulate in tumours and prevent their development. This was a starting point for the hypothesis of using Ga compounds as an anti-tumour agent [89].

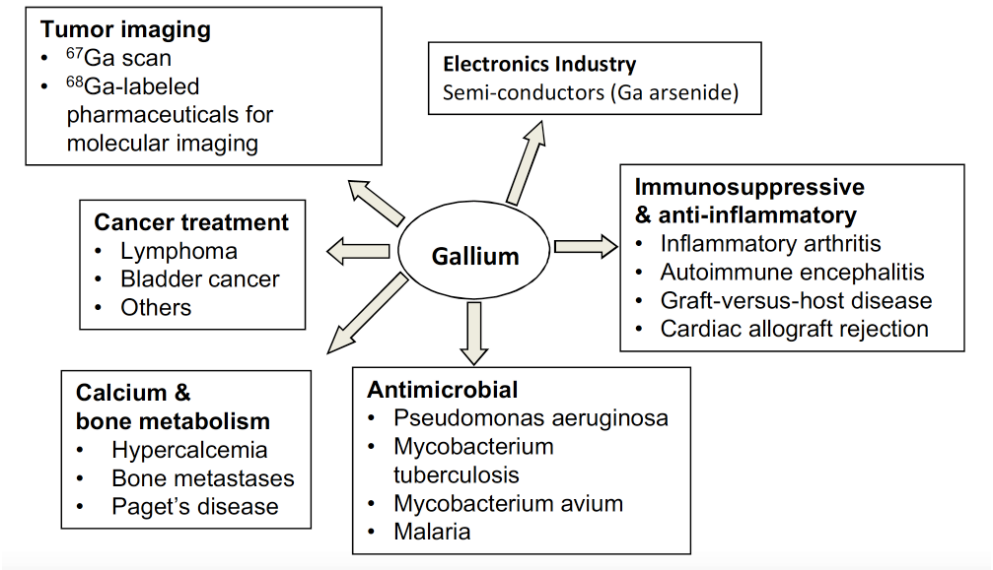

Figure 1.7. Gallium compounds medical applications. Gallium has a range of different medical and therapeutic applications, including cancer therapy, bone metabolism diseases, infections, and imaging [90].

1.9.1 Gallium antineoplastic properties

The fact that ^{67}Ga could be localised in tumour cells prompted researchers to investigate the antineoplastic properties of salts of the group IIIa metals aluminium, gallium, indium, and thallium in CDF1 mice and Sprague-Dawley rats [25]. Amongst these, $Ga(NO_3)_3$ demonstrated the highest efficacy for tumour suppression with the lowest toxicity. $Ga(NO_3)_3$ has been intravenously administered with a dosage of up to 300 mg/Kg using protracted venous infusion. This delivery protocol has been shown to be effective against cancer hypercalcemia, bladder carcinoma, carcinoma of the urothelium and lymphoma. However, side effects such as granulocytopenia grade 3 and 4 despite the use of growth factors, renal function alteration grade 3 or 4, hypocalcemia grade 3 or 4, thrombocytopenia and temporary blindness have been reported in some of the tested patients [91].

While early studies were undertaken to assess Ga^{3+} antitumor properties, the studies also reported that patients treated with $Ga(NO_3)_3$ showed a substantial reduction in calcium levels in the blood of patients with hypercalcemia [25]. One of the benefits of $Ga(NO_3)_3$ is that it does not cause myelosuppression, unlike other chemotherapeutic medications, and thus could be used in patients with very low white blood cell or platelet counts. *In vitro* studies demonstrate that Ga is in synergy with fludarabine, interferon-alpha, gemcitabine, paclitaxel,

and fludarabine, indicating that combination therapy with these drugs can be very effective. Furthermore, Ga therapeutic compounds do not seem to share cross-resistance with traditional chemotherapeutic drugs, as clinical responses have been observed in patients with difficulty reacting to several other medications [25, 89]. Zeimaran *et al.* fabricated Ga silicate containing bioactive glass to produce poly (octanediol citrate) scaffolds containing microparticles of Bioglass. Due to the addition of bioactive glass in the formulation, the mechanical aspects of the scaffolds were enhanced. The osteoblast cell viability on these scaffolds was evaluated, and it was reported that adding 10 wt. % of glass particles stimulated osteoblast cell attachment and viability. Even though the article stated the possible usage of such scaffolds for bone grafts affecting OS patients, the effect of such scaffolds on OS cells has not been investigated [92].

1.9.2 Gallium mechanism of action

To maximise Ga's medicinal uses, a better comprehension of its pharmacology, mechanisms of action, clinical effectiveness, and possible adverse effects is necessary. Although Ga has no recognised physiological function, it is metabolised in the human body in a manner similar to that of iron in circulation. It can, however, disrupt vital biological proteins and signalling pathways, especially those involved in iron metabolism. Due to its distinct behaviour, several gallium-based compounds have been developed as therapeutic agents and diagnostic instruments with uses in the treatment of infectious illnesses, cancer, and metabolic bone diseases [25].

Gallium ions are taken up by cancer cells primarily through transferrin receptor-mediated endocytosis, where gallium-transferrin complexes bind to the cell surface. The uptake of gallium occurs through both transferrin receptor-dependent and -independent mechanisms, which may vary depending on the cell type involved [25, 93]. The proposed cellular mechanisms of gallium’s action are illustrated in Figure 1.8.

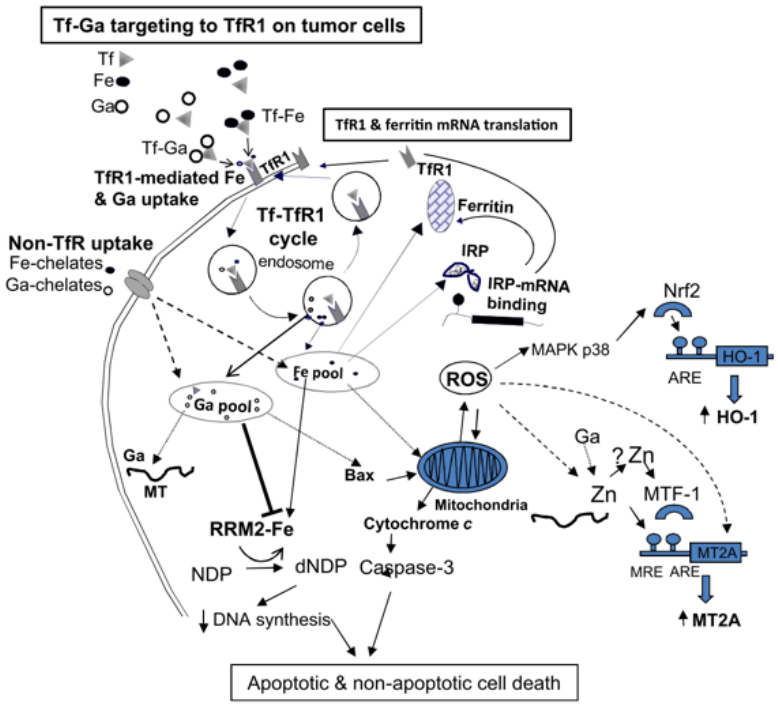

Figure 1.8. Gallium transport and cellular uptake. gallium's binding to transferrin (Tf) in the blood circulation which is then taken up by transferrin receptor1 (TfR1)-mediated endocytosis of Tf-Ga complexes. The absorption of cellular iron can be inhibited as Tf-Ga compounds will compete with Tf-Fe compounds for binding to TfR. Cells Initially subjected to Ga may induce a cytoprotective reaction in which the cellular reactive oxygen species (ROS) produced by gallium causes the expression of heme oxygenase-1 (HO-1) and metallothionine-2A (MT-2A) p38 and metal transcription factor-1 (MTF-1) mechanisms, respectively [90].

Ga's mechanism of action is complicated and occurs in two steps. The first step includes Ga binding (as Tf-Ga) to the transferrin receptor of tumour cells. In the second step, Ga interferes with the metabolism of cellular iron by disrupting transferrin-mediated iron uptake and endosomal iron release from transferrin to the cytoplasm which results in iron deprivation and inactivation of iron-dependent ribonucleotide reductase, an essential enzyme for the synthesis of DNA [93-95]. In fact, Ga is proven to suppress ribonucleotide reductase enzyme function in cell lysates specifically; this suggests that Ga blocks the synthesis of deoxyribonucleotide via two mechanisms: a blockage of intracellular iron transportation to the enzyme and a direct effect on the enzyme, which is independent of iron transport [89]. Ga's anti-cancer mechanisms are summarised in Table 1.2.

Table 1.2. Summary of Ga's anticancer mechanisms.

Mechanism	Description	Effect on Cancer Cells	Ref
Iron Mimicry and Disruption of Iron Metabolism	Ga mimics iron (Fe^{3+}) and binds to transferrin, interfering with iron-dependent cellular functions.	Inhibits DNA synthesis, disrupts mitochondrial function, and impairs cell proliferation.	[96]
Inhibition of Ribonucleotide Reductase (RR)	Ga prevents RR from converting ribonucleotides to deoxyribonucleotides, which are required for DNA synthesis.	Reduces DNA replication, leading to cell cycle arrest in **S-phase**.	[97]
Caspase Activation and Apoptosis Induction	Ga triggers intrinsic apoptosis via mitochondrial pathways and caspase-3/7 activation.	Promotes programmed cell death (apoptosis) in cancer cells.	[98]
Disruption of Mitochondrial Function	Ga interferes with mitochondrial iron homeostasis and induces oxidative stress.	Leads to mitochondrial membrane damage and release of cytochrome C, triggering apoptosis.	[99]
Inhibition of Cell Proliferation	Gallium alters iron-dependent enzyme activity, affecting key metabolic pathways.	Suppresses cancer cell growth by impairing metabolic function.	[100]
TfR Overexpression Targeting	Cancer cells have increased TfR expression for iron uptake. Ga exploits this to preferentially enter tumour cells.	Enhances selective cytotoxicity, limiting damage to healthy cells.	[101]
Inhibition of Angiogenesis	Ga disrupts VEGF pathways, reducing new blood vessel formation.	Prevents tumour vascularisation, limiting nutrient supply.	[102]
Suppression of Cancer Cell Migration and Invasion	Ga downregulates matrix metalloproteinases (MMPs), reducing extracellular matrix degradation.	Limits metastasis by restricting tumour cell invasion.	[103]

1.10 Clinical applications of gallium for cancer treatment

Gallium nitrate, a basic gallium salt is regarded as a 'first-generation' gallium compound that was explored for its anticancer potential in humans. Consequently, it serves as the benchmark for evaluating the effectiveness of newer gallium-based treatments [89].

In a clinical trial efficacy and safety of gallium nitrate was investigated as a continuous seven-day infusion in patients with advanced malignant lymphoma (NCT00054808). This study aims to establish the role of gallium nitrate in a targeted group of patients who have previously undergone treatment. Early clinical investigations have indicated promising evidence of antitumor activity in individuals with relapsed or refractory non-Hodgkin's Lymphoma who were treated with gallium nitrate. The trial commenced in June 2002 and included 47 participants, both male and female, aged 18 and above, who had malignant lymphoma including, Hodgkin's disease, diffuse histiocytic lymphoma (DHL), Diffuse poorly differentiated lymphocytic lymphoma (DPDL), Nodular poorly differentiated lymphocytic lymphoma (NPDL), Cutaneous T-cell lymphoma (mycosis fungoides). The treatment regime was the administration of Gallium nitrate via continuous infusion over seven days. Four dose levels were tested (200 mg/m²/day to 400 mg/m²/day), with 300 mg/m²/day identified as the optimal dose for further evaluation. Infusions initially took place in the hospital but later transitioned to outpatient administration via portable infusion pumps. Tumour response was assessed using CT scans, lymphangiography, and bone marrow biopsies. Blood parameters, kidney function, and electrolyte levels were closely monitored throughout the treatment. Out of 47 evaluable patients, 34% (16 patients) demonstrated a significant positive response to the treatment and achieved major tumour responses. Response rates varied by lymphoma type as following:

- Hodgkin's disease: 18% (3/17 patients)
- Diffuse histiocytic lymphoma (DHL): 40% (6/15 patients)
- Diffuse poorly differentiated lymphocytic lymphoma (DPDL): 50% (5/10 patients)
- Nodular poorly differentiated lymphocytic lymphoma (NPDL): 40% (2/5 patients)

Renal Toxicity occurred in 8% of patients treated at 300 mg/m²/day, but was reversible with hydration. The study concluded that continuous infusion of gallium nitrate (300 mg/m²/day) is effective, well-tolerated, and improves therapeutic outcomes with manageable side effects. Outpatient administration via portable pumps was safe and practical, and the drug may also help treat cancer-related hypercalcemia [104].

Gallium maltolate (GaM), known chemically as tris(3-hydroxy-2-methyl-4H-pyran-4-onato) gallium, is an oral gallium compound developed for therapeutic use. Evidence supporting its

anticancer potential in humans was reported by Bernstein *et al.* [105] in their study, a patient with advanced hepatocellular carcinoma who had previously failed treatment with sorafenib showed significant improvement after receiving 1500 mg/day of oral gallium maltolate. The patient's symptoms improved markedly, and imaging studies confirmed a notable reduction in the size of the hepatic tumour. This outcome followed radiogallium scanning, which indicated high gallium uptake by the tumour [105].

Another clinical trial, which began on May 8, 2024, is investigating the Expanded Access to Gallium Maltolate (GaM) (NCT06404034). This ongoing trial is still recruiting participants and aims to provide GaM for compassionate use in adult patients (both male and female) aged 18 and above with relapsed/refractory glioblastoma who have exhausted standard treatment options. Eligible patients must be diagnosed with histologic or molecular glioblastoma in accordance with WHO 2021 guidelines. GaM is administered as 500 mg capsules, taken once daily on an empty stomach in 28-day cycles. Patients initially receive a 3-cycle prescription for home self-administration. The treating physician has the flexibility to adjust therapies or discontinue GaM at any time. Additionally, consultation with xCures and Imaging Biometrics is required before introducing non-emergent anti-cancer therapies or modifying the treatment schedule [106]. This program offers a compassionate treatment option for glioblastoma patients with limited alternatives and continues to recruit participants to expand its impact.

Tris(8-quinolonato) gallium (III) (KP46), a gallium complex contains an organic ligand 8-quinolinol is in clinical trials as an oral gallium compound. In a clinical trial Phase I and Pharmacokinetic Study of FFC11 (KP46) in Solid Tumours was investigated. FFC11 (KP46) is an orally available gallium complex with antitumor activity through ribonucleotide reductase inhibition, S phase arrest, and apoptosis induction. Preclinical models indicated that FFC11 is more potent than gallium nitrate and effective in treating tumour-associated hypercalcemia. FFC11 was administered orally for 14 days, followed by a 14-day recovery period (one treatment cycle). The Initial dose was 30 mg/m², with dose escalation by 100% increments until toxicity criteria were met. Tumour response was assessed using RECIST criteria, and pharmacokinetics (PK) were evaluated using a one-compartment model. In this trial, 7 patients with solid tumours (including parotid gland, stomach, renal cell, and ovarian cancer) participated. Adverse events included Neutropenia (G2) and anaemia (G2) at 30 mg/m², Stomatitis and conjunctivitis (G1) at 60 mg/m², Dizziness, headache, and acne (G1) at 240

mg/m², Fatigue (G1) and diarrhoea (G3) at 480 mg/m², the latter being dose-limiting toxicity (DLT). However, due to feasibility concerns, enrolment at the highest dose level was halted. Pharmacokinetics showed Peak plasma levels occurred 5-7 hours post-administration. The drug showed a long half-life (28 hours), high clearance (42 L/h), and a large volume of distribution (1700 L). One patient with renal cell carcinoma (RCC) showed an unconfirmed partial response after 8 weeks. Another RCC patient achieved stable disease for 29 weeks. Overall FFC11 demonstrated good tolerability with early signs of efficacy in renal cell carcinoma [107]. These findings support further exploration of gallium compounds in combination therapies or for other cancer types requiring effective tumour management.

1.11 Gallium-doped bioactive glasses

Gallium-doped bioactive glasses (Ga-BGs) are novel materials that combine bioactivity with antibacterial and anticancer properties, making them promising for biomedical applications. These glasses combine the medicinal advantages of Ga ions with the well-established qualities of BGs [108]. The BGs under investigation in this research project is silicate-based and is modified by incorporating gallium oxide (Ga_2O_3) into the glass structure. Structurally, Ga can act both as a network former, integrating into the glass matrix, or as a network modifier, disrupting the glass network structure depending on its concentration and the glass composition [109]. At lower Ga concentrations, Ga behaves similarly to Al^{3+}, forming stable GaO_4 (tetrahedral) or GaO_6 (octahedral) units. The incorporation of Ga leads to increased chemical durability and enhanced structural flexibility [110, 111]. Notably, the addition of Ga has been shown to reduce the glass Tg by weakening directional covalent bonds in the Si–O–Si network. This occurs as Ga forms Si–O–Ga bonds, which are more ionic than Si–O–Si bonds, enhancing the flexibility of the glass structure [112].

Apart from its structural function, Ga-BGs exhibits a few significant biological impacts. Ga-BGs show potent antibacterial properties, particularly against Gram-negative bacteria such as *E. coli*. Studies have shown that the release of Ga ions can inhibit bacterial growth by interfering with iron-dependent metabolic processes in bacteria, effectively mimicking Fe^{3+} ions and disrupting key bacterial functions [112]. The antibacterial efficiency has been shown to rise with higher Ga_2O_3 concentrations, demonstrating promising results for infection control in biomedical applications [113]. Furthermore, Ga-BGs have demonstrated biocompatibility and

enhanced bone regenerative potential. Studies involving osteoblast-like cells have reported improved cell attachment, increased mitochondrial activity, and enhanced cell viability in the presence of Ga-BGs [108]. Ga incorporation has also been shown to promote the secretion of vascular endothelial growth factor (VEGF), supporting angiogenesis and improved vascularisation, which is vital for effective bone healing and regeneration [109].

In addition to their antibacterial and regenerative properties, Ga-BGs have demonstrate promising anticancer effects. Research has demonstrated that Ga ions effectively reduce the viability of osteosarcoma cells such as MG-63 and Saos-2 cell lines [110, 111]. Ga ions selectively target cancer cells by exploiting their increased demand for iron, which is critical for their rapid growth and division. Ga interferes with iron metabolism in cancer cells by mimicking Fe2+ ions, which eventually hinders cell division and stimulates apoptosis [100]. Notably, Ga-doped glasses selectively target cancer cells without compromising the viability of healthy osteoblast cells, enhancing their therapeutic potential in cancer treatment [110].

Ga-doped bioactive glasses have been investigated in preclinical research to further improve the functioning of composite materials like hydrogels. Ga-BG-based hydrogels have been shown to improve antibacterial performance, vascularisation potential, and mechanical strength, making them suitable for a variety of clinical applications [114]. Additionally, injectable Ga-containing gels have demonstrated enhanced compressive strength and prolonged working time, improving the material's handling properties for surgical use.

The therapeutic potential of Ga has inspired some preliminary studies on its incorporation into BGs (Table 1.3). To completely investigate its advantages and improve patient outcomes using gallium-containing bioactive glasses, further research is necessary. A study by Phull *et al.* explored the development of a gallium-doped cement aimed at treating bone cancers. The research investigated the effect of substituting ZnO with Ga_2O_3 in an ionomeric glass series (1-5 mol%, substitution) and examined the resulting glass polyalkenoate cements (GPCs) for their rheological, mechanical, pH, and ion-eluting properties. X-ray diffraction confirmed the amorphous glass structure, and energy dispersive x-ray fluorescence validated the successful incorporation of Ga into the glass series. The study demonstrated a controlled release of Ga across the GPC series, which is advantageous for potential therapeutic applications. However, while the Ga-doped cement shows promise for localised Ga delivery in bone cancer treatment, the study did not assess its cytotoxic effects on OS cells, nor did it include any direct cell studies to evaluate its anticancer efficacy. Further *in vitro* investigations are

necessary to determine the potential cytotoxic effects and therapeutic value of this Ga-doped cement in bone cancer treatment [115].

The study by Medeiros *et al.* investigated the development of Ga-BGs for bone regeneration and cancer therapy. The researchers synthesised bioactive glasses containing Ga and niobium (Nb) using a sol-gel method coupled with self-propagating combustion. The addition of Ga^{3+} ions were shown to enhance network connectivity by replacing calcium ions with Ga ions, which act as network formers. This increased the polymerisation degree of the glass structure and improved its chemical stability. The controlled release of Ga^{3+} ions were identified as a potential therapeutic strategy for targeting bone cancer cells, leveraging gallium's known ability to mimic iron, disrupt cancer cell metabolism, and induce apoptosis. Additionally, the incorporation of Ga enhanced the antibacterial properties of the material. While the study demonstrated promising characteristics for Ga-doped bioactive glasses, no direct cytotoxicity tests on osteosarcoma cells or *in vitro* cell studies were performed. Further investigation is needed to evaluate the anticancer potential and biocompatibility of this material in relevant biological models [116].

Zeimaran *et al.* (2015) developed silica-based bioactive glass containing 0.08 mol% Ga_2O_3 and incorporated it into poly (octanediol citrate) scaffolds infused with bioglass microparticles. The inclusion of BG particles enhanced the mechanical properties of the scaffolds. Additionally, osteoblast cell viability studies indicated improved cell attachment and survival when 10 wt% glass particles were added to the scaffolds. Although the authors suggested the potential application of these scaffolds in bone grafts for osteosarcoma patients, the study did not investigate their direct effects on osteosarcoma cells [92].

This research investigates the development of an injectable calcium phosphate cement (CPC) loaded with gallium maltolate (GaM) for controlled drug release in bone cancer treatment. The study highlights the synthesis process, physicochemical properties, mechanical strength, and the controlled release profile of GaM within the cement. The incorporation of GaM improved the injectability and cohesiveness of the cement, while its mechanical strength, though slightly reduced, remained within acceptable clinical standards. According to the study, GaM was released gradually over time, suggesting that it may be used as a localised therapy for bone metastases. However, the research lacks cytotoxicity and *in vitro* efficacy studies and biological response, which are important for investigating GaM's therapeutic

efficacy on bone cancer therapy, leaving important gaps in its potential clinical applicability [117].

Overall, Ga-BGs provide a versatile and highly promising approach for biomedical applications. Their distinctive combination of bioactivity, antibacterial properties, and antineoplastic features makes them an advantageous material for future developments in orthopaedic implants, bone cancer treatments, and infection control strategies. The multifunctional role of Ga ions in altering the structure of the glass and impacting biological responses emphasises their capacity to tackle multiple clinical challenges, further positioning Ga-BGs as a cutting-edge approach in biomaterial research.

Table 1.3. Applications of Gallium-Doped Bioactive Glasses with Preclinical Findings.

Application Area	Glass Composition	Preclinical Findings	Key Outcomes	Ref
Bone Regeneration and Vascularisation	SiO_2–CaO glasses with 2–4 mol% Ga_2O_3	Improved osteoblast cell attachment, increased mitochondrial activity, and enhanced cell viability. Increased secretion of Vascular Endothelial Growth Factor (VEGF), promoting angiogenesis.	Gallium promotes osteoblast proliferation and supports bone regeneration. Ga enhances vascularization, supporting faster tissue healing.	[109]
Antibacterial Properties	SiO_2–CaO–ZnO glasses with 3 wt% Ga_2O_3	Significant inhibition of *E. coli* and *S. aureus*. Antibacterial efficiency increased with higher Ga_2O_3 concentration.	Ga ions mimic Fe^{3+}, disrupting bacterial metabolism and inhibiting growth.	[118]
Cancer Treatment	SiO_2–CaO–Na_2O–ZnO–Ga_2O_3 glasses in CMC-Dex hydrogel composites	Reduced viability of MG-63 cells to 69% after 30 days of exposure	Ga disrupts cancer cell iron metabolism, selectively targeting tumour cells.	[119]
OS Treatment	45S5 BG rods with up to 3 mol% Ga_2O_3	Viability of Saos-2 OS cells reduced to **50%** after 72 hours.	Ga-containing glasses significantly reduce cancer cell growth.	[110]
Cardiac Tissue Engineering	SiO_2–CaO–P_2O_5–CaO–Al_2O_3 glasses with 18 mol% Ga_2O_3 in alginate hydrogel	Enhanced compressive strength (4× higher than standard requirements) and prolonged working time for material application.	Ga addition improves mechanical strength and material handling in cardiac tissue engineering.	[120]
Antifungal Properties	SiO_2–Na_2O–CaO–ZnO–Ga_2O_3 glasses in hydrogel composites	Strong inhibitory effect against *Candida albicans* in broth dilution and agar disc diffusion tests.	Ga-BG hydrogels exhibited enhanced antifungal activity in direct contact.	[111]
Implantable Device Coating	Ga-modified polylactic acid (PLA) films with Defensin (De) coating	Significant reduction in *Acinetobacter baumannii* biofilm formation and decreased inflammation via reduced IL-1β release.	Ga-coated surfaces effectively prevent biofilm formation and reduce inflammatory response.	[121]

1.12 Research objectives and thesis structure

1.12.1 Research Objectives

This research aims to investigate the potential of gallium-doped bioactive glasses as multifunctional materials for bone cancer treatment, with a focus on their structural, mechanical, antibacterial, and anticancer properties. The following specific objectives have been established to achieve this aim:

1. To fabricate gallium-doped bioactive glasses with varying Ga_2O_3 concentrations using a melt-quenching method.
2. To characterise the physicochemical properties, ion release profile and chemical stability of the synthesised glasses using techniques such as fourier-transform infrared spectroscopy (FTIR), scanning electron microscopy (SEM), inductively coupled plasma (ICP) analysis, and energy dispersive X-ray spectroscopy (EDS).
3. To investigate the cytotoxic effects of Ga-doped bioactive glasses on OS cells and their biocompatibility with normal osteoblast cells.
4. To evaluate the efficacy of Ga-BG on a broader range of OS cells, as well as human mesenchymal stem cells, and to investigate the mechanism of Ga-induced toxicity in OS cells using gene expression analysis and cellular apoptosis studies.
5. To assess the antibacterial properties of Ga-doped bioactive glasses against *Escherichia coli* (E. coli) and *Staphylococcus aureus* (S. aureus) to investigate their potential for infection control.

This research aims to provide insights into the potential of Ga-doped bioactive glasses as multifunctional materials for bone cancer treatment, ultimately aiming to improve clinical outcomes in orthopaedic and oncological applications.

1.12.2 Thesis Structure

This thesis is structured into six chapters, each addressing specific research objectives and experimental approaches. The organisation is designed to systematically present the research progression, from material fabrication and characterisation to biological evaluation and therapeutic potential.

Chapter 1: Introduction

This chapter introduces the background, context, and significance of the study. It outlines the clinical challenges associated with bone cancer treatment and the potential of gallium-doped bioactive glasses (Ga-BGs) as multifunctional biomaterials. The research aims, objectives and overall thesis structure are presented to guide the reader through the following chapters.

Chapter 2: Fabrication and Characterisation of Gallium-Doped Bioactive Glasses

This chapter details the fabrication of Ga-doped bioactive glasses with varying Ga_2O_3 concentrations using the melt-quenching method. The methodology for preparing glass compositions with precise Ga_2O_3 content is described, including material preparation, melting conditions, and quenching procedures. Characterisation techniques such as FTIR, SEM, ICP, and EDS are employed to assess the physicochemical properties, ion release profile, and chemical stability of the synthesised glasses. This chapter aims to provide a comprehensive understanding of the materials' structure and stability in simulated physiological environments.

Chapter 3: Cytotoxicity and Biocompatibility of Gallium-Doped Bioactive Glasses

This chapter investigates the cytotoxic effects of Ga-doped bioactive glasses on OS cells and evaluates their biocompatibility with normal osteoblast cells. The experimental design includes cell culture conditions, MTT viability assays, live/dead staining, and scratch wound assays. The results aim to evaluate Ga-BG toxicity in cancer cells while ensuring minimal adverse effects on healthy bone cells.

Chapter 4: Mechanistic Studies of Ga-BG-Induced Cytotoxicity

This chapter extends the investigation by evaluating Ga-BG efficacy on a broader range of OS cells and human mesenchymal stem cells. The experimental design includes gene expression

analysis and apoptosis studies to explore the underlying mechanisms of Ga-induced cytotoxicity. This chapter aims to provide mechanistic insights into how Ga ions affect cancer cell survival and proliferation, further validating Ga-BGs as potential therapeutic agents.

Chapter 5: Antibacterial Properties of Gallium-Doped Bioactive Glasses

This chapter examines the antibacterial potential of Ga-doped bioactive glasses by evaluating their efficacy against common pathogens such as *Escherichia coli* (E. coli) and *Staphylococcus aureus* (S. aureus). Antibacterial testing methods include viability assays, time-kill assays, and bacterial live/dead staining. The findings from this chapter aim to determine Ga-BG's potential in reducing implant-related infections and enhancing clinical outcomes in orthopaedic treatments.

Chapter 6: Conclusion and Future Work

The final chapter provides a summary of key findings from the study and evaluates the extent to which the research objectives have been achieved. The clinical implications of Ga-doped bioactive glasses are discussed, along with recommendations for future research to address remaining knowledge gaps and expand the potential applications of Ga-BG materials in bone cancer treatment and infection control.

1.13 References

[1] P. A. Meyers and R. Gorlick, "OSTEOSARCOMA," *Pediatr Clin North Am*, vol. 44, no. 4, pp. 973–989, Aug. 1997, doi: 10.1016/S0031-3955(05)70540-X.

[2] A. Abarrategi *et al.*, "Osteosarcoma: Cells-of-Origin, Cancer stem cells, and targeted therapies," 2016, *Hindawi Limited*. doi: 10.1155/2016/3631764.

[3] E. Kobayashi *et al.*, "Reduced argininosuccinate synthetase is a predictive biomarker for the development of pulmonary metastasis in patients with osteosarcoma," *Mol Cancer Ther*, vol. 9, no. 3, pp. 535–544, Mar. 2010, doi: 10.1158/1535-7163.MCT-09-0774.

[4] K. Ando, M. F. Heymann, V. Stresing, K. Mori, F. Rédini, and D. Heymann, "Current therapeutic strategies and novel approaches in osteosarcoma," Jun. 2013. doi: 10.3390/cancers5020591.

[5] L. Tattersall, D. C. Gagui, V. L. Tippett, N. B. Ab Latif, K. M. Shah, and A. Gartland, "A Systematic Review of the Expression, Signalling and Function of P2 Receptors in Primary Bone Cancer," Apr. 01, 2022, *Bioscience Research Institute*. doi: 10.31083/j.fbl2704122.

[6] J. S. Wunder *et al.*, "TP53 mutations and outcome in osteosarcoma: A prospective, multicenter study," *Journal of Clinical Oncology*, vol. 23, no. 7, pp. 1483–1490, 2005, doi: 10.1200/JCO.2005.04.074.

[7] R. A. Weinberg, "The Retinoblastoma Protein and Cell Cycle Control Review," 1995.

[8] D. M. Thomas *et al.*, "The Retinoblastoma Protein Acts as a Transcriptional Coactivator Required for Osteogenic Differentiation," *Mol Cell*, vol. 8, no. 2, pp. 303–316, Aug. 2001, doi: 10.1016/S1097-2765(01)00327-6.

[9] L. Tattersall and U. Kingdom, "Osteosarcoma," pp. 1–17, 2019, doi: 10.1016/B978-0-12-801238-3.62259-6.

[10] B. A. Lindsey, J. E. Markel, and E. S. Kleinerman, "Osteosarcoma Overview," *Rheumatol Ther*, vol. 4, no. 1, pp. 25–43, 2017, doi: 10.1007/s40744-016-0050-2.

[11] H. Ma *et al.*, "Localized Co-delivery of Doxorubicin, Cisplatin, and Methotrexate by Thermosensitive Hydrogels for Enhanced Osteosarcoma Treatment," *ACS Appl Mater Interfaces*, vol. 7, no. 49, pp. 27040–27048, 2015, doi: 10.1021/acsami.5b09112.

[12] P. F. M. Choong, M. L. Broadhead, J. C. M. Clark, D. E. Myers, and C. R. Dass, "The molecular pathogenesis of osteosarcoma: A review," *Sarcoma*, vol. 2011, 2011, doi: 10.1155/2011/959248.

[13] C. Gerrand *et al.*, "UK guidelines for the management of bone sarcomas," *Clin Sarcoma Res*, vol. 6, no. 1, p. 7, Dec. 2016, doi: 10.1186/s13569-016-0047-1.

[14] A. M. Florea and D. Büsselberg, "Cisplatin as an anti-tumor drug: Cellular mechanisms of activity, drug resistance and induced side effects," Mar. 2011. doi: 10.3390/cancers3011351.

[15] D. P. M. Hughes, "How the NOTCH Pathway Contributes to the Ability of Osteosarcoma Cells to Metastasize," 2009, pp. 479–496. doi: 10.1007/978-1-4419-0284-9_28.

[16] S. S. Bielack *et al.*, "Second and Subsequent Recurrences of Osteosarcoma: Presentation, Treatment, and Outcomes of 249 Consecutive Cooperative

Osteosarcoma Study Group Patients," *Journal of Clinical Oncology*, vol. 27, no. 4, pp. 557–565, Feb. 2009, doi: 10.1200/JCO.2008.16.2305.

[17] Z. Nie and H. Peng, "Osteosarcoma in patients below 25 years of age: An observational study of incidence, metastasis, treatment and outcomes," *Oncol Lett*, vol. 16, no. 5, pp. 6502–6514, Nov. 2018, doi: 10.3892/ol.2018.9453.

[18] R. Sullivan *et al.*, "The Lancet Oncology Commission Global cancer surgery: delivering safe, aff ordable, and timely cancer surgery," 2015. [Online]. Available: http://www.socialstyrelsen.se

[19] H. T. Ta, C. R. Dass, P. F. M. Choong, and D. E. Dunstan, "Osteosarcoma treatment: state of the art," *Cancer and Metastasis Reviews*, vol. 28, no. 1–2, pp. 247–263, Jun. 2009, doi: 10.1007/s10555-009-9186-7.

[20] B. R. Eaton *et al.*, "Osteosarcoma," *Pediatr Blood Cancer*, vol. 68, no. S2, May 2021, doi: 10.1002/pbc.28352.

[21] N. Zhu, H. Ni, S. Guo, Y. Q. Shen, and Q. Chen, "Bone complications of cancer treatment," *Cancer Treat Rev*, vol. 130, p. 102828, Nov. 2024, doi: 10.1016/J.CTRV.2024.102828.

[22] M. Barbosa-Azevedo, A. Dias-Carvalho, F. Carvalho, and V. M. Costa, "Chemotherapy-induced cognitive impairment and glia: A new take on chemobrain?," *Toxicol Appl Pharmacol*, vol. 492, p. 117085, Nov. 2024, doi: 10.1016/J.TAAP.2024.117085.

[23] T. A. Greenhalgh and R. P. Symonds, "Principles of chemotherapy and radiotherapy," *Obstet Gynaecol Reprod Med*, vol. 24, no. 9, pp. 259–265, Sep. 2014, doi: 10.1016/J.OGRM.2014.06.004.

[24] B. A. Chabner and T. G. Roberts, "Chemotherapy and the war on cancer," *Nat Rev Cancer*, vol. 5, no. 1, pp. 65–72, Jan. 2005, doi: 10.1038/nrc1529.

[25] C. R. Chitambar, "Medical applications and toxicities of gallium compounds," *Int J Environ Res Public Health*, vol. 7, no. 5, pp. 2337–2361, 2010, doi: 10.3390/ijerph7052337.

[26] J. Ma and D. J. Waxman, "Combination of antiangiogenesis with chemotherapy for more effective cancer treatment," *Mol Cancer Ther*, vol. 7, no. 12, pp. 3670–3684, Dec. 2008, doi: 10.1158/1535-7163.MCT-08-0715.

[27] R. Schwarz, O. Bruland, A. Cassoni, P. Schomberg, and S. Bielack, "The Role of Radiotherapy in Oseosarcoma," 2009, pp. 147–164. doi: 10.1007/978-1-4419-0284-9_7.

[28] M. Baumann *et al.*, "Radiation oncology in the era of precision medicine," *Nat Rev Cancer*, vol. 16, no. 4, pp. 234–249, Apr. 2016, doi: 10.1038/nrc.2016.18.

[29] J. R. Jones, "Review of bioactive glass: From Hench to hybrids," *Acta Biomater*, vol. 9, no. 1, pp. 4457–4486, Jan. 2013, doi: 10.1016/J.ACTBIO.2012.08.023.

[30] M. Montazerian and E. D. Zanotto, "Bioactive and inert dental glass-ceramics," *J Biomed Mater Res A*, vol. 105, no. 2, pp. 619–639, Feb. 2017, doi: 10.1002/jbm.a.35923.

[31] M. Vallet-Regí, Ed., *Bio-Ceramics with Clinical Applications*. Wiley, 2014. doi: 10.1002/9781118406748.

[32] S. K. Nandi, A. Mahato, B. Kundu, and P. Mukherjee, "Doped Bioactive Glass Materials in Bone Regeneration," in *Advanced Techniques in Bone Regeneration*, InTech, 2016. doi: 10.5772/63266.

[33] J. Jones and Alexis Clare, *Bio-glasses: an introduction.* John Wiley & Sons, 2012.

[34] W. H. Zachariasbn, “THE ATOMIC ARRANGEMENT IN GLASS,” 1932. [Online]. Available: https://pubs.acs.org/sharingguidelines

[35] L. L. Hench and J. R. Jones, “Bioactive Glasses: Frontiers and Challenges,” *Front Bioeng Biotechnol*, vol. 3, p. 194, Nov. 2015, doi: 10.3389/fbioe.2015.00194.

[36] H. Larry L and P. Julia M, “Third-generation biomedical materials,” *Science (1979)*, vol. 295, no. February, pp. 1014–1017, 2002.

[37] J. R. Jones, “Reprint of: Review of bioactive glass: From Hench to hybrids,” *Acta Biomater*, vol. 23, no. S, pp. S53–S82, 2015, doi: 10.1016/j.actbio.2015.07.019.

[38] C. Calahoo and L. Wondraczek, “Ionic glasses: Structure, properties and classification,” *Journal of Non-Crystalline Solids: X*, vol. 8, p. 100054, Dec. 2020, doi: 10.1016/J.NOCX.2020.100054.

[39] H. R. Fernandes, A. Gaddam, A. Rebelo, D. Brazete, G. E. Stan, and J. M. F. Ferreira, “Bioactive Glasses and Glass-Ceramics for Healthcare Applications in Bone Regeneration and Tissue Engineering,” *Materials*, vol. 11, no. 12, p. 2530, Dec. 2018, doi: 10.3390/ma11122530.

[40] J. R. Jones, E. Gentleman, and J. Polak, “Bioactive Glass Scaffolds for Bone Regeneration,” *Elements*, vol. 3, no. 6, pp. 393–399, Dec. 2007, doi: 10.2113/GSELEMENTS.3.6.393.

[41] L. L. Hench, “Bioceramics,” *Journal of the American Ceramic Society*, vol. 81, no. 7, pp. 1705–1728, 1998, doi: 10.1111/j.1151-2916.1998.tb02540.x.

[42] R. D. Aspasio, R. Borges, and J. Marchi, “Biocompatible Glasses for Cancer Treatment,” 2016, pp. 249–265. doi: 10.1007/978-3-319-44249-5_10.

[43] D. M. SANDERS and L. L. HENCH, “Mechanisms of Glass Corrosion,” *Journal of the American Ceramic Society*, vol. 56, no. 7, pp. 373–377, Jul. 1973, doi: 10.1111/j.1151-2916.1973.tb12689.x.

[44] J. R. Jones and I. R. Gibson, “1.3.4 - Ceramics, Glasses, and Glass-Ceramics: Basic Principles,” in *Biomaterials Science (Fourth Edition)*, Fourth Edi., W. R. Wagner, S. E. Sakiyama-Elbert, G. Zhang, and M. J. Yaszemski, Eds., Academic Press, 2020, pp. 289–305. doi: https://doi.org/10.1016/B978-0-12-816137-1.00022-2.

[45] J. R. Jones, P. Sepulveda, and L. L. Hench, “Dose-dependent behavior of bioactive glass dissolution,” *J Biomed Mater Res*, vol. 58, no. 6, pp. 720–726, 2001, doi: 10.1002/jbm.10053.

[46] “The story of Bioglass.pdf.”

[47] J. Wilson and S. B. Low, “Bioactive ceramics for periodontal treatment: Comparative studies in the patus monkey,” *Journal of Applied Biomaterials*, vol. 3, no. 2, pp. 123–129, Jun. 1992, doi: 10.1002/jab.770030208.

[48] C. Vitale-Brovarone, E. Vernè, M. Bosetti, P. Appendino, and M. Cannas, “Microstructural and in vitro characterization of SiO2-Na2O-CaO-MgO glass-ceramic bioactive scaffolds for bone substitutes,” *J Mater Sci Mater Med*, vol. 16, no. 10, pp. 909–917, Oct. 2005, doi: 10.1007/s10856-005-4425-0.

[49] J. E. Gough, J. R. Jones, and L. L. Hench, “Nodule formation and mineralisation of human primary osteoblasts cultured on a porous bioactive glass scaffold,” *Biomaterials*, vol. 25, no. 11, pp. 2039–2046, May 2004, doi: 10.1016/J.BIOMATERIALS.2003.07.001.

[50] E. A. B. E. Kaufmann, P. Ducheyne, and I. M. Shapiro, “Effect of varying physical properties of porous, surface modified bioactive glass 45S5 on osteoblast proliferation and maturation,” *J Biomed Mater Res*, vol. 52, no. 4, pp. 783–796, Dec. 2000, doi: 10.1002/1097-4636(20001215)52:4<783::AID-JBM24>3.0.CO;2-J.

[51] I. D. Xynos, A. J. Edgar, L. D. K. Buttery, L. L. Hench, and J. M. Polak, “Gene-expression profiling of human osteoblasts following treatment with the ionic products of Bioglass® 45S5 dissolution,” *J Biomed Mater Res*, vol. 55, no. 2, pp. 151–157, 2001, doi: 10.1002/1097-4636(200105)55:2<151::AID-JBM1001>3.0.CO;2-D.

[52] I. A. Silver, J. Deas, and M. Erecińska, “Interactions of bioactive glasses with osteoblasts in vitro: effects of 45S5 Bioglass®, and 58S and 77S bioactive glasses on metabolism, intracellular ion concentrations and cell viability,” *Biomaterials*, vol. 22, no. 2, pp. 175–185, Jan. 2001, doi: 10.1016/S0142-9612(00)00173-3.

[53] L. L. Hench, “Genetic design of bioactive glass,” *J Eur Ceram Soc*, vol. 29, no. 7, pp. 1257–1265, 2009, doi: 10.1016/j.jeurceramsoc.2008.08.002.

[54] L. L. Hench, J. M. Polak, I. D. Xynos, and L. D. K. Buttery, “Bioactive materials to control cell cycle,” *Materials Research Innovations*, vol. 3, no. 6, pp. 313–323, 2000, doi: 10.1007/s100190000055.

[55] A. L. B. Maçon *et al.*, “A unified in vitro evaluation for apatite-forming ability of bioactive glasses and their variants,” *J Mater Sci Mater Med*, vol. 26, no. 2, pp. 1–10, 2015, doi: 10.1007/s10856-015-5403-9.

[56] E. M. Valliant and J. R. Jones, “Softening bioactive glass for bone regeneration: Sol-gel hybrid materials,” *Soft Matter*, vol. 7, no. 11, pp. 5083–5095, 2011, doi: 10.1039/c0sm01348j.

[57] L. L. Hench and J. K. West, “The sol-gel process,” *Chem Rev*, vol. 90, no. 1, pp. 33–72, Jan. 1990, doi: 10.1021/cr00099a003.

[58] J. R. Jones, D. S. Brauer, L. Hupa, and D. C. Greenspan, “Bioglass and Bioactive Glasses and Their Impact on Healthcare,” *Int J Appl Glass Sci*, vol. 7, no. 4, pp. 423–434, 2016, doi: 10.1111/ijag.12252.

[59] N. C. Lindfors, I. Koski, J. T. Heikkilä, K. Mattila, and A. J. Aho, “A prospective randomized 14-year follow-up study of bioactive glass and autogenous bone as bone graft substitutes in benign bone tumors,” *J Biomed Mater Res B Appl Biomater*, vol. 94, no. 1, pp. 157–164, 2010, doi: 10.1002/jbm.b.31636.

[60] J. S. Zamet *et al.*, “Particulate bioglass® as a grafting material in the treatment of periodontal intrabony defects,” *J Clin Periodontol*, vol. 24, no. 6, pp. 410–418, Jun. 1997, doi: 10.1111/j.1600-051X.1997.tb00205.x.

[61] L. Aalto-Setälä, M. Siekkinen, N. Lindfors, and L. Hupa, “Dissolution of Glass–Ceramic Scaffolds of Bioactive Glasses 45S5 and S53P4,” *Biomedical Materials and Devices*, vol. 1, no. 2, pp. 871–881, 2023, doi: 10.1007/s44174-022-00059-4.

[62] Z. Jin, D. R. Neuville, and D. S. Brauer, “Glasses for bone regeneration: structural features controlling physical properties and ion release of bioactive glasses 45S5, S53P4 and 13-93,” *RSC Adv*, vol. 15, no. 7, pp. 4997–5006, 2025, doi: 10.1039/d4ra06081d.

[63] Huang X, Li R, Feng Y, and Wang Y, “Remineralization of demineralized dentin induced by bioactive glass NovaMin.,” *Journal of Central South University. Medical Sciences.*, vol. 43, no. 6, pp. 619–24, Jun. 2018.

[64] J. M. Gomez-Vega, E. Saiz, A. P. Tomsia, G. W. Marshall, and S. J. Marshall, "Bioactive glass coatings with hydroxyapatite and Bioglass® particles on Ti-based implants. 1. Processing," *Biomaterials*, vol. 21, no. 2, pp. 105–111, Jan. 2000, doi: 10.1016/S0142-9612(99)00131-3.

[65] N. Moritz *et al.*, "Implants coated with bioactive glass by CO_2-laser, an in vivo study," *J Mater Sci Mater Med*, vol. 15, no. 7, pp. 795–802, Jul. 2004, doi: 10.1023/B:JMSM.0000032820.50983.c1.

[66] P. Jaiswal, "The Use of Ceramics in Total Hip Arthroplasty," *Orthopedics and Rheumatology Open Access Journal*, vol. 4, no. 3, Jan. 2017, doi: 10.19080/OROAJ.2017.04.555636.

[67] B. J. McEntire, B. S. Bal, M. N. Rahaman, J. Chevalier, and G. Pezzotti, "Ceramics and ceramic coatings in orthopaedics," *J Eur Ceram Soc*, vol. 35, no. 16, pp. 4327–4369, Dec. 2015, doi: 10.1016/J.JEURCERAMSOC.2015.07.034.

[68] M. S. Nickoli and W. K. Hsu, "Ceramic-Based Bone Grafts as a Bone Grafts Extender for Lumbar Spine Arthrodesis: A Systematic Review," *Global Spine J*, vol. 4, no. 3, pp. 211–216, Aug. 2014, doi: 10.1055/s-0034-1378141.

[69] E. Mohseni, E. Zalnezhad, and A. R. Bushroa, "Comparative investigation on the adhesion of hydroxyapatite coating on Ti–6Al–4V implant: A review paper," *Int J Adhes Adhes*, vol. 48, pp. 238–257, Jan. 2014, doi: 10.1016/J.IJADHADH.2013.09.030.

[70] G. Dearnaley and J. H. Arps, "Biomedical applications of diamond-like carbon (DLC) coatings: A review," *Surf Coat Technol*, vol. 200, no. 7, pp. 2518–2524, Dec. 2005, doi: 10.1016/J.SURFCOAT.2005.07.077.

[71] B. J. McEntire, B. S. Bal, M. N. Rahaman, J. Chevalier, and G. Pezzotti, "Ceramics and ceramic coatings in orthopaedics," *J Eur Ceram Soc*, vol. 35, no. 16, pp. 4327–4369, Dec. 2015, doi: 10.1016/J.JEURCERAMSOC.2015.07.034.

[72] Abbasi Za, Bahrololoom ME, Shariat MH, and Bagheri R, "Bioactive Glasses in Dentistry: A Review," *J Dent Biomater*, vol. 2, no. 1, pp. 1–9, Jan. 2015.

[73] N. Shadjou and M. Hasanzadeh, "Graphene and its nanostructure derivatives for use in bone tissue engineering: Recent advances," *J Biomed Mater Res A*, vol. 104, no. 5, pp. 1250–1275, May 2016, doi: 10.1002/jbm.a.35645.

[74] S. Utneja, R. R. Nawal, S. Talwar, and M. Verma, "Current perspectives of bio-ceramic technology in endodontics: calcium enriched mixture cement - review of its composition, properties and applications," *Restor Dent Endod*, vol. 40, no. 1, p. 1, 2015, doi: 10.5395/rde.2015.40.1.1.

[75] R. Hegde and J. Thakkar, "Comparative evaluation of the effects of casein phosphopeptide-amorphous calcium phosphate (CPP-ACP) and xylitol-containing chewing gum on salivary flow rate, pH and buffering capacity in children: An in vivo study," *Journal of Indian Society of Pedodontics and Preventive Dentistry*, vol. 35, no. 4, p. 332, 2017, doi: 10.4103/JISPPD.JISPPD_147_17.

[76] S. Najeeb *et al.*, "Modifications in Glass Ionomer Cements: Nano-Sized Fillers and Bioactive Nanoceramics," *Int J Mol Sci*, vol. 17, no. 7, p. 1134, Jul. 2016, doi: 10.3390/ijms17071134.

[77] Z. Özkurt and E. Kazazoğlu, "Zirconia Dental Implants: A Literature Review," *Journal of Oral Implantology*, vol. 37, no. 3, pp. 367–376, Jun. 2011, doi: 10.1563/AAID-JOI-D-09-00079.

[78] F. Baino and I. Potestio, “Orbital implants: State-of-the-art review with emphasis on biomaterials and recent advances,” *Materials Science and Engineering: C*, vol. 69, pp. 1410–1428, Dec. 2016, doi: 10.1016/J.MSEC.2016.08.003.

[79] D. R. Jordan and S. R. Klapper, “Controversies in Enucleation Technique and Implant Selection: Whether to Wrap, Attach Muscles, and Peg?,” 2010, pp. 195–209. doi: 10.1007/978-3-540-85542-2_14.

[80] C. T. Catalu, S. L. Istrate, L. M. Voinea, C. Mitulescu, V. Popescu, and C. Radu, “Ocular implants-methods of ocular reconstruction following radical surgical interventions.,” *Rom J Ophthalmol*, vol. 62, no. 1, pp. 15–23, 2018.

[81] “Study Details | Comparison of Bioactive Glass and Beta-Tricalcium Phosphate as Bone Graft Substitute | ClinicalTrials.gov.” Accessed: Mar. 22, 2025. [Online]. Available: https://clinicaltrials.gov/study/NCT00841152

[82] N. C. Lindfors, I. Koski, J. T. Heikkilä, K. Mattila, and A. J. Aho, “A prospective randomized 14-year follow-up study of bioactive glass and autogenous bone as bone graft substitutes in benign bone tumors,” *J Biomed Mater Res B Appl Biomater*, vol. 94B, no. 1, pp. 157–164, Jul. 2010, doi: 10.1002/jbm.b.31636.

[83] “Study Details | Complete Twelve Month Bone Remodeling With a Bi-phasic Injectable Bone Substitute in Benign Bone Tumors | ClinicalTrials.gov.” Accessed: Mar. 22, 2025. [Online]. Available: https://clinicaltrials.gov/study/NCT02567084

[84] R. P. Warrell, R. S. Bockman, C. J. Coonley, M. Isaacs, and H. Staszewski, “Gallium nitrate inhibits calcium resorption from bone and is effective treatment for cancer-related hypercalcemia.,” *Journal of Clinical Investigation*, vol. 73, no. 5, pp. 1487–1490, May 1984, doi: 10.1172/JCI111353.

[85] R. J. Martens, N. A. Miller, N. D. Cohen, J. R. Harrington, and L. R. Bernstein, “Chemoprophylactic Antimicrobial Activity of Gallium Maltolate against Intracellular Rhodococcus equi,” *J Equine Vet Sci*, vol. 27, no. 8, pp. 341–345, Aug. 2007, doi: 10.1016/J.JEVS.2007.06.007.

[86] D. M. Pickup *et al.*, “Structural characterization by x-ray methods of novel antimicrobial gallium-doped phosphate-based glasses,” *J Chem Phys*, vol. 130, no. 6, Feb. 2009, doi: 10.1063/1.3076057.

[87] C. R. Chitambar, “Gallium and its competing roles with iron in biological systems,” *Biochimica et Biophysica Acta (BBA) - Molecular Cell Research*, vol. 1863, no. 8, pp. 2044–2053, Aug. 2016, doi: 10.1016/J.BBAMCR.2016.04.027.

[88] M. M. Hart and R. H. Adamson, “Antitumor Activity and Toxicity of Salts of Inorganic Group IIIa Metals: Aluminum, Gallium, Indium, and Thallium,” *Proceedings of the National Academy of Sciences*, vol. 68, no. 7, pp. 1623–1626, Jul. 1971, doi: 10.1073/pnas.68.7.1623.

[89] C. R. Chitambar, “Gallium-containing anticancer compounds,” *Future Med Chem*, vol. 4, no. 10, pp. 1257–1272, 2012, doi: 10.4155/fmc.12.69.

[90] C. R. Chitambar, “The therapeutic potential of iron-targeting gallium compounds in human disease: From basic research to clinical application,” *Pharmacol Res*, vol. 115, pp. 56–64, 2017, doi: 10.1016/j.phrs.2016.11.009.

[91] P. Collery, B. Keppler, C. Madoulet, and B. Desoize, “Gallium in cancer treatment,” *Crit Rev Oncol Hematol*, vol. 42, no. 3, pp. 283–296, 2002, doi: 10.1016/S1040-8428(01)00225-6.

[92] E. Zeimaran *et al.*, "Fabrication and characterization of poly(octanediol citrate)/gallium-containing bioglass microcomposite scaffolds," *J Mater Sci*, vol. 50, no. 5, pp. 2189–2201, 2015, doi: 10.1007/s10853-014-8782-2.

[93] R. S. Bockman, A. L. Boskey, N. C. Blumenthal, N. W. Alcock, and R. P. Warrell, "Gallium increases bone calcium and crystallite perfection of hydroxyapatite," *Calcif Tissue Int*, vol. 39, no. 6, pp. 376–381, Nov. 1986, doi: 10.1007/BF02555174.

[94] C. R. Chitambar, W. G. Matthaeus, W. E. Antholine, K. Graff, and W. J. O'Brien, "Inhibition of Leukemic HL60 Cell Growth by Transferrin-Gallium: Effects on Ribonucleotide Reductase and Demonstration of Drug Synergy With Hydroxyurea," *Blood*, vol. 72, no. 6, pp. 1930–1936, Dec. 1988, doi: 10.1182/BLOOD.V72.6.1930.1930.

[95] J. Narasimhan, W. E. Antholine, and C. R. Chitambar, "Effect of gallium on the tyrosyl radical of the iron-dependent M2 subunit of ribonucleotide reductase," *Biochem Pharmacol*, vol. 44, no. 12, pp. 2403–2408, Dec. 1992, doi: 10.1016/0006-2952(92)90686-D.

[96] C. R. Chitambar, "The therapeutic potential of iron-targeting gallium compounds in human disease: From basic research to clinical application," *Pharmacol Res*, vol. 115, pp. 56–64, 2017, doi: 10.1016/j.phrs.2016.11.009.

[97] C. R. Chitambar *et al.*, "Gallium maltolate disrupts tumor iron metabolism and retards the growth of glioblastoma by inhibiting mitochondrial function and ribonucleotide reductase," *Mol Cancer Ther*, vol. 17, no. 6, pp. 1240–1250, 2018, doi: 10.1158/1535-7163.MCT-17-1009.

[98] C. R. Chitambar, D. P. Purpi, J. Woodliff, M. Yang, and J. P. Wereley, "Development of gallium compounds for treatment of lymphoma: Gallium maltolate, a novel hydroxypyrone gallium compound, induces apoptosis and circumvents lymphoma cell resistance to gallium nitrate," *Journal of Pharmacology and Experimental Therapeutics*, vol. 322, no. 3, pp. 1228–1236, 2007, doi: 10.1124/jpet.107.126342.

[99] L. Todorov, I. Kostova, and M. Traykova, "Lanthanum, Gallium and their Impact on Oxidative Stress," *Curr Med Chem*, vol. 26, no. 22, pp. 4280–4295, Sep. 2019, doi: 10.2174/0929867326666190104165311.

[100] C. R. Chitambar, "Gallium and its competing roles with iron in biological systems," *Biochim Biophys Acta Mol Cell Res*, vol. 1863, no. 8, pp. 2044–2053, 2016, doi: 10.1016/j.bbamcr.2016.04.027.

[101] F. Minandri, C. Bonchi, E. Frangipani, F. Imperi, and P. Visca, "Promises and failures of gallium as an antibacterial agent," 2014, *Future Medicine Ltd.* doi: 10.2217/fmb.14.3.

[102] S. Hijazi, D. Visaggio, M. Pirolo, E. Frangipani, L. Bernstein, and P. Visca, "Antimicrobial activity of gallium compounds on ESKAPE pathogens," *Front Cell Infect Microbiol*, vol. 8, no. SEP, Sep. 2018, doi: 10.3389/fcimb.2018.00316.

[103] I. Strazic-Geljic *et al.*, "Gallium, a promising candidate to disrupt the vicious cycle driving osteolytic metastases," *Biochem Pharmacol*, vol. 116, pp. 11–21, Sep. 2016, doi: 10.1016/J.BCP.2016.06.020.

[104] "Study Details | Phase II Gallium Nitrate in Relapsed or Refractory Non-Hodgkin's Lymphoma | ClinicalTrials.gov." Accessed: Mar. 17, 2025. [Online]. Available: https://clinicaltrials.gov/study/NCT00054808?cond=Lymphoma,Non-Hodgkin&intr=Gallium%20nitrate&rank=1

[105] L. R. Bernstein, J. J.M. van der Hoeven, and R. O. Boer, “Hepatocellular Carcinoma Detection by Gallium Scan and Subsequent Treatment by Gallium Maltolate: Rationale and Case Study,” *Anticancer Agents Med Chem*, vol. 11, no. 6, pp. 585–590, Jul. 2011, doi: 10.2174/187152011796011046.

[106] “Study Details | Expanded Access to Gallium Maltolate (GaM) | ClinicalTrials.gov.” Accessed: Mar. 17, 2025. [Online]. Available: https://clinicaltrials.gov/study/NCT06404034?cond=cancer&intr=Gallium%20Maltolate&rank=2

[107] C. Dittrich *et al.*, “Phase I and pharmacokinetic study of the oral tris-(8-quinolinolato)gallium(III) complex (FFC11, KP46) in patients with solid tumors - a study of the CESAR Central European Society for Anticancer Drug Research - EWIV,” *Journal of Clinical Oncology*, vol. 23, no. 16_suppl, pp. 3205–3205, Jun. 2005, doi: 10.1200/jco.2005.23.16_suppl.3205.

[108] A. Wajda, W. H. Goldmann, R. Detsch, A. Grünewald, A. R. Boccaccini, and M. Sitarz, “Structural characterization and evaluation of antibacterial and angiogenic potential of gallium-containing melt-derived and gel-derived glasses from CaO-SiO2 system,” *Ceram Int*, vol. 44, no. 18, pp. 22698–22709, Dec. 2018, doi: 10.1016/j.ceramint.2018.09.051.

[109] A. Wajda, W. H. Goldmann, R. Detsch, A. Grünewald, A. R. Boccaccini, and M. Sitarz, “Structural characterization and evaluation of antibacterial and angiogenic potential of gallium-containing melt-derived and gel-derived glasses from CaO-SiO2 system,” *Ceram Int*, vol. 44, no. 18, pp. 22698–22709, Dec. 2018, doi: 10.1016/j.ceramint.2018.09.051.

[110] K. S. Rana, L. P. De Souza, M. A. Isaacs, F. N. S. Raja, A. P. Morrell, and R. A. Martin, “Development and Characterization of Gallium-Doped Bioactive Glasses for Potential Bone Cancer Applications,” *ACS Biomater Sci Eng*, vol. 3, no. 12, pp. 3425–3432, 2017, doi: 10.1021/acsbiomaterials.7b00283.

[111] T. J. Keenan, L. M. Placek, M. M. Hall, and A. W. Wren, “Antibacterial and antifungal potential of Ga-bioactive glass and Ga-bioactive glass/polymeric hydrogel composites,” *J Biomed Mater Res B Appl Biomater*, vol. 105, no. 5, pp. 1102–1113, Jul. 2017, doi: 10.1002/jbm.b.33655.

[112] E. Zeimaran *et al.*, “Antibacterial properties of poly (octanediol citrate)/gallium-containing bioglass composite scaffolds,” *J Mater Sci Mater Med*, vol. 27, no. 1, p. 18, Jan. 2016, doi: 10.1007/s10856-015-5620-2.

[113] F. Kurtuldu, N. Mutlu, A. R. Boccaccini, and D. Galusek, “Gallium containing bioactive materials: A review of anticancer, antibacterial, and osteogenic properties,” *Bioact Mater*, no. December, 2022, doi: 10.1016/j.bioactmat.2021.12.034.

[114] A. Wajda, W. H. Goldmann, R. Detsch, A. Grünewald, A. R. Boccaccini, and M. Sitarz, “Structural characterization and evaluation of antibacterial and angiogenic potential of gallium-containing melt-derived and gel-derived glasses from CaO-SiO2 system,” *Ceram Int*, vol. 44, no. 18, pp. 22698–22709, Dec. 2018, doi: 10.1016/J.CERAMINT.2018.09.051.

[115] S. Phull, A. Rahimnejad Yazdi, and M. R. Towler, “A Gallium-doped cement for the treatment of bone cancers. The effect of ZnO ↔ Ga_2O_3 substitution of an ionomeric glass series on the rheological, mechanical, pH and ion-eluting properties of their

corresponding glass polyalkenoate cements," *Mater Res Express*, vol. 8, no. 6, p. 065401, Jun. 2021, doi: 10.1088/2053-1591/ac07e5.

[116] G. S. Medeiros *et al.*, "A perfect pair: Niobium- and gallium-doped ceramic biomaterial enabled by coupled synthesis method with potential application for bone regeneration and cancer-targeted therapy," *J Non Cryst Solids*, vol. 599, p. 121962, Jan. 2023, doi: 10.1016/j.jnoncrysol.2022.121962.

[117] M. Dupleichs *et al.*, "Controlled release of gallium maltolate complex from injectable phosphocalcic cements," *Mater Res Express*, vol. 9, no. 9, p. 095401, Sep. 2022, doi: 10.1088/2053-1591/ac8a3c.

[118] L. Rimondini, C. Della Valle, A. Cochis, B. Azzimonti, and R. Chiesa, "The Biofilm Formation onto Implants and Prosthetic Materials May Be Contrasted Using Gallium (3+)," *Key Eng Mater*, vol. 587, pp. 315–320, Nov. 2013, doi: 10.4028/www.scientific.net/KEM.587.315.

[119] T. J. Keenan, L. M. Placek, A. Coughlan, G. M. Bowers, M. M. Hall, and A. W. Wren, "Structural characterization and anti-cancerous potential of gallium bioactive glass/hydrogel composites," *Carbohydr Polym*, vol. 153, pp. 482–491, Nov. 2016, doi: 10.1016/j.carbpol.2016.07.100.

[120] O. M. Clarkin *et al.*, "Novel injectable gallium-based self-setting glass-alginate hydrogel composite for cardiovascular tissue engineering," *Carbohydr Polym*, vol. 217, pp. 152–159, Aug. 2019, doi: 10.1016/j.carbpol.2019.04.016.

[121] S. K. Divakarla *et al.*, "Antimicrobial and Anti-inflammatory Gallium–Defensin Surface Coatings for Implantable Devices," *ACS Appl Mater Interfaces*, vol. 14, no. 7, pp. 9685–9696, Feb. 2022, doi: 10.1021/acsami.1c19579.

[122] P. Vizureanu, M. Simona Bălțatu, A. Victor Sandu, D. Cristian Achitei, D. Doru Burduhos Nergis, and M. Cristina Perju, "New Trends in Bioactive Glasses for Bone Tissue: A Review," 2022. doi: 10.5772/intechopen.100567.

Chapter 2

Fabrication and Characterisation of Gallium-Doped Bioactive Glass and the Analysis of Dissolution Behaviour

2.1 Introduction

Silica-based bioactive glasses (BGs) are among the most widely studied biomaterials due to their ability to release therapeutic ions in a controlled manner, enabling local modulation of cellular responses and tissue regeneration [1, 2]. Their compositional flexibility allows the incorporation of trace elements such as zinc, copper, magnesium, silver, and gallium to tailor biological activity [3-5].

In silica-based glasses, silicon atoms form SiO_4 tetrahedra linked by Si–O–Si bonds, creating a stable network with low dissolution. Introducing network modifiers such as Ca^{2+}, Na^{+}, or K^{+} generates non-bridging oxygens (NBOs) that disrupt this network, increasing ion exchange, dissolution rate, and silanol group formation. This modification enhances the glass's bioactivity and enables the design of new therapeutic glass compositions [6, 7].

Gallium (Ga^{3+}) is a clinically approved metal ion with therapeutic, and diagnostic uses in cancer, infections, and bone diseases. It treats osteoporosis and cancer by inhibiting osteoclastic bone resorption without affecting osteoblasts, lowers blood calcium levels, and exhibits antibacterial properties [8, 9]. Some of the biomedical applications of gallium are demonstrated in Figure 2.1.

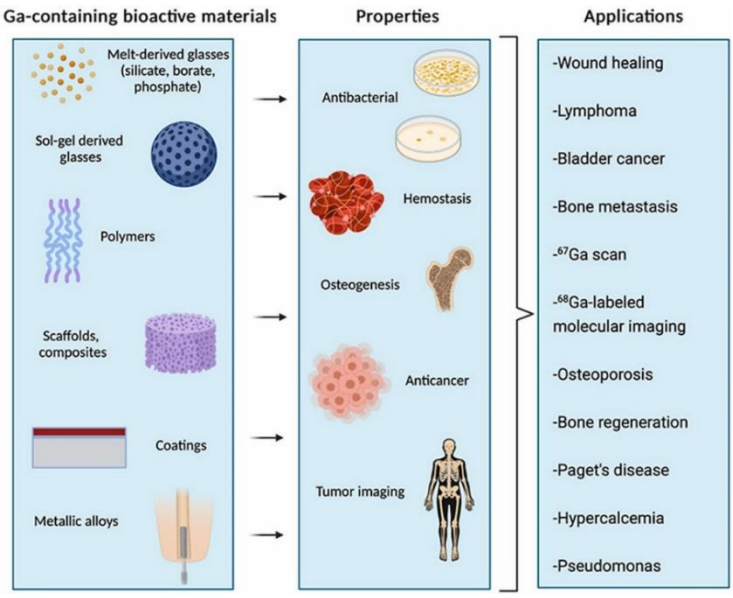

Figure 2.1. Biomedical application areas of gallium containing biomaterials (8).

In silicate glasses, Ga can act as both a network former and modifier, like Al^{3+} [10, 11]. It integrates in glass structure as tetrahedral (coordination number CN=4, GaO_4) or octahedral

(CN=6, GaO_6) structural units [12]. It functions as a glass former with high concentrations of alkali and alkali earth oxides, but it may also function as a glass modifier in glasses with high silica content. Ga ions can function as network formers at low concentrations in the silicate system, resulting in the protonation of the BO of the Si–O–Ga groups and the formation of Bronsted acidic sites (Figure 2.2). In the SiO_2-CaO system containing Ga, Tg temperature decreases as the number of Si–O covalent bonds decreases, increasing the flexibility of the glass structure. Thus, the decrease in Tg results from a "weakened" glass network [13-15].

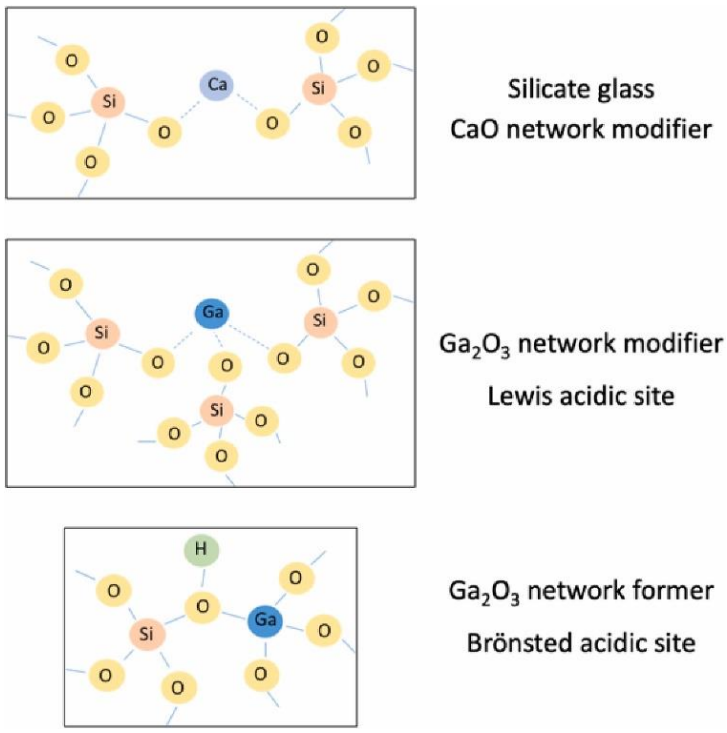

Figure 2.2. Effect of gallium in the silicate glass structure [8,9].

This chapter will discuss the manufacturing and characterisation of novel gallium-doped Bioglass-based bioactive glasses with increasing content of gallium oxide (Ga_2O_3). The fabricated glasses were studied using Fourier transform infrared (FTIR) spectroscopy, scanning electron microscopy-energy dispersive spectroscopy (SEM-EDS) and inductively coupled plasma optical emission spectrometry ICP-OES. The main purpose is to study different parameters linked to the dissolution behaviour of the Ga doped bioactive glasses, as well as the glass structural and compositional analysis.

2.2 Aims

The aim of this chapter is the fabrication of gallium-doped BG and the investigation of the structural characteristics, compositional analysis, and their dissolution behaviour pre- and post-exposure to simulated body fluid (SBF). This was accomplished through the examination of,

- Fabrication of Ga doped BG with Ga content of 0-5 mol%
- Molecular structure, composition, and interactions within the BG network via FTIR analysis
- Elemental compositional analysis via SEM-EDS
- Ion release analysis via ICP-OES

2.3 Materials and methods

2.3.1 Glass preparation

Gallium doped bioactive glasses (Ga-BGs) were prepared by melt-quenched method using the following reagents: ammonium phosphate hydrate (H_6NO_4P, ≥99.5% purity; Sigma-Aldrich, USA), sodium carbonate (Na_2CO_3, ≥99.5% purity; Sigma-Aldrich, USA), calcium carbonate ($CaCO_3$, ≥99.5% purity Alfa Aesar, Thermo Fisher Scientific, USA), silicon dioxide (SiO_2, ≥99.5% purity; Alfa Aesar, USA) and gallium (III) oxide (Ga_2O_3, ≥99.99% purity; Thermo Fisher Scientific, USA). Six different compositions of Ga doped bioactive glasses were manufactured as shown in Table 2.1. All the compositions had a fixed concentration of Na_2O, CaO and P_2O_5 while the Ga_2O_3 and SiO_2 were varied.

Table 2.1. Summary of glass compositions, showing molar concentration of precursors.

Glass Code	Glass Composition (mol%)				
	Na_2O	CaO	P_2O_5	SiO_2	Ga_2O_3
45S5	24.4	26.9	2.6	46.1	0
Ga glass 1%	24.4	26.9	2.6	43.1	0.97
Ga glass 2%	24.4	26.9	2.6	40.22	1.92
Ga glass 3%	24.4	26.9	2.6	37.45	2.82
Ga glass 4%	24.4	26.9	2.6	34.79	3.69
Ga glass 5%	24.4	26.9	2.6	32.22	4.53

The precursors were weighed and mixed in a 90% platinum-10% rhodium crucible (GLC alloys Ltd Middlesex, UK). All the precursors are mixed thoroughly and placed into the Lindberg/Blue M™ Moldatherm™ box furnace (Thermo Scientific™, USA) at room temperature and heated at a rate of 10°C/min to 1450 °C and held at this temperature for 90 minutes. The melted glass was poured between two graphite blocks at room temperature. Bioactive glass compound with 5% Ga content was quenched into distilled water to cool the molten rapidly, to avoid the formation of crystalline structures and maintain an amorphous state due to the high content of Ga compound.

Each glass composition was ground with a planetary ball mill (PM100, Retsch) and sieved (Retsch GmbH, Germany) to obtain the particle size between 40 and 63 µm. The glass powders were used for characterisation analysis and cell studies. Each glass composition was kept into a desiccator to prevent the atmosphere moisture through the glass compositions.

2.3.2 Sample preparation for bioactivity testing

Simulated body fluid was prepared as outlined by Macon *et al* [16]. It contains precise procedure to create a solution which mimic human blood plasma. The reagents shown in Table 2.2 are mixed one by one in order in 700 ml 37 ˚C deionised (DI) water. The solution was constantly mixed using a Isotemp™ magnetic stirrer (Thermo Fisher Scientific, USA). Each reagent was added gradually and the pH of the solution was continuously monitored using a Fisherbrand™ accumet™ Basic AB315 benchtop pH/mV meter (Thermo Fisher Scientific, USA) to prevent a rapid increase, which can result in precipitation. Finally, the solution was transferred to a 1000 mL volumetric flask and was topped up to 1000 mL.

All experiments were performed in triplicate (n = 3) using samples prepared from the same glass production batch to ensure consistency and reproducibility across all analyses. Bioactive glass samples with particle sizes between 40 and 63 µm were soaked in SBF at concentrations of 10 and 20 mg/mL. They were incubated at 37 ˚C with 95% humidity and 5% CO_2 for a period of 7 days. After 7 days, the glass powders were removed from the solution using Whatman® qualitative filter paper, Grade 1 (Sigma-Aldrich, USA), washed twice with distilled water, and then rinsed with acetone 99+% (Thermo Scientific™, USA) to halt any further reactions and eliminate the residual elements of SBF. The samples were then dried in an incubator at 60 °C overnight and were used for characterisation analysis, including SEM-EDS elemental analysis and FTIR to investigate the potential of apatite formation.

Table 2.2. Reagents used for the preparation of 1000 mL SBF.

Order	Reagent	Amount (g/L)
1	NaCl (≥99.0% purity; Sigma-Aldrich, USA)	8.035
2	$NaHCO_3$ (≥99.5% purity Sigma-Aldrich, USA)	0.355
3	KCl (≥99.0% purity; Sigma-Aldrich, USA)	0.225
4	K_2HPO_4 $3H_2O$ (≥99.0% purity; Sigma-Aldrich, USA)	0.231
5	$MgCl_2$ $6H_2O$ (≥97.0% purity; Thermo Scientific™, USA)	0.311
6	HCl 1M (≥99.0% purity; Sigma-Aldrich, USA)	38 mL
7	$CaCl_2$ $2H_2O$ (≥99.0% purity; Sigma-Aldrich, USA)	0.386
8	Na_2SO_4 (≥99.0% purity; Sigma-Aldrich, USA)	0.072
9	Tris (≥99.0% purity; Thermo Scientific™, USA)	6.118

2.3.3 FTIR analysis

Fourier transform infrared spectroscopy was performed using a PerkinElmer Frontier FTIR equipped with PEAK technologies GladiATR sampling accessory (PIKE Technologies, USA). The FTIR measurements were undertaken with a spectral resolution of 4 cm^{-1} from 4000 to 400 cm^{-1} at room temperature, and a mean of 32 scans were recorded per sample. The data was plotted as the percentage of transmission. The glass powder with the particle size between 40 and 63 µm was used as samples. FTIR analysis was performed on untreated glass compounds as well as glass compounds which were exposed to SBF for a period of 7 days.

2.3.4 Elemental compositional analysis

Elemental analysis of the Ga-BGs was undertaken using Energy-dispersive X-ray spectroscopy using a JEOL JCM-6000 Plus Neoscope Scanning Electron Microscope (JEOL Ltd., Japan) equipped with an EDS detection laser. EDS measurements were undertaken using an excitation energy of 15 KeV. BGs were measured initially to determine their compositions directly after manufacture. A second measurement was also undertaken on the glasses after they had been exposed to SBF to determine the change in surface composition and potential bioactivity of the glasses. For each sample multiple regions were analysed to ascertain representative outcomes.

2.3.5 Ion release study

The stock solution of all the bioactive glass compounds at the concentrations of 10 mg/mL was prepared in distilled water for the quantification of ionic dissolution profile using inductively coupled plasma optical emission spectrometry ICP-OES (iCAP 7000 Plus Series, Thermo Fisher Scientific, USA). ICP-OES is a method for determining the concentration of trace metal ions in a sample. The samples were passed through a nebuliser to form aerosols, which were then driven through ICP at high temperatures, resulting in the formation of excited ions. The ions were separated and identified via an optical emission spectrometer.

The stock solutions were kept in an ES-20 compact shaker-incubator (Grant Instruments, GRT-ES-20, UK) at 200 rpm at 37 ˚C for 1, 3 and 7 days. Following the time points, the solutions were filtered using a 0.4 µm Ministart filter (Fisher Scientific, UK) to eliminate the glass particles from the solution. Reference standards of Ga^{3+}, Si^{4+}, Ca^{2+}, and Na^{+} were diluted with distilled water at 1, 10, 20, and 100 ppm to create calibration curves. The concentrations of ions were calculated using the linear portion of the plotted standard curve as ppm. The samples for each timepoint were analysed for the presence of cations, including Ga^{3+}, Si^{4+}, Ca^{2+}, and Na^{+} and anion PO_4^{3-}. For each glass compound and concentration, 3 independent samples were analysed to validate the accuracy of the data.

2.4 Results

2.4.1 FTIR analysis

FTIR spectroscopy was employed to investigate the compositional and structural modification in Ga-BGs. The purpose was to identify characteristic functional groups and investigate any changes as a result of Ga doping. FTIR analysis was performed on all the Ga doped glass compounds, 0-5% Ga containing at the concentration of 10 and 20 mg/mL. Figure 2.4 shows the FTIR spectra for the Ga-BGs at 10 mg/mL after being immersed in SBF for 7 days. IR absorption bands are clearly visible at ~ 565 and 605cm^{-1} and are attributed to the PO_4^{-3} tetrahedra, which had been observed in all the glass compounds. It is clear that the absorption bands for the glass compounds at the concentration of 20 mg/mL were more intense than 10 mg/mL (Figures 2.4 and 2.5). The peak ~ 1030 cm^{-1} is assigned to the P-O bending. Bands detected ~ 875, 1420 and 1,460 cm^{-1} are assigned to the carbonate group CO_3^{-2} which are commonly observed for the formation of apatite on BG [17, 18].

Note, there is no evidence of CO_3^{-2} or PO_4^{-3} IR bands in the unreacted '*as prepared*' bioactive glasses (Figure 2.3). The corresponding peaks for PO_4^{-3} and CO_3^{-2} for Ga containing samples exposed to the SBF agree with Ga free samples. The key absorption bands observed which correspond to the amorphous nature of the bioactive glass compounds at 900-1100 cm^{-1} correspond to Si-O-Si and Si-O stretching modes and 450 cm^{-1} corresponds to Si-O-Si bending mode. These bands indicate the presence of the silicate group. Table 2.3 summarises the main peaks seen in the FTIR spectra of Ga doped BG pre- and post-SBF exposure, showing the significant alterations [19, 20].

Table 2.3. Main FTIR peaks pre- and post-SBF immersion.

Peak Position (cm^{-1})	Assignment	Before immersion	After immersion 10 mg/mL	After immersion 20 mg/mL	References
900-1100	Si-O-Si/ Si-O Stretching	Present	Decreased	Decreased	[20]
415-540	Si-O-Si/ Si-O Bending	Present	Present	Present	[20]
560	P-O Stretching	Present	Increased	Increased	[21]
500-600	P-O Bending (HA)	Absent	Present	Present	[17, 18, 22]
1080-1350	P-O Stretching (HA)	Absent	Present	Present	[17, 18]
870,1420,1460	Carbonate Group (HA)	Absent	Present	Present	[23]
950	NBO	Present	Decreased	Decreased	[24]

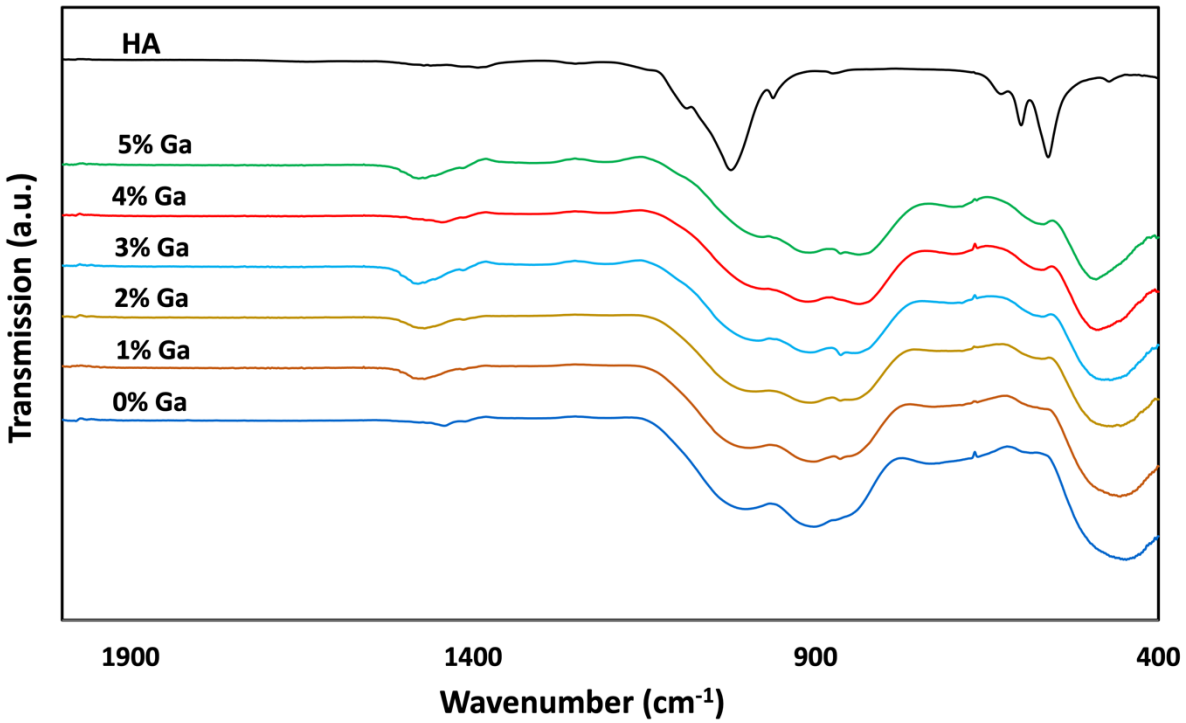

Figure 2.3. FTIR for BG before immersion in SBF. HA is shown for reference. Data sets are offset for clarity.

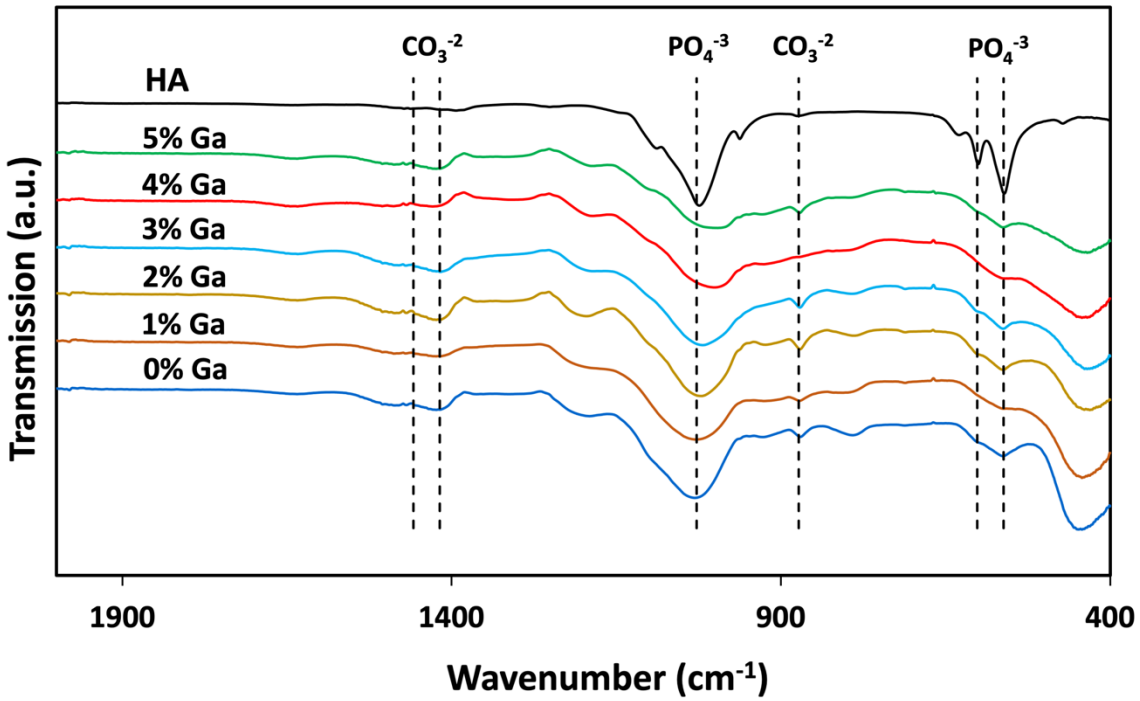

Figure 2.4. FTIR bands for BG following 7 days of immersion in SBF. HA is shown for reference. Data sets are offset for clarity (10 mg/mL Static).

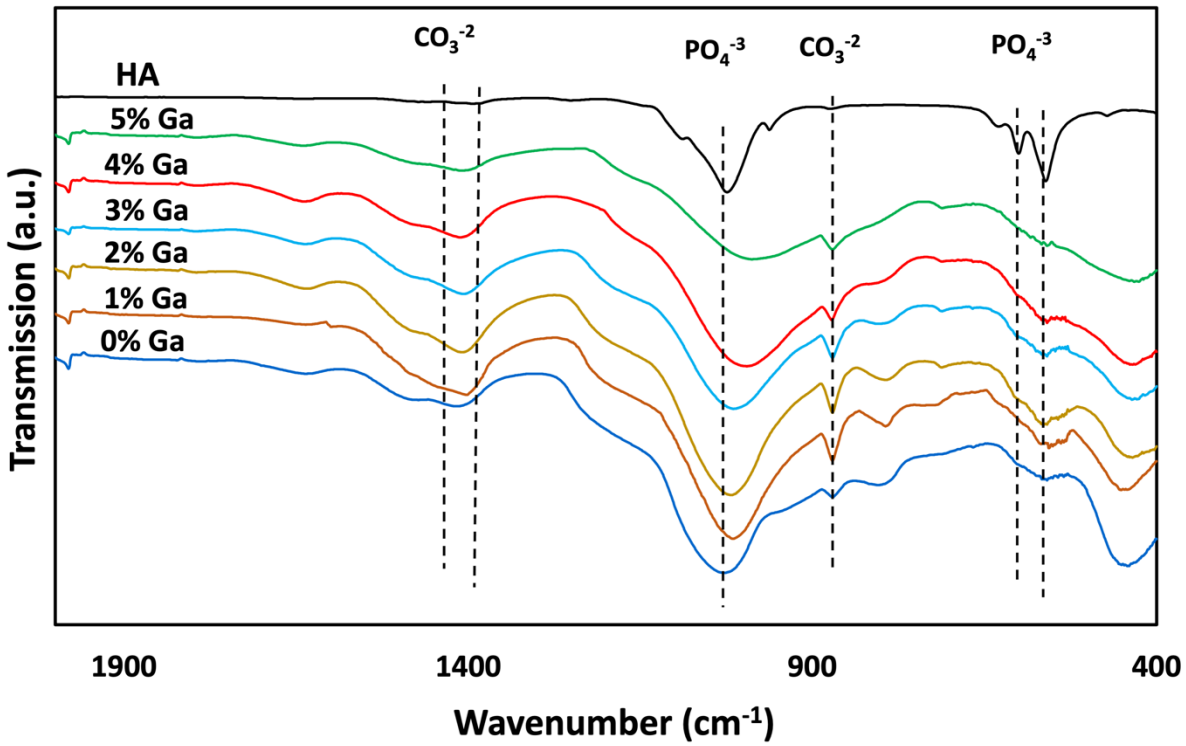

Figure 2.5. FTIR bands for BG following 7 days of immersion in SBF. HA is shown for reference. Data sets are offset for clarity (20 mg/mL Static).

2.4.2 EDS analysis

EDS analysis was performed to investigate the elemental composition and distribution of the ions within the glass network. This study aimed to confirm the presence of Ga ions and other compositional elements in the BG as well as to evaluate the homogeneity of the compositional elements in the glass matrix. It was performed on all the glass compounds before and after exposure to SBF at the concentration of 10 and 20 mg/mL. The results from EDS analysis confirmed the presence of Ga, Ca, P, Si and Na in the BG. Glass compositional values obtained from EDS are given in Table 2.4. The compositional data obtained from EDS analysis further supported the formation of a calcium / phosphorus-rich apatite layer for the glass compounds after incubation for 7 days in SBF (Tables 2.5 and 2.6).

Values obtained from EDS agree with the expect theoretical values, within experimental errors. Nominal Ga_2O_3 values are 0 to 5 mol% in increments of 1%. The average variation between the theoretical and measured value is just 0.1 mol % with a maximum difference of 0.5 mol % observed for the 4 mol% Ga glass. Sodium is within 1% of the expected nominal values and Ca within 4%. SiO_2 and CaO values are ~10% below and above the theoretical values respectively. However, this is a consistent and systematic difference across all samples and is attributed to an error in the calibration standards rather than a deviation from the expected nominal theoretical values.

Tables 2.5 and 2.6 show the compositional values of the Ga doped glass compounds after incubating in SBF at concentrations of 10 and 20 mg/mL for 7days of incubation. The release rate of ions is broadly as expected. A systematic increase is observed for Ga with the increasing Ga_2O_3 content, Si content decreases as expected as the concentration of SiO_2 is reduced by 3 times the concentration of Ga_2O. Ca is reasonably stable whilst Na in seen to increase significantly. As shown, the SiO_2 content has increased by on average 14 mol % across the whole series for soaked samples in SBF compared to the pre-soak. This is due to ions such as Na leaching from the glass, leaving behind a silicon-rich phase. A significant decrease in Na_2O content has been observed for the glass samples after 7 days of immersion in SBF in both 10 and 20 mg/mL glass samples. As seen, the P_2O_5 content has doubled after exposure to SBF compared to the unreacted glasses for all the samples.

Table 2.4. Compositional values of BGs as prepared were obtained from EDS before immersion in SBF.

Glass code	Composition (mol%)				
	SiO_2	CaO	Na_2O	P_2O_5	Ga_2O_3
45S5	43.6 ± 1.0 (46.1)	30.1 ± 0.8 (26.9)	24.0 ± 0.7 (24.4)	2.2 ± 0.4 (2.6)	0 (0)
1% Ga	41.9 ± 1.1 (44.0)	30.1 ± 0.8 (27.5)	24.4 ± 0.7 (24.9)	2.7 ± 0.5 (2.7)	0.9 ± 0.7 (1.0)
2% Ga	37.9 ± 1.5 (41.9)	32.1 ± 1.2 (28.0)	25.6 ± 1.1 (25.4)	2.1 ± 0.6 (2.7)	2.2 ± 1.2 (2.0)
3% Ga	36.9 ± 0.9 (39.8)	32.3 ± 0.8 (28.6)	25.2 ± 0.7 (25.9)	3.0 ± 0.4 (2.8)	2.6 ± 0.8 (3.0)
4% Ga	32.1 ± 1.5 (37.7)	34.8 ± 1.4 (29.1)	26.5 ± 1.2 (26.4)	3.1 ± 0.8 (2.8)	3.5 ± 1.5 (4.0)
5% Ga	32.6 ± 1.4 (35.5)	33.2 ± 1.2 (29.7)	26.5 ± 1.1 (26.9)	2.5 ± 0.7 (2.9)	5.2 ± 1.5 (5.0)

Table 2.5. Composition values of BGs at 10 mg/mL after immersion in SBF for 7 days obtained from EDS.

Glass code	Composition (mol%)				
	SiO_2	CaO	Na_2O	P_2O_5	Ga_2O_3
45S5	60.1 (±2.5)	34.3 (±1.9)	0.9 (±0.4)	4.7 (±1.3)	0.0 (0)
1% Ga	57.6 (±1.8)	29.3 (±1.3)	5.9 (±0.6)	5.5 (±1.0)	1.8 (±0.9)
2% Ga	57.1 (±2.5)	32.6 (±1.8)	2.3 (±0.7)	5.8 (±1.3)	2.9 (±1.4)
3% Ga	47.8 (±1.2)	38.8 (±1.0)	4.5 (±0.4)	4.8 (±0.7)	4.1 (±0.9)
4% Ga	46.8 (±1.9)	32.2 (±1.4)	10.5 (±0.9)	4.3 (±1.0)	6.2 (±1.6)
5% Ga	44.5 (±2.0)	38.2 (±1.7)	5.8 (±0.8)	4.9 (±1.1)	6.7 (±1.7)

Table 2.6. Composition values of BGs at 20 mg/mL after immersion in SBF for 7 days obtained from EDS.

Glass code	Composition (mol%)				
	SiO_2	CaO	Na_2O	P_2O_5	Ga_2O_3
45S5	64.8 (±0.4)	26.3 (±0.8)	4.9 (±0.4)	4 (±0.6)	0.0 (0)
1% Ga	50.6 (±1.6)	29.8 (±1.2)	14 (±0.8)	3.9 (±0.8)	1.8 (±0.9)
2% Ga	59.6 (±1.3)	30.2 (±0.9)	2.3 (±0.4)	5.8 (±0.7)	2.2 (±0.7)
3% Ga	53.8 (±2.3)	32.9 (±1.7)	4.7 (±0.8)	4.1 (±1.1)	4.4 (±1.6)
4% Ga	53.2 (±1.2)	29 (±0.9)	7.2 (±0.5)	4.3 (±0.6)	6.3 (±1.0)
5% Ga	46.9 (±1.1)	29.9 (±0.8)	10.6 (±0.5)	4.6 (±0.6)	8.0(±1.1)

Figures 2.6 and 2.7 demonstrate the EDS spectrum, which confirms the presence of each element with the characteristic peaks attributed to Ca, Si, Na, P and Ga ions. More importantly the presence of Ga was noted with the distinct peak at 1.1 keV.

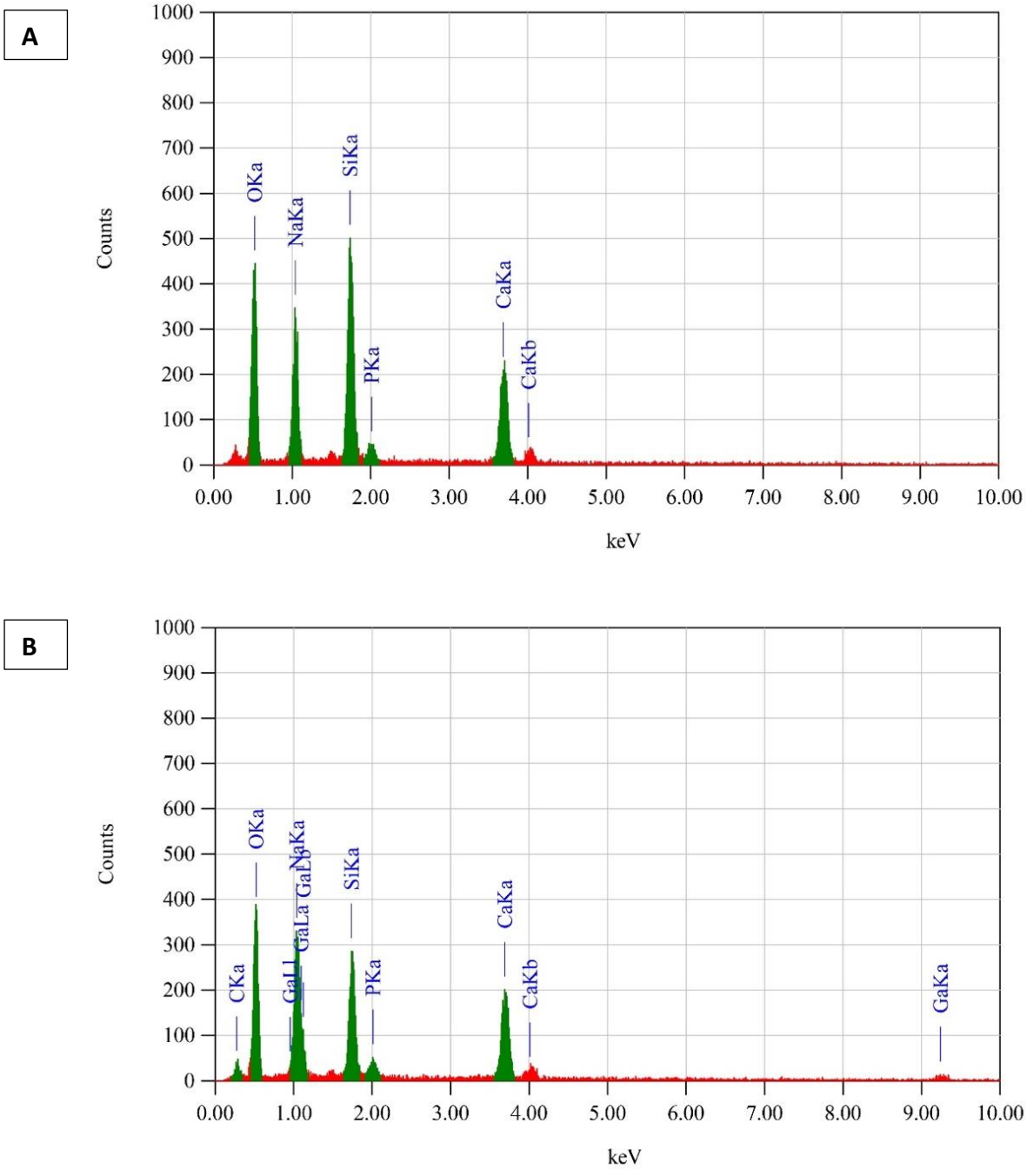

Figure 2.6. EDS spectra of BG samples before SBF immersion **(A)** 45S5 **(B)** 5% Ga.

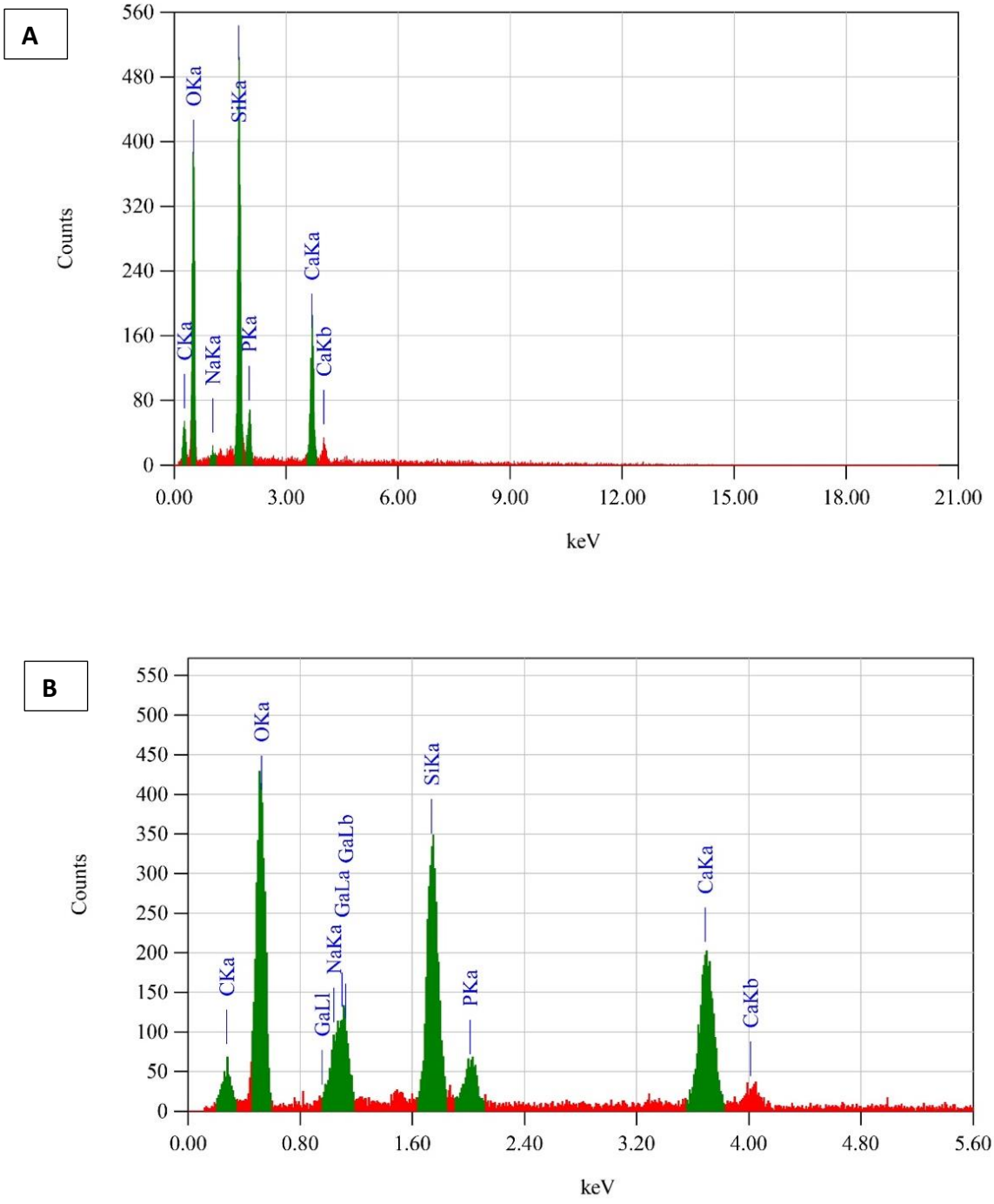

Figure 2.7. EDS spectra of BG samples immersed in SBF for 7 days **(A)** 45S5 **(B)** 5% Ga.

2.4.3 Dissolution profiles of bioactive glasses

To investigate the ions concentration leaching out of the Ga doped glass compounds, ICP analysis was performed. All the bioactive glass compounds were investigated to analyse the accumulation of Ga^{3+}, Si^{4+}, Ca^{2+}, and Na^{+} ions in distilled water at the concentrations of 10 mg/mL over 24 hours. Figure 2.8 shows the dissolution profile of the Ga^{3+}, Si^{4+}, Ca^{2+}, and Na^{+} glass compounds.

The release of ions has an ascending trend for the glass compounds in the first 3 days. The ICP results confirm the successful integration of Ga in the BG network, since the concentrations of Ga nearly correspond to the desired levels of doping. The findings show that with time, gallium, calcium, and silicon ions are released gradually. Based on ICP results, Ga^{3+}, Si^{4+}, Ca^{2+}, and Na^{+} ions leached out of the glass samples in a controlled manner. These patterns point to the glass matrix partially leaching out and the subsequent development of a bioactive layer, likely hydroxyapatite (HA), on the glass surface[19, 20].

A faster rate of Na^{+} ion release was observed in the first three days, followed by a steady decline in the accumulation of Na^{+} except for 4 and 5% Ga containing glasses, which had an upward trend for the 7 days course. After seven days, a significant decrease in calcium levels was noted. This suggests that the supersaturation of the surrounding fluid caused by the ion release facilitates the precipitation of calcium phosphate phases [25].

The silicon contents demonstrate a moderate decrease after 3 days of incubation. Due to the continuous processes of dissolution and re-precipitation, the silicon contents showed a modest reduction. In addition, the formation of Ca/P rich layer partially inhibits the release of Si.

The glasses compound investigated showed a significant release of Ga ions in a controlled and sustained manner over the period of 7 days. The Ga^{3+} is released at a higher rate in the first 3 days. For the glass compounds with 4 and 5%, the Ga release had an upward trend. The anticancer and antibacterial activity properties are enhanced by this regulated release [7]. There was no trace of gallium ions in 45S5 (the gallium-free samples), which is expected.

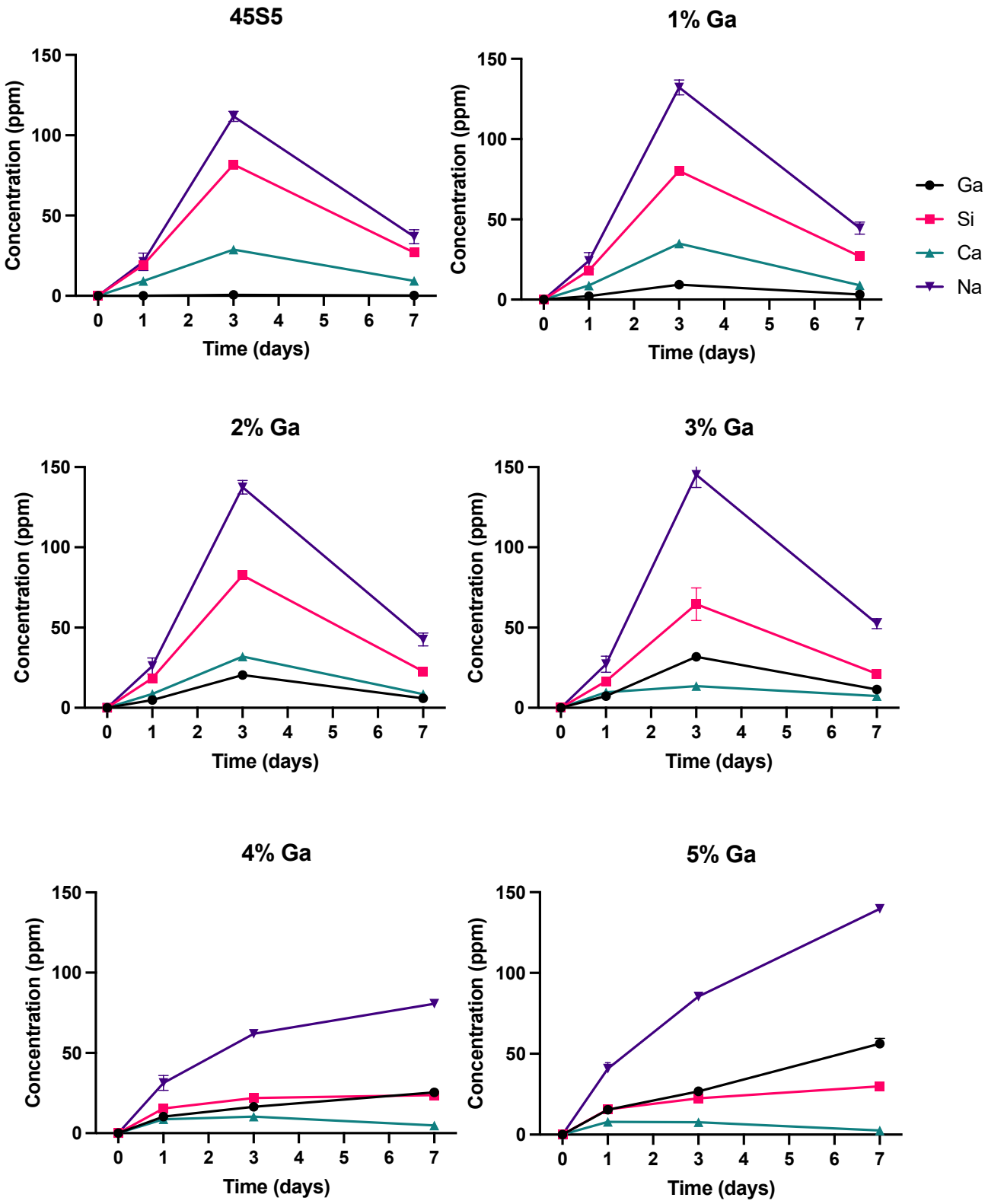

Figure 2.8. Elemental concentration release for Ca, Na, Ga, and Si as determined by ICP analysis of solutions resulting from the dissolution of 45S5, 1-5% Ga doped BG in dH_2O for a period of 7 days (Error bars = ±SD for triplicate samples).

Table 2.7 presents the dissolution profile of Ga-doped glass samples following 24 hours of incubation in distilled water at a concentration of 10 mg/mL. The overall ion release patterns align with expectations. A progressive increase in Ga release is observed with higher Ga_2O_3 content, while silicon levels decrease, consistent with the reduction of SiO_2 set at three times the Ga_2O_3 concentration. Ca release remains relatively stable, whereas Na levels increase markedly. This is in line with the renormalisation of the glass composition, where reductions in SiO_2 result in proportionally higher concentrations of CaO and Na_2O. Although the 5% Ga-doped glass initially appears to exhibit a faster dissolution rate than anticipated, the normalised values remain within two standard deviations of the expected trend, suggesting the variation is still statistically acceptable.

Table 2.7. Ion accumulation of all the glass compounds in diH_2O at the concentrations of 10 mg/mL after 24 hours of incubation. The data are represented as ppm.

Glass code	Concentration (ppm)			
	Na	Ca	Si	Ga
45S5	21.1	9.1	19.2	0.1
1% Ga	24.2	8.9	18.2	2.2
2% Ga	26.0	8.6	18.5	4.8
3% Ga	27.2	9.7	16.5	7.3
4% Ga	31.4	8.7	15.5	10.3
5% Ga	40.8	8.0	15.6	15.4

2.5 Discussion

A series of Ga-BGs was successfully fabricated and characterised. The process of ions leaching out BG compounds is a complicated process that depends on several variables including temperature, shaking intensity, and surrounding conditions, in addition to the composition and structure of the glass [26]. The aim of this chapter was to study the surface reactivity and its ability to form HA post immersion into biological fluids via FTIR and EDS techniques as well as the investigation of the glass compounds dissolution profile by ICP.

FTIR analysis was performed on fabricated glasses before and after immersion in SBF for a period of 7 days. In the pre-soaked glasses only the characteristic peaks of Si-O-Si bands were observed. After immersion the glasses in SBF, an ion exchange between the glass and the biological fluid occurs which results in precipitation of PO_4^{-3} anions and CO_3^{-2} cations on the BG surface. They form an amorphous Ca-P which ultimately crystalise to hydroxycarbonate apatite (HCA) [17, 23]. The process of HA formation on bioactive glasses summarized in the following stages [27],

1. Initial Surface Reactions:

When bioactive materials come into the contact with biological fluids like SBF or human plasma, the ion exchange process occures. The H^+ or H_3O^+ ions from the biological solution exchange with alkaline earth (e.g., Ca^{2+}) cations and alkali (e.g., Na^+) ions from glass. As a result, the pH increases near the glass surface and silanol (Si-OH) groups forms on the glass surface because the bonds of silicon and oxygen are broken and rehydrated.

2. Silica Gel Layer Formation:

On the glass surface, the silanol groups condense to produce a gel layer that is rich in silica which is an amorphous and porous layer. At the same time, the surrounding solution is exposed to soluble silica ($Si(OH)_4$), which might condense further and contribute to the gel layer.

3. Formation of Calcium Phosphate layer

The Bioglass surface, enriched with silanol groups on the silica gel layer, initiates the precipitation of calcium and phosphate ions from the surrounding fluid as the pH rises, further increasing the concentration of silanol groups on the surface.

The first layer to develop is an amorphous calcium phosphate (ACP) layer. This layer acts as hydroxyapatite's predecessor.

4. Crystalisation of HA

Over the course of many maturation processes, the amorphous calcium phosphate layer eventually changes into a crystalline HA layer. In order to align into the HA structure, more calcium and phosphate ions from the solution are incorporated during this process.

The overall process leading to the creation of HA is shown by:

$$10Ca^{2+}+6PO_4^{3-}+2OH^- \rightarrow Ca_{10}(PO_4)_6(OH)_2 \quad (2.1)$$

5. Growth and Maturation:

Following HA nucleation, the layer thickens as a result of the solution's constant addition of calcium and phosphate ions. The BG eventually has a layer of HA covering its whole surface. This layer creates a biocompatible interface that encourages tissue integration and bone bonding.

The generated data for FTIR showed the formation of PO_4^{-3} bonds in glasses in both 10 and 20 mg/mL concentration. However, the peaks were more intense for glass samples at 20 mg/mL. That is expected because with a higher concentration of bioactive glasses, the ions exchange occurs at a higher level/rate, and subsequent precipitation processes that lead to the formation of HA occur at a faster rate.

Pure HA is less likely to precipitate in SBF because it is saturated with regard to mildly carbonated apatite, in which carbonates replace orthophosphates in the crystal lattice. These CO_3^{-2} bands have previously been identified and attributed to carbonated apatite precipitation ($Ca_9(HPO_4)_{0.5}(CO_3)_{0.5}(PO_4)_5OH$) which preferentially forms rather than pure hydroxyapatite [18], [28]. Furthermore, BG immersion in SBF occur in the presence of air, so the CO_2 from atmosphere may have dissolved into the solution, partially substituting CO_3^{2-} for OH^- in the precipitated layer and ultimately forming HCA in place of HA [29].

No significant difference had been identified in Ga containing and Ga free bioactive glasses which suggest that the addition of Ga ions did not impact the glass network structure. Even the compounds with highest Ga percentage (mol 5%) demonstrate similar trends in the peaks as Ga free BGs.

Another interesting finding of FTIR result was the corresponding peaks for PO_4^{-3} and $CO_3^{-2}$for Ga containing glass samples were in agreement with Ga free glasses. This suggests that the addition of the Ga ions did not affect the bioactivity of the bioactive glasses and exposure of the Ga-BGs to the biological fluids provoke the same bioactivity and bioavailability as 45S5

bioactive glass. This is very important because the Ga ions have antineoplastic properties, and it not only creates cytotoxicity for the cancer cells but also has the properties of 45s5 bioactive glass, which stimulates bone regeneration for healthy bone cells.

The peaks at 1030 cm^{-1} and 600 cm^{-1}, are correspond to HA formation, which shows the bioactivity of the BG. Furthermore, a peak attributed to carbonate groups at around 870 cm^{-1} implies the development of a bioactive layer of carbonated HA [18, 23, 28]. Overall, the results from FTIR suggest the fabricated glasses are biologically active due to the formation of amorphous HCA on the glass surface and have a strong potential for bone regeneration purposes.

EDS analysis was performed to investigate the incorporation of the compositional elements of BG. As seen in the results, Ga ions had been incorporated and distributed uniformly, indicating that the doping procedure was successful and did not cause phase separation or clustering. This homogenous distribution is essential for the bioactive properties of the glass and the potential anticancer effects *in vitro* and *in vivo* [30-32].

According to the results from EDS analysis, the SiO_2 content had increased by average of 14% and this to be expected as Na_2O, P_2O_5 and to a lesser extent CaO are known to leach rapidly from the glass. Consequently, after the removal of these elements from the glass, followed by renormalising the remaining components back to 100%, a significant increase is observed for the remaining SiO_2 [33]. The Na_2O content has significantly decreased, as expected. Initially, it is expected that CaO and P2O5 would both leach out of the glass; however, after a 7-day incubation period, the formation of an amorphous calcium phosphate/carbonate apatite layer begins to occur. The P_2O_5 content has been doubled after immersion in SBF (Table 2.5 and 2.6) compared to the unreacted glasses (Table 2.4). This is further evidence of the formation of an amorphous calcium phosphate/apatite layer on the glass surface, indicating the initial stages of bone regeneration. A calcium to phosphorous ratio of 1.67:1 would be expected for hydroxyapatite ($Ca_{10}(PO_4)_6(OH)_2$) if only the uppermost surface layer was being probed[28]. However, the EDS contains a mixture of signals including the bulk glass as well as the apatite formation layer. One would therefore not expect to see an optimal ratio of 1.67:1. It is clear the ratio moves in the correct direction as the Ca:P ratio of the unreacted glass is ~ 15:1 whilst for the SBF reacted glass the ratio moves to ~7:1. This indicated that ~half of the signal is related to the bulk glass.

The EDS results from both 10 and 20 mg/mL agree which suggest that using the higher concentration of the Ga-BGs induces the formation of HA and did not interfere the process of Ca and P deposition on the glass surface. This is an important finding as the higher concentration of the Ga doped glass compounds induces higher toxicity for the cancer cells at a faster rate, while the bone regeneration side of the glass, which is important for the glass integration to the bone tissue of the host tissue, would stay the same [7].

The EDS data demonstrates that the fabricated glasses, which were exposed to the SBF for 7 days, developed a Ca and P-rich layer on the surface of the glass compounds.

ICP results demonstrate the dissolution profile of the Ga-BGs compounds after incubating in distilled water at the concentration of 10 mg/mL for 7 days of incubation. The release rate of ions is broadly as expected. A systematic increase is observed for Ga with the increasing Ga_2O_3 content. It is anticipated that Ga release will be reduced while the HA layer builds up over time and the glass degrades over a long period of time, which is beneficial for the therapeutic purposes [9]. Si content decreases as expected as the concentration of SiO_2 is reduced by 3 times the concentration of Ga_2O_3. The fast release of Si^{4+} could be due to the breaking of the network's outer layers of silica. Silica breaks down into monosilicic acid $Si(OH)_4$, upon the saturation of the solution [26]. The higher the concentration of the Ga ions in each glass compound the lower is the silicon content. This is expected as with the increase in the Ga ion content, the Si ions decrease in the formulation of the glass compounds. Accumulation of Ca^{2+} ions increases for the first 3 days and decreases steadily over the 7 days of incubation, which is due to the calcium ions combining with phosphorus ions to form a Ca-P saturated layer on the glass surface. Therefore, the rate of HCA formation will rise with increasing concentration of glass. The quantity of Na ions released from the glass was significantly high amongst all the other ions which agrees with results from Jones *et al* 2001 [27]. CaO and SiO_2 concentrations are expected to increase as the glass composition is renormalised following the reduction is Na_2O. At first inspection, it appears as though the glass dissolves more rapidly for the 5% Ga glass than expected; however, the value (after normalising by composition) is still within 2 standard deviations of the expected trend. These analyses confirmed the successful incorporation of Ga in the glass network as well as the bioavailability of Ga at the intended doping levels.

Ga^{3+}, Si^{4+}, Ca^{2+}, and Na^{+} ions were released gradually in the diH_2O, which indicates the partial dissolution of the glass and its bioactivity. It is noteworthy to emphasise that the fabricated

BG that are biodegradable, as evidenced by the release of Si and Ca ions. This is important since it pertains to bone regeneration and repair. Additionally, it is anticipated that the release of biologically active ions would increase the particles' bioactivity [30-32].

The analysis to assess the ionic dissolution product of Ga doped glass compounds had been performed in distilled water. ICP analysis is often performed in diH2O to enable direct comparison with the literature. Conducting dissolution in other conditions, such as SBF, is challenging because the high concentration of ions in SBF can dominate the signal and would not give accurate results.

2.6. Conclusion

A series of melt-quenched Ga-doped bioactive glasses (0-5 mol% Ga_2O_3) was successfully synthesised with fixed Na_2O, CaO, P_2O_5 content and varying Ga_2O_3/SiO_2 ratios. Elemental analysis confirmed the effective incorporation of Ga into the glass network, with compositions closely matching nominal values. FTIR spectra of the as-prepared glasses showed the characteristic Si-O-Si bands typical of amorphous silicate structures, while immersion in SBF for seven days produced PO_4^{3-} and CO_3^{2-} absorption peaks, confirming HCA formation and, therefore, bioactivity. EDS analysis supported these findings, revealing Na_2O depletion and P_2O_5 enrichment after immersion, consistent with ion exchange, silica-gel formation, and calcium-phosphate deposition on the glass surface.

ICP-OES analysis demonstrated a controlled, composition-dependent release of Ga^{3+}, Ca^{2+}, Na^+, and Si species over seven days, with gallium release scaling with Ga_2O_3 content. Importantly, Ga incorporation up to 5 mol% did not alter the glass structure or hinder bioactivity, indicating that Ga can be introduced without compromising the dissolution–reprecipitation behaviour characteristic of 45S5 bioactive glass. Across FTIR/EDS/ICP data, Ga doping (up to 5 mol%) did not impair HA/HCA formation or the canonical dissolution–reprecipitation sequence relative to 45S5, indicating that Ga can be introduced without sacrificing bioactivity. Overall, these findings confirm that Ga-doped bioactive glasses provide bioactive surfaces capable of HCA formation combine bioactivity with sustained Ga^{3+} ion release whose magnitude increases with Ga content, establishing a strong basis for the biological evaluations in the following chapter focused on their cytotoxic selectivity and mechanism of action against osteosarcoma as well as healthy osteoblast cells.

2.7. References

[1] M. Vallet-Regí and E. Ruiz-Hernández, "Bioceramics: From bone regeneration to cancer nanomedicine," *Advanced Materials*, vol. 23, no. 44, pp. 5177–5218, 2011, doi: 10.1002/adma.201101586.

[2] P. Saravanapavan and L. L. Hench, "Low-temperature synthesis, structure, and bioactivity of gel-derived glasses in the binary CaO-SiO2 system," *J Biomed Mater Res*, vol. 54, no. 4, pp. 608–618, 2001, doi: 10.1002/1097-4636(20010315)54:4<608::AID-JBM180>3.0.CO;2-U.

[3] A. Rahimnejad Yazdi, L. Torkan, S. D. Waldman, and M. R. Towler, "Development of a novel bioactive glass suitable for osteosarcoma-related bone grafts," *J Biomed Mater Res B Appl Biomater*, vol. 106, no. 3, pp. 1186–1193, 2018, doi: 10.1002/jbm.b.33930.

[4] L. Fiocco, S. Li, M. M. Stevens, E. Bernardo, and J. R. Jones, "Biocompatibility and bioactivity of porous polymer-derived Ca-Mg silicate ceramics," *Acta Biomater*, vol. 50, no. 0, pp. 56–67, 2017, doi: 10.1016/j.actbio.2016.12.043.

[5] S. Chen *et al.*, "Biodegradable zinc-containing mesoporous silica nanoparticles for cancer therapy," *Mater Today Adv*, vol. 6, p. 100066, 2020, doi: 10.1016/j.mtadv.2020.100066.

[6] A. Hoppe, N. S. Güldal, and A. R. Boccaccini, "A review of the biological response to ionic dissolution products from bioactive glasses and glass-ceramics," *Biomaterials*, vol. 32, no. 11, pp. 2757–2774, 2011, doi: 10.1016/j.biomaterials.2011.01.004.

[7] F. Kurtuldu, N. Mutlu, A. R. Boccaccini, and D. Galusek, "Gallium containing bioactive materials: A review of anticancer, antibacterial, and osteogenic properties," *Bioact Mater*, no. December, 2022, doi: 10.1016/j.bioactmat.2021.12.034.

[8] C. R. Chitambar, "Gallium-containing anticancer compounds," *Future Med Chem*, vol. 4, no. 10, pp. 1257–1272, 2012, doi: 10.4155/fmc.12.69.

[9] K. S. Rana, L. P. De Souza, M. A. Isaacs, F. N. S. Raja, A. P. Morrell, and R. A. Martin, "Development and Characterization of Gallium-Doped Bioactive Glasses for Potential Bone Cancer Applications," *ACS Biomater Sci Eng*, vol. 3, no. 12, pp. 3425–3432, 2017, doi: 10.1021/acsbiomaterials.7b00283.

[10] M. Franchini, G. Lusvardi, G. Malavasi, and L. Menabue, "Gallium-containing phospho-silicate glasses: Synthesis and in vitro bioactivity," *Materials Science and Engineering: C*, vol. 32, no. 6, pp. 1401–1406, Aug. 2012, doi: 10.1016/J.MSEC.2012.04.016.

[11] O. M. Clarkin *et al.*, "Novel injectable gallium-based self-setting glass-alginate hydrogel composite for cardiovascular tissue engineering," *Carbohydr Polym*, vol. 217, pp. 152–159, Aug. 2019, doi: 10.1016/J.CARBPOL.2019.04.016.

[12] N. Gómez-Cerezo *et al.*, "The response of pre-osteoblasts and osteoclasts to gallium containing mesoporous bioactive glasses," *Acta Biomater*, vol. 76, pp. 333–343, Aug. 2018, doi: 10.1016/J.ACTBIO.2018.06.036.

[13] A. W. Wren *et al.*, "A preliminary investigation into the structure, solubility and biocompatibility of solgel SiO2–CaO–Ga2O3 glass-ceramics," *Mater Chem Phys*, vol. 148, no. 1–2, pp. 416–425, Nov. 2014, doi: 10.1016/J.MATCHEMPHYS.2014.08.006.

[14] G. Lusvardi, G. Malavasi, L. Menabue, and S. Shruti, "Gallium-containing phosphosilicate glasses: Functionalization and in-vitro bioactivity," *Materials Science and Engineering: C*, vol. 33, no. 6, pp. 3190–3196, Aug. 2013, doi: 10.1016/J.MSEC.2013.03.046.

[15] A. Wajda, W. H. Goldmann, R. Detsch, A. Grünewald, A. R. Boccaccini, and M. Sitarz, "Structural characterization and evaluation of antibacterial and angiogenic potential of

gallium-containing melt-derived and gel-derived glasses from CaO-SiO2 system," *Ceram Int*, vol. 44, no. 18, pp. 22698–22709, Dec. 2018, doi: 10.1016/J.CERAMINT.2018.09.051.

[16] A. L. B. Maçon *et al.*, "A unified in vitro evaluation for apatite-forming ability of bioactive glasses and their variants," *J Mater Sci Mater Med*, vol. 26, no. 2, pp. 1–10, 2015, doi: 10.1007/s10856-015-5403-9.

[17] N. F. Ibrahim, H. Mohamad, and S. N. F. Mohd Noor, "Characterization on melt-derived bioactive glass powder from SiO2-CaO-Na2O-P2O5 system," *J Non Cryst Solids*, vol. 462, pp. 23–31, Apr. 2017, doi: 10.1016/J.JNONCRYSOL.2017.01.040.

[18] O. Peitl, E. Dutra Zanotto, and L. L. Hench, "Highly bioactive P2O5–Na2O–CaO–SiO2 glass-ceramics," *J Non Cryst Solids*, vol. 292, no. 1–3, pp. 115–126, Nov. 2001, doi: 10.1016/S0022-3093(01)00822-5.

[19] J. R. Jones, "Reprint of: Review of bioactive glass: From Hench to hybrids," *Acta Biomater*, vol. 23, no. S, pp. S53–S82, 2015, doi: 10.1016/j.actbio.2015.07.019.

[20] L. L. Hench, "Bioceramics: From Concept to Clinic."

[21] A. Saboori, M. Rabiee, F. Moztarzadeh, M. Sheikhi, M. Tahriri, and M. Karimi, "Synthesis, characterization and in vitro bioactivity of sol-gel-derived SiO2–CaO–P2O5–MgO bioglass," *Materials Science and Engineering: C*, vol. 29, no. 1, pp. 335–340, Jan. 2009, doi: 10.1016/J.MSEC.2008.07.004.

[22] R. Ravarian, F. Moztarzadeh, M. S. Hashjin, S. M. Rabiee, P. Khoshakhlagh, and M. Tahriri, "Synthesis, characterization and bioactivity investigation of bioglass/hydroxyapatite composite," *Ceram Int*, vol. 36, no. 1, pp. 291–297, Jan. 2010, doi: 10.1016/J.CERAMINT.2009.09.016.

[23] F. Z. Mezahi, A. L. Girot, H. Oudadesse, and A. Harabi, "Reactivity kinetics of 52S4 glass in the quaternary system SiO2–CaO–Na2O–P2O5: Influence of the synthesis process: Melting versus sol–gel," *J Non Cryst Solids*, vol. 361, no. 1, pp. 111–118, Feb. 2013, doi: 10.1016/J.JNONCRYSOL.2012.10.013.

[24] J. P. Borrajo *et al.*, "Influence of the Network Modifier Content on the Bioactivity of Silicate Glasses," in *Key Engineering Materials*, Trans Tech Publications Ltd, 2004, pp. 23–26. doi: 10.4028/www.scientific.net/kem.254-256.23.

[25] J. R. Jones and I. R. Gibson, "1.3.4 - Ceramics, Glasses, and Glass-Ceramics: Basic Principles," in *Biomaterials Science (Fourth Edition)*, Fourth Edi., W. R. Wagner, S. E. Sakiyama-Elbert, G. Zhang, and M. J. Yaszemski, Eds., Academic Press, 2020, pp. 289–305. doi: https://doi.org/10.1016/B978-0-12-816137-1.00022-2.

[26] L. L. Hench, "Bioceramics," *Journal of the American Ceramic Society*, vol. 81, no. 7, pp. 1705–1728, 1998, doi: 10.1111/j.1151-2916.1998.tb02540.x.

[27] J. R. Jones, P. Sepulveda, and L. L. Hench, "Dose-dependent behavior of bioactive glass dissolution," *J Biomed Mater Res*, vol. 58, no. 6, pp. 720–726, 2001, doi: 10.1002/jbm.10053.

[28] G. A. Stanciu *et al.*, "Investigation of the Hydroxyapatite Growth on Bioactive Glass Surface," *Journal of Biomedical & Pharmaceutical Engineering*, vol. 1, pp. 34–39, 2007.

[29] A. Rahimnejad Yazdi and M. Towler, "The effect of the addition of gallium on the structure of zinc borate glass with controlled gallium ion release," *Mater Des*, vol. 92, pp. 1018–1027, 2016, doi: 10.1016/j.matdes.2015.12.082.

[30] Q. Nawaz *et al.*, "New insights into the crystallization process of sol-gel–derived 45S5 bioactive glass," *Journal of the American Ceramic Society*, vol. 103, no. 8, pp. 4234–4247, 2020, doi: 10.1111/jace.17124.

[31] D. De *et al.*, “Assessing behaviour of osteoblastic cells in dynamic culture conditions using titanium-doped phosphate glass microcarriers”, doi: 10.1177/2041731419825772.

[32] R. A. Martin *et al.*, “Characterizing the hierarchical structures of bioactive sol-gel silicate glass and hybrid scaffolds for bone regeneration,” *Philosophical Transactions of the Royal Society A: Mathematical, Physical and Engineering Sciences*, vol. 370, no. 1963, pp. 1422–1443, 2012, doi: 10.1098/rsta.2011.0308.

[33] I. M. Asif, R. M. Shelton, P. R. Cooper, O. Addison, and R. A. Martin, “In vitro bioactivity of titanium-doped Bioglass.”

Chapter 3

In-vitro Cellular Response to Gallium Doped Bioactive Glass

3.1 Introduction

The application of a bioactive glass for the treatment of bone cancer is based on two important functions of bioactive glasses: 1) targeted drug delivery to the tumour site 2) introducing a regenerative scaffold to stimulate the growth of new tissue [1]. Gallium (Ga) compounds play an important role in the management and treatment of a variety of cancers [2, 3]. It interferes with iron-dependent growth pathways in tumour cells by acting as an iron mimetic [4]. For cancer therapy, different types of bioactive glasses, including granular particles and 3D scaffolds, may be used. Ga doped bioactive glasses (Ga-BGs) introduce a localised drug delivery system, which increases the bioavailability of Ga compared to oral administration. In addition, it is more convenient and less invasive compared to intravenous infusion [5]. In this context, Ga-BGs have been reported as a potential scaffold for dual action of the cancer therapy and bone tissue engineering [6]. There has been a lot of interest in the development and improvement of bioactive glass ceramics for bone tissue engineering. However, there has been little or no attention on BG for bone cancer applications.

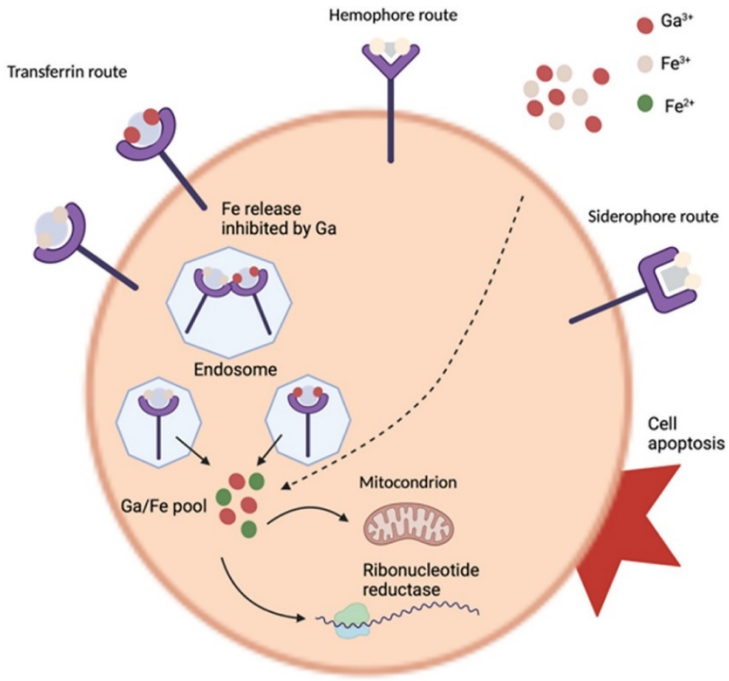

Figure 3.1. Schematic of Ga's anticancer action. Fe and Ga enter cells via transferrin-dependent and independent pathways. In acidic endosomes, they are released into the intracellular pool. Ga disrupts iron availability, inhibiting processes like ribonucleotide reductase and mitochondrial function.

In the previous chapter, Ga-BGs with increasing Ga_2O_3 content were successfully fabricated and characterised. The results proved that the Ga ions have been integrated effectively in the structure of the silica-based bioactive glasses (BGs) without forming crystalline phases, which obstruct and compromise the bioactivity of the glasses [7], [8]. Also, the results demonstrated that an amorphous layer of Ca-P has been formed after the glass particulates were exposed to the growth medium for a period of 7 days.

This chapter focuses on evaluating the biological performance of Ga-BGs using osteosarcoma (Saos-2) and normal human osteoblast (NHOst) cell models. The cytocompatibility and selective anticancer effects of Ga-BGs were assessed through multiple *in vitro* assays, including MTT viability, Live/Dead staining, and real-time IncuCyte imaging. Additionally, scratch-wound and PicoGreen DNA assays were conducted to investigate cell migration, wound closure, and cytotoxicity. The fundamental composition of the Ga-BGs is based on the sodium calcium phosphor-silica Bioglass 45S5 [9-11]. For *in vitro* analysis, 45S5 Bioglass was used as a reference to assess the osteostimulatory, osteoconductive, and osteoinductive properties of the samples. Its biological activity arises from the release of Si, Ca, P, and Na ions, which stimulate the bone regeneration [12]. However, incorporating gallium oxide may alter glass composition and reduce bioactivity; therefore, it is essential to evaluate both the bioactivity and cytotoxicity of Ga-doped glasses to ensure therapeutic effectiveness and safety for healthy tissue

These experiments aim to identify the optimal Ga concentration and exposure conditions that maximise osteosarcoma suppression while preserving healthy osteoblast function, key parameters for developing effective bone-graft materials for osteosarcoma-related defects.

3.2 Aims

The aim of this chapter is to investigate the effect of Bioglass 45S5 and Ga-BGs (containing 1, 2, 3, 4, and 5 mol% % Ga_2O_3) on the viability of human drive OS and healthy osteoblast cells. This was accomplished by investigating,

- The effect of the glass dissolution product on the cells' viability and proliferation using MTT viability assay and IncuCyte image analysis
- Cell toxicity analysis using Live/Dead assay, which was performed on the cells exposed to the conditioned medium for a period of 10 days.
- Cell proliferation using IncuCyte Live-Cell Imaging Systems
- Scratch wound assay and investigate wound healing in OS cells using IncuCyte Live-Cell Imaging Systems
- Cell death, using the PicoGreen assay on the cell supernatant.

3.3 Materials and methods

The bioactive glasses used in this study were manufactured using the melt-quench, method described in Chapter 2, Section 2.3.1 (Glass preparation). The compositions and processing conditions were identical to those detailed in chapter 2. All experiments were performed in triplicate (n = 3) using samples prepared from the same glass production batch to ensure consistency and reproducibility across all analyses.

3.3.1 Conditioned medium preparation

Conditioned medium was prepared through the addition of the glass particles (particle size range from 40-63 µm) at a concentration of 10 and 20 mg/mL to serum-free McCoy's 5A medium (Thermo Fisher Scientific, USA) for Saos-2 cells and OGM ™ medium (Lonza, Switzerland) for NHOst cells. The medium was incubated at 37 ˚C for 24 hours in an ES-20 compact shaker-incubator at 200 rpm. After the incubation, the conditioned medium was filtered using Millex™-GS 0.22 µm syringe filter (Sigma-Aldrich, USA) to remove the glass particles and also to sterilise the stock solution. The conditioned medium for Saos-2 was supplemented with 15% Fetal bovine serum (FBS) (Gibco™, Thermo Fisher Scientific, USA), while 10% FBS was added to the conditioned medium for NHOst (Lonza, Switzerland). The glass composition usually increases the pH of the medium during dissolution. The increase in pH occurs during the ion exchange mechanism when the cations, such as Na^+ and Ca^{2+}, are released from the glass structure and exchange with protons (H+/H3O+) from the solution. With an increase in glass concentration, the pH increases more due to a greater quantity of cations which are available for ion exchange [10]. For neutralising pH and gaining the appropriate pH for the treatment of the cells, medium was incubated overnight using a Cytomat™ 10C automated incubator (Thermo Scientific™, USA) with 5% CO_2/ 95% air at 37 ˚C. This way, the CO_2 in the incubator mediated the buffering, and it helps in the elimination of any detrimental cytotoxic effects of high pH of the conditioned medium. Cell culture medium contains bicarbonate ions. The 5% CO_2 from the incubator dissolve in the medium and forms carbonic acid, which creates an equilibrium with the HCO_3^- ions and reduces the pH. The presence of HCO_3^- drives the equation to the left, subtracting H^+ and it increases the pH[6].

$$H_2O + CO_2 \Leftrightarrow H_2CO_3 \Leftrightarrow H^+ + HCO_3^- \quad (3.1)$$

3.3.2 Cell culture of human osteosarcoma (Saos-2)

Saos-2 (ATCC® HTB-85™) cells were purchased from the American Type Culture Collection (ATCC®, USA) and grown according to the manufacturer's instructions in McCoy's 5A medium containing 1.5 mM L-glutamine and 2200 mg/L sodium bicarbonate (Gibco™, Thermo Fisher Scientific, USA). Medium was supplemented with 15% FBS. The cell line was kept at 37 °C in a humidified atmosphere of 5% CO_2/95% air. The cells were seeded in T-75, and the medium was swapped with fresh growth medium every 2-3 days. The cells were split upon 80% confluency. Cell culture assays were performed in accordance with ISO 10993-5:2009 guidelines to evaluate the cytocompatibility of the bioactive glass samples.

3.3.3 Cell culture of normal human osteoblast (NHOst)

Primary Normal Human Osteoblasts (NHOst) cells were purchased from Lonza and grow according to the manufacturer's instructions in Clonetics OGM Osteoblast growth medium (Lonza, Switzerland), which was supplemented with 10% FBS, gentamicin sulfate-Amphotericin (GA-1000) 0.50 mL, and Ascorbic Acid 0.50 mL. Cells were maintained at 37 °C in a humidified atmosphere of 5% CO_2/95% air. Cell culture assays were performed in accordance with ISO 10993-5:2009 guidelines to evaluate the cytocompatibility of the bioactive glass samples.

3.3.4 Cell viability assay

Cell viability assays were conducted using the MTT viability assay kits from Invitrogen, Thermo Fisher Scientific (Waltham, MA, USA), to investigate the cytotoxic effect of the Ga doped bioactive glasses *in vitro* in accordance with the principles outlined in ISO 10993-5:2009. OS cells Saos-2 were seeded into 48 well plates with the density of 5000 cells/cm^2 in McCoy's 5A Medium supplemented with 15% FBS and maintained overnight in a cell culture incubator at 37 ˚C /5% CO_2/95% air. NHOst cells were seeded as described above in Clonetics OGM osteoblast growth medium, which was supplemented with 10% FBS, gentamicin sulfate-Amphotericin (GA-1000) 0.50 mL, and Ascorbic Acid 0.50 mL. The next day the growth medium was swapped with the conditioned medium containing either 10 or 20 mg/mL Ga doped bioactive glass ionic dissolution. The MTT assays were performed at day 1, 3, 5, 7 and 10 after the addition of conditioned medium to the cells. The conditioned medium was

changed on day 3 for the time point day 5, 7 and 10 also on day 7 for the time-point of day 10. Ethanol 70% (v/v) was used as an etoposide to represent the positive control while the cells grow in normal growth medium represent the negative control. For the MTT assay, a 12 mM stock solution of 3-(4.5-dimethylthiazol-2-yl)-2.5-diphenyltetrazolium bromide (MTT) was prepared as per the manufacturer's instructions and diluted 1/10 in Dulbecco's Modified Eagle Medium (DMEM) phenol-red free medium (Gibco™, Thermo Fisher Scientific, USA) before being added to the cells. After treating the stock solution to the cells, the plates were incubated for 4 hours at 37 °C. After the incubation, 150 µL of the treatment was removed and 50 µL of Dimethyl sulfoxide (DMSO), (Sigma-Aldrich, USA) was added and left to incubate at 37 °C for more 10 minutes. Metabolically active cells reduce MTT to formazan and after formazan extraction, the optical density was measured using Ascent MultiScan GO spectrophotometer (Fisher Scientific, Leicester, UK) at 570 nm. This assay was performed in 5 replicates. Cell free blank samples containing DMEM medium and MTT reagent were considered for detection and subtracting background.

3.3.5 LIVE/DEAD assay

Cell viability was assessed using the LIVE/DEAD™ Viability Assay Kit (Invitrogen™, Thermo Fisher Scientific, Waltham, MA, USA), following the principles outlined in ISO 10993-5:2009. It is a simple and quick colorimetric assay that uses two stains: Calcein-AM, a green fluorescent nucleic acid stain, and the red-fluorescent nucleic acid stain, ethidium homodimer-1 (EthD-1). The Calcein-AM stain can penetrate all cells, but EthD-1 only penetrates the cells where membranes are damaged. However, the fluorescent intensity is reduced for Calcein-AM when EthD-1 is present. Therefore, live cells with an undamaged cell membrane represent green, while dead cells with a damaged cell membrane appear red.

Saos-2 cells were seeded at a concentration of 5000/cm^2 in a 48-well plate and incubated for 24 hours. NHOst cells were also seeded as described. After 24 hours, the growth medium was swapped with conditioned medium and the LIVE/DEAD assay was performed at the time-points days 1, 3, 5, 7 and 10 post the addition of conditioned medium to the cells.

The working concentration of Calcein-AM at 0.5 µM and EthD-1 at 2.5 µM were mixed into one solution with Phosphate-buffered saline (PBS), (Gibco™, Thermo Fisher Scientific, USA), and 200 µL of this master mix was added to each well and incubated at room temperature (in

dark) for 1 hour. Cells were photographed using a LAS X Widefield Systems fluorescence microscope (Leica Microsystems, Germany) at 10x magnification.

3.3.6 IncuCyte cell proliferation and migration assay

Cell proliferation and cell migration studies were performed using a label-free, non-invasive cellular confluence assay by IncuCyte Live-Cell Imaging Systems (Essen Bioscience, Ann Arbor, MI, USA). Saos-2 cells were seeded into 48-well plates at a density of 5000 cells per well in McCoy's 5A medium and supplemented with 15% FBS and maintained in a cell culture incubator at 37 ˚C with 5% CO_2/95% air overnight. The next day, the medium was swapped with the conditioned medium, and the plate was transferred to the IncuCyte imaging system for a period of 10 days. Images were captured every 2 hours using 10X objective to monitor the cell proliferation in real time. Cell confluence was calculated using Fiji image analysis.

To investigate cell migration, a scratch wound assay was performed on Saos-2 cells. Saos-2 cells were seeded onto a 6-well plate with 5×10^5 cells per well in complete growth medium. Cells were grown for 24 hours to form a 90% confluent monolayer. A scratch ~ 3um wide was made using a sterile micropipette tip (Corning®, Axygen®, USA). Media was removed, and the residue of the lifted cells was washed twice with PBS, and the cells were cultured in the absence and presence of conditioned medium containing gallium compounds. Images were acquired immediately following media replacement and then every 2 hours for a period of 10 days using the IncuCyte Live-Cell imaging system (Essen Bioscience, Ann Arbor, MI, USA) at 10x magnification. The final images were analysed using ImageJ (National Institutes of Health) to examine the wound area distance. Cells were kept under sterile culture conditions at 37 °C in an atmosphere containing 5% CO_2 during image collection. The percentage of wound area was plotted over time for each concentration. Data are presented as mean ± SD. The percentage (%) of wound closure was calculated using,

$$Wound\ closure\ (\%) = \frac{W_0 - W_t}{W_0} \times 100 \qquad (3.1)$$

where W_0 is the initial width of the scratch wound at day zero and W_t is the width of the scratch after time *t*.

3.3.7 Fiji image analysis

An enhanced image-analysis software titled Fiji (http://Fiji.sc/Downloads) on the open-source ImageJ was used to analyse the image outputs of the IncuCyte system. To begin, all the images were converted to 8-bit black and white, and the scale was converted from pixels into micrometres (µm). According to the scale bar of the images, 290 pixels equal 400 µm, which was applied to all the images (each image was 1280x944 pixels originally). By employing the "Freehand Selections" tool, the areas covered by the cells were selected manually and filled with white colour (by selecting "Fill" option under the "Edit" in menu bar) to maximise the distinction in pixel intensities between areas covered by cells and cell absence zone (which had been filled with black colour by selecting "Clear Outside" option under the "Edit" in menu bar). "Set Measurements" tool was then opened under the "Analyse" tab on the menu bar in order to choose "Area" and "Area Fraction" options. "Measure" tool was used under the "Analyse" tab to get the percentage of confluency.

3.3.8 Cell cytotoxicity assay

Cell death was assessed using Quant-iT™ Picogreen ® dsDNA kit (Invitrogen™, Thermo Fisher Scientific, USA). Saos-2 cells were seeded into 48-well plates at a density of 5000 cells/cm^2 and in McCoy's 5A Medium supplemented with 15% FBS and maintained overnight in a cell culture incubator at 37 ˚C /5% CO_2/95% air. The next day, the growth medium was swapped with the conditioned medium.

The samples were measured in quadruplicate for each condition and analysed on days 3, 5, 7, and 10. At each time point, the supernatant was collected in an eppendorf tube from each well and spun at 300 g for 5 minutes. After centrifugation, the supernatant was discarded while the pellet, which contained the dead cells, was resuspended in 1 mM ammonium acetate buffer and 0.05 v/w Proteinase K. Proteinase K is a digestive reagent for DNA extraction. It digests unwanted and contaminating proteins that are present. It also digests nucleases enzymes and protects the nucleic acid from the enzymatic attack.

The samples were stored at -80°C until processing. A day prior to the experiment, samples were thawed at 37 °C, pipetted up and down and incubated in the dry oven at 60˚C overnight for the process of digestion. On the day of the experiment, a set of high range standards was prepared using Lambda DNA, which was provided with the kit. The DNA concentration for the

high range standard was 1000, 100, 10, and 1 ng/mL. For each standard, 50 µL was transferred into a 96-well tissue culture (TC)-treated flat-bottom black microplates (Corning® Falcon®, Sigma-Aldrich, USA) in 5 repeats. A working solution of the PicoGreen reagent was prepared by making a 1:50 dilution in TE buffer and kept in aluminium foil, as the working solution is light sensitive. 50 µL of the working solution was added to each sample/standard. The plate was shaken and incubated in the dark for five minutes at RT. The plate was read at 485 nm emission and 520 nm emission using a fluorescent plate reader (Synergy HT, BioTek, USA). To perform the Picogreen assay on the samples, a 1:1 proportion of the DNA samples mix with TE buffer to reduce the concentration of the DNA samples. Then 50 µL of this master-mix was mixed with 50 µL of working solution in a black 96-well plate, and the fluorescence was measured at the mentioned excitation and emission. Three independent experiments were performed with four replicates per condition.

3.3.9 Statistical analysis

All the experiments described were performed in at least three independent experiments, with typically 4 replicates per experiment. The data were analysed using GraphPad Prism 8 software (https://www.graphpad.com/scientific-software/prism/). The results are expressed as the mean ± standard deviation. Two-way ANOVA and Tukey's multiple comparisons test were performed to test for significance, with statistically significant values defined as $p < 0.05$ for a precise comparison between the viability of the cells exposed to different glass compositions at different time points.

3.4 Results

3.4.1 Cytotoxic analysis of Ga doped bioactive glasses *in vitro*

3.4.1.1. Cell cytotoxic analysis for osteosarcoma Saos-2 cells

The viability of Saos-2 cells was investigated by MTT viability assay following exposure to the conditioned medium containing Bioglass 45S5, 1, 2, 3, 4, 5 mol% Ga doped powder at 10 and 20 mg/mL (Figure 3.2 A and B). The cell viability was assessed as a percentage of the negative control (unconditioned medium). There is a clear dose-dependent inhibition of Saos-2 cell growth with the increase in the accumulation of Ga ions in the medium with all three different concentrations of the glass ($p < 0.0001$). Specifically, a significant cytotoxic effect was observed in the cell growth exposed to the conditioned medium containing 20 mg/mL Ga glass with increasing Ga ions content compared to the control ($p < 0.0001$). Cell growth exposed to 10 mg/mL also demonstrated a steady and significant decrease compared to the control ($p < 0.0001$) in the viability of the cells, but in comparison to the 20 mg/mL Ga glass concentration, cell cytotoxicity was less pronounced.

Ga doped glasses with 1 and 2 mol % showed the least cytotoxic effect on the Saos-2 cell growth, with over 50% of the cell's viability after 10 days of exposure to conditions medium containing 10 mg/mL glass concentration. This was the same with the cells exposed to the medium containing 20 mg/mL, and no significant decrease in cell growth was observed, and over 50% of the cells were viable after 10 days of exposure ($p \geq 0.05$). For the concentration of 10 mg/mL Ga glasses with 4 and 5 mol % a significant decrease in cell growth was observed, with 60% and less than 10% viability after 10 days ($p < 0.05$ and $p < 0.0001$, respectively). Cells treated with conditioned medium containing 20 mg/mL of 4% Ga showed approximately less than 40% of Saos-2 cell viability. Cells exposed to 10 mg/mL 5 mol% of Ga glass compound showed almost 80% cell death after 10 days of treatment with the conditioned medium ($p < 0.0001$). While for the cells treated with the medium containing 20 mg/mL of 5% Ga glasses 100% cell death had been observed after a period of 10 days treatment. There was no significant cell growth reduction by day 10 in Soas-2 cells which were treated with both 10 and 20 mg/mL ($p \geq 0.05$) of Ga free (Bioglass 45S5) conditioned medium comparing to the negative control cells. In all the MTT experiments, etoposide was used, where the cells were

treated with 70% ethanol for 30 minutes as the inducer of the cell death ($p<0.0001$). Two-way ANOVA and Tukey's multiple comparisons test were conducted to test for significance, data are presented as mean ± SD. Significance was set at $p \leq 0.05$, N=5.

3.4.1.2. Cell viability analysis for normal human osteoblast cells

The viability of NHOst cells was investigated by MTT viability assay post exposure to the conditioned medium containing Bioglass 45S5, 1, 2, 3, 4, 5 mol% Ga doped powder at 10 and 20 mg/mL (Figure 3.3 A and B). No significant cytotoxic effect against NHOst cells has been observed after treatment with 10 and 20 mg/mL of all the Ga free as well as Ga containing conditioned medium for a period of 10 days ($p \geq 0.05$). Even the glass concentration of 10 and 20 mg/mL with highest content of Ga (5%) did not cause significant cytotoxicity for the NHOst cells ($p \geq 0.05$). In all the MTT experiment etoposide was used where the cells were treated with 70% ethanol for 30 minutes as the inducer of the cell death ($p<0.0001$).

Two-way ANOVA and Tukey's multiple comparisons test was conducted to test for significance, data are presented as mean ± SD. Significance was set at $p \leq 0.05$, N=5.

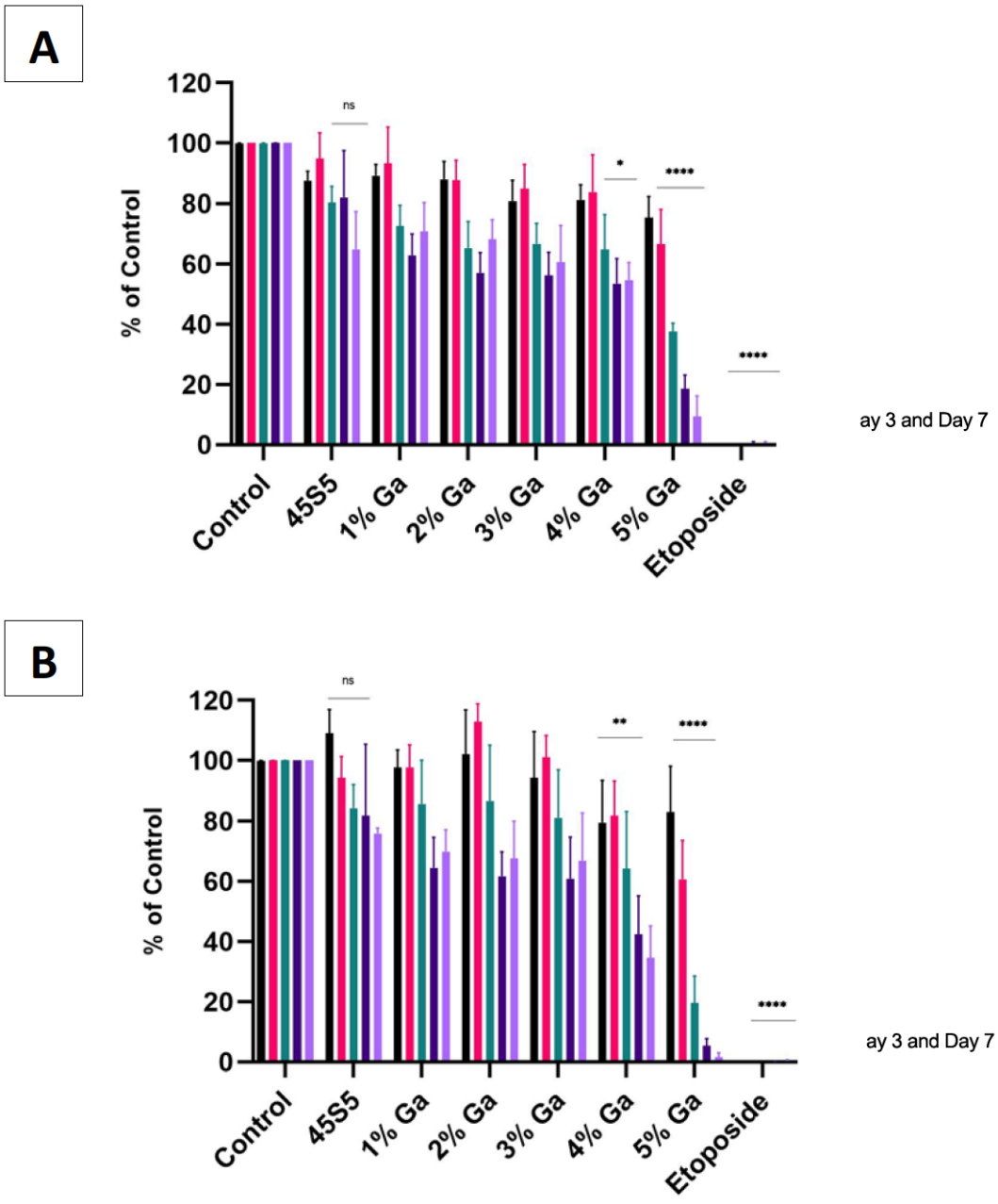

Figure 3.2. The effect of the dissolution products of Bioglass 45S5 and Ga doped silica based bioactive glasses (1-5 mol%) on Saos-2 cells using MTT viability assay. The data is represented as Mean ± SD (N=5) **A)** 10 mg/mL. **B)** 20 mg/mL.

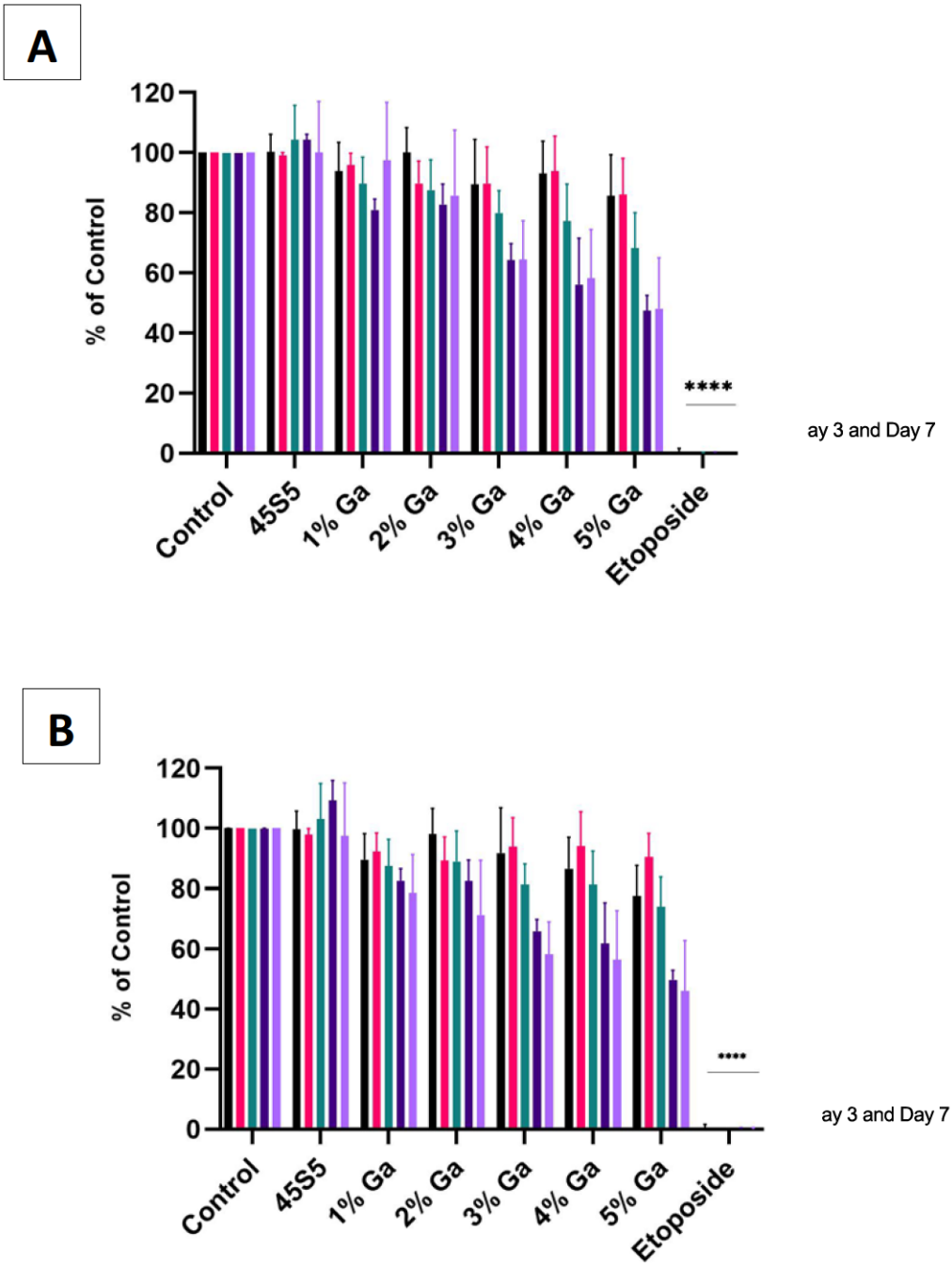

Figure 3.3. The effect of the dissolution products of Bioglass 45S5 and Ga doped silica based bioactive glasses (1-5 mol%) on NHOst cells using MTT viability assay. The data is represented as Mean ± SD (N=5) **A)** 10 mg/mL. **B)** 20 mg/mL.

3.4.2 Investigation of cell viability by Live/Dead assay

Live/Dead assay was used to investigate the cytotoxic effect of the glass dissolution products on the cell's viability. Both Saos-2 and NHOst cells were exposed to the conditioned medium containing 10 and 20 mg/mL of the glass dissolution product for a period of 10 days and the cytotoxic effect was evaluated at the time points day 1, 3, 5, 7, and 10. Live cells are illustrated in green while the dead cells are in red.

As is clear in Figures 3.4 and 3.5 Saos-2 cells treated with dissolution products of bioactive glass 45S5 at 10 and 20 mg/mL for 10 days demonstrated similar viability as the cells cultured in osteosarcoma cell media i.e., negative control. Amongst all the Ga doped glass compounds, Saos-2 cells showed the lowest susceptibility towards the conditioned media of 1 and 2 mol% Ga containing compounds over the course of 10 days at both concentrations of 10 and 20 mg/mL. However, the suppression of the cell growth has started to become more pronounced from the 3% Ga containing glass. The dissolution product of Ga doped glass containing 4 and 5% of Ga demonstrated a significant reduction of the Saos-2 cell growth, both at the concentration of 10 and 20 mg/mL. The cytotoxic effect of Ga ions is obvious from day 3 for 4 and 5% of Ga containing medium, as the cell growth is inhibited alongside cell death. Saos-2 cells treated with conditioned medium containing 5% Ga demonstrated a significant decrease in cell growth. The cell growth was controlled over the course of 10 days, and at the time point of day 10, very few viable cells were observed.

The viability of NHOst cells exposed to the dissolution product of Ga doped glass composition was investigated (Figures 3.6 and 3.7). Unlike for Saos-2 cells, all Ga containing conditioned medium, including 5% Ga content, did not induce severe cytotoxicity for NHOst cells. Cells exposed to the conditioned medium at 10 mg/mL demonstrated any significant detrimental effect on the viability of NHOst cells and even after 10 days of treatment the dissolution product remains nontoxic against the NHOst cells (Figure 3.6), but concentration of 20 mg/mL showed a mild cell growth inhibition for 3-5% Ga (Figure 3.7). The viability of the cells treated with Ga free glass compound (Bioglass 45S5) demonstrated that the dissolution product of the glass both at 10 and 20 mg/mL was non-toxic as the cell viability was the same compared to the negative control (cells grown in medium).

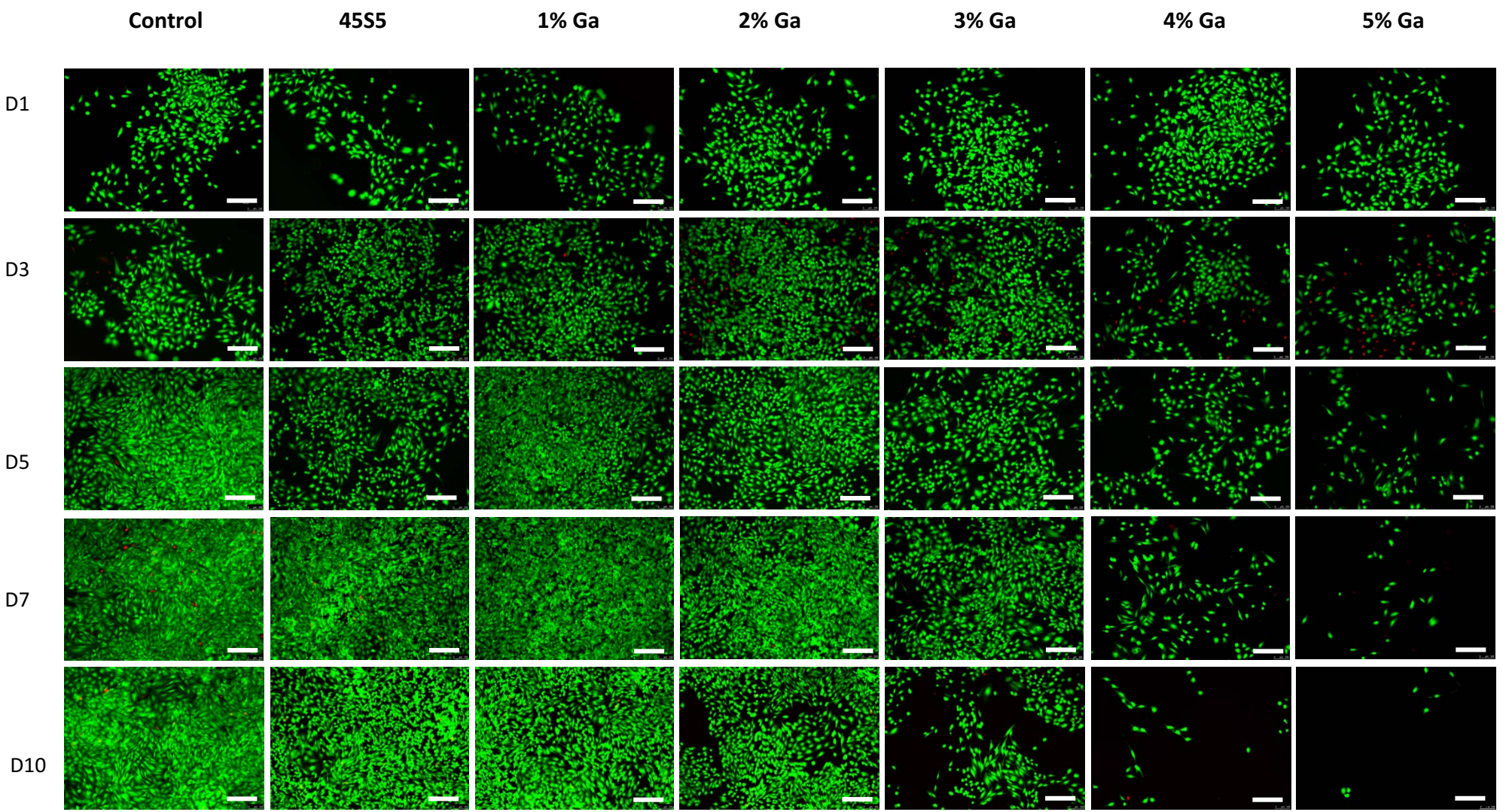

Figure 3.4. Fluorescence images of Live/Dead assay of Saos-2 cells treated with 10 mg/mL of Ga-doped glass dissolution product with time-points of day 1, 3, 5, 7, and 10 (each row represents each time point). Images were taken using a fluorescent microscope at 10x magnification. Live =green and dead=red. Scale bar indicates 100 µm.

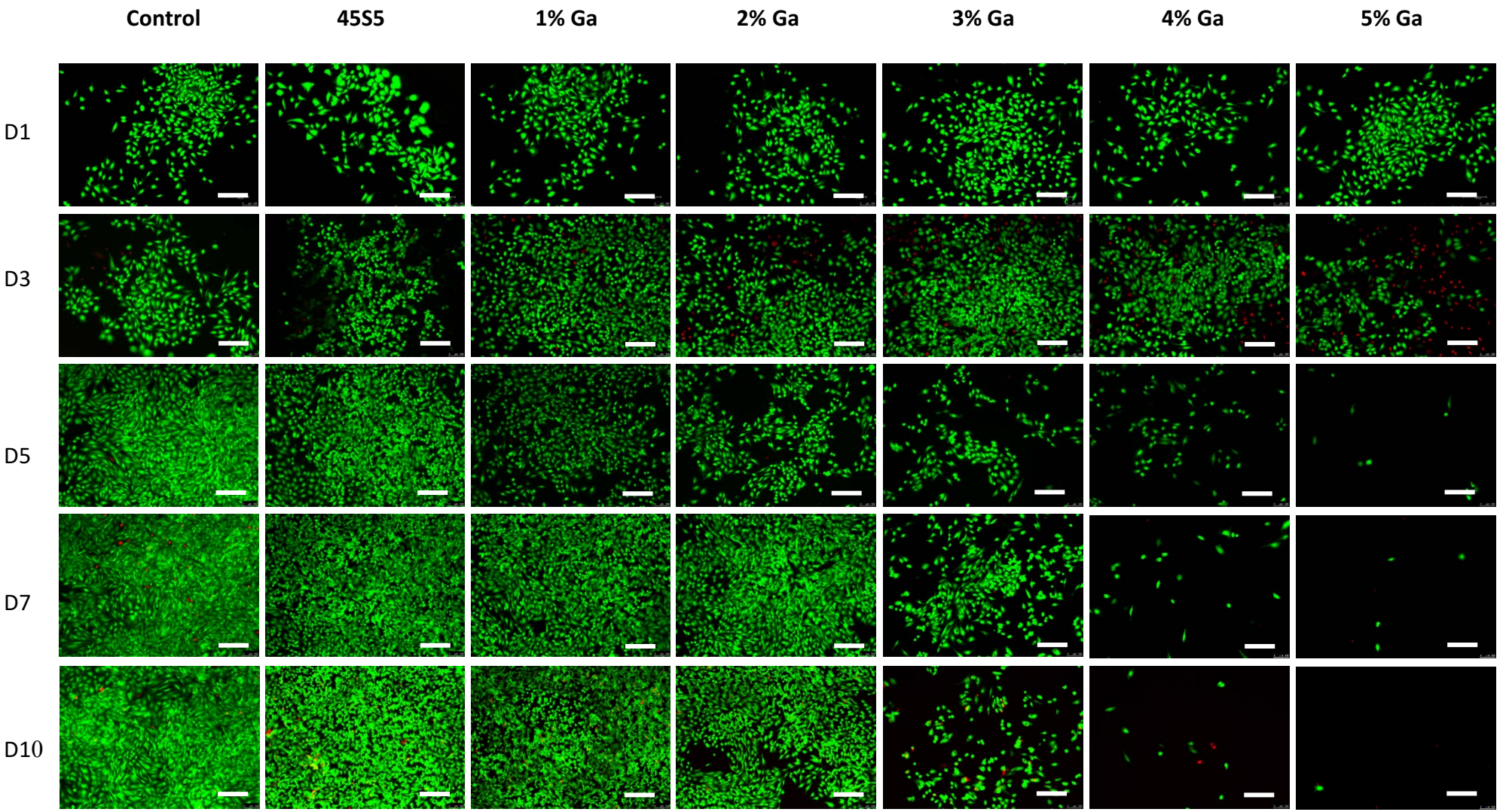

Figure 3.5. Fluorescence images of Live/Dead assay of Saos-2 cells treated with 20 mg/mL of Ga-doped glass dissolution product with time points of day 1, 3, 5, 7, and 10 (each row represents each time point). Images were taken using a fluorescent microscope at 10x magnification. Live =green and dead=red. Scale bar indicates 150 µm.

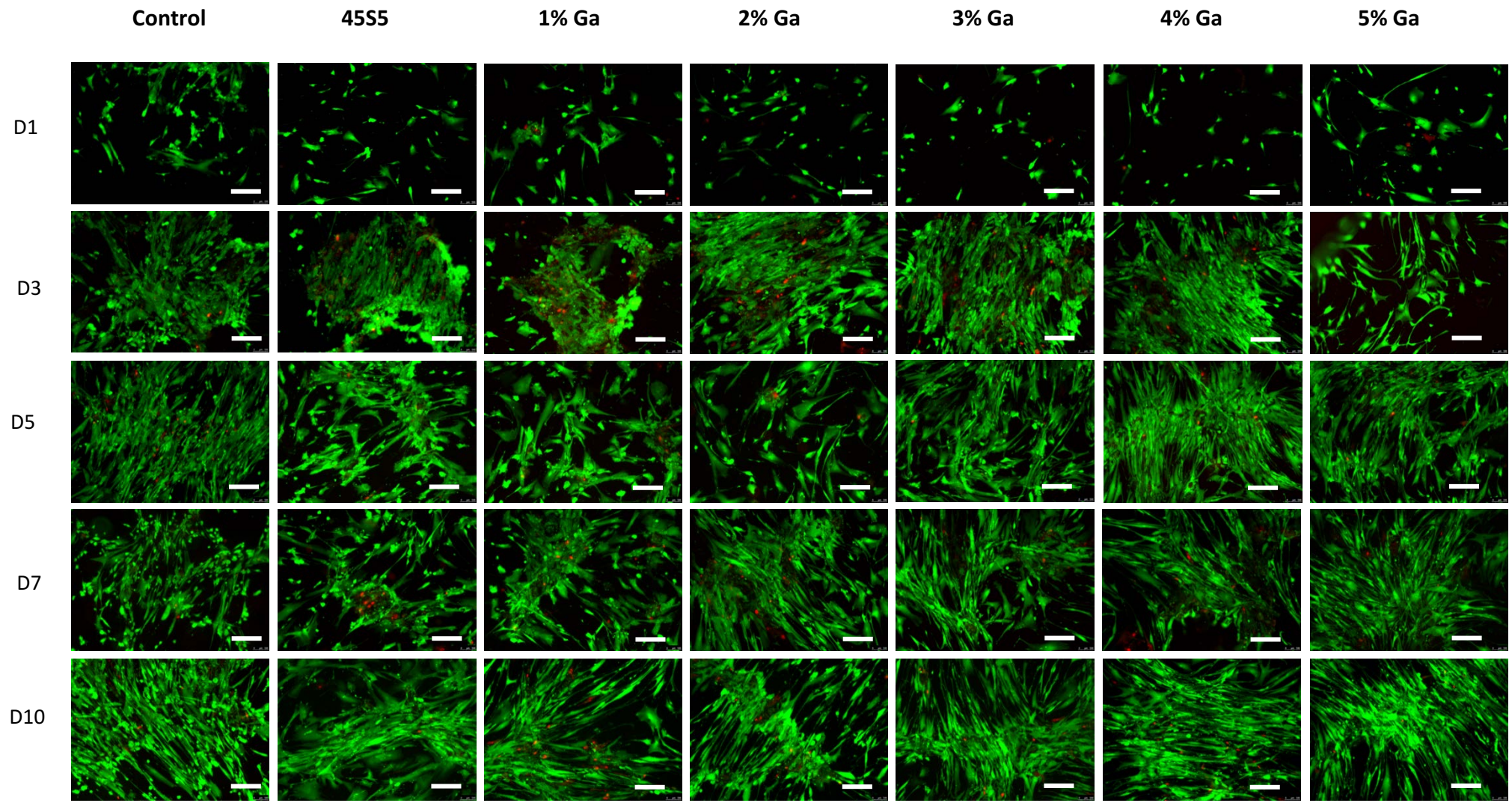

Figure 3.6. Fluorescence images of Live/Dead assay of NHOst cells treated with 10 mg/mL of Ga-doped glass dissolution product with time points of day 1, 3, 5, 7, and 10 (each row represents each time point). Images were taken using a fluorescent microscope at 10x magnification. Live =green and dead = red. Scale bar indicates 150 µm.

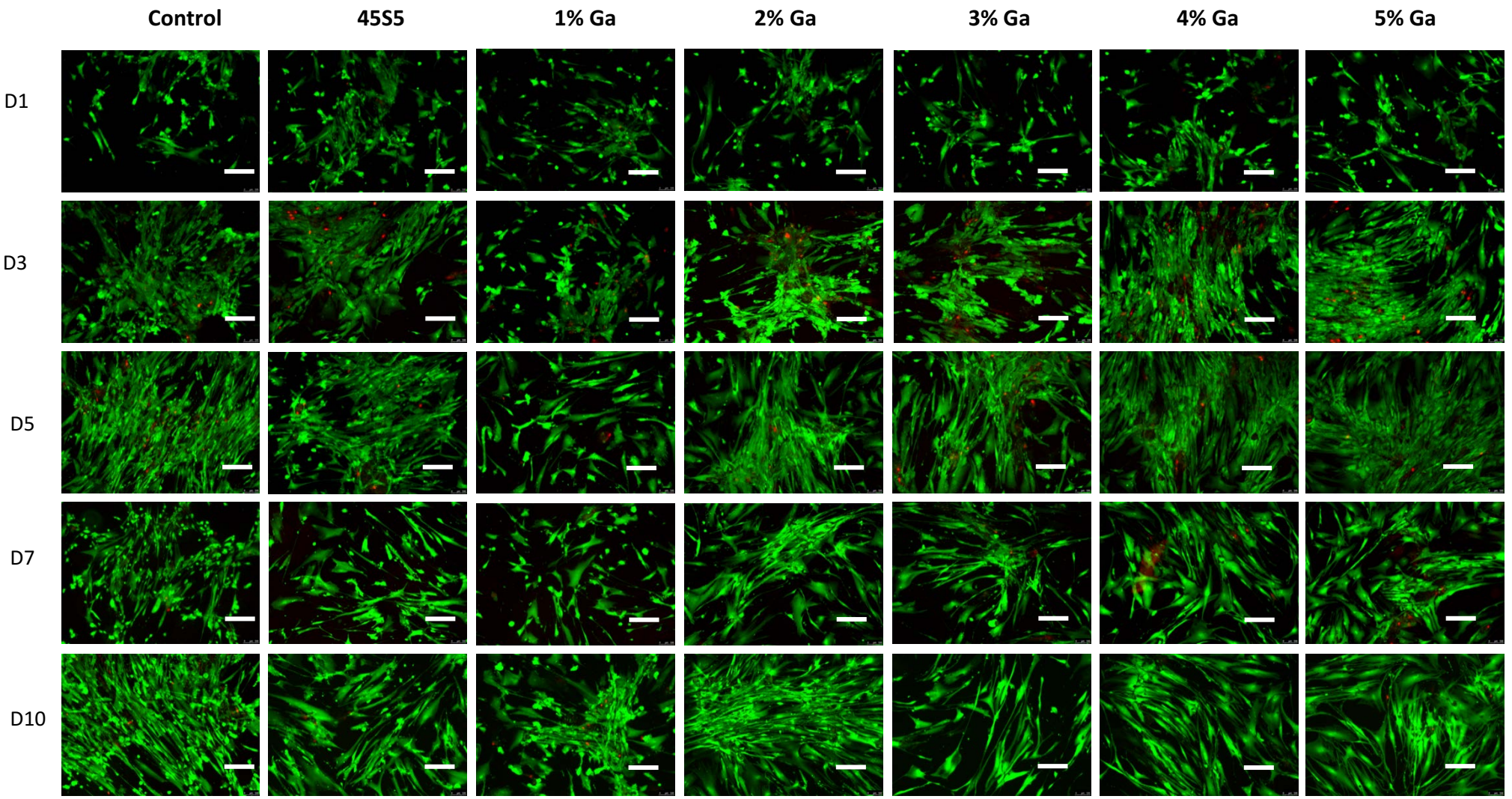

Figure 3.7. Fluorescence images of Live/Dead assay of NHOst cells treated with 20 mg/mL of Ga-doped glass dissolution product with timepoints of day 1, 3, 5, 7, and 10 (each row represents each time point). Images were taken using a fluorescent microscope at 10x magnification. Live =green and dead = red. Scale bar indicates 150 µm.

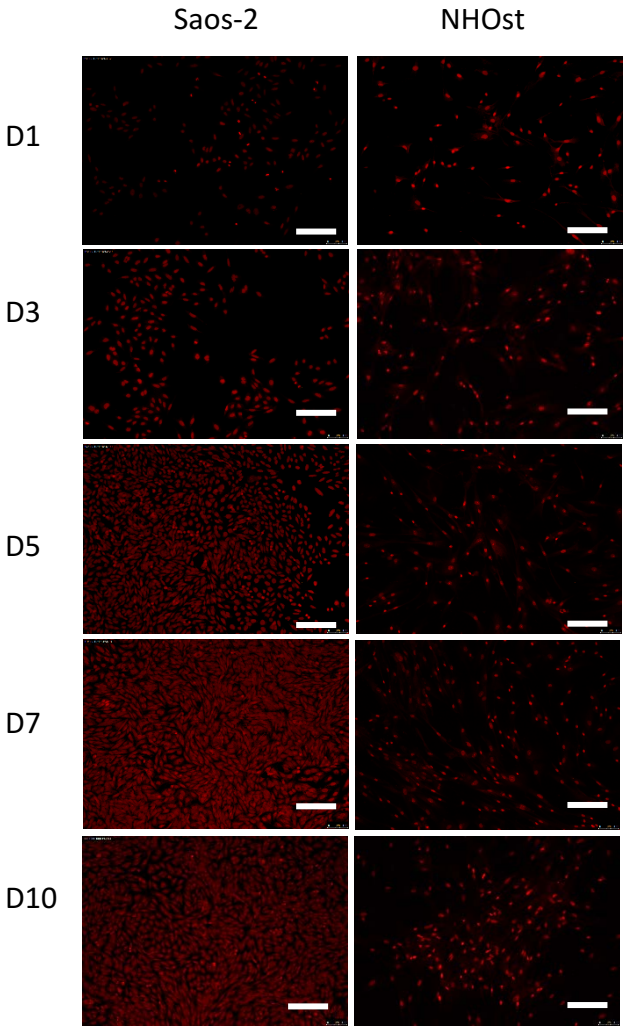

Figure 3.8. Fluorescence images of Live/Dead assay positive controls for Saos-2 and NHOst cells. Cells were treated with 70% ethanol to induce complete cell death and serve as a positive control for cytotoxicity. Fluorescence staining using the Live/Dead viability Kit shows predominant red fluorescence, indicating loss of membrane integrity and non-viable cells. Images were taken using a fluorescent microscope at 10x magnification. Scale bar indicates 150 µm.

3.4.3 Cell proliferation analysis, IncuCyte Live-Cell Analysis system

Cell proliferation was measured using the IncuCyte imaging analyser system. Figures 3.9 and 3.9 represent the microscopic images of Saos-2 cell proliferation exposed to the conditioned medium, captured by IncuCyte imaging system. The results clearly indicate that Ga-BGs can suppress the growth of osteosarcoma Saos-2 cells in a dose-dependant manner in both concentrations of 10 and 20 mg/mL. The cell growth exposed to the conditioned medium containing 45S5 BGs was approximately 90% and 85% for the concentrations of 10 and 20 mg/mL (respectively) for the course of 10 days. This indicates that the composition of Bioglass 45S5 compound does not interfere with the growth of Saos-2 and in fact, the cell growth suppression is due to the increased concentration of Ga ions rather than the composition of the bioactive glass itself. The cells exposed to the conditioned media containing 1 and 2 mol% Ga at the concentration of 10 mg/mL showed the lowest susceptibility after 10 days of treatment. The cells exposed to the conditioned medium containing 3 and 4 mol% Ga-BGs at the concentration of 10 mg/mL demonstrated about 70% cell growth while the concentration of 20 mg/mL showed 30% growth of the cell for the mentioned compounds. The 5 mol % Ga doped glass showed the highest cell growth suppression for both concentrations of 10 and 20 mg/mL. The cell growth was under 5% for 10 mg/mL, while less than 1 % of the cells were alive in 20 mg/mL at day 10, with a faster rate of cell growth inhibition, whereby less than 10% of the cells were viable at day 5.

NHOst cells were exposed to conditioned medium as mentioned above. None of the conditioned media containing Ga ions had detrimental effects on cellular proliferation and conformation. Even the cells exposed to 5% Ga-BGs at both 10 and 20 mg/mL concentration proliferate and had over 90% confluency after 10 days of treatment (Figures 3.11 and 3.12).

3.4.4 Cell migration analysis-IncuCyte Live-Cell Analysis system

Cell migration data for Saos-2 cells as a function of time is shown in Figures 3.13 and 3.14. Quantitative data for the scratch wound as a percentage of the original scratch width is shown in Figure 3.14 B. As shown, the wound is almost completely closed for the negative control (~70% closed) and the 45S5 bioactive glass control (~60% closed) within 24 hours. After 3 days, the wound is completely closed for negative control, Ga free and the 1-3% Ga-BGs. However, cells exposed to media conditioned using the 4 and 5% Ga at the concentration of

20 mg/mL still had clearly visible scratch wounds. Specifically, the scratch size for the samples exposed to the 5% Ga containing samples started to become wider on day 10 which suggest the cytotoxic effects of Ga ions on the OS cells.

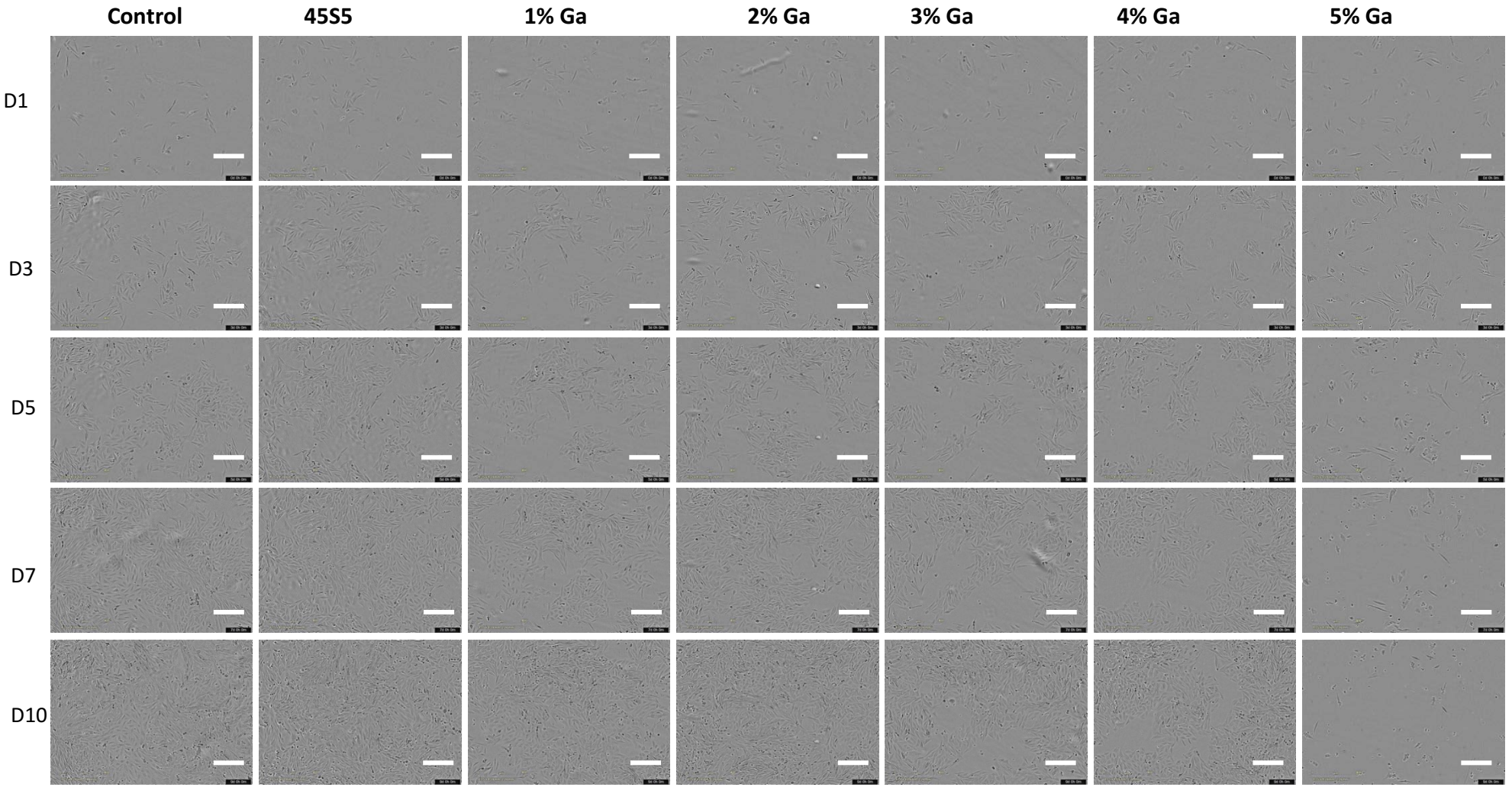

Figure 3.9. Representative microscopic images of Saos-2 cell proliferation treated with bioactive glass composition conditioned medium containing 10 mg/mL glass dissolution product. Cell growth monitored in real time using IncuCyte image analyser 10X objective over a 10-day period. The images captured on day 1, 3, 5, 7 and 10. Scale bars=400 µm.

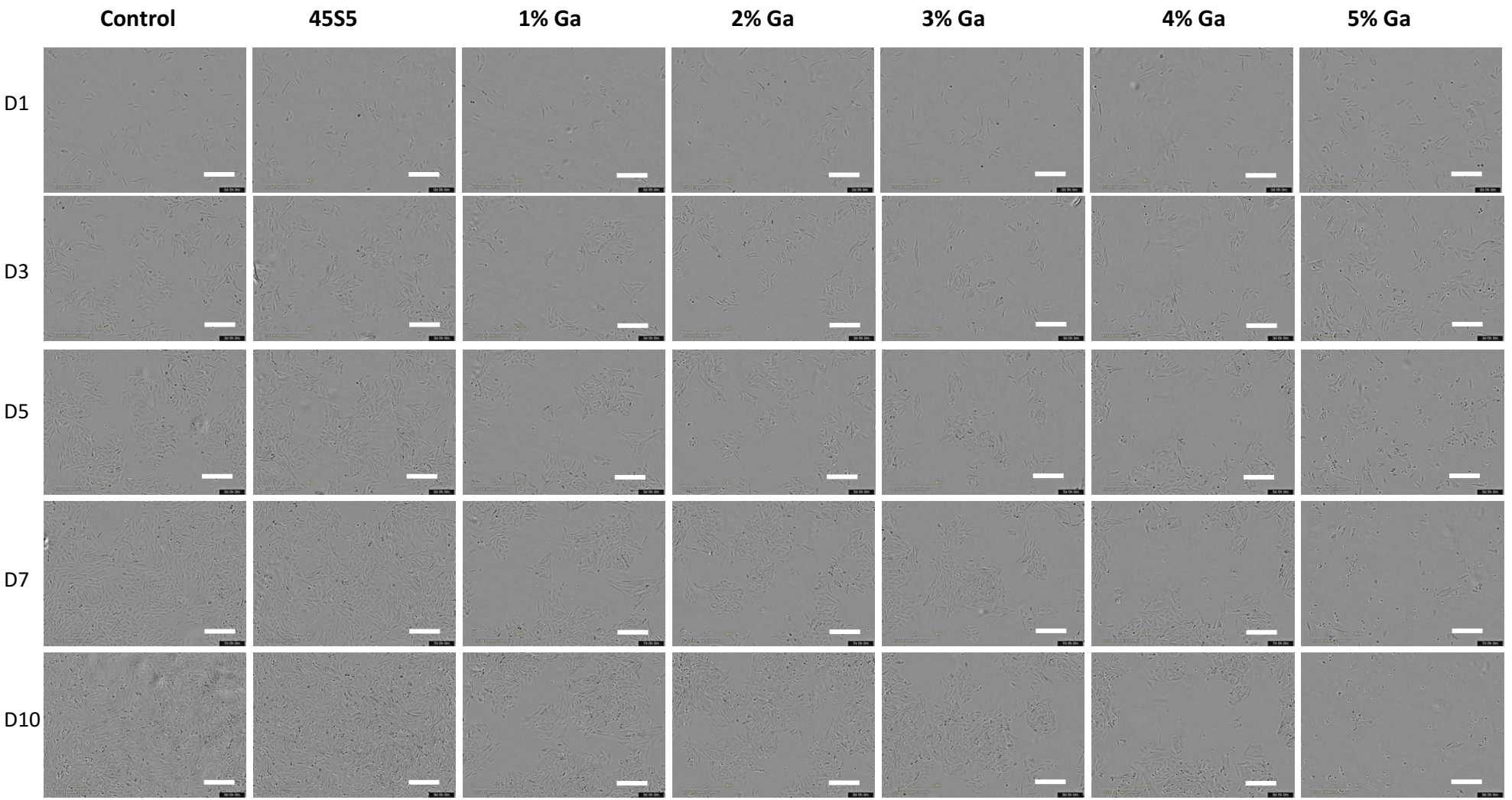

Figure 3.10. Representative microscopic images of Saos-2 cell proliferation treated with bioactive glass composition conditioned medium containing 20 mg/mL glass dissolution product. Cell growth was monitored in real time using an IncuCyte image analyser with a 10X objective over a 10-day period. The images were captured on days 1, 3, 5, 7 and 10. Scale bars = 400 µm.

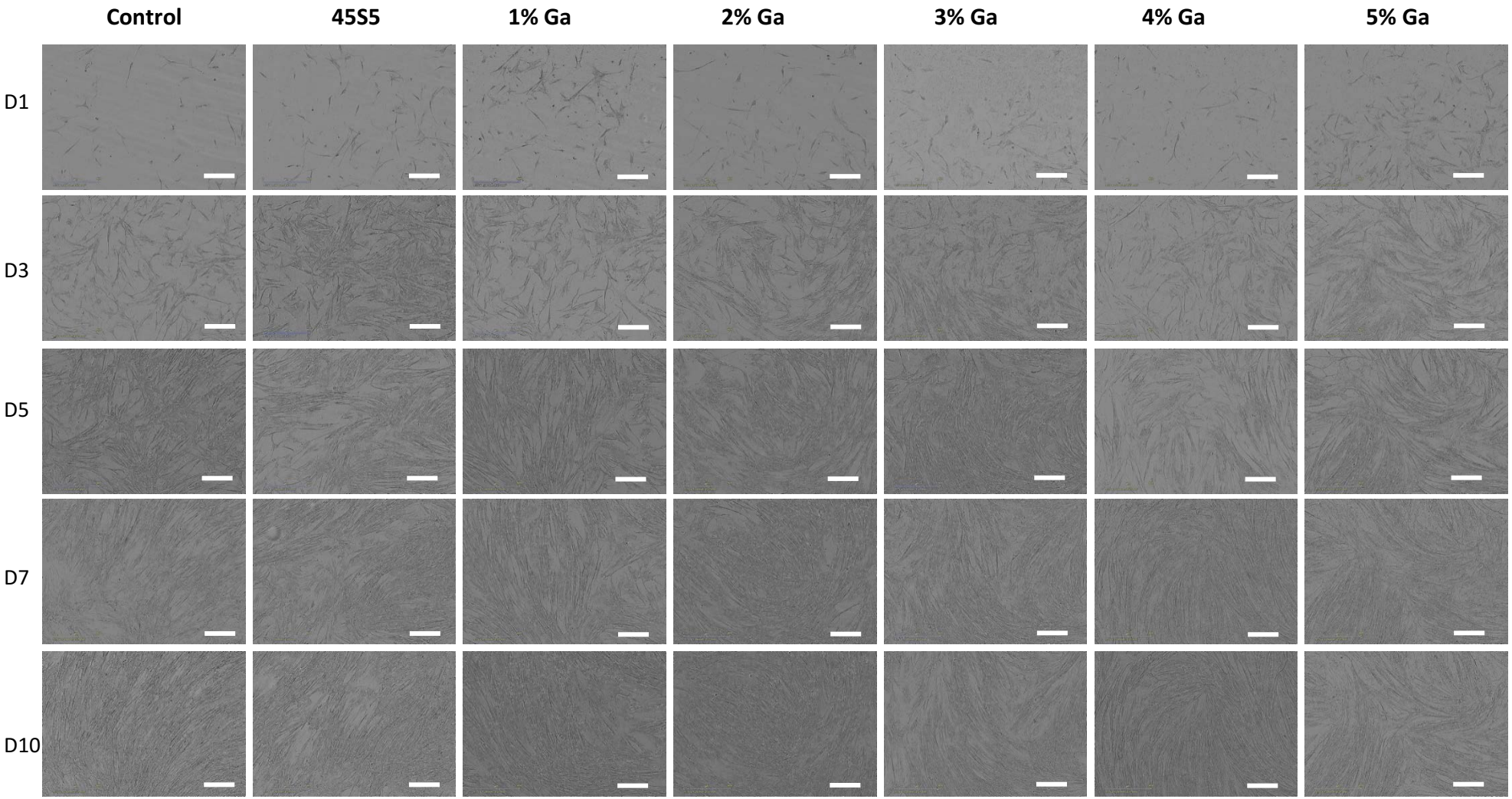

Figure 3.11. Representative microscopic images of NHOst cell proliferation treated with bioactive glass composition conditioned medium containing 10 mg/mL glass dissolution product. Cell growth was monitored in real time using an IncuCyte image analyser with a 10X objective over a 10-day period. The images were captured on day 1, 3, 5, 7 and 10. Scale bars = 400 µm.

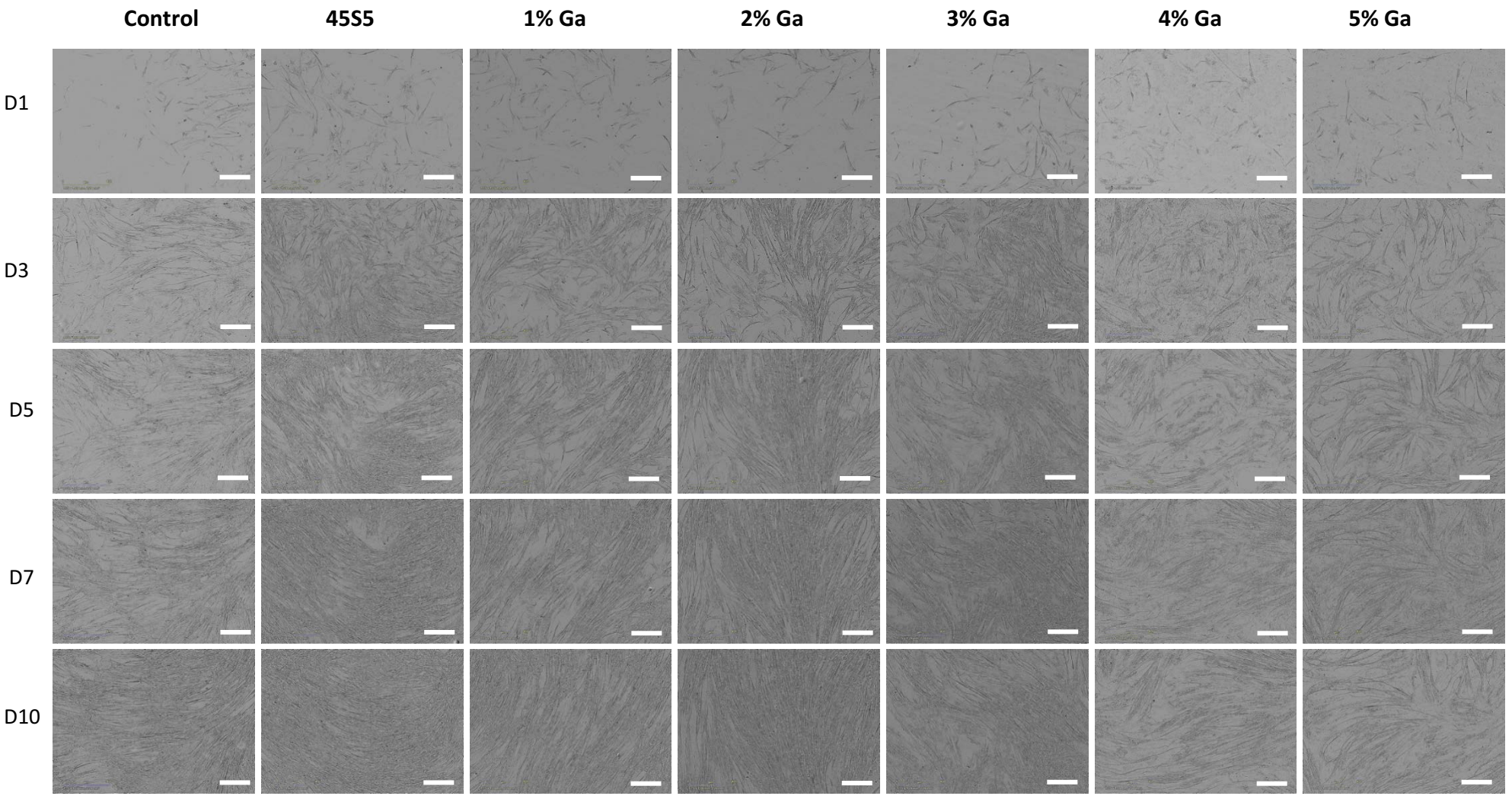

Figure 3.12. Representative microscopic images of NHOst cell proliferation treated with bioactive glass composition conditioned medium containing 20 mg/mL glass dissolution product. Cell growth was monitored in real time using an IncuCyte image analyser with a 10X objective over a 10-day period. The images were captured on day 1, 3, 5, 7 and 10. Scale bars = 400 µm.

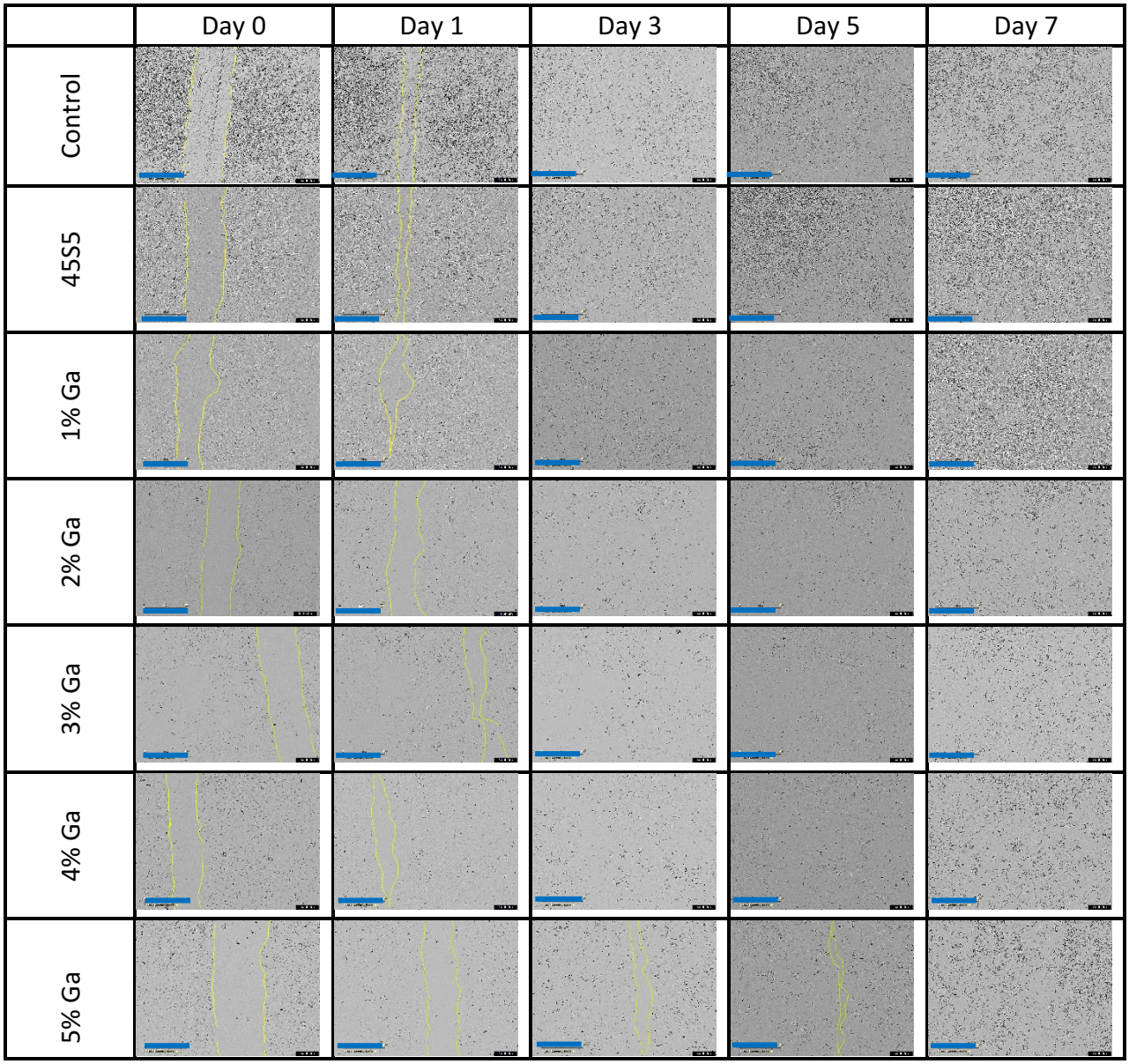

Figure 3.13. Cell migration images for Saos-2 cells as a function of time at 10 mg/mL.

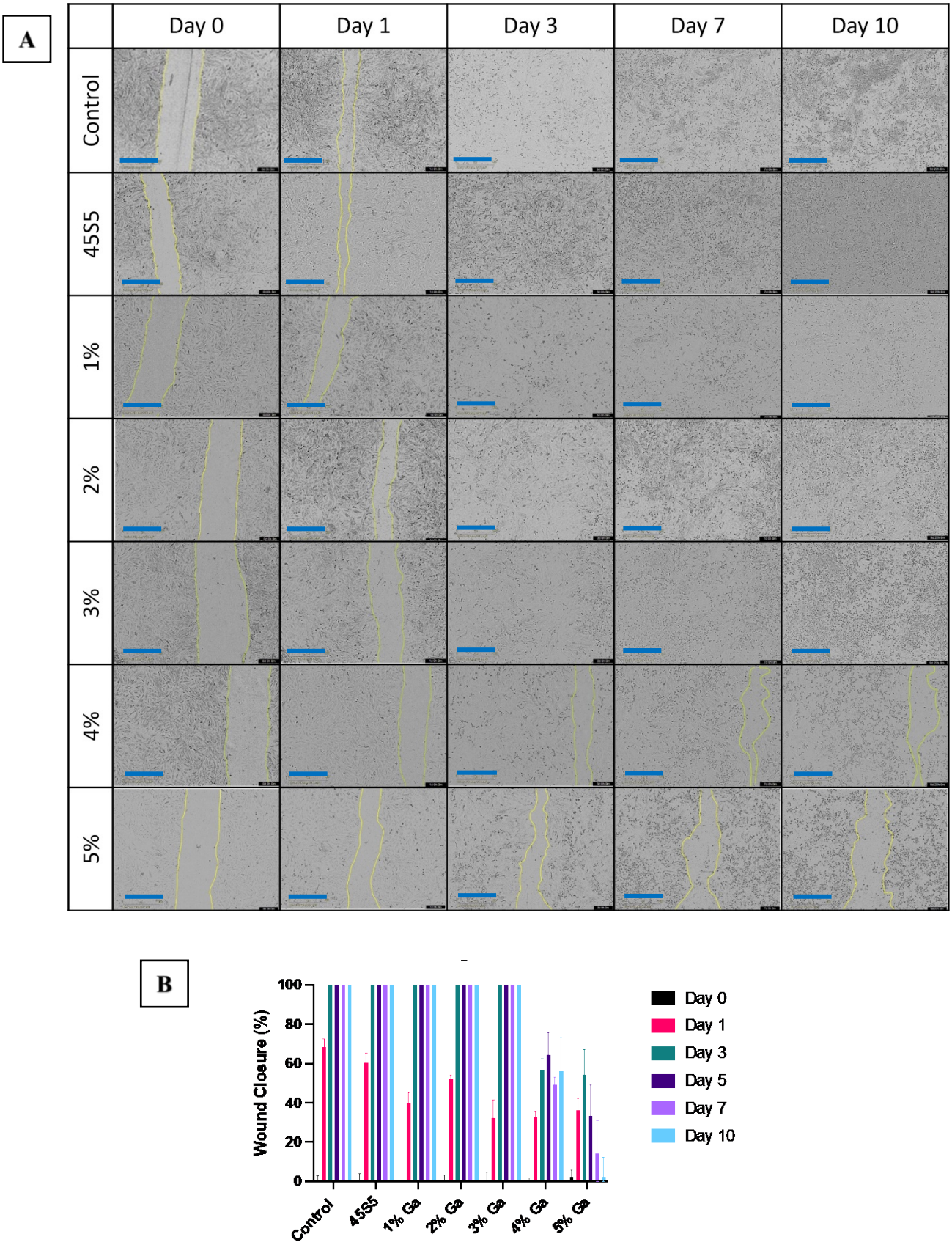

Figure 3.14. (A) Cell migration images for Saos-2 cells at 20 mg/mL as a function of time. **(B)** Quantification of the scratch wound data.

3.4.5 PicoGreen ® assay

Saos-2 and NHOst cells were exposed to the Ga containing conditioned medium as well as Ga free glass compositions. The cytotoxic effect of the glass compounds on the cells was investigated by measuring the dead cells in the cells' supernatant for a period of 10 days and comparing the results with the controls. The PicoGreen ® assay was used to evaluate the DNA content of the cells post-exposure to the conditioned medium with the time points at day 3, 5, 7, and 10 (Figure 3.15 and Figure 3.16). This assay is based on the quantification of DNA content within the cell lysate, while other tests, such as MTT, measure the metabolic activity of the cells. Therefore, it is possible to measure accurately the DNA content of the dead cells for each cell culturing with the conditioned medium to investigate the glass cytotoxicity against the cells.

As seen in Figure 3.15 the cell death has a slow rate during the first 7 days of treatment for the control and Ga free glass composition (Bioglass 45S5) at both concentration of 10 and 20 mg/mL (around 100 to 150 ng/mL) while for the time point of day 10 the cell death is significantly higher (approximately 400 ng/mL). The cells treated with conditioned medium containing Ga ions demonstrated a significant cell death during the first 5 to 7 days for both concentrations of the glasses comparing to the controls. Cell death for samples exposed to 10 mg/mL of 3% and 4% Ga ion containing conditioned medium is slightly higher comparing to the 5% Ga glass composition on day 10 while this is the case only for the 3% Ga ions content glass compounds for the concentration of 20 mg/mL and 4% and 5% Ga glass compositions both showed slightly lower cell death on time-point day 10.

Figure 3.16 demonstrates the PicoGreen® assay results for the NHOst cells exposed to the conditioned medium containing Ga doped bioactive glasses, and as it is clear, the cellular behaviour post-exposure to the conditioned medium is different in comparison with Saos-2 cells. The NHOst showed significantly lower content of dsDNA in the cell supernatant and therefore lower cell death compared with Saos-2. The highest content of dsDNA in cell supernatant was observed in the samples exposed to 20 and 10 mg/mL of 5% Ga content conditioned medium with the values of around 40 and 30 ng/mL, respectively. However, this value is 10-fold lower compared to the PicoGreen® assay results of Saos-2 cells. The other composition of the Ga doped glasses showed an extremely low level of cell death regardless of the concentration of the bioactive glasses in the conditioned medium.

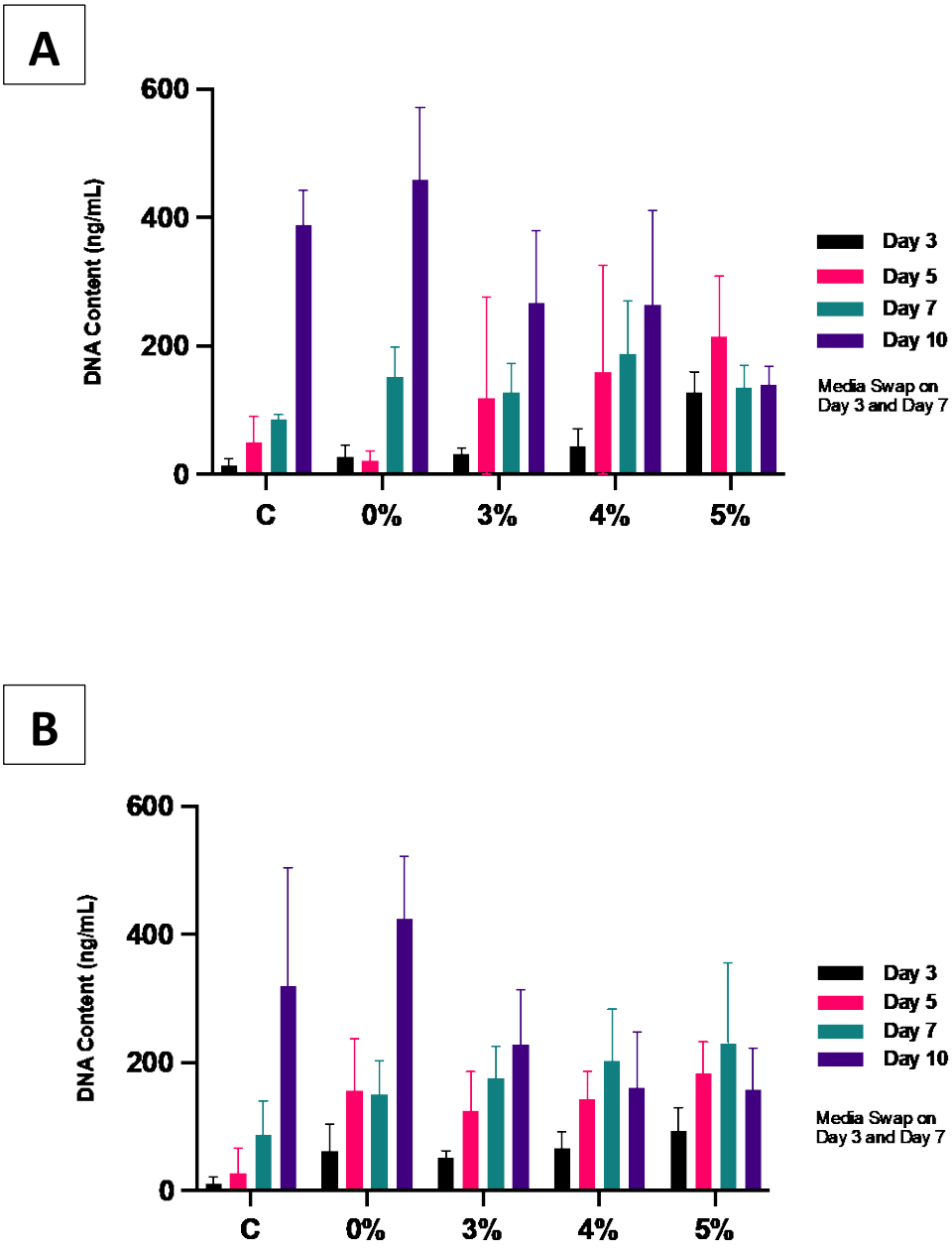

Figure 3.15. Saos- 2 cells exposed to Ga doped glasses conditioned medium containing 3%, 4% and 5% of Ga **A)** 10 mg/mL. **B)** 20 mg/mL. The data is represented as Mean ± SD (N=4).

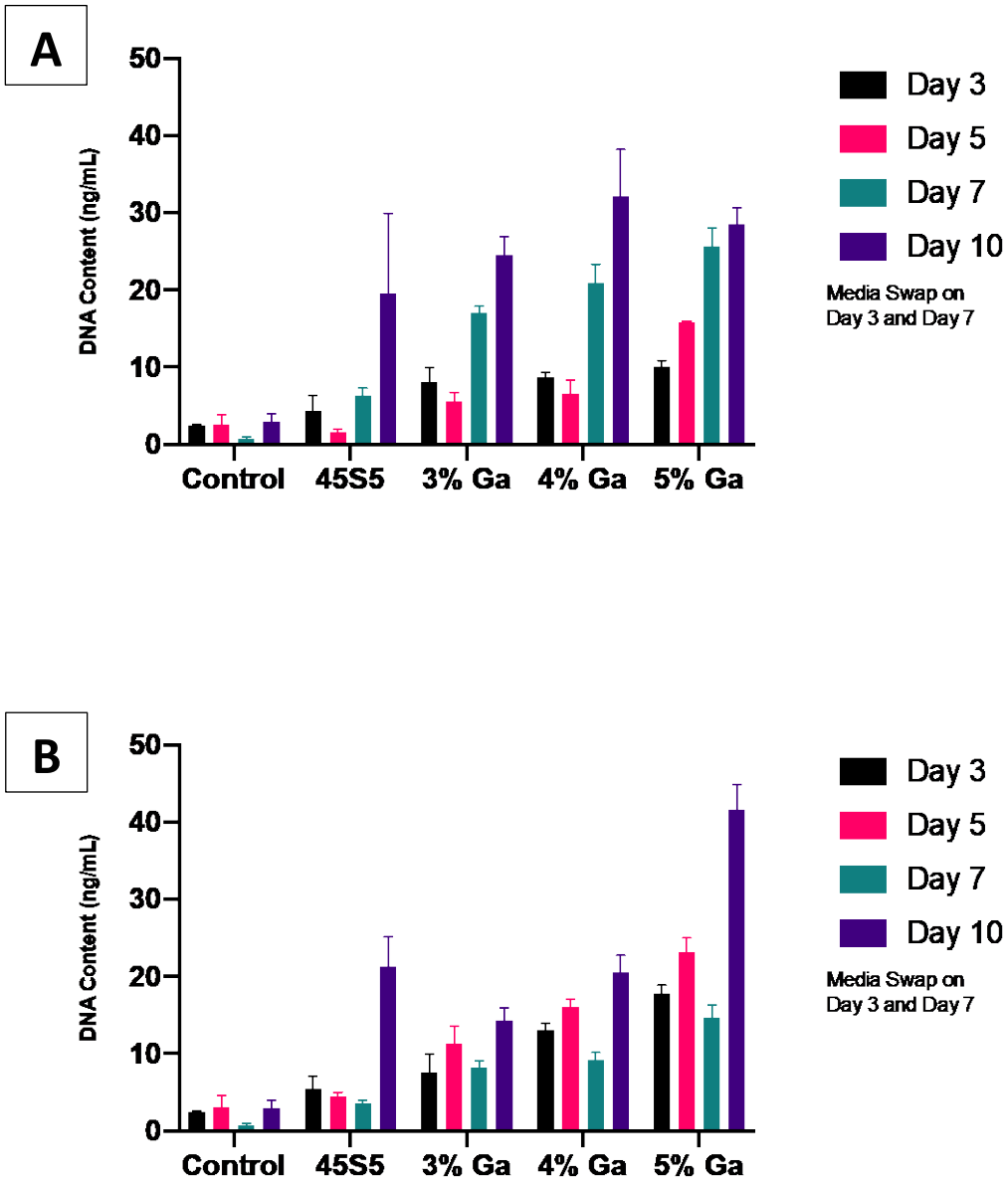

Figure 3.16. NHOst cells exposed to Ga doped glasses conditioned medium containing 3%, 4% and 5% of Ga **A)** 10 mg/mL **B)** 20 mg/mL. The data is represented as Mean ± SD (N=4).

3.5 Discussion

During the last few decades, a wide range of different bioactive glass-ceramics have been introduced with clinical applications, with a focus on orthopaedic treatments due to their remarkable properties, such as bioactivity, cytocompatibility, osteostimulativity and osteoconductivity [13]. Bioactive glass stimulates the formation of an apatite layer on its surface when implanted into the body. This layer is formed due to the release of Ca and P ions from the glass. The precipitation of hydroxyapatite (HA) stimulates strong integration of the bioactive glass with the host tissue [14-16]. The incorporation of other therapeutic elements into the structure of bioactive glasses can improve their therapeutic performance as well as modifying their physical and mechanical characteristics, for example borate based bioactive glass for purpose of tissue regeneration, silver (Ag) incorporation can induce anti-inflammatory and antimicrobial properties or doping copper (Cu) ions in bioactive glass to induce antineoplastic properties for hyperthermia therapy [17, 18].

Osteosarcoma is a highly malignant tumour in bones with an extremely poor prognosis. Patients who go through resection and adjuvant and neoadjuvant chemotherapy may result in 5-year survival rates of over 60%, but a fatal outcome due to drug resistance, regional recurrences or tumour metastasis are unavoidable. Thus, identifying a reliable platform is critical for detecting high-risk patients and administering early treatments to enhance osteosarcoma patients' survival rates [19]. Gallium is the most commonly used metal ion for the treatment of cancer after platinum. It is a great choice to manipulate the properties of bioactive glass because of antineoplastic effects when it is in its ionic form, antibacterial and anti-inflammatory characteristics, and its capacity to control bone resorption [20, 21]

The aim of this study was to investigate the cytotoxic effects of 45S5 and 1-5 mol% Ga doped glasses on the viability and proliferative behaviour of osteosarcoma Saos-2 and primary NHOst cells. This was accomplished by evaluating the effect of dissolution products of bioactive glasses on the mentioned cells. Ga ions were effectively integrated into the silica-based bioactive glasses and were found to generate a strong cytotoxicity for Saos-2 cells. A significant reduction in the Saos-2 cell’s viability has been observed in a dose dependant manner in MTT results which is due to the Ga content of the bioactive glasses present in the dissolution product of the conditioned medium. When compared to Ga-free glass and control medium, Ga-containing glasses were found to have minimal reduction in cell viability of

NHOst cells. This suggests Ga ions selectively stimulate toxicity in OS cells while sparing NHOst cells. This selective mechanism of toxicity in Ga containing OS cells can be attributed to the differing uptake of Ga ions by cancer cells, which disrupts essential cellular processes like DNA synthesis and mitochondrial function. The conditioned medium containing 20 mg/mL of 4 and 5% Ga was the most toxic glass composition for the Saos-2 cells with almost 60% and 99% reduction in viable Saos-2 cells respectively, in the MTT assay.

The results from the Live/Dead assay were also in agreement with the MTT for the level of cytotoxic effect of Ga doped bioactive glass on Saos-2 and NHOst cells. The results showed the selective cytotoxic effects of Ga ions in Saos-2 cells. According to Live/Dead results, the Saos-2 cell population decreased with increasing Ga content of conditioned media. However, this cytotoxic effect does not show as an increase in the red fluorescence signal, which is indicative of dead cells at higher Ga concentrations. The reason is that dead cells often lose their ability to adhere to the culture surface due to the breakdown of cell-matrix interactions and cytoskeletal structures and are washed during the Live/Dead assay washing steps. However, the results from the proliferation assay performed by IncuCyte real-time imaging highlight the dose-dependent nature of this selective cytotoxic effect, which indicates the accuracy of the Live Dead assay method. It suggests Ga-BGs stimulate a strong cytotoxic effect on Saos-2 in a dose-dependent manner. In contrast, the Live/Dead images showed NHOst cells kept a high level of viability across different concentrations of Ga ions. This was evidenced by the green fluorescence in the assay images. Therefore, it was proven again that Ga ions selectively induce cytotoxic effects. The data obtained was supported by IncuCyte Live-Cell Imaging systems and the PicoGreen assay.

These findings align with earlier studies that have demonstrated the selective toxicity of Ga-containing compounds against cancer cells. For instance, Yazdi *et al* reported zinc borate-based bioactive glasses with 5 wt % Ga using glass degradation extracts that can suppress osteosarcoma cell growth without severe cytotoxic effects on preosteoblast cells through MTT and LIVE/DEAD assay [5]. It was reported that the mentioned dissolution product had an inhibitory impact on Saos-2 cells' growth after 28 days of exposure.

Many studies have proven the cytotoxic effect of the different Ga compounds on the cancerous cells [21-24]. However, the method of administration is an important factor in the efficacy of Ga ions for the treatment of cancer, as well as the cytotoxic effects on different

healthy tissues. It has been reported in several studies, Ga bioavailability is low following oral administration. Also, other studies stated that oral administration can have dose-dependent repressing effect on biosynthesis of heme and hepatic oxidative stress along with the primary immune response. On the other hand, the parenteral route generates great bioavailability and efficacy, but renal toxicity is one of the limiting factors to achieve appropriate efficacy [25]. Kelsen *et al.* demonstrated that a considerable dose of Ga is excreted through the kidneys, which reduces the efficacy of Ga and also has implications for its renal toxicity [26]. Also, another negative aspect of intravenous injection is the requirement for a facility for gallium nitrate injection, such as a pump device for continuous infusion.

Bioactive glasses naturally release compositional ions and gradually degrade post exposure to the aqueous medium, which are calcium, silicon, sodium, phosphorus, and gallium in this present case. Ga-BGs provide a platform for the safe delivery of Ga ions, which specifically target cancer cells, stimulating the cell death of the bone cancer cells. However, not very many studies used glass as a delivery system for Ga ions for OS applications with minimum side effects of the method of administration.

It has been proven that Ga ions localised into the cancer cells via surface transferrin receptors (TfR) [27]. It is important to know that tumour cells possess significantly more TfR compared to non-cancer cells, as TfR1 expression is extremely elevated in highly proliferative cells, including cancer, intestinal epithelium, basal epidermis, and certain activated immune cells [28]. TfR is an ideal choice to target cancer cells due to its high proportion in malignant cells, its relevance in cancer, and its extracellular accessibility[29]. It is often overexpressed at levels several-fold higher than normal cells, and that is the reason it has been recognised as a universal cancer marker [30]. The expression of iron metabolism genes was investigated in tumour tissues and adjacent tissues. The expression of *TFRC* was increased by 3-fold in cancer compared to the normal tissue, which demonstrated higher iron intake in cancer progression. Also, the expression of *FTH1,* which is a cellular iron utilisation gene and *FLCVCR1,* an iron efflux genes, were increased in tumour tissue by over 5-fold [31].

Ga mechanisms of action have been illustrated by current research studies, including 3D DNA structure alteration, DNA polymerisation inhibition and protein synthesis dysregulation. In addition, it has been observed that Ga induces apoptosis via the mitochondrial pathway. Ga can activate Bax protein, which translocates to mitochondria, and this results in piercing in

the mitochondrial membrane and the release of mitochondrial cytochrome C and activation of caspase-3. These sets of events ultimately result in the cell's apoptosis [32-34].

In the current study, results from MTT, Live/Dead and PicoGreen assay demonstrated the non-toxic nature of Ga free glass compositions as the conditioned medium has no detrimental effect on the cell growth, neither Saos-2 nor NHOst cells. Cell viability was 70% and 80% for Saos-2 cells post-treatment with G-free conditioned medium at 10 and 20 mg/mL, respectively, after 10 days of treatment. While for NHOst cells, the viability at the mentioned concentrations was 100%. This was supported by results from the IncuCyte image analysis, as the cellular morphology was similar for cells exposed to undoped conditioned medium and controls, and no unusual cellular conformation had been observed. This was in line with data from LIVE/Dead assay. Therefore, it is evident from the data that the composition of bioactive glass is not the reason of the cell growth inhibition, and the toxicity is due to the efficacy of the Ga ions in the conditioned medium rather than the composition of the glass and the other ions released into the conditioned medium (Na, Ca, P and Si). However, according to the PicoGreen results a higher cell death for Saos-2 cells, around 400 ng/mL for both 10 and 20 mg/mL, has been observed for the mentioned glass at the time-point of day 10. This is due to the extremely high population of the cells after 10 days of treatment. The cellular confluency after day 7 is extremely high, and the cells cannot grow any more due to a high cell population, nutrient consumption and a rise in cytotoxic metabolites, and the cells go from the stationary phase to the death phase, which ultimately results in cell death [35].

Scratch wound assay was performed to investigate the effect of Ga ions on the migratory capacity of saoos-2 cells, which is a critical factor in cancer metastasis. The results showed a significant inhibition of migration in Saos-2 cells. The wound closure was markedly slower in treated cells, particularly at higher Ga concentrations, compared to untreated controls. This indicates that the presence of gallium ions decreased cell mobility in the wound healing assay. The results show that the number of cells moving into the scratched region was considerably lower in the groups exposed to 4 and 5% gallium-containing media from time points 72 hours onwards. After a period of 10 days, the wound size of the cells exposed to 20 mg/mL of 5% gallium conditioned medium was almost the same as the initial scratch.

The quantitative analysis demonstrated that after 24 hours, the wound area in the group treated with Ga-BGs was only 40% closed, in contrast to a 70% closure in the control group.

The assay images clearly demonstrated decreased cell migration in the presence of Ga, suggesting a dose-dependent inhibition of cell motility for 4% and 5% Ga containing samples. Cells treated with 5% Ga conditioned media started to increase the wound area from day 5 and at day 10 the wound closure area was ~ 5%. This indicates the extreme cytotoxic effects of Ga ions on Saos-2 cells. The inhibition of Saos-2 cell migration by Ga-BGs may be linked to disruptions in cytoskeletal organisation and the cellular signalling pathways that govern motility. Ga ions are known to disrupt iron metabolism, which is essential for several cellular functions, including migration. The observed decrease in wound closure could result from impaired cell proliferation and motility caused by these disruptions. The notable decrease in Saos-2 cell migration observed in this study indicates that Ga-BGS have a promising potential for inhibiting OS metastasis. By limiting the spread of cancer cells, this material may enhance the efficacy of localised treatments and improve overall patient outcomes [36, 37].

The PicoGreen results of the cells treated with Ga containing conditioned medium demonstrated a noticeable cell death during the initial stage of the cell growth for both 10 and 20 mg/mL, which is the result of the cytotoxic effect of Ga ions present in the conditioned medium. Due to high cell death post the initial treatment with 5% Ga conditioned medium the cell population decrease dramatically, and this explains the lower rate of cell death during day 10 comparing to the controls. The cell death for the cells were exposed to 10 mg/mL of conditioned medium with 3, 4 and 5% Ga follow a dose dependant manner as for the 3% there are more cell death than 4% than 5%, 260, 250 and 140 ng/mL respectively. This is because the cytotoxic effect of the 3 and 4% glass composition induces less severe toxicity for the cells compared to 5% Ga composition; therefore, this results in more cell growth and higher cell population, as well as confluency of the cells and higher cell death is expected. While the 20 mg/mL concentration of the conditioned medium only 3% Ga content showed higher cell death by day 10 (230 ng/mL) and had an upward trend. The cells exposed to the 4 and 5% Ga content medium follow the same pattern up to day 7 and on the day 10 the cell death decreased (160 and 150 ng/mL in order). That is because the concentration of 20 mg/mL stimulates a higher level of toxicity for the cells post the initial treatment and the cytotoxic effect during the first 7 days is extremely strong, preventing more cell growth and causing high cell death and by day 10 the cell population is lower. These results are in line with the results from MTT and Live/Dead assay results. Taken together, these findings suggest that the

Ga doped glass composition not only induces toxicity for the OS cells with increase in the content of Ga in each glass composition, but also with the increase in the concentration, they stimulate a higher level of toxicity. In contrast, the viability results for the NHOst cells exposed to the Ga doped bioactive glasses showed extremely high levels of viability and minor toxicity compared to the Saos-2 cells. This is extremely promising as it confirm, even the highest content and concentration of the Ga-BGs do not cause any significant toxicity for the healthy osteoblast cells and higher dsDNA of the cells exposed to the 5% Ga content conditioned medium (30 and 40 ng/mL on day 10 for 10 and 20 mg/mL respectively). It could be probably due to the mild reaction of the cells to the Ga ions. However, this value is not considerable especially comparing to the extreme cytotoxic side effects of other conventional method of cancer therapy, including chemotherapy and radiotherapy. The nature of chemotherapy agents is to generate cytotoxicity for the cells, so they damage cancer as well as normal cells. Most of the chemo and radiotherapy side effects are debilitating, even fatal. Hemopoietic cell precursors located in the bone marrow initiate cell division faster than other organs. Therefore, they are more susceptible to cytotoxic medications. Chemotherapeutic agents operate predominantly on proliferative cells. As a result, one of the most common adverse effects of these types of medications is bone marrow depression. Another common side effect is red blood cell macrocytosis, which is induced by methotrexate, hydroxyurea, cytarabine, and other antimetabolites [38]. Furthermore, radiation toxicity can be broad as radiotherapy cannot distinguish healthy tissue from cancerous one. Therefore, they induce damage to healthy tissue via accelerating DNA damage and formation of free radicals, which initiate the formation of secondary tumours [39].

Ga-releasing materials have been investigated at non-toxic levels and have been demonstrated to have many advantages in regard to bone metabolism. It has been observed that in hypercalcemia and Paget's disease patients, Ga can reduce the bone turnover. It accumulates in bones and decreases bone resorption by suppressing the activity of osteoclasts. For both the *in vivo* and *in vitro* experiments, $Ga(NO_3)_3$ has been used to suppress bone resorption without cytotoxicity on healthy bone cells [40], [41]. Studies performed using Ga-treated rat calvaria indicate that Ga^{3+} can directly influence osteoblasts at the gene expression level. It has been noticed that $Ga(NO_3)_3$ treatment may inhibit the stimulation of osteocalcin (OC), a protein synthesised by osteoblasts; depletion of OC synthesis *in vivo* is

correlated with increased mineralisation [42, 43]. It is believed that OC plays a role as an osteoblast-synthesised signal molecule to begin bone resorption[44, 45]. Inhibition of resorption would imply to the cells that formation of collagen and bone is preferred, thereby stimulating proliferation of preosteoblasts.

A study was performed with CMC-Dex hydrogel, which contains SiO_2–CaO–Na_2O–ZnO-Ga_2O_3 glasses, with the purpose of cancer therapy using MG-63 osteosarcoma cells. The conditioned media from the glass with 16 mol% Ga suppress cell viability up to 79%, while the conditioned media from the composite inhibited the cell viability to 69% after a period of 30 days of exposure. Keenan *et al* reported that neither the glass composition nor the composite did not reduced the viability of MC3T3-E1 osteoblast cells at the same time point [46]. They proposed that gallium influences protein synthesis in relation to the osteoblast differentiation process, suggesting that an appropriate concentration of Ga may enhance the proliferation and differentiation of preosteoblasts.

Wren *et al* introduced the application of Ga containing glass ionomer cements (GICs) for OS treatment, where Ga was considered as the antineoplastic reagent. While the cements were labelled "anti-cancerous", the release of ions and appropriate cell behaviour analysis were not documented to support the authors' hypothesis of the cements with anti-tumour properties. Furthermore cements were designed to be much less soluble and would therefore be unlikely to release sufficient Ga ions to be effective against OS [47].

Deliormanlı produced silicate-based BG particles containing Ga (5 wt %) via sol-gel method. The impact of Ga on the mechanical properties and bioactivity of the glasses was investigated *in vitro,* and it was stated that introducing Ga ions did not adversely influence the glass's *in vitro* bioactivity and HA forming capacity [48]. Considering this study, it validates that the addition of Ga ions not only interferes with the bioactivity of the Ga doped glass compounds but also stimulates the formation of HCA, which helps with the bone regeneration application.

This current study thus demonstrates that the fabricated Ga containing silicate BG induced an efficient release of the ionic product. The observed cytotoxicity in Saos-2 cells results from the increased absorption of Ga ions through TfR, which are overexpressed in cancer cells. This absorption likely disrupts cellular iron metabolism, causing oxidative stress, impaired DNA synthesis, and eventual apoptosis. The minimal effect on NHOst cells suggests they absorb less Ga. The selective toxicity of Ga-BGs towards OS cells underscores their potential as a

targeted therapeutic agent for bone cancer treatment. The fact that Ga is incorporated with bioactive glass provides a convenient and effective way of Ga administration as bone grafting for localised delivery of Ga to the bone cancerous tissue while sparing healthy tissues surrounding the tumour and stimulating bone regeneration. Therefore, Ga doped bioactive glasses can provide a targeted localised delivery of Ga to a tissue with the potential to not only target osteosarcoma cells but also stimulate new bone formation due to the characteristics of bioactive glass [49-51].

3.6 Conclusion

The effect of bioactive glasses containing 0-5% Ga was investigated for Saos-2 and NHOst cells using MTT, Live/Dead, proliferation and migration analysis by IncuCyte Live-Cell Imaging systems and PicoGreen assays. Cells were exposed to conditioned medium containing the dissolution product of the bioactive glass composition. Viability results showed a high percentage of osteosarcoma cell growth inhibition in a dose-dependent manner, with the highest cell death in bioactive glass compositions containing 5% Ga content (which achieved a 99% kill after 10 days). However, the mentioned Ga doped glass compositions did not have a significant detrimental effect against the proliferation of healthy normal human-derived osteoblast cells, and they remained largely unaffected. The results showed that bioactive glasses containing 1 and 2 % Ga produced limited cytotoxicity in OS cells and did not achieve the predefined efficacy threshold, while preserving viability in non-malignant osteogenic cells. By contrast, Ga 3–5 mol% consistently suppressed OS cell viability in a dose- and time-dependent manner and showed a favourable therapeutic window relative to healthy cells. Therefore, Chapter 4 focuses on 3, 4 and 5 mol% Ga to confirm efficacy across additional OS lines (HOS, U2). Based on the findings so far, it can be confirmed confidently that suppression of OS cell growth was due to the toxicity of the Ga ions within bioactive glasses. The results suggest that gallium-doped bioactive glasses have high potential for osteosarcoma-related bone grafting applications.

3.7 References

[1] J. R. Jones, "Review of bioactive glass: From Hench to hybrids," *Acta Biomater*, vol. 9, no. 1, pp. 4457–4486, Jan. 2013, doi: 10.1016/J.ACTBIO.2012.08.023.

[2] M. S. Chua, L. R. Bernstein, R. Li, and S. K. S. So, "Gallium maltolate is a promising chemotherapeutic agent for the treatment of hepatocellular carcinoma," *Anticancer Res*, vol. 26, no. 3 A, pp. 1739–1743, 2006.

[3] S. Pourshahrestani *et al.*, "Gallium-containing mesoporous bioactive glass with potent hemostatic activity and antibacterial efficacy," *J Mater Chem B*, vol. 4, no. 1, 2016, doi: 10.1039/c5tb02062j.

[4] C. R. Chitambar, "Gallium and its competing roles with iron in biological systems," *Biochimica et Biophysica Acta (BBA) - Molecular Cell Research*, vol. 1863, no. 8, pp. 2044–2053, Aug. 2016, doi: 10.1016/J.BBAMCR.2016.04.027.

[5] A. Rahimnejad Yazdi, L. Torkan, S. D. Waldman, and M. R. Towler, "Development of a novel bioactive glass suitable for osteosarcoma-related bone grafts," *J Biomed Mater Res B Appl Biomater*, vol. 106, no. 3, pp. 1186–1193, 2018, doi: 10.1002/jbm.b.33930.

[6] K. S. Rana, L. P. De Souza, M. A. Isaacs, F. N. S. Raja, A. P. Morrell, and R. A. Martin, "Development and Characterization of Gallium-Doped Bioactive Glasses for Potential Bone Cancer Applications," *ACS Biomater Sci Eng*, vol. 3, no. 12, pp. 3425–3432, 2017, doi: 10.1021/acsbiomaterials.7b00283.

[7] M. Plewinski, K. Schickle, M. Lindner, A. Kirsten, M. Weber, and H. Fischer, "The effect of crystallization of bioactive bioglass 45S5 on apatite formation and degradation," *Dental Materials*, vol. 29, no. 12, pp. 1256–1264, Dec. 2013, doi: 10.1016/J.DENTAL.2013.09.016.

[8] "The story of Bioglass.pdf."

[9] M. Bosetti and M. Cannas, "The effect of bioactive glasses on bone marrow stromal cells differentiation," *Biomaterials*, vol. 26, no. 18, pp. 3873–3879, Jun. 2005, doi: 10.1016/J.BIOMATERIALS.2004.09.059.

[10] J. R. Jones, P. Sepulveda, and L. L. Hench, "Dose-dependent behavior of bioactive glass dissolution," *J Biomed Mater Res*, vol. 58, no. 6, pp. 720–726, 2001, doi: 10.1002/jbm.10053.

[11] J. R. Jones, D. S. Brauer, L. Hupa, and D. C. Greenspan, "Bioglass and Bioactive Glasses and Their Impact on Healthcare," *Int J Appl Glass Sci*, vol. 7, no. 4, pp. 423–434, 2016, doi: 10.1111/ijag.12252.

[12] M. Montazerian and E. D. Zanotto, "A guided walk through Larry Hench's monumental discoveries," *J Mater Sci*, vol. 52, no. 15, pp. 8695–8732, 2017, doi: 10.1007/s10853-017-0804-4.

[13] F. Baino, S. Hamzehlou, and S. Kargozar, "Bioactive glasses: Where are we and where are we going?," *J Funct Biomater*, vol. 9, no. 1, 2018, doi: 10.3390/jfb9010025.

[14] L. L. Hench and J. R. Jones, "Bioactive Glasses: Frontiers and Challenges," *Front Bioeng Biotechnol*, vol. 3, p. 194, Nov. 2015, doi: 10.3389/fbioe.2015.00194.

[15] M. Miola *et al.*, "Glass-ceramics for cancer treatment: So close, or yet so far?," *Acta Biomater*, vol. 83, pp. 55–70, 2019, doi: 10.1016/j.actbio.2018.11.013.

[16] L. C. Palmer, C. J. Newcomb, S. R. Kaltz, E. D. Spoerke, and S. I. Stupp, "Biomimetic systems for hydroxyapatite mineralization inspired by bone and enamel," *Chem Rev*, vol. 108, no. 11, pp. 4754–4783, Nov. 2008, doi: 10.1021/cr8004422.

[17] O. Leppäranta *et al.*, "Antibacterial effect of bioactive glasses on clinically important anaerobic bacteria in vitro," *J Mater Sci Mater Med*, vol. 19, no. 2, pp. 547–551, Feb. 2008, doi: 10.1007/s10856-007-3018-5.

[18] R. Koohkan, T. Hooshmand, D. Mohebbi-Kalhori, M. Tahriri, and M. T. Marefati, "Synthesis, Characterization, and in Vitro Biological Evaluation of Copper-Containing Magnetic Bioactive Glasses for Hyperthermia in Bone Defect Treatment," *ACS Biomater Sci Eng*, vol. 4, no. 5, pp. 1797–1811, May 2018, doi: 10.1021/acsbiomaterials.7b01030.

[19] S. Xin and G. Wei, "Prognostic factors in osteosarcoma: A study level meta-analysis and systematic review of current practice," *J Bone Oncol*, vol. 21, p. 100281, Apr. 2020, doi: 10.1016/J.JBO.2020.100281.

[20] C. R. Chitambar, "Medical applications and toxicities of gallium compounds," *Int J Environ Res Public Health*, vol. 7, no. 5, pp. 2337–2361, 2010, doi: 10.3390/ijerph7052337.

[21] S. Phull, A. Rahimnejad Yazdi, and M. R. Towler, "A Gallium-doped cement for the treatment of bone cancers. The effect of ZnO ↔ Ga2O3substitution of an ionomeric glass series on the rheological, mechanical, pH and ion-eluting properties of their corresponding glass polyalkenoate cements," *Mater Res Express*, vol. 8, no. 6, Jun. 2021, doi: 10.1088/2053-1591/ac07e5.

[22] M. Kulkarni *et al.*, "The management impact of 68gallium-tris(hydroxypyridinone) prostate-specific membrane antigen (68Ga-THP-PSMA) PET-CT imaging for high-risk and biochemically recurrent prostate cancer," *Eur J Nucl Med Mol Imaging*, vol. 47, no. 3, pp. 674–686, Mar. 2020, doi: 10.1007/s00259-019-04643-7.

[23] J. Qi *et al.*, "Synthesis, antiproliferative activity and mechanism of gallium(III)-thiosemicarbazone complexes as potential anti-breast cancer agents," *Eur J Med Chem*, vol. 154, pp. 91–100, Jun. 2018, doi: 10.1016/J.EJMECH.2018.05.016.

[24] E. Halevas *et al.*, "Structurally characterized gallium-chrysin complexes with anticancer potential," *Dalton Transactions*, vol. 49, no. 8, pp. 2734–2746, Feb. 2020, doi: 10.1039/c9dt04540f.

[25] S. J. S. Flora, P. Kumar, G. M. Kannan, and G. P. Rai, "Acute oral gallium arsenide exposure and changes in certain hematological, hepatic, renal and immunological indices at different time intervals in male Wistar rats," *Toxicol Lett*, vol. 94, no. 2, pp. 103–113, Jan. 1998, doi: 10.1016/S0378-4274(97)00110-0.

[26] D. P. Kelsen, N. Alcock, S. Yeh, J. Brown, and C. Young, "Pharmacokinetics of gallium nitrate in man," *Cancer*, vol. 46, no. 9, pp. 2009–2013, Nov. 1980, doi: 10.1002/1097-0142(19801101)46:9<2009::AID-CNCR2820460919>3.0.CO;2-A.

[27] T. R. Daniels *et al.*, "The transferrin receptor and the targeted delivery of therapeutic agents against cancer," *Biochimica et Biophysica Acta (BBA) - General Subjects*, vol. 1820, no. 3, pp. 291–317, Mar. 2012, doi: 10.1016/J.BBAGEN.2011.07.016.

[28] T. R. Daniels, T. Delgado, J. A. Rodriguez, G. Helguera, and M. L. Penichet, "The transferrin receptor part I: Biology and targeting with cytotoxic antibodies for the treatment of cancer," *Clinical Immunology*, vol. 121, no. 2, pp. 144–158, Nov. 2006, doi: 10.1016/J.CLIM.2006.06.010.

[29] C. R. Chitambar, "Gallium-containing anticancer compounds," *Future Med Chem*, vol. 4, no. 10, pp. 1257–1272, 2012, doi: 10.4155/fmc.12.69.

[30] A. Essaghir and J.-B. Demoulin, "A Minimal Connected Network of Transcription Factors Regulated in Human Tumors and Its Application to the Quest for Universal Cancer

Biomarkers," *PLoS One*, vol. 7, no. 6, p. e39666, Jun. 2012, doi: 10.1371/journal.pone.0039666.

[31] Y. Shen *et al.*, "Iron metabolism gene expression and prognostic features of hepatocellular carcinoma," *J Cell Biochem*, vol. 119, no. 11, pp. 9178–9204, Nov. 2018, doi: 10.1002/jcb.27184.

[32] C. R. Chitambar, "10. GALLIUM COMPLEXES AS ANTICANCER DRUGS," in *Metallo-Drugs: Development and Action of Anticancer Agents*, De Gruyter, 2018, pp. 281–302. doi: 10.1515/9783110470734-010.

[33] J. Narasimhan, W. E. Antholine, and C. R. Chitambar, "Effect of gallium on the tyrosyl radical of the iron-dependent M2 subunit of ribonucleotide reductase," *Biochem Pharmacol*, vol. 44, no. 12, pp. 2403–2408, Dec. 1992, doi: 10.1016/0006-2952(92)90686-D.

[34] C. R. Chitambar and W. E. Antholine, "Iron-targeting antitumor activity of gallium compounds and novel insights into triapine®-metal complexes," Mar. 10, 2013. doi: 10.1089/ars.2012.4880.

[35] B. Krampe and M. Al-Rubeai, "Cell death in mammalian cell culture: Molecular mechanisms and cell line engineering strategies," Jun. 2010. doi: 10.1007/s10616-010-9274-0.

[36] J. Fornetti, A. L. Welm, and S. A. Stewart, "Understanding the Bone in Cancer Metastasis," Dec. 01, 2018, *John Wiley and Sons Inc.* doi: 10.1002/jbmr.3618.

[37] C. Marques, J. M. F. Ferreira, E. Andronescu, D. Ficai, M. Sonmez, and A. Ficai, "Multifunctional materials for bone cancer treatment," May 28, 2014, *Dove Medical Press Ltd*. doi: 10.2147/ijn.s55943.

[38] K. Singh, M. Bhori, Y. A. Kasu, G. Bhat, and T. Marar, "Antioxidants as precision weapons in war against cancer chemotherapy induced toxicity – Exploring the armoury of obscurity," *Saudi Pharmaceutical Journal*, vol. 26, no. 2, pp. 177–190, Feb. 2018, doi: 10.1016/J.JSPS.2017.12.013.

[39] E. Harper and C. J. Talbot, "Is it Time to Change Radiotherapy: The Dawning of Chronoradiotherapy?," *Clin Oncol*, vol. 31, no. 5, pp. 326–335, May 2019, doi: 10.1016/J.CLON.2019.02.010.

[40] T. J. Hall and T. J. Chambers, "Gallium inhibits bone resorption by a direct effect on osteoclasts," *Bone Miner*, vol. 8, no. 3, pp. 211–216, Mar. 1990, doi: 10.1016/0169-6009(90)90106-P.

[41] G. Cournot-Witmer *et al.*, "Bone modeling in gallium nitrate-treated rats," *Calcif Tissue Int*, vol. 40, no. 5, pp. 270–275, 1987, doi: 10.1007/BF02555260.

[42] R. S. Bockman, P. T. Guidon, L. C. Pan, R. Salvatori, and A. Kawaguchi, "Gallium nitrate increases type I collagen and fibronectin mRNA and collagen protein levels in bone and fibroblast cells," *J Cell Biochem*, vol. 52, no. 4, pp. 396–403, Aug. 1993, doi: 10.1002/jcb.240520404.

[43] "Bone repair process in calvarial defects using biactive glass and calcium sulfate barrier."

[44] P. T. Guidon, R. Salvatori, and R. S. Bockman, "Gallium nitrate regulates rat osteoblast expression of osteocalcin protein and mRNA levels," *Journal of Bone and Mineral Research*, vol. 8, no. 1, pp. 103–112, Jan. 1993, doi: 10.1002/jbmr.5650080113.

[45] J. D. Malone, S. L. Teitelbaum, G. L. Griffin, R. M. Senior, and A. J. Kahn, "Recruitment of osteoclast precursors by purified bone matrix constituents.," *J Cell Biol*, vol. 92, no. 1, pp. 227–230, Jan. 1982, doi: 10.1083/jcb.92.1.227.

[46] T. J. Keenan, L. M. Placek, A. Coughlan, G. M. Bowers, M. M. Hall, and A. W. Wren, “Structural characterization and anti-cancerous potential of gallium bioactive glass/hydrogel composites,” *Carbohydr Polym*, vol. 153, pp. 482–491, Nov. 2016, doi: 10.1016/j.carbpol.2016.07.100.

[47] A. W. Wren, A. Coughlan, L. Placek, and M. R. Towler, “Gallium containing glass polyalkenoate anti-cancerous bone cements: Glass characterization and physical properties,” *J Mater Sci Mater Med*, vol. 23, no. 8, pp. 1823–1833, 2012, doi: 10.1007/s10856-012-4624-4.

[48] A. M. Deliormanlı, “Synthesis and characterization of cerium- and gallium-containing borate bioactive glass scaffolds for bone tissue engineering,” *J Mater Sci Mater Med*, vol. 26, no. 2, pp. 1–13, Feb. 2015, doi: 10.1007/s10856-014-5368-0.

[49] S. P. Valappil *et al.*, “Controlled delivery of antimicrobial gallium ions from phosphate-based glasses,” *Acta Biomater*, vol. 5, no. 4, pp. 1198–1210, May 2009, doi: 10.1016/J.ACTBIO.2008.09.019.

[50] S. P. Valappil *et al.*, “Antimicrobial Gallium-Doped Phosphate-Based Glasses,” *Adv Funct Mater*, vol. 18, no. 5, pp. 732–741, Mar. 2008, doi: 10.1002/adfm.200700931.

[51] P. Collery, B. Keppler, C. Madoulet, and B. Desoize, “Gallium in cancer treatment,” *Crit Rev Oncol Hematol*, vol. 42, no. 3, pp. 283–296, 2002, doi: 10.1016/S1040-8428(01)00225-6.

Chapter 4

In-vitro Cytotoxic and Apoptotic Effects of Ga-Doped Bioactive Glass on Osteosarcoma Cells

4.1 Introduction

Bioactive glass (BG) is a multifunctional material valued for its bioactivity, cytocompatibility, and ability to release therapeutic ions in a controlled manner, making it suitable for cancer-related bone regeneration. Among its many applications, BG is particularly advantageous for bone cancer treatment, where it can fill defects following tumour resection, promote bone regeneration, and enable local delivery of therapeutic ions [1, 2]. The tunability of BG composition allows tailoring of properties such as porosity, degradation rate, and ion-release profile for specific biomedical requirements [3, 4].

In this research project, bioactive glass 45S5 was doped with gallium ions to harness the dual functionality of the material, combining the well-established bone regenerative properties of Bioglass with the antineoplastic activity of gallium ions. Owing to its chemical similarity to Fe^{3+}, Ga^{3+} competes with iron in metabolic pathways essential for tumour cell growth, thereby disrupting iron-dependent enzymes and mitochondrial function [5, 6]. Its therapeutic potential has been demonstrated in various cancer models; however, its application in bone cancer remains underexplored. Incorporating Ga^{3+} into BG enables targeted, localised delivery, improving bioavailability and minimising systemic toxicity compared with conventional administration routes [7].

OS cells overexpress TfRs to meet their heightened iron demand for vital metabolic functions for DNA synthesis, respiration, and other metabolic processes. This upregulation, which may also occur under iron-deficient conditions, enables enhanced iron uptake via TfR1-mediated endocytosis, distinguishing malignant from healthy cells. Consequently, TfRs represent attractive targets for cancer therapy [8]. Ga, which mimics iron and enters cells through TfRs, disrupts DNA synthesis and mitochondrial function by inducing iron deprivation and reactive oxygen species (ROS) generation, ultimately leading to apoptosis. Since tumour cells depend heavily on iron for mitochondrial activity, ribonucleotide reductase, and signalling pathways such as mammalian target of rapamycin (mTOR) and Wingless-related integration site (WNT), dysregulation of iron homeostasis promotes iron-dependent tumour growth [9]. Although Ga compounds (e.g., gallium nitrate, gallium chloride, and radioisotopes ^{67}Ga and ^{68}Ga) have shown anticancer potential, their application in bone cancer remains underexplored [10]. Figure 1 illustrates the key mechanisms by which Ga disrupts cellular iron metabolism.

In the previous chapters, Ga-doped bioactive glasses (Ga-BGs) were fabricated and characterised, and their cytotoxic effects were examined on OS (Saos-2) and normal human osteoblast (NHOst) cells. Results showed dose-dependent inhibition of Saos-2 proliferation with minimal toxicity to healthy osteoblasts, confirming selective anticancer efficacy.

Building on these findings, this chapter investigates the mechanistic aspects of Ga-BG-induced cytotoxicity across a broader range of osteosarcoma cell lines human osteosarcoma (HOS) and U2 OS, representing distinct levels of tumour aggressiveness, alongside human mesenchymal stem cells (hMSCs), which play a key role in bone regeneration. According to several studies, HOS is one of the most aggressive OS cells, with U2 being less aggressive compared to HOS. This can be observed via parameters, such as faster proliferation rates and higher migratory and invasive properties [11, 12]. Therefore, we decided to investigate the effect of Ga-BGs on these two types of OS cells. Cell viability, proliferation, and cytotoxicity were evaluated using MTT and Live/Dead assays to determine dose-dependent effects.

Furthermore, the study explores the mechanism of Ga-mediated cytotoxicity by examining transferrin receptor (TfR) expression in HOS, U2 OS, and hMSC cells, followed by caspase-activity assays to assess apoptosis induction. These analyses provide insight into the selective cytotoxic mechanisms of Ga ions and their potential in developing multifunctional therapeutic materials for osteosarcoma-related bone repair.

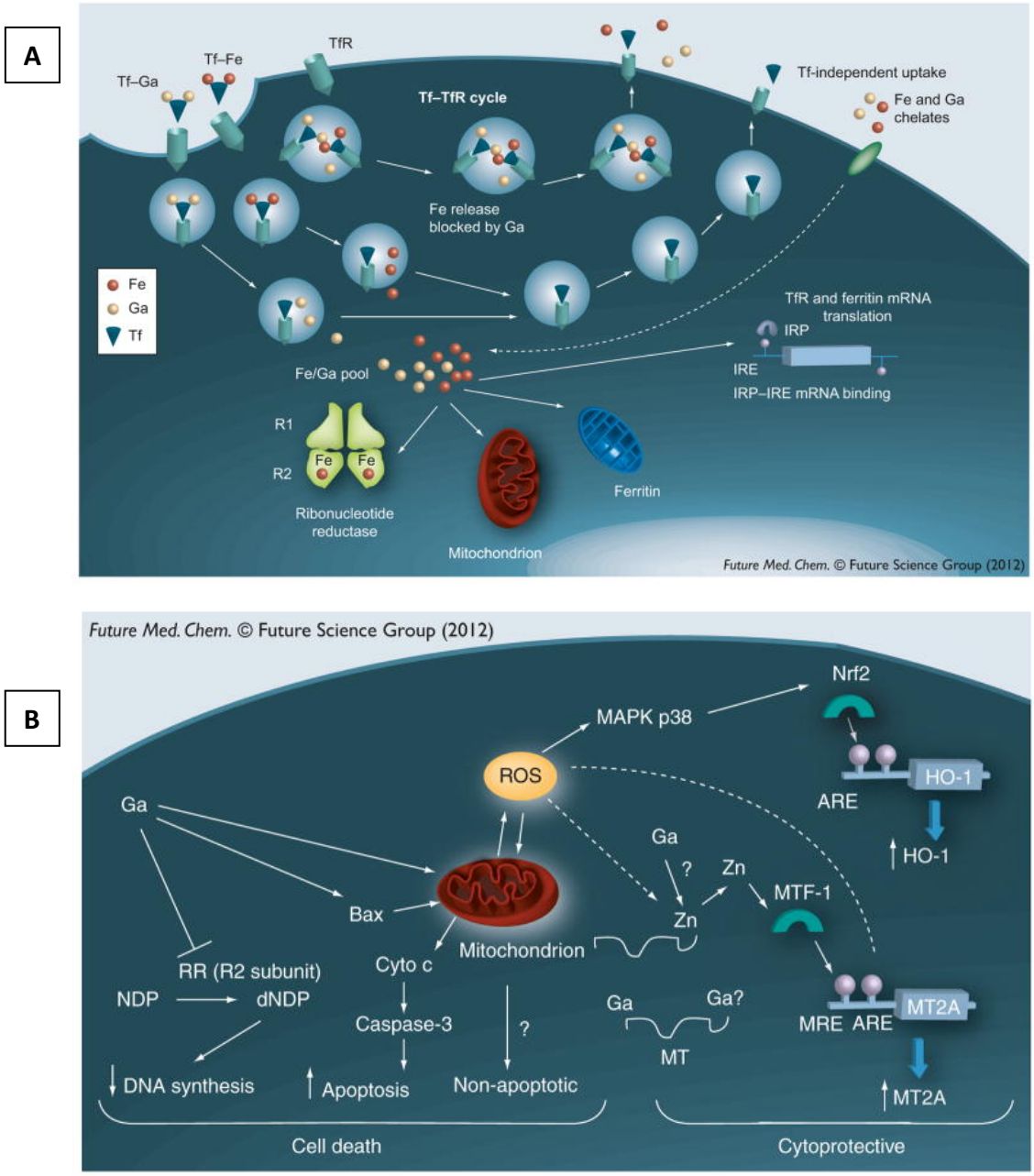

Figure 4.1. A) Cellular uptake and interaction of iron and gallium. **B)** Proposed model of gallium nitrate action involving its intracellular targets, highlights both cytotoxic and cytoprotective effects [13].

4.2 Aims

The aim of this chapter is to investigate the effect of BGs 4555 and Ga doped BG (3, 4, and 5 mol% %) on the viability of human drive osteosarcoma HOS and U2, as well as hMSC cells. Moreover, further investigation was performed to elucidate the mechanism by which Ga ions impact cellular functions. This was accomplished by,

- Assessing the influence of the glass dissolution product on cell viability and proliferation using the MTT viability assay
- Investigating Live/Dead assay on the cells exposed to the conditioned media
- Measurement of the TfR expression level in the cells
- Evaluating the apoptosis by quantifying caspase activity.

4.3 Materials and methods

The bioactive glasses used in this study were manufactured using the melt-quench, method described in Chapter 2, Section 2.3.1 (Glass preparation). The compositions and processing conditions were identical to those detailed in chapter 2. All experiments were performed in triplicate (n = 3) using samples prepared from the same glass production batch to ensure consistency and reproducibility across all analyses.

4.3.1 Conditioned media preparation

Conditioned media were prepared by mixing glass particles (particle size range from 40-63 µm) at concentrations of 10 and 20 mg/mL with serum-free Eagle's Minimum Essential Medium (EMEM) (ATCC® 30-2003™, USA). serum-free Eagle's Minimum Essential Medium (EMEM) for HOS cells purchased from Sigma-Aldrich and Gibco™ McCoy's 5A (Modified) Medium, HEPES (Thermo Fisher Scientific, USA) to treat U2 cells and Dulbecco's Modified Eagle Medium (DMEM) high glucose, (Sigma-Aldrich, USA). for hMSCs cells. The media was incubated in a shaker incubator at 200 rpm and 37 °C for 24 hours. After incubation, the conditioned media was filtered with a 0.2 µm syringe filter to remove the glass particles and to also sterilise the stock solution. All conditioned media were supplemented with the recommended components according to the supplier's guidelines. The media was then incubated overnight with 5% CO_2/ 95% air at 37 °C prior to use. This buffers the pH and ensures false positive results are not present due to the elevated pH of the conditioned media.

4.3.2 Cell culture of human-derived osteosarcoma (HOS and U2)

HOS (ATCC® CRL-1543™) and U2 (ATCC® HTB-96™) OS cells were purchased from the American Tissue Culture Collection and were grown according to the manufacturer's instructions.

HOS cells were grown in Eagle's minimum essential media (EMEM) modified to contain Earle's Balanced Salt Solution, non-essential amino acids, 2 mM L-glutamine, 1 mM sodium pyruvate, and 1500 mg/L sodium bicarbonate. U2 OS cells were grown in McCoy's 5A media containing 1.5 mM L-glutamine and 2200 mg/L sodium bicarbonate. Media for both OS cell lines were supplemented with 10% FBS, (Gibco™, Thermo Fisher Scientific, USA). The cells were growing in T-75 flasks at 37 °C in a humidified atmosphere of 5% CO_2/ 95% air.

4.3.3 Cell culture of human Mesenchymal Stem Cell (hMSC)

Human Mesenchymal Stem Cells (hMSC) obtained from Promo Cell (Germany) of healthy donors (63-75 years old) and grown in Dulbecco's Modified Eagle's Media (DMEM) - high glucose. The media was supplemented with 10% FBS, 1% sodium pyruvate solution (Sigma-Aldrich, USA), 1% Minimum Essential Medium (MEM) non-essential amino acid solution (Sigma-Aldrich, USA), 1% L-glutamine and 1% pen-strep (Invitrogen, Thermo Fisher Scientific, USA). The cells were growing in T-75 flasks at 37 °C in a humidified atmosphere of 5% CO_2/ 95% air.

4.3.4 Cell viability assay

Cell viability was assessed by 3-(4,5-dimethylthiazol-2-yl)-2,5-diphenyltetrazolium bromide (MTT) proliferation kit. The relative cytotoxicity of Ga ions against different cell lines (HOS, U2 OS and hMSCs) was investigated by MTT assay. Generally, the cells were seeded in a 48-well plate at a concentration of 5000 cells/cm^2, in complete growth media. The cells grew for 24 hours, and then their media was swapped with conditioned media containing Ga doped ions for a period of 10 days, while the media was replaced on days 3 and 7. The viability of the cells was investigated at the time points of day 1, 3, 5, 7 and 10 post-treatments with conditioned media. At each time point, the optical density was measured using an Ascent MultiScan GO spectrophotometer at 570 nm. Ethanol 70% (v/v) was used to represent the positive control, while the cells grown in normal growth media represent the negative control. The assay was performed in 3 independent experiments.

4.3.5 LIVE/DEDA assay

Cell viability was investigated using a LIVE/DEAD™ Viability assay Kit. The assay contains two fluorescent nucleic acid stains: Calcein-AM, which is green, and ethidium homodimer-1 (EthD-1), which is red. Calcein-AM permeates living cells. Upon entering the cell, the intracellular esterases cleave the acetoxymethyl (AM) ester group, trapping the Calcein fluorescent green dye within the living cell. EthD-1, the fluorescent red dye, can only penetrate cells with damaged membranes, when it then binds to nucleic acid. Therefore, live cells with an undamaged cell membrane appear green while dead cells with a damaged cell membrane appear red.

OS HOS and U2, as well as hMSCs cells, were seeded at 5000/cm^2 in 48-well plates, and the viability of the cells was evaluated post-exposure to the conditioned media. The LIVE/DEAD assay was performed at time-points of 1, 3, 5, 7 and 10 days with media changes on days 3 and 7. Calcein-AM at 2 µM and EthD-1 at 4 µM were mixed into a single solution with Dulbecco's phosphate-buffered saline (D-PBS), and 200 µL of this master mix was added to each well and incubated at room temperature (under dark conditions) for 1 hour. Cells were photographed using a Leica fluorescent microscope at 10x magnification.

4.3.6 Transferrin Receptor (TfR) Expression

The expression of TfR, which is the receptor responsible for gallium and iron cellular uptake, was investigated using TfR antibody treatment run by Flow cytometer. OS HOS and U2, as well as hMSCs cells, were seeded at 5000/cm^2 in T-25 flasks in complete growth media. The cells growth for 24 hours and then their media was swapped with conditioned media containing Ga doped ions. The cells were treated with conditioned media for 24 hours, and then the expression of transferrin (Tf) was investigated using APC anti-human TfR (CD71) antibody (Biolegend 334108, 1:100). After 24 hours, the supernatant was taken out, and the cells were washed with PBS. Then the cells were incubated with Accutase (Sigma-Aldrich, USA) for 5 minutes at 37 °C. Detached cells were collected with fresh, warm complete media and spun at 300 g for 5 minutes. The cells were washed with PBS to remove excess Accutase. Finally, the pellet was resuspended in the Human transferrin receptor (TfR) CD71 antibody (R&D Systems, AF2474, USA) and Purified Mouse IgG1, κ Isotype Control Antibody (BioLegend, USA) as Isotype control antibody and incubated for 30 minutes in the dark on ice. After incubation, the cells were washed twice with PBS, and the final pellet was resuspended in flow buffer. Finally, the samples were run on a BD Accuri™ C6 Plus flow cytometer (BD Biosciences, USA), and a minimum of 10000 cells per sample were analysed.

Antibody preparation: the antibody was diluted with flow buffer at 1:100.

4.3.7 Caspase activity

The effect of Ga doped BG on Caspase-3/7 activity in cells was investigated by using CellEvent™ Caspase-3/7 Detection Reagents (Invitrogen™, Thermo Fisher Scientific, USA), which are based on the enzymatic cleavage of the fluorogenic caspase-3 substrate of a four-amino acid peptide, DEVD. DEVD is conjugated with a dye that binds nucleic acids. In

non-apoptotic cells, there is no fluorescent reaction, while in apoptotic cells, caspase-3 and caspase-7, which are activated, cleave the DEVD peptide, allowing the dye to bind to DNA and emit a bright, fluorogenic signal.

All the cells were treated with Ga doped conditioned media for 72 hours. The caspase 3/7 reagent was added to each well and incubated at 37 °C for 1 hour in the dark. After the incubation, the fluorescent signal was measured using a FLUOstar Omega Filter-based microplate reader (BMG Labtech, Germany) as well as imaging the cells using a fluorescent microscope. The generation of fluorescent signal in each reaction was measured at 503/530 nm and expressed as arbitrary relative fluorescent units. Cells were photographed using a Leica fluorescent microscope at 10x magnification.

4.4 Results

4.4.1 Cytotoxic analysis of Ga doped bioactive glasses *in vitro*

4.4.1.1. Cell cytotoxic analysis for osteosarcoma HOS and U2 cells

Cell viability of HOS and U2 cells was assessed using the MTT assay after treatment with conditioned media containing Bioglass 45S5 or Ga-doped bioactive glass (3-5 mol%) at concentrations of 10 and 20 mg/mL (Figure 4.2 a-d). Cell viability was expressed as a percentage relative to the negative control (unconditioned medium). A significant dose-dependent inhibition of cell proliferation was observed in both OS cells with increasing accumulation of Ga ions in the medium across all Ga containing glass compounds ($p < 0.0001$). The cells were treated for a period of 10-day and the viability was measured after 1, 3, 5, 7 and 10 days.

A significant cytotoxic effect was observed for the HOS cells treated with both 10 and 20 mg/mL of 5% Ga glasses. Cell viability began to decrease from day 3 and on day 5 no viable cells were observed ($p < 0.0001$). HOS cells which were exposed to the 4% Ga doped conditioned media showed a significant cell growth inhibition in the course of 10 days. The cell viability for 10 and 20 mg/mL were 16 and 9% respectively on time point day 10 ($p < 0.0001$). There was no significant cell growth reduction in the HOS cells which were exposed to the Ga free conditioned media compared to the negative control ($p>0.9999$).

There was a significant cytotoxic effect on U2 cells which were exposed to both 10 and 20 mg/mL of Ga doped conditioned media. The viability of the cells which were exposed to the 10 mg/mL of 5% Ga doped conditioned media decreased significantly on day 7 to around 30% and on day 10 the viability was approximately 4% compared to the negative control ($p < 0.0001$). In addition, it was noted that 4% Ga conditioned media cause a significant cell cytotoxicity, and the viability was 34% on time point day 10 ($p < 0.0001$). Exposure to 20 mg/mL of 5% Ga-doped conditioned medium led to a marked reduction in cell viability, decreasing to approximately 20% by day 7 and further to around 4% by day 10, compared to the negative control ($p < 0.0001$). Similarly, the 4% Ga-doped medium also exhibited significant cytotoxicity, with cell viability dropping to 32% on day 10 ($p < 0.0001$).

There was no significant cell growth reduction in the U2 cells which were exposed to the Ga free conditioned media compared to the negative control ($p > 0.05$).

4.4.1.2. Cell viability analysis for hMSC cells

The cytotoxic effect of Ga-doped bioactive glass on hMSC cells was evaluated over a 10-day period using conditioned media containing 10 and 20 mg/mL of each glass composition Bioglass 45S5 or Ga-doped powders (3-5 mol%). The samples which were treated with 10 mg/mL conditioned media showed no significant cytotoxic effect in cell viability across all the glass compounds. Neither Ga free nor Ga doped conditioned media caused toxicity for hMSC cells. At 4 and 5% Ga content conditioned media, which caused significant cytotoxicity for OS cells, failed to affect the viability in the same manner for hMSCs cells after treating for 10 days ($p>0.9999$). In all 3 cell types exposed to 70% ethanol demonstrated total cell death of the population as anticipated ($p<0.0001$).

The metabolic activity of hMSCs was investigated at 20 mg/mL of each glass composition. On day 1, all treatment groups, including 45S5 and Ga-doped samples, exhibited viability levels comparable to the control, indicating no acute cytotoxicity at early time points. However, by day 3, cells treated with 45S5-conditioned media showed a marked decrease in viability, while all Ga-doped groups (3–5%) maintained higher metabolic activity, with 5% Ga demonstrating the most consistent performance across all time points. From day 5 onward, hMSCs in the Ga-treated groups showed a gradual recovery and proliferation, whereas the 45S5 group remained significantly lower ($p<0.0001$). By day 10, viability in Ga-treated cells approached or exceeded control levels, suggesting enhanced compatibility and sustained support for cell metabolism. These findings highlight the improved cytocompatibility of Ga-doped bioactive glass over traditional 45S5, particularly in maintaining hMSC viability during the period of exposure.

A two-way ANOVA and Tukey's multiple comparisons test were performed to test for significance, and the data are presented as mean ± SD, and significance was set at $p \leq 0.05$, N=3.

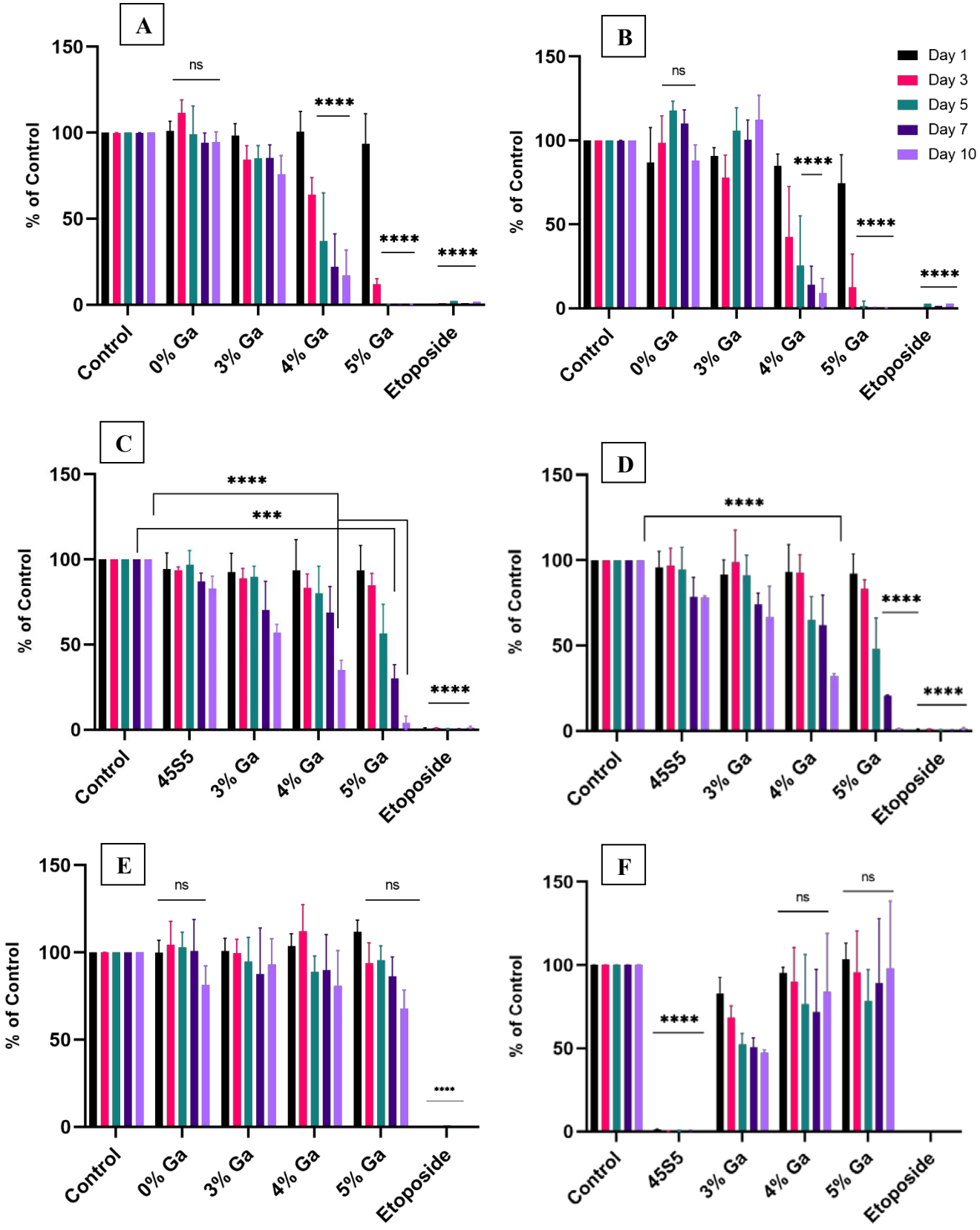

Figure 4.2. The effect of the dissolution products of Bioglass 45S5 and Ga doped silica based BG (3-5 mol%) on the cellular metabolic activity using MTT viability assay. The data is represented as Mean ± SD (N=5). **A, B)** HOS cells exposed to the 10 and 20 mg/mL conditioned media. **C, D)** U2 OS cells exposed to the 10 and 20 mg/mL conditioned media. **E, F)** hMSC cells exposed to the 10 and 20 mg/mL conditioned media.

4.4.2 Investigation of cell viability by Live/Dead assay

Live/Dead images are shown in Figures 4.3 to 4.8 for OS cells HOS and U2 as well as hMSC. Live cells are illustrated in green while the dead cells are in red. All the cell types were exposed to the conditioned media containing 10 and 20 mg/mL of the glass dissolution product for a period of 10 days. The Live/Dead staining was performed on day 1, 3, 5, 7 and 10.

HOS cells exposed to 10 and 20 mg/mL of 4 and 5% Ga conditioned media both show the highest cytotoxicity in cell viability (Figures 4.3 and 4.4). The viability of HOS cells exposed to 10 and 20 mg/mL of 5% Ga compounds was less than 1% after exposure for 10 days. These results agree with the results observed in the MTT assay. The cells' viability for the group exposed to Ga free conditioned media was similar to the negative control, which suggests that the glass composition does not have any detrimental effect on the cell viability, and the cytotoxicity comes from the Ga compounds.

The Live/Dead results for OS U2 cells demonstrate that Ga doped conditioned media affect the cells' viability in a dose-dependent manner. Figures 4.5 and 4.6 show that the viability of U2 cells exposed to 10 and 20 mg/mL of 4 and 5% Ga doped conditioned media has been compromised after a course of 10 days. The viability of cells exposed to 5% Ga compounds was less than 1% for both 10 and 20 mg/mL. In addition, 4% Ga compounds demonstrated a significant cytotoxicity at 20 mg/mL, while this is less intense at the concentration of 10 mg/mL; however, it is still significant cell growth inhibition. It can clearly be seen that Ga free conditioned media did not affect the cell viability, which is similar to the negative control group.

In contrast, OS cell hMSC cells did not demonstrate any cytotoxicity after being exposed to Ga doped conditioned media. As shown in Figures 4.7 and 4.8, the cells were treated for a period of 10 days and even in 5% Ga compound, which has the highest toxicity for both OS HOS and U2 cells did not affect the viability of hMSC cells. The viability of 455S (Ga free compounds) at 10 mg/mL was similar to the negative control.

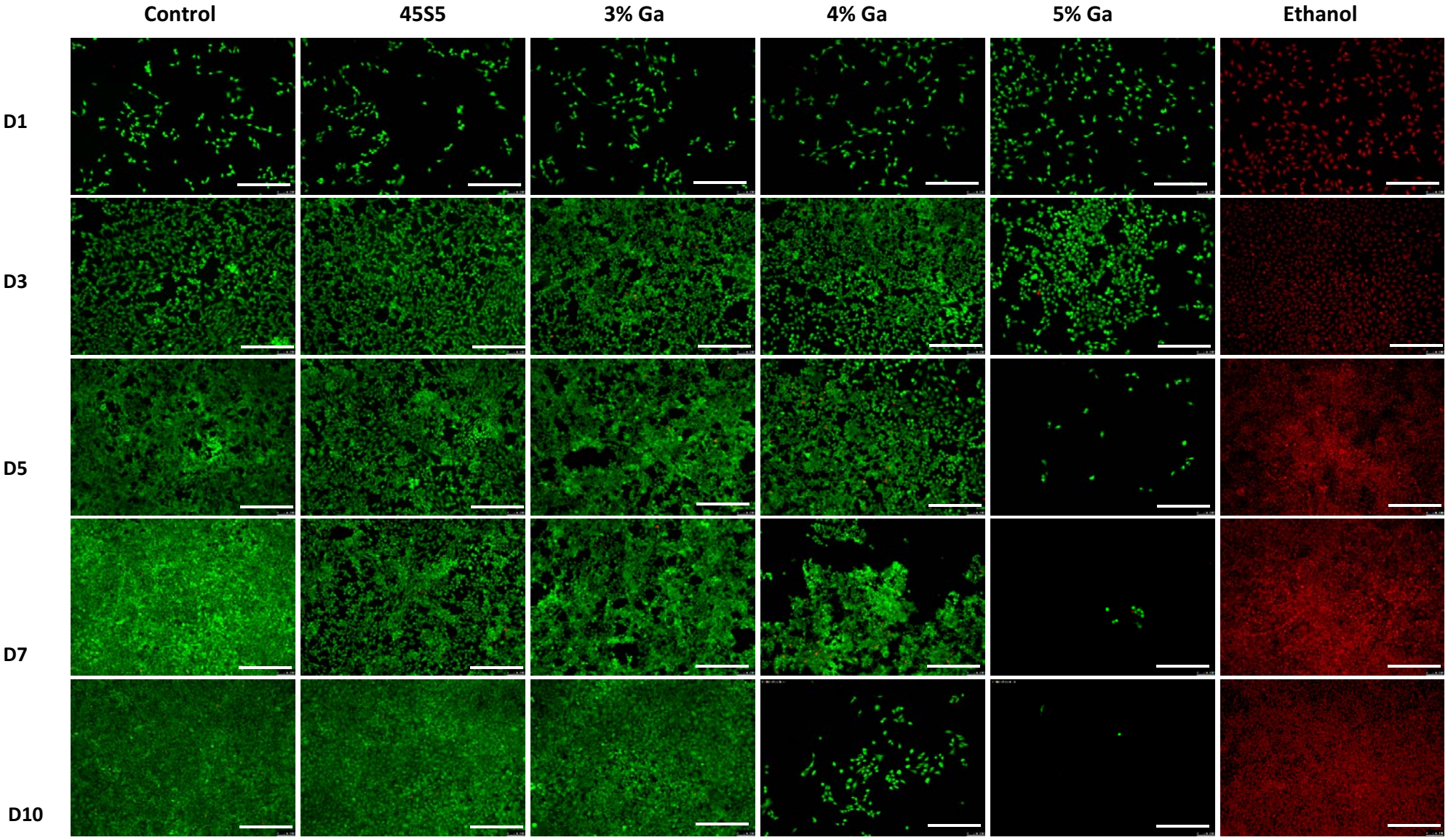

Figure 4.3. Fluorescence images of Live/Dead assay of HOS cells treated with 10 mg/mL of Ga-doped glass dissolution product with time points of day 1, 3, 5, 7, and 10 (each row represents each time point). Images were taken using a fluorescent microscope at 10x magnification. Live =green and dead=red. Scale bar indicates 300 µm.

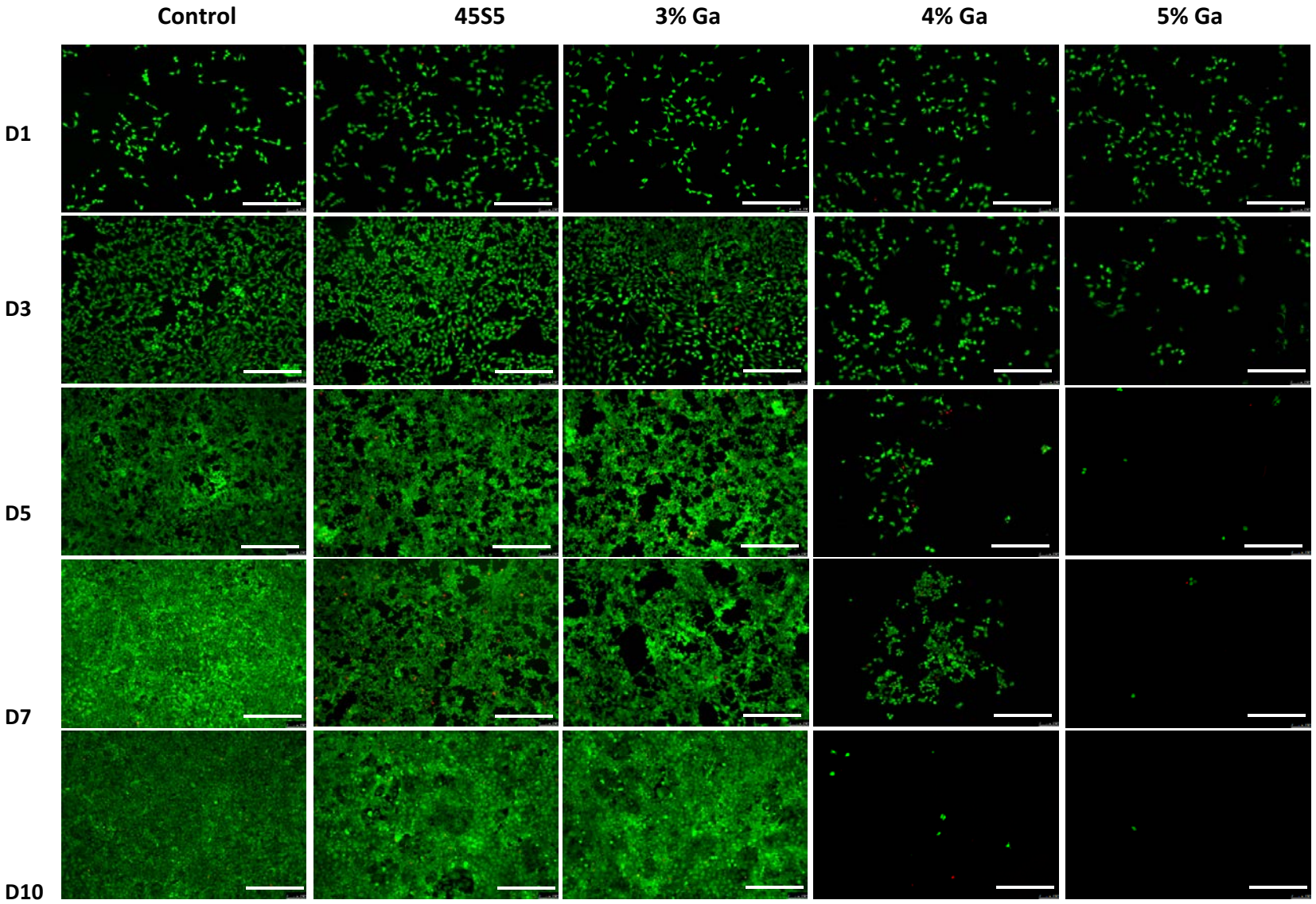

Figure 4.4. Fluorescence images of Live/Dead assay of HOS cells treated with 20 mg/mL of Ga-doped glass dissolution product with time points of day 1, 3, 5, 7, and 10 (each row represents each time point). Images were taken using a fluorescent microscope at 10x magnification. Live =green and dead=red. Scale bar indicates 300 µm.

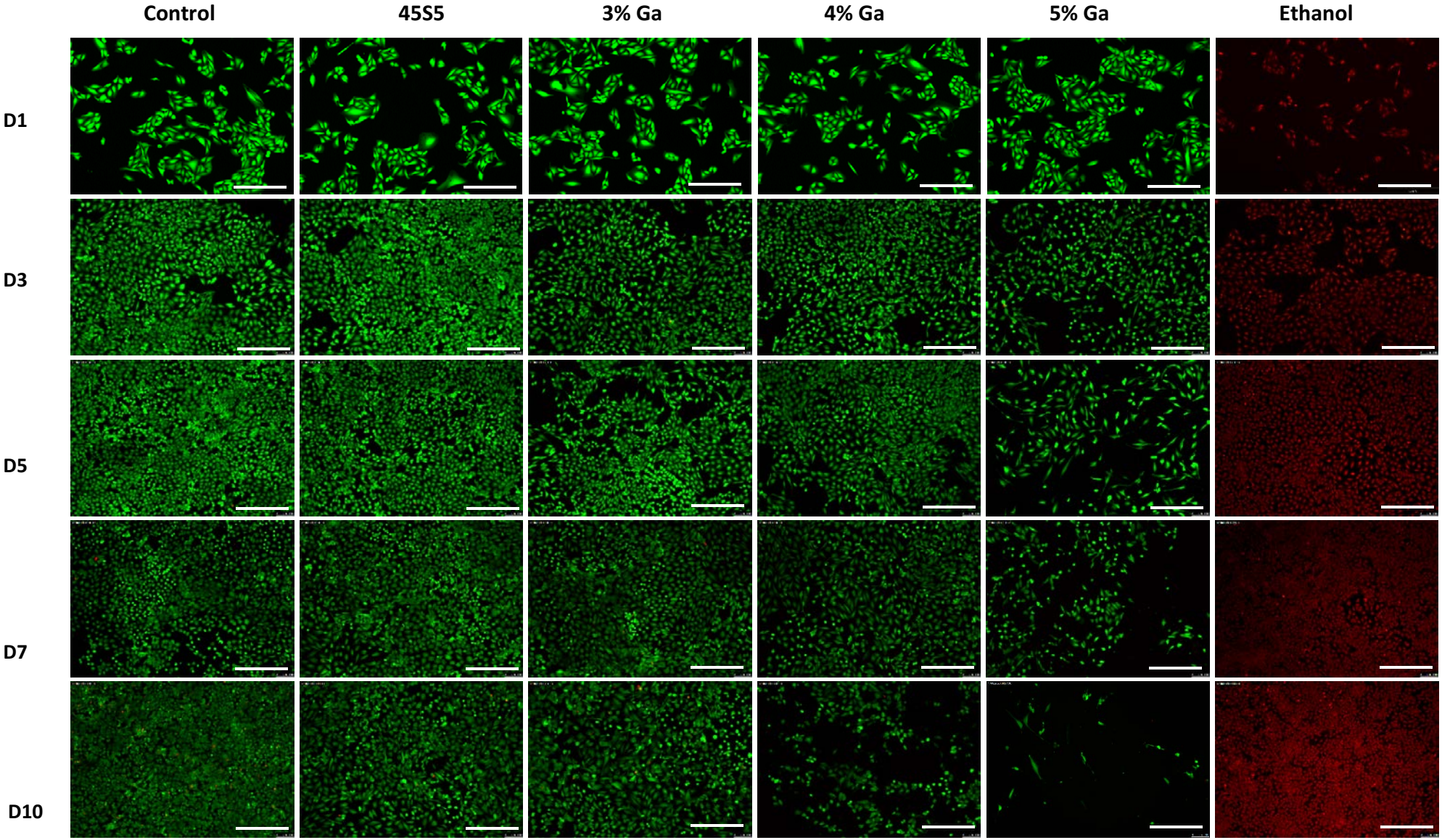

Figure 4.5. Fluorescence images of Live/Dead assay of U2 cells treated with 10 mg/mL of Ga-doped glass dissolution product with time points of day 1, 3, 5, 7, and 10 (each row represents each time point). Images were taken using a fluorescent microscope at 10x magnification. Live =green and dead = red. Scale bar indicates 300 µm.

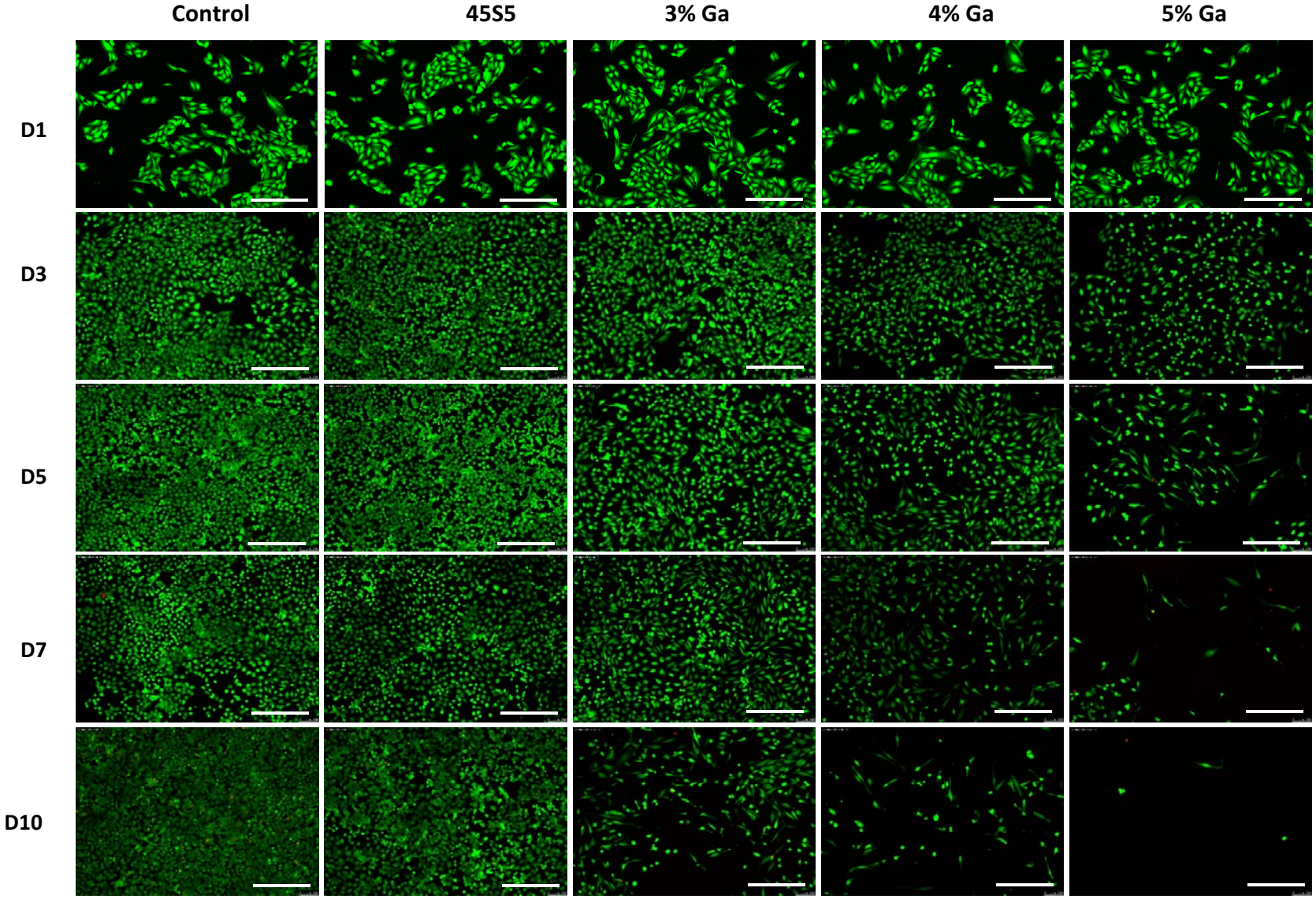

Figure 4.6. Fluorescence images of Live/Dead assay of U2 cells treated with 20 mg/mL of Ga-doped glass dissolution product with time points of day 1, 3, 5, 7, and 10 (each row represents each time point). Images were taken using a fluorescent microscope at 10x magnification. Live =green and dead = red. Scale bar indicates 300 µm.

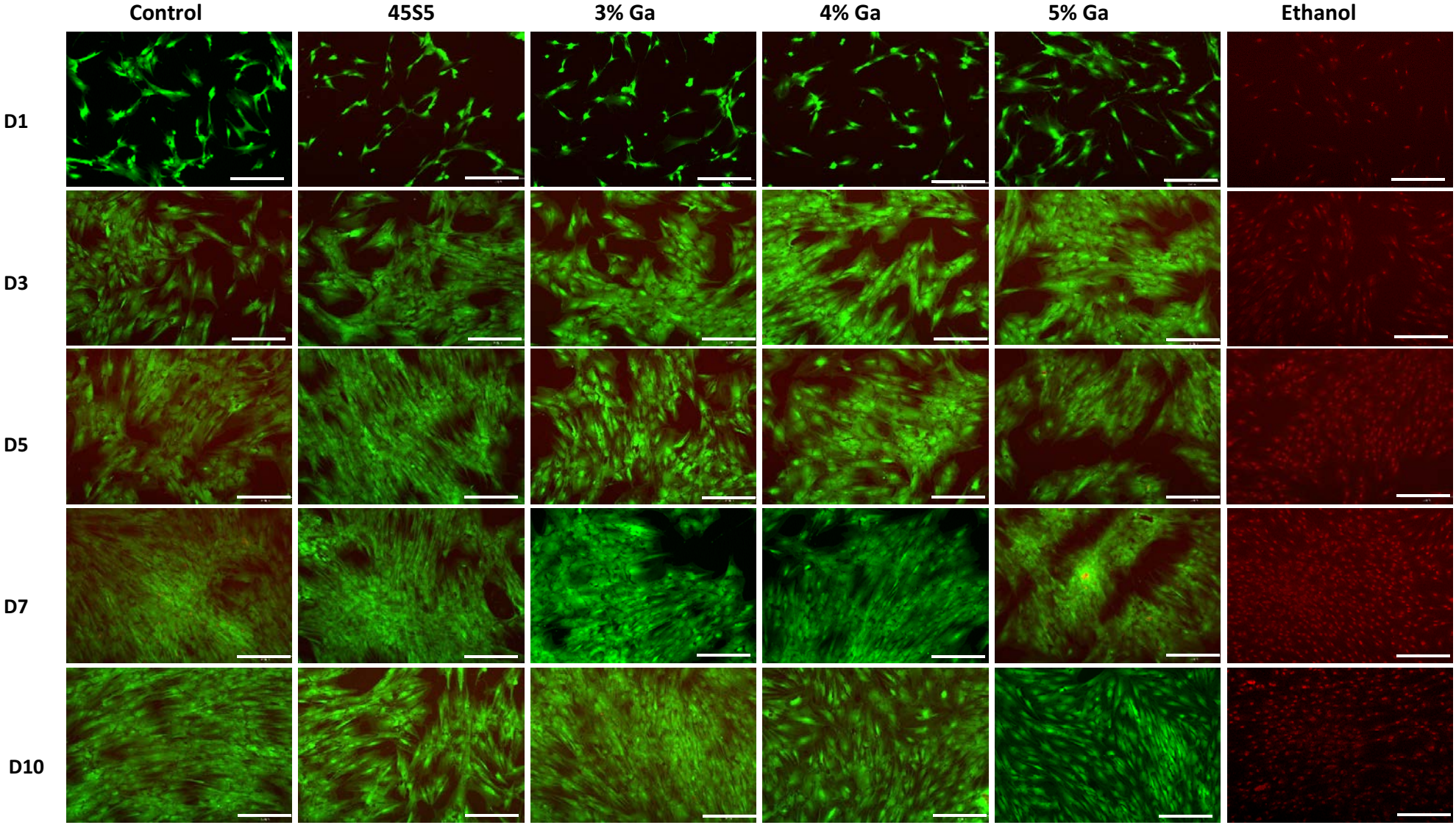

Figure 4.7. Fluorescence images of Live/Dead assay of hMSC cells treated with 10 mg/mL of Ga-doped glass dissolution product with time points of day 1, 3, 5, 7, and 10 (each row represents each time point). Images were taken using a fluorescent microscope at 10x magnification. Live =green and dead = red. Scale bar indicates 300 µm.

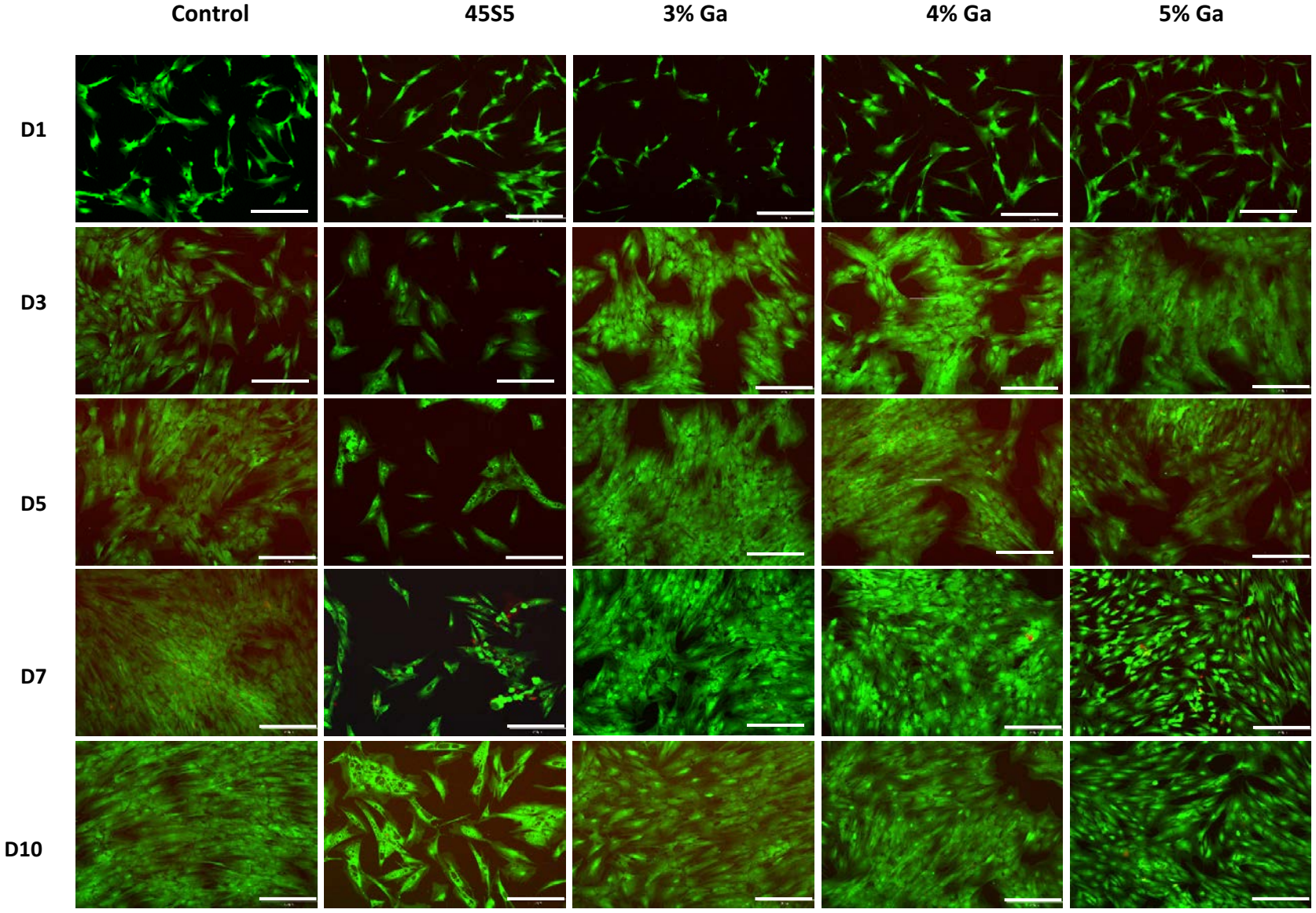

Figure 4.8. Fluorescence images of Live/Dead assay of hMSC cells treated with 20 mg/mL of Ga-doped glass dissolution product with time points of day 1, 3, 5, 7, and 10 (each row represents each time point). Images were taken using a fluorescent microscope at 10x magnification. Live =green and dead=red. Scale bar indicates 300 µm.

4.4.3 Expression of transferrin receptor

To evaluate the impact of bioactive glass on iron-regulating proteins, the level of TfR expression was examined in OS cells HOS and U2, as well as hMSC cells using the Human CD71 antibody binding properties via a flow cytometry system. The glass compounds 0 and 5% Ga doped glasses at the concentration of 10 mg/mL were used to investigate the level of surface transferrin.

As shown in Figure 4.9, expression of TfR for both OS HOS and U2 cells in negative control samples was significantly higher than the hMSC cells (~30000, 33000 and 4000 in order). It is interesting to note that the expression in all the cell types increased by 1.3 folds exposing them to 5% Ga conditioned media.

The expression of TfR was observed in hMSC cells, and the level of expression was significantly lower compared to the cancer cell line (~4000). No significant difference was observed between the samples, which were treated with Ga free glass compounds and the negative control. However, the TfR expression level was increased for the samples which were exposed to 5% Ga containing medium.

It is evident from the results that analysis of the antibody binding to TfRs on intact cells, as seen in Figure 4.9, compared to hMSC cells, HOS and U2 cells had 7 folds more Tf binding sites.

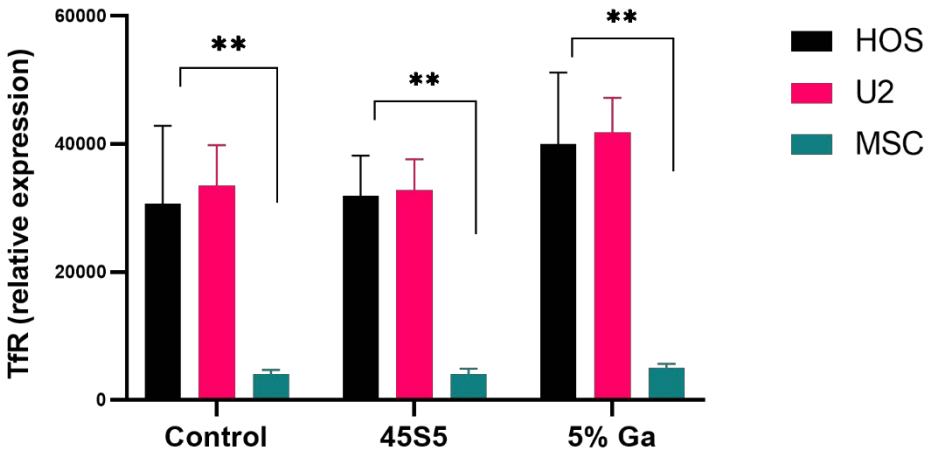

Figure 4.9. Cells seeded at 5000 cells/cm^2 and let them grow for 24 hours in T25 flasks. Then the media was swapped with conditioned media and the expression of transferrin receptor was investigated after 24 hours.

4.4.4 Caspase activity

Caspase proteins, in particular caspases 3 and 7, are essential to the process of apoptosis, or programmed cell death [14]. One important aspect of the cytotoxicity impact of anticancer medicinal agents is their capacity to activate caspase proteins. Caspase 3/7 activity was investigated across three cell types: HOS and U2 (osteosarcoma cell line) and hMSC following treatment with different conditions: Negative control, 45S5, 5%, and H2O2 (positive control) (Figure 4.10).

Under control conditions, all three cell lines displayed minimal baseline caspase 3/7 activity, indicating low levels of apoptosis. Treatment with the 5% Ga compounds significantly increased caspase 3/7 activity in HOS and U2 cells relative to the control ($p < 0.0001$ and $p < 0.001$, respectively). HOS cells showed approximately 1.5 fold higher caspase activity than U2 cells and nearly 3-fold higher activity than hMSC under this condition, suggesting selective induction of apoptosis in OS cell lines. The difference between the control and 5% treatment groups was statistically significant, while the comparison between the 45S5 treated and control groups was non-significant (ns), indicating no meaningful increase in caspase activity in response to Ga-free samples. As demonstrated in Figure 4.10 A, the Ga ions did not stimulate the activation of caspase in hMSC. Conditioned media with 5% Ga compounds have had the highest cytotoxic effect on OS cells so far. However, the hMSC cells exhibited minimal impact on the caspase activity. For the positive control, the cells were treated with hydrogen peroxide, and it is shown it induced a high cytotoxic effect as expected.

To visualise caspase activity in cells treated with conditioned media, image analysis was conducted. This provides the prospect of visualisation as well as quantification of apoptosis, providing insights into the efficacy of Ga compounds in inducing apoptosis. Images were captured using a Leica fluorescent microscope at 10x magnification. As shown in Figure 4.10. B, HOS, and U2 OS cells demonstrated a significant increase in caspase 3 and 7 positive cells in the samples treated with 5% Ga conditioned media, as compared to the control group. However, the results show that the effect of Ga doped conditioned media was more intense on HOS cells compared to U2 OS cells. The observed images of cellular efficacy of Ga doped conditioned media on hMSC cells suggest the low impact of Ga ions on hMSC cells.

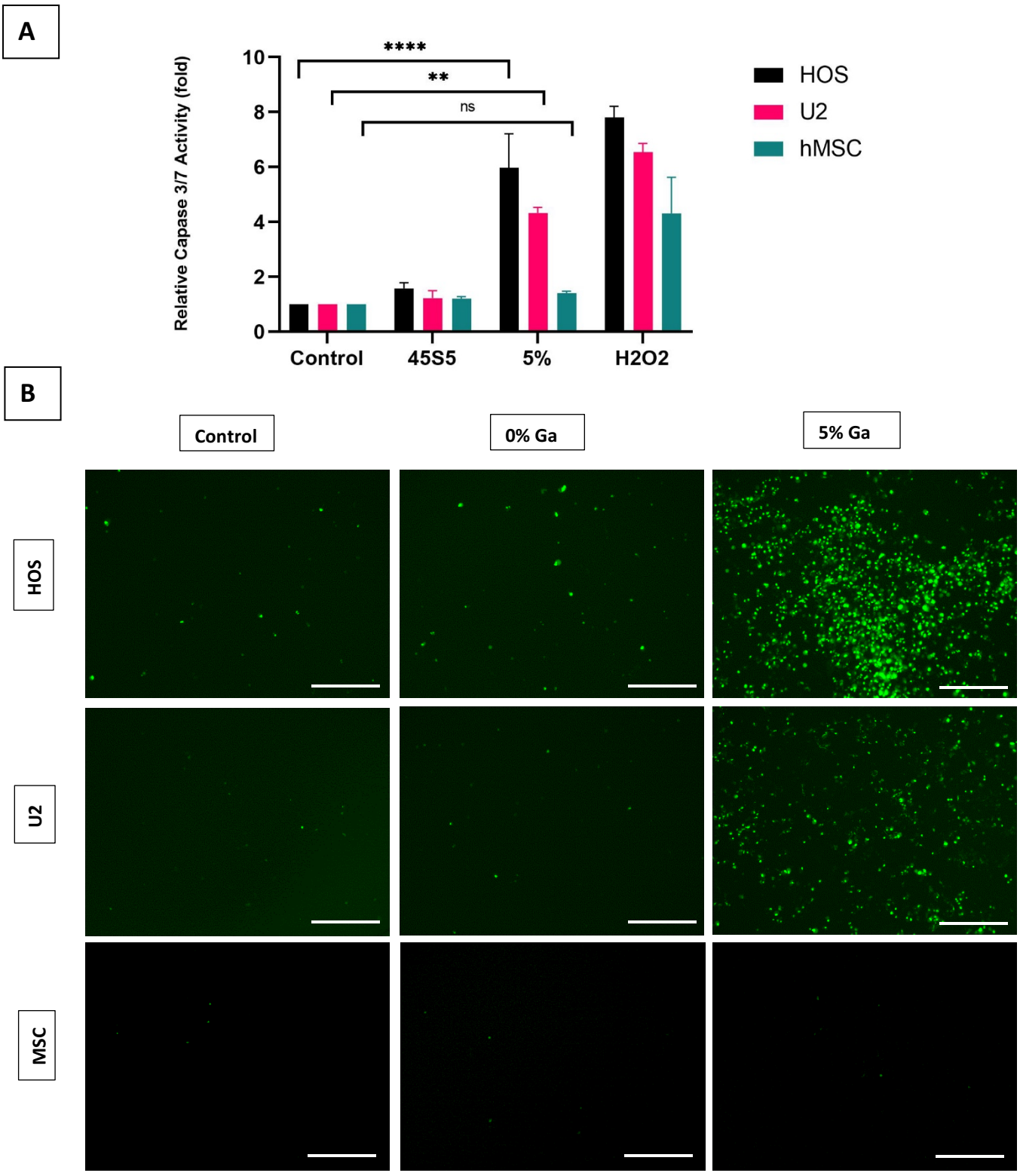

Figure 4.10. A) Relative caspase 3/7 activity in HOS, U2, and hMSC cells following treatment with Control, 45S5, 5% Ga, and H2O2. Data are presented as fold change in caspase activity relative to the control condition. Statistical significance is indicated by *p < 0.01; **p < 0.001; ****p < 0.0001; ns = not significant. **B)** Representative fluorescent microscopy images of HOS, U2, and hMSC cells stained for apoptosis markers following treatment with Control, 45S5, 5%, and H2O2 using Caspase 3/7 Green detection kit. Images were captured using a Leica fluorescent microscope. Scale bar = 300 µm.

4.5 Discussion

As stated in the introductory chapter, several studies have investigated the cytotoxic effect of bioactive glass on various types of cancer. However, very few studies have elucidated its impact against OS. The aim of this study was to investigate the cytotoxic effect of Ga-doped BG on OS cancer cells (HOS and U2) as well as human mesenchymal stem cells (hMSC). We used BG 4555 and Ga-doped BG with a 3-5 mol% Ga content and investigated the effect of the dissolution products of the BGs on the growth and viability of these cells. We further investigated the mechanism of action of Ga ions by analysing their cellular uptake and assessing their ability to induce apoptosis.

In the context of bone cancer, the role of hMSC cells is extremely important, where, in post-amputation they promote healing and regeneration due to their differentiation into osteoblasts. Moreover, they are very important for the process of wound healing due to their capability in the modulation of immune response and promoting angiogenesis, which is vital for the process of healing [15, 16]. Therefore, it is important to investigate the toxic effect of Ga doped BG on hMSC.

In order to investigate the cytotoxic effect of Ga doped BG conditioned media, the dissolution product of the BGs was used, which was exposed to OS cells, HOS and U2, as well as hMSC cells, for a period of 10 days. The cytotoxic effect was analysed using the MTT assay at the time points mentioned earlier. The dissolution product of Ga doped glass was found to have a strong cytotoxic impact on OS, HOS and U2 cells. MTT assay results revealed a dose-dependent decrease in the OS cell viability after treatment with conditioned media. This indicates a significant cytotoxic effect on OS cells resulting from the efficacy of Ga ions present in the conditioned media. The viability of the cells exposed to the Ga free samples was not compromised which indicates that the cytotoxic effect is due to the efficacy of Ga compounds rather than the composition of the BG. These findings align with previous studies, which have demonstrated Ga compounds have been shown to exert cytotoxic effects on various cancer cell lines, including breast and prostate cancer cells [17, 18]. Gallium binds Tf, facilitating the cellular uptake of iron and gallium through TR-mediated endocytosis. Intracellular gallium inhibits cell proliferation by blocking ribonucleotide reductase, an iron-containing enzyme crucial for DNA synthesis and repair. It also induces apoptosis via the mitochondrial pathway by activating proapoptotic BAX and caspase-3 [19-21]. Our study extends this understanding

and demonstrates that in osteosarcoma cells, gallium-doped bioactive glass is effective in reducing cell viability for these cells.

The selective cytotoxicity in OS cells observed with Ga doped glasses is encouraging when compared with other studies. In one such study by Souza et al. demonstrated application of Ga doped BG induced only a 40% decline in viability in OS Saos-2 cells [22]. Another study by Medeiros et al. introduced a new niobium and Ga glass with potential for bone cancer application, which was applied through a sol-gel method of glass fabrication. However, in this work, no cell study has been performed to determine the efficacy of the fabricated glass on OS cells. Moreover, in the characteristic analysis, no ICP assay was performed to demonstrate the ion release profile of the glass [23]. Considering the fact that the bioactivity and ion bioavailability of the glasses can be illustrated after exposing the glass compounds to biological fluids, further investigations for this study were crucial to claim the glass's potential for cancer-targeted therapy. A different study by Deliormanlı et al. fabricated silica-based BG with trivalent rare-earth ions (Eu^{3+}, Gd^{3+}, and Yb^{3+}) for bone cancer treatment and their results demonstrated less than 50% cell viability reduction for the OS Saos-2 cell line after 7 days of treatment. While the results show approximately 50% cell viability reduction against healthy fibroblast cells, which indicates high toxicity [24]. In this current study, the MTT results show that Ga-doped conditioned media have minimal side effects on healthy hMSCs. Notably, samples containing 5 mol% Ga, which induces the highest toxicity in cancer cells, did not compromise the viability of healthy hMSCs, with no significant reduction in cell viability observed.

Despite being applied at the same concentration, 5% Ga-doped BG did not exhibit cytotoxic effects on hMSCs, in contrast to the significant reduction in cell viability observed with conventional 45S5 bioglass at the concentration of 20 mg/mL. This discrepancy highlights the impact of glass composition on cytocompatibility. The inclusion of Ga appears to modulate the material’s dissolution behaviour, potentially resulting in a more controlled release of ions and a stabilized pH environment. In comparison, 45S5 is known for its rapid ion exchange, which can lead to sudden increases in alkalinity and osmotic stress, conditions that are detrimental to cell health [25, 26]. It is also possible that Ga incorporation alters the glass network structure in a way that buffers excessive calcium or silicate ion release, thus reducing cellular stress responses [27]. Together, these findings suggest that Ga-doping not only

preserves the antineoplastic properties of the glass but also enhances its cytocompatibility, making it a promising candidate for clinical applications.

In the context of this study, we have managed to fabricate Ga doped BG with a higher mol% of gallium content (5%), which induces over 99% cell death against 3 different OS cells, Saos-2, HOS and U2, with minimum side effects and toxicity on healthy NHOst and hMSC cells. This was indeed confirmed in chapter 3 of this study, where in NHOst cells, no significant toxicity was observed after 10 days of treatment with Ga containing conditioned media.

To further evaluate the cytotoxic effects of Ga-doped BG, we also performed a cytotoxic Live/Dead assay on the aforementioned OS cells, HOS and U2, as well as hMSC. As shown in Figures 4.3 to 4.6, over 99% cell death was observed after 10 days of treatment with Ga-doped BG containing 5% Ga for OS HOS and U2. The results from the Live/Dead assay align well with the MTT in terms of cytotoxic effect of Ga doped bioactive glass on the osteosarcoma cells. Therefore, it can be concluded that Ga-doped glass compositions not only induce toxicity in osteosarcoma cells as the Ga content increases but also stimulate higher toxicity levels with increasing concentrations. In contrast, the viability results for hMSC cells exposed to Ga-doped bioactive glasses showed extremely high viability and minimal toxicity compared to OS cells. This is highly promising as it confirms that even the highest Ga content and concentration in bioactive glasses do not cause significant toxicity to hMSCs.

In clinical practice, gallium compounds are utilised as both diagnostic and therapeutic agents for cancer and conditions affecting calcium and bone metabolism. Numerous studies have demonstrated that gallium is absorbed by various malignant cells *in vitro* via cell surface transferrin receptor-mediated endocytosis of Ga-transferrin complexes. Cancer cells have a higher demand for iron than other rapidly growing cells, they have a higher level of TfR expression [28].

Previous studies demonstrated that gallium and iron shared chemical properties with respect to their ionic radius. Gallium shares some properties with iron (III). The octahedral ionic radius of Ga^{3+} is 0.620 Å, compared to 0.645 Å for high spin Fe^{3+}. In tetrahedral coordination, the ionic radii are 0.47 Å for Ga3+ and 0.49 Å for Fe^{3+}. The ionisation potential and electron affinity for Ga^{3+} are 64 eV and 30.71 eV, respectively, while those for high spin Fe^{3+} are 54.8 eV and 30.65 eV, respectively [29]. Due to these similarities, it is assumed that the uptake mechanism for gallium and iron is similar. Ga ions can form a bond with transferrin, which is the iron transport protein in blood, and internalise into the cells. Therefore, understanding the level

of TfR expression in OS cells (HOS and U2-OS) might help determine the Ga mechanism of efficacy on these cells and the potential of Ga doped bioactive glass as therapeutic targets for the treatment of OS [30]. The significance of the TfR in cellular absorption of Ga has been demonstrated. Therefore, it stands to reason that cells with more TfRs would be more sensitive to Ga ions.

The level of TfRs on intact cells was investigated using the Human CD71 antibody binding evaluation, in order to understand whether, the difference in susceptibility to Ga ions between OS cells and healthy hMSC cells may be connected to variations in TfRs on the cell surface. OS HOS and U2, as well as hMSC cells, were treated with Ga containing medium, and the level of surface transferrin receptor was investigated using flow cytometry. According to our results TfR level increased in both HOS and U2 cells, which can be related to their aggressive proliferation rates which is the main characteristics of cancer cells. OS cells demonstrated a significantly higher level of surface TfR compared to hMSC, which showed a markedly lower level of TfR. This disparity highlights the modified iron metabolism in cancer cells [31]. These results are consistent with previous studies that have observed similar increases in transferrin receptor expression in various cancers, such as bladder, lymphoma, and breast cancer [32-34]. Our findings expand this understanding to osteosarcoma, providing additional evidence of the common strategy employed by cancer cells to meet their iron requirements. The high expression of TfRs in OS cells offers a promising target for therapeutic intervention. Therapies aimed at inhibiting TfR activity or delivering cytotoxic agents specifically via these receptors could selectively target OS cells while minimising detrimental effects on non-cancerous cells with lower receptor levels. These findings not only enhance our understanding of iron metabolism in cancer cells but also pave the way for the development of TfR-targeted therapies for osteosarcoma.

Gallium compounds have been investigated intensively due to their cytotoxic properties on cancer cells. It is therefore essential to comprehend the Ga mechanism of cell death to maximise their therapeutic efficiency and reduce side effects. The protease enzyme family known as caspases is activated during apoptosis. In order to verify the induction of apoptosis, caspase assays quantify the activity of these enzymes [35]. The increase in caspase activity is the main indication that the Ga doped BG stimulated apoptosis in cancer cells [36]. The caspase cascade is responsible for executing programmed cell death, which is followed by cytochrome c release [35].

In order to investigate if the growth inhibitory effects of Ga ions were caused by apoptosis induction, OS cells as well as hMSC cells were incubated with the Ga doped bioactive glass with the highest Ga content and caspase activity was investigated to analyse the apoptotic effect. Results showed a significant activation of caspase 3/7 in OS cells, which were exposed to Ga doped conditioned media, which indicated robust induction of apoptosis. In comparison to the untreated control group, the treated cells exhibited significantly elevated caspase activity. This indicates that Ga doped bioactive glass successfully activates apoptotic pathways, whereas the control cells retained their baseline caspase levels. The apoptotic effects of Ga compounds align with prior research indicating that gallium compounds can disturb mitochondrial function, resulting in cytochrome c release and subsequent caspase activation [37, 38]. Our results are consistent with Chitambar et al., who observed comparable rises in caspase activity in cancer cells treated with gallium-based compounds [36]. However, our study advances this knowledge by illustrating that gallium-doped bioactive glass induces apoptosis specifically in osteosarcoma cells, which is a novel discovery in this field. The findings indicate that caspase activity was significantly lower for samples which were exposed to Ga free conditioned media, indicating that cytotoxicity effects on the cells are due to the presence of the Ga ions rather than the compositional elements of the BGs (Figure 4.10).

It is interesting to note that the effect of the Ga containing conditioned media is more intense in HOS cells compared to U2 and OS cells. This was observed both in the qualitative and quantitative data. The results consistently demonstrated that HOS cells show more aggressive properties than U2 cells. This conclusion is supported by several key observations. Firstly, HOS cells proliferated at a much higher rate than U2 cells, indicating a greater capacity for rapid growth, which is a characteristic of aggressive cancer phenotypes. Wound healing and migration assays showed that HOS cells possess enhanced migratory and invasive abilities compared to U2 cells. The fast rate of wound closure in HOS cultures suggests a greater potential for metastasis. These findings provide strong evidence that HOS cells are more aggressive than U2 cells [39-41].

The results showed the minimal effect of caspase activation in the hMSC cells exposed to the Ga doped bioactive glasses. This was expected due to their reduced expression of transferrin receptors compared to OS cells. Therefore, Ga compounds enter the cells at significantly lower levels compared to cancer cells. The results are consistent with the findings from the

TfR expression level experiments are discussed earlier in the chapter. Earlier studies had reported Ga induced cell death involves mitochondrial pathways [19, 42]. Studies reported that when human leukaemia/lymphoma cells are exposed to gallium compounds, inositol phosphatidylserine, an early sign of apoptosis, is translocated to the cell surface. That leads to loss of mitochondrial membrane, followed by release of cytochrome c from the mitochondria into the cytoplasm and the activation of caspase-3 and 7, which causes morphological changes associated with apoptosis [19, 36, 37]. In general, these results indicate that Ga-doped BG has a significant impact on caspase activity in cancer cells, with only a minor effect observed on hMSC cells at the highest concentration tested.

Figure 4.10 B represents the qualitative data that was generated by fluorescence microscopic image capture post-treatment with caspase reagents. As the results demonstrated, an increase in caspase activity was observed in cancer cells compared with untreated control samples, suggesting that the gallium compound triggers apoptosis. Furthermore, contrasting the activity of caspase in cancer and normal cells may shed light on the Ga-doped BG selectivity and possible therapeutic window. Caspases 3 and 7 are identified as executioner caspases due to their key roles in the induction and completion of apoptosis [43]. Upon activation, they cleave to a range of cellular substrates, resulting in programmed cell death, which is the distinctive morphological and biochemical alterations of apoptosis, which include membrane blebbing, DNA fragmentation, and shrinking of the cell [14, 44]. Investigation of caspases 3 and 7 can confirm that the mechanism of cell death is indeed apoptosis, rather than that of other forms of cell death, such as necrosis. This is a more chaotic and damage-induced form of cell death, which can lead to inflammation, whilst apoptosis is a regulated and planned process [45, 46]. In both cancer cells, caspase activity has increased post-treatment with Ga doped conditioned medium, which indicates the high efficacy of Ga compounds against OS cells. The results suggest that the Ga compounds have target specificity as compared to the caspase 3 and 7 activity, versus non-cancerous cells, can reveal that the treatment selectively triggers apoptosis in OS cells, while in hMSC cells, no caspase activity was observed. This is an important finding, as it suggests that the Ga compounds have minimal side effects for normal, healthy cells.

4.6 Conclusion:

The effect of bioactive glasses 45S5 and Ga doped 3-5% glasses on the viability of OS, HOS, and U2, as well as hMSC cells, was examined using MTT and Live/Dead assays. The results showed strong, dose- and time-dependent cytotoxicity in HOS and U2 cells, with 5 mol% Ga the most potent: HOS showed no viable cells by day 5 at both 10 and 20 mg/mL, 4 mol% Ga also caused marked inhibition. Ga-free 45S5 did not reduce OS viability. Selectivity for cancer over healthy cells was maintained across conditions. hMSCs retained high viability at both 10 and 20 mg/mL for all Ga contents, including 5 mol%, whereas conventional 45S5 at 20 mg/mL depressed hMSC metabolic activity. These findings define a therapeutic window in which Ga-doped glasses kill OS cells effectively while sparing hMSCs.

Mechanistically, OS cells displayed substantially higher TfR levels than hMSCs, with an additional ~1.3-fold increase after exposure to 5 mol% Ga conditioned media, consistent with TfR-mediated Ga uptake. Caspase-3/7 activity rose significantly in HOS and U2 but not in hMSCs, indicating apoptosis as the predominant death pathway and supporting cancer-cell selectivity. Together, these data link efficacy to a plausible uptake mechanism and an apoptotic mode of action.

Based on efficacy, selectivity, and mechanistic readouts, 3-5 mol% Ga meets performance criteria in OS models, with 5 mol% Ga emerging as the lead composition; earlier investigated 1-2 mol% Ga was sub-efficacious and hence were not taken forward. Therefore, this chapter established that Ga-BGs (3-5 mol% Ga) and particularly 5 mol% deliver potent, selective anti-osteosarcoma activity via TfR-linked uptake and caspase-mediated apoptosis while preserving hMSC viability.

4.7 References

[1] F. Kurtuldu, N. Mutlu, A. R. Boccaccini, and D. Galusek, "Gallium containing bioactive materials: A review of anticancer, antibacterial, and osteogenic properties," *Bioact Mater*, no. December, 2022, doi: 10.1016/j.bioactmat.2021.12.034.

[2] R. D. Aspasio, R. Borges, and J. Marchi, "Biocompatible glasses for cancer treatment," *Advanced Structured Materials*, vol. 53, pp. 249–265, 2016, doi: 10.1007/978-3-319-44249-5_10.

[3] I. D. Xynos, M. V. J. Hukkanen, J. J. Batten, L. D. Buttery, L. L. Hench, and J. M. Polak, "Bioglass ®45S5 stimulates osteoblast turnover and enhances bone formation in vitro: Implications and applications for bone tissue engineering," *Calcif Tissue Int*, vol. 67, no. 4, pp. 321–329, 2000, doi: 10.1007/s002230001134.

[4] M. Vallet-Regí and E. Ruiz-Hernández, "Bioceramics: From bone regeneration to cancer nanomedicine," *Advanced Materials*, vol. 23, no. 44, pp. 5177–5218, 2011, doi: 10.1002/adma.201101586.

[5] P. Collery, B. Keppler, C. Madoulet, and B. Desoize, "Gallium in cancer treatment," *Crit Rev Oncol Hematol*, vol. 42, no. 3, pp. 283–296, 2002, doi: 10.1016/S1040-8428(01)00225-6.

[6] C. R. Chitambar and W. E. Antholine, "Iron-targeting antitumor activity of gallium compounds and novel insights into triapine®-metal complexes," Mar. 10, 2013. doi: 10.1089/ars.2012.4880.

[7] H. S. Alhajala *et al.*, "The cytotoxicity of gallium maltolate in glioblastoma cells is enhanced by metformin through combined action on mitochondrial complex 1," 2020. [Online]. Available: www.oncotarget.com

[8] C. R. Chitambar *et al.*, "Gallium maltolate disrupts tumor iron metabolism and retards the growth of glioblastoma by inhibiting mitochondrial function and ribonucleotide reductase," *Mol Cancer Ther*, vol. 17, no. 6, pp. 1240–1250, Jun. 2018, doi: 10.1158/1535-7163.MCT-17-1009.

[9] C. R. Chitambar, "Medical applications and toxicities of gallium compounds," 2010, *MDPI*. doi: 10.3390/ijerph7052337.

[10] C. Shang, H. Zhou, W. Liu, T. Shen, Y. Luo, and S. Huang, "Iron chelation inhibits mTORC1 signaling involving activation of AMPK and REDD1/Bnip3 pathways," *Oncogene*, vol. 39, no. 29, pp. 5201–5213, Jul. 2020, doi: 10.1038/s41388-020-1366-5.

[11] S. U. Lauvrak *et al.*, "Functional characterisation of osteosarcoma cell lines and identification of mRNAs and miRNAs associated with aggressive cancer phenotypes," *Br J Cancer*, vol. 109, no. 8, pp. 2228–2236, Oct. 2013, doi: 10.1038/bjc.2013.549.

[12] L. Ottaviano *et al.*, "Molecular characterization of commonly used cell lines for bone tumor research: A trans-European EuroBoNet effort," *Genes Chromosomes Cancer*, vol. 49, no. 1, pp. 40–51, Jan. 2010, doi: 10.1002/gcc.20717.

[13] C. R. Chitambar, "Gallium-containing anticancer compounds," *Future Med Chem*, vol. 4, no. 10, pp. 1257–1272, 2012, doi: 10.4155/fmc.12.69.

[14] S. Kumar, "Caspase function in programmed cell death," Jan. 2007. doi: 10.1038/sj.cdd.4402060.

[15] M. Kazemi, M. M. Dehghan, and M. Azami, "Biological evaluation of porous nanocomposite scaffolds based on strontium substituted β-TCP and bioactive glass: An in vitro and in vivo

study," *Materials Science and Engineering C*, vol. 105, no. July, p. 110071, 2019, doi: 10.1016/j.msec.2019.110071.

[16] R. Guillamat-Prats, "The role of MSC in wound healing, scarring and regeneration," Jul. 01, 2021, *MDPI*. doi: 10.3390/cells10071729.

[17] S. M. El-sonbaty, F. S. M. Moawed, E. I. Kandil, and A. M Tamamm, "Antitumor and Antibacterial Efficacy of Gallium Nanoparticles Coated by Ellagic Acid," *Dose-Response*, vol. 20, no. 1, Jan. 2022, doi: 10.1177/15593258211068998.

[18] S. C. Dixon *et al.*, "In vitro effect of gallium nitrate when combined with ketoconazole in the prostate cancer cell line PC-3," *Cancer Lett*, vol. 113, no. 1–2, pp. 111–116, Feb. 1997, doi: 10.1016/S0304-3835(97)04603-X.

[19] C. R. Chitambar, J. P. Wereley, and S. Matsuyama, "Gallium-induced cell death in lymphoma: Role of transferrin receptor cycling, involvement of Bax and the mitochondria, and effects of proteasome inhibition," *Mol Cancer Ther*, vol. 5, no. 11, pp. 2834–2843, Nov. 2006, doi: 10.1158/1535-7163.MCT-06-0285.

[20] J. Narasimhan, W. E. Antholine, and C. R. Chitambar, "Effect of gallium on the tyrosyl radical of the iron-dependent M2 subunit of ribonucleotide reductase," *Biochem Pharmacol*, vol. 44, no. 12, pp. 2403–2408, Dec. 1992, doi: 10.1016/0006-2952(92)90686-D.

[21] C. R. Chitambar, W. G. Matthaeus, W. E. Antholine, K. Graff, and W. J. O'Brien, "Inhibition of Leukemic HL60 Cell Growth by Transferrin-Gallium: Effects on Ribonucleotide Reductase and Demonstration of Drug Synergy With Hydroxyurea," *Blood*, vol. 72, no. 6, pp. 1930–1936, Dec. 1988, doi: 10.1182/BLOOD.V72.6.1930.1930.

[22] L. Souza, F. V. Ferreira, J. H. Lopes, J. A. Camilli, and R. A. Martin, "Cancer Inhibition and in Vivo Osteointegration and Compatibility of Gallium-Doped Bioactive Glasses for Osteosarcoma Applications," *ACS Appl Mater Interfaces*, vol. 14, no. 40, pp. 45156–45166, Oct. 2022, doi: 10.1021/acsami.2c12102.

[23] G. S. Medeiros *et al.*, "A perfect pair: Niobium- and gallium-doped ceramic biomaterial enabled by coupled synthesis method with potential application for bone regeneration and cancer-targeted therapy," *J Non Cryst Solids*, vol. 599, p. 121962, Jan. 2023, doi: 10.1016/J.JNONCRYSOL.2022.121962.

[24] A. M. Deliormanlı, M. Ensoylu, and H. Atmaca, "Preparation of trivalent rare-earth element-substituted bioactive glass robocast scaffolds for osteosarcoma treatment: structural, morphological, mechanical, drug delivery, and biological properties," *Appl Phys A Mater Sci Process*, vol. 130, no. 3, Mar. 2024, doi: 10.1007/s00339-024-07334-9.

[25] K. S. Rana, L. P. De Souza, M. A. Isaacs, F. N. S. Raja, A. P. Morrell, and R. A. Martin, "Development and Characterization of Gallium-Doped Bioactive Glasses for Potential Bone Cancer Applications," *ACS Biomater Sci Eng*, vol. 3, no. 12, pp. 3425–3432, 2017, doi: 10.1021/acsbiomaterials.7b00283.

[26] A. W. Wren *et al.*, "A preliminary investigation into the structure, solubility and biocompatibility of solgel SiO2–CaO–Ga2O3 glass-ceramics," *Mater Chem Phys*, vol. 148, no. 1–2, pp. 416–425, Nov. 2014, doi: 10.1016/J.MATCHEMPHYS.2014.08.006.

[27] A. Hoppe, N. S. Güldal, and A. R. Boccaccini, "A review of the biological response to ionic dissolution products from bioactive glasses and glass-ceramics," *Biomaterials*, vol. 32, no. 11, pp. 2757–2774, 2011, doi: 10.1016/j.biomaterials.2011.01.004.

[28] C. R. Chitambar, “The therapeutic potential of iron-targeting gallium compounds in human disease: From basic research to clinical application,” *Pharmacol Res*, vol. 115, pp. 56–64, Jan. 2017, doi: 10.1016/J.PHRS.2016.11.009.

[29] L. R. Bernstein, “Mechanisms of Therapeutic Activity for Gallium,” 1998. [Online]. Available: http://www.pharmrev.org

[30] C. R. Chitambar, “Gallium and its competing roles with iron in biological systems,” *Biochim Biophys Acta Mol Cell Res*, vol. 1863, no. 8, pp. 2044–2053, 2016, doi: 10.1016/j.bbamcr.2016.04.027.

[31] K. Salnikow, “Role of iron in cancer,” *Semin Cancer Biol*, vol. 76, pp. 189–194, Nov. 2021, doi: 10.1016/J.SEMCANCER.2021.04.001.

[32] X. Wu, R. E. Sells, and S. T. Hwang, “Upregulation of Inflammatory Cytokines and Oncogenic Signal Pathways Preceding Tumor Formation in a Murine Model of T-Cell Lymphoma in Skin,” *Journal of Investigative Dermatology*, vol. 131, no. 8, pp. 1727–1734, Aug. 2011, doi: 10.1038/JID.2011.89.

[33] K. C. Gatter, G. Brownt, I. S. Trowbridget, R.-E. Woolston, and D. Y. Mason, “Transferrin receptors in human tissues: their distribution and possible clinical relevance,” 1983. [Online]. Available: http://jcp.bmj.com/

[34] N. W. SMITH *et al.*, “Transferrin Receptor Expression in Primary Superficial Human Bladder Tumours Identifies Patients who Develop Recurrences,” *Br J Urol*, vol. 65, no. 4, pp. 339–344, Apr. 1990, doi: 10.1111/j.1464-410X.1990.tb14752.x.

[35] J. Li and J. Yuan, “Caspases in apoptosis and beyond,” Oct. 20, 2008. doi: 10.1038/onc.2008.297.

[36] C. R. Chitambar, D. P. Purpi, J. Woodliff, M. Yang, and J. P. Wereley, “Development of gallium compounds for treatment of lymphoma: Gallium maltolate, a novel hydroxypyrone gallium compound, induces apoptosis and circumvents lymphoma cell resistance to gallium nitrate,” *Journal of Pharmacology and Experimental Therapeutics*, vol. 322, no. 3, pp. 1228–1236, Sep. 2007, doi: 10.1124/jpet.107.126342.

[37] C. R. Chitambar, “Gallium-containing anticancer compounds,” Jun. 2012. doi: 10.4155/fmc.12.69.

[38] C. R. Chitambar, “10. GALLIUM COMPLEXES AS ANTICANCER DRUGS,” in *Metallo-Drugs: Development and Action of Anticancer Agents*, De Gruyter, 2018, pp. 281–302. doi: 10.1515/9783110470734-010.

[39] C. R. Walkley, *Modeling osteosarcoma: In vitro and in vivo approaches*, Second Edi. Elsevier Inc., 2015. doi: 10.1016/B978-0-12-416721-6.00017-0.

[40] A. Abarrategi *et al.*, “Osteosarcoma: Cells-of-Origin, Cancer stem cells, and targeted therapies,” *Stem Cells Int*, vol. 2016, 2016, doi: 10.1155/2016/3631764.

[41] D. A. Fernandes, A. A. Costa, and P. Lahdenperä, “Osteosarcoma Genetics and Epigenetics: Emerging Biology and Candidate Therapies,” *International Journal of Construction Management*, vol. 18, no. 6, pp. 482–496, 2018, doi: 10.1080/15623599.2017.1344913.

[42] C. R. Chitambar, “The therapeutic potential of iron-targeting gallium compounds in human disease: From basic research to clinical application,” *Pharmacol Res*, vol. 115, pp. 56–64, 2017, doi: 10.1016/j.phrs.2016.11.009.

[43] S. A. Lakhani *et al.*, “Caspases 3 and 7: Key mediators of mitochondrial events of apoptosis,” *Science (1979)*, vol. 311, no. 5762, pp. 847–851, Feb. 2006, doi: 10.1126/science.1115035.

[44] T. J. Fan, L. H. Han, R. S. Cong, and J. Liang, “Caspase family proteases and apoptosis,” *Acta Biochim Biophys Sin (Shanghai)*, vol. 37, no. 11, pp. 719–727, Nov. 2005, doi: 10.1111/j.1745-7270.2005.00108.x.

[45] A. Boice and L. Bouchier-Hayes, “Targeting apoptotic caspases in cancer,” *Biochimica et Biophysica Acta (BBA) - Molecular Cell Research*, vol. 1867, no. 6, p. 118688, Jun. 2020, doi: 10.1016/J.BBAMCR.2020.118688.

[46] M. A. Savitskaya and G. E. Onishchenko, “Mechanisms of apoptosis,” Nov. 01, 2015, *Maik Nauka Publishing / Springer SBM*. doi: 10.1134/S0006297915110012.

Chapter 5

Antimicrobial Effect of Gallium-Doped Bioactive Glass

5.1 Introduction

Orthopaedic surgical site infections (SSIs) represent a significant complication following bone and joint procedures, contributing to considerable morbidity, prolonged hospital stays, and increased healthcare costs. These infections commonly occur following implantation of prosthetic devices, fracture fixation hardware, or joint replacements, where foreign materials provide a favourable surface for microbial colonisation and biofilm formation [1]. Among the most frequently implicated pathogens are both Gram-positive and Gram-negative bacteria, notably *Staphylococcus aureus* (*S. aureus*) and *Escherichia coli (E. coli*) [2], [3].

The incidence of SSIs in orthopaedic surgery varies depending on the procedure and patient risk factors, but it is estimated to occur in up to 2-5% of joint arthroplasties and as high as 10% in trauma-related implant surgeries. Once established, these infections are notoriously difficult to eradicate due to biofilm-mediated resistance to conventional antimicrobial agents and immune evasion. This has a major influence on functional results and quality of life since many patients need revision operations, long-term antimicrobial medication, systemic infection, delayed tissue healing, or even implant removal. Additionally, because orthopaedic SSIs frequently cost more than tens of thousands of dollars each case, they significantly strain healthcare systems financially. In an era of rising antimicrobial resistance, the effective prevention and management of orthopaedic SSIs has become an urgent clinical and research priority [4].

Bioactive glasses which originally developed for bone healing, have evolved into versatile delivery platforms for therapeutic agents and ions, enabling tailored biological responses such as antibacterial, angiogenic, and osteogenic effects [5, 6]. Moreover, several metal oxides, including copper, cobalt, and zinc, have demonstrated intrinsic broad-spectrum antimicrobial activity. The ability of BGs to release therapeutic ions during dissolution, thereby promoting osteogenesis and angiogenesis, has been extensively studied [7].

Gallium (Ga), a transition metal oxide with strong antimicrobial potential, mimics iron and disrupts essential bacterial metabolic processes. By competing with iron for uptake through bacterial transport systems, Ga interferes with iron-dependent functions such as DNA synthesis, respiration, and enzyme activity, ultimately leading to bacterial death [8, 9].

Given this promising profile, the present study aims to investigate the antimicrobial efficacy of Ga within a BG network, specifically targeting *E. coli* and *S. aureus* as representative Gram-

negative and Gram-positive pathogens, respectively. To achieve this, we employed a combination of quantitative and qualitative methodologies, including viability assays, time-kill assays, and BacLight Live/Dead assays.

The underlying rationale of this study is that gallium-doped bioactive glass (Ga-BG) can exert its antibacterial activity at the earliest stages of bacterial contamination, thereby preventing the establishment of infection by inhibiting initial bacterial adhesion and biofilm formation. By delivering localised, sustained antibacterial action, Ga-BGs have the potential to neutralise residual pathogens introduced during surgery. The primary goal of this approach is to improve patient outcomes and implant success by actively preventing infection rather than just treating it.

The results reported in this chapter significantly impact the development of Ga-doped bioactive glasses as multipurpose materials for therapeutic applications. This work advances our knowledge of Ga-BGs structural elements affecting bacterial susceptibility by assessing the dose-dependent effects of Ga on both *S. aureus* and *E. coli*. Additionally, the use of complementary assays bridges the gap between *in vitro* research and practical clinical applications by offering a comprehensive evaluation of Ga's antibacterial properties.

5.2 Aim

The aim of this chapter is to evaluate the antimicrobial effects of dissolution products from Ga-doped bioactive glasses (Ga-BGs) on the bacterial strains *E. coli* and *S. aureus*. This was accomplished by investigating,

- The effect of the glass dissolution product on the bacterial strains' viability.
- Time kill assay to assess the antimicrobial activity of Ga-BG dissolution products over time.
- Viability via Live/Dead assay on *E. coli* which were exposed to the conditioned media for a period of 24 hours.

5.3 Materials and methods

The bioactive glasses used in this study were manufactured using the melt-quench, method described in Chapter 2, Section 2.3.1 (Glass preparation). The compositions and processing conditions were identical to those detailed in chapter 2. All experiments were performed in triplicate (n = 3) using samples prepared from the same glass production batch to ensure consistency and reproducibility across all analyses.

5.3.1 Microbial strains

Two bacterial strains, *Escherichia coli* (NCTC 10538) and *Staphylococcus aureus* (ATCC 6538) were used in this study. The strains were stored at -80°C on MicroBank beads (Pro-Lab Diagnostics, Neston, Cheshire, UK). When required, the beads were inoculated into their respective broths and incubated overnight at 37 °C under aerobic conditions. The resulting cultures were sub-cultured onto agar plates and stored at 4°C for short-term storage until use in experiments. The cultures were diluted in sterile broth for antimicrobial testing to obtain the desired cell density.

5.3.2 Microbiological media

In this study, Nutrient Agar (NA) and Nutrient Broth (NB) were used to culture both strains, as following the manufacturer's guidelines (Thermo Fisher Scientific, USA). The media were sterilised by autoclaving at 121°C for 15 minutes. After sterilisation, the agar was allowed to cool to 55 °C before being dispensed into sterile Petri dishes (Sarstedt Ltd, Leicester, UK). The prepared plates and broths were stored at 4°C until use. PBS was sourced from Fisher Scientific (UK) and prepared by dissolving one tablet in 100 mL of distilled water. The solution was autoclaved at 121°C for 15 minutes to ensure sterility.

5.3.3 Bacterial viability assay using gallium-doped bioactive glass

A bacterial viability assay was performed to evaluate the antimicrobial effects of Ga-BGs on *E. coli* as well as *S. aureus*. This assay assessed bacterial growth through turbidity measurements, providing insight into the BG's potential bacteriostatic and bactericidal properties. The turbidity-based approach was chosen due to its simplicity, reproducibility, and ability to detect subtle changes in bacterial proliferation over time. *E. coli* and *S. aureus* were cultured overnight in nutrient broth at 37 °C to reach the logarithmic phase. The bacterial

suspensions were adjusted to a final concentration of 10^5 CFU/mL using sterile nutrient broth. Bacterial suspensions were mixed at a 1:1 ratio with bioactive glass samples containing varying concentrations of Ga (0%, 3%, 4%, and 5%). In a 96-well microplate, 100 µL of the adjusted bacterial suspension was combined with 100 µL of bioactive glass dissolution product, resulting in a total volume of 200 µL per well. Samples containing only bacteria (without bioactive glass) served as negative controls. In addition to experimental samples containing bacteria and bioactive glass, controls containing sterile nutrient broth and bioactive glass (without bacteria) were prepared. These samples were used to account for any background absorbance contributed by the bioactive glass or broth alone. The absorbance values from these controls were subtracted from the corresponding experimental readings to ensure an accurate representation of bacterial growth and minimise interference from non-bacterial sources. The microplate was incubated under static conditions at 37 °C for 24 hours to allow interaction between the bacteria and bioactive glass. This incubation period was selected to mimic physiological conditions and provide sufficient time to evaluate the inhibitory effects of Ga-BGs on bacterial growth. Bacterial viability was assessed by measuring the absorbance of the turbidity for the samples using a microplate reader (Agilent BioTek™ 800 TS, USA). Absorbance was recorded at 570 nm to reflect bacterial growth. Higher absorbance values indicated increased bacterial proliferation, while reduced absorbance suggested inhibited growth or bacterial death. All measurements were performed in triplicate to ensure reproducibility and minimise variability.

5.3.4 Time kill assay

A time-kill assay was performed as outlined by White *et al,* [11] to evaluate the antimicrobial activity of bioactive glass containing varying concentrations of Ga (0%, 3%, 4%, and 5%) against *E. coli* and *S. aureus*. All experimental tubes were inoculated with an initial microbial density of 10^5 CFU/mL. For the assay, the strains were grown in the nutrient broth to the logarithmic phase at 37 °C. The bacterial suspension was adjusted to 10^5 CFU/mL using sterile broth, and was confirmed using Miles and Misra method. Equal volumes of the adjusted bacterial suspension were mixed 1:1 with bioactive glass samples containing 0%, 3%, 4%, or 5% Ga. A bacterial suspension without bioactive glass served as the negative control. A control containing broth only was prepared as well. The mixtures were incubated statically at 37 °C for 24 hours. At designated time points (0, 2, 6, and 24 hours), 100 µL aliquots were

withdrawn, serially diluted 1:10 in PBS, and plated onto nutrient agar. Plates were incubated at 37 °C for 24 hours, and colony-forming units (CFUs) were counted to determine bacterial viability. All experiments were performed in triplicate to ensure reproducibility.

5.3.5 Bacterial viability staining using LIVE/DEAD® BacLight™ kit

The viability of *E. coli* was evaluated using the LIVE/DEAD® BacLight™ Bacterial Viability Kit (L7012, Molecular Probes, USA). This assay distinguishes live from dead bacteria by exploiting the differential permeability of two nucleic acid stains, SYTO 9 and propidium iodide. SYTO 9 labels all bacterial cells, whereas propidium iodide only penetrates cells with compromised membranes, leading to red fluorescence in dead cells and green fluorescence in live cells.

E. coli cultures were grown in nutrient broth at 37 °C to the logarithmic phase. The following day, the bacterial suspension was adjusted to a final concentration of 10^5 CFU/mL. The bacterial suspension's equal volumes (1:1) were mixed with bioactive glass samples containing 0%, 3%, 4%, and 5% Ga ions. A bacterial suspension without bioactive glass served as the negative control. The mixtures were incubated overnight at 37 °C under static conditions. After 24 hours of incubation, bacterial viability was assessed using the LIVE/DEAD® BacLight™ bacterial viability kit. Bacterial samples were collected by centrifugation at 10,000 ×g for 10 minutes and washed once with 0.85% NaCl to remove any remaining culture medium. To produce positive control samples, the bacterial suspension was incubated in 70% isopropanol for 1 hour at room temperature, with periodic mixing every 15 minutes. Both live and killed bacteria were pelleted by centrifugation and resuspended in 0.85% NaCl. The working stain solution was mixed with equal volumes of SYTO 9 (Component A, 3.34 mM) and propidium iodide (Component B, 20 mM). A 3 µL aliquot of this dye mixture was added to 1 mL of the bacterial suspension. The samples were incubated in the dark at room temperature for 15 minutes for proper staining. After incubation, 5 µL of the stained suspension was placed onto a glass slide and sealed under an 18 mm coverslip (Thermo Fisher Scientific, USA). The samples were examined under a fluorescence microscope equipped with filter sets optimised for SYTO 9 (green fluorescence) and propidium iodide (red fluorescence). Bacteria with intact membranes fluoresced green, while those with damaged membranes appeared red. Fluorescence images were captured using an EVOS™ M5000 Imaging System (Invitrogen™, Thermo Fisher Scientific, USA) at 40X magnification.

5.3.6 Statistical analysis

Statistical significance was assessed using a two-way analysis of variance (ANOVA) with GraphPad Prism software version 9. If a significant difference was found, a Tukey test was performed to identify which specific values differed significantly. Differences were considered statistically significant at a threshold of $P < 0.05$.

5.4 Results

5.4.1 Viability assay

The antimicrobial effects of Ga-doped BGs were evaluated through turbidity measurements of *E. coli* and *S. aureus* cultures following 24-hour exposure. The absorbance at 570 nm provided insight into bacterial viability and the growth-inhibitory properties of Ga-containing bioactive glass.

Exposure to bioactive glass containing Ga resulted in a dose-dependent reduction in *E. coli* viability in 10 and 20 mg/mL (Figure 5.1 A). Ga-free bioactive glass samples (0% Ga) exhibited high turbidity, indicating robust bacterial growth. In contrast, samples treated with bioactive glass containing 3% Ga showed a moderate reduction in turbidity, suggesting partial inhibition of bacterial proliferation in both 10 and 20 mg/mL.

The 4% Ga group experienced a more pronounced decrease in absorbance, with bacterial viability reduced by around 60% and 90% at 10 and 20 mg/mL, respectively, compared to the control. The 5% Ga bioactive glass exhibited the strongest antimicrobial effect, with a significant reduction in turbidity, indicating approximately 90% and 99% *E. coli* death at 10 and 20 mg/mL, respectively.

Unlike *E. coli, S. aureus* displayed greater resistance to the antimicrobial effects of Ga-BGs (Figure 5.1 B). Treatment with 3%, 4% and 5% Ga bioactive glass resulted in minimal reductions in absorbance, with bacterial growth inhibited by over 50%. Furthermore, no significant difference was observed between Ga-free and Ga-containing samples. In the 5% Ga group, a modest reduction in turbidity was observed, corresponding to bacterial growth inhibition. However, *S. aureus* viability remained significantly higher than *E. coli* under the same conditions. Statistical analysis revealed a significant reduction in *E. coli* viability at higher Ga concentrations ($p < 0.05$), while the effect on *S. aureus* was less pronounced and not statistically significant ($p > 0.05$).

These results suggest that Ga-BGs exhibit strong antibacterial activity against *E. coli* but have limited efficacy against *S. aureus*.

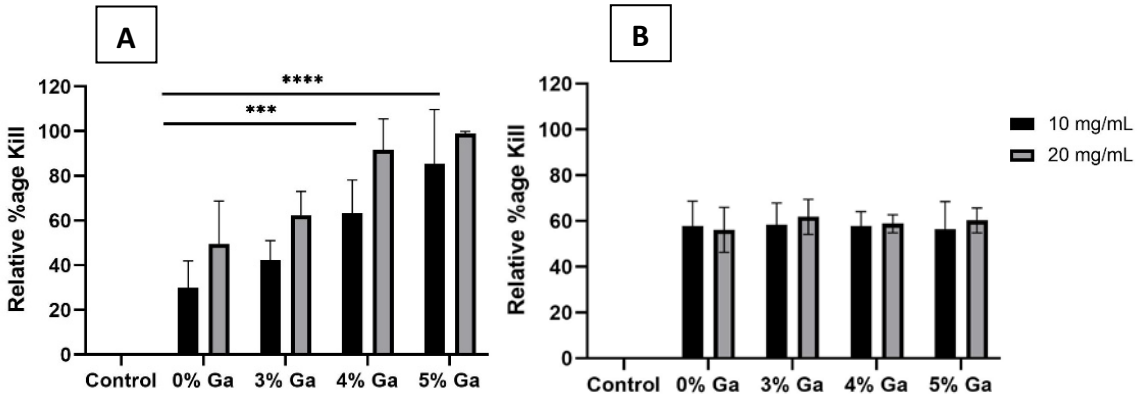

Figure 5.1. The effect of the dissolution products of Bioglass 45S5 and Ga doped silica-based BG (3-5 mol%) at 10 mg/mL and 20 mg/mL concentrations on the viability of *E. coli* **A)**, and *S. aureus* **B)** was assessed after 24-hour of exposure. The absorbance at 570 nm was recorded to determine bacterial growth, and the relative percentage kill was calculated by comparing the absorbance of treated samples to the untreated control. Bars represent mean values ± SD from three independent experiments. Statistical significance was determined using two-way ANOVA with Tukey's post hoc test ***$p < 0.001$, ****$p < 0.0001$.

5.4.2 Time kill assay

5.4.2.1 Time kill assay for E. coli exposed to gallium-doped bioactive glass

The antimicrobial activity of Ga-doped BGs against *E. coli* was evaluated at two concentrations (10 mg/mL and 20 mg/mL) over 2, 6, and 24 hours. The bacterial viability was measured through CFU counts and recorded as log CFU/mL (Figure 5.2 A and B).

After 2 hours, bacterial growth was evident in the control and 45S5 groups, with CFU counts increasing to approximately log 5 CFU/mL. Samples treated with 3%, 4%, and 5% Ga-doped BGs did not exhibit reduced growth, and the CFU counts remained close to baseline levels.

By 6 hours, the control and 45S5 groups continued to proliferate, reaching around 8 and 6 CFU/mL in order. The 3% and 4% Ga groups showed moderate growth inhibition. In comparison, the 5% Ga-treated group demonstrated the most pronounced reduction in bacterial growth, with CFU counts around log 4 CFU/mL, suggesting early inhibition of bacterial growth.

At 24 hours, bacterial counts in the control and 45S5 groups reached at log 8 CFU/mL, reflecting substantial growth over time. In the 3% and 4% Ga groups, bacterial growth persisted but was slower, with counts near log 7 CFU/mL. The 5% Ga group demonstrated a significant bactericidal effect, with bacterial counts falling below the detection limit (log 0 CFU/mL), indicating near-complete eradication of *E. coli*.

The antimicrobial effect was more pronounced at the higher 20 mg/mL concentration. At 2 hours, bacterial counts remained similar to the baseline in the control, 45S5, and 3% groups. However, 4% and 5% Ga-doped BG groups exhibited lower CFU counts, with the 5% Ga group showing the most significant inhibition (~log 3 CFU/mL).

By 6 hours, bacterial growth persisted in the control group, with CFU counts nearing log 8 CFU/mL. In contrast, bacterial growth in the 45S5 and 3% Ga groups plateaued, indicating limited inhibition. The 4% Ga group displayed a modest reduction in bacterial counts, suggesting partial bacteriostatic activity. Notably, the 5% Ga group demonstrated significant bactericidal activity, leading to a sharp decline in CFU counts to approximately log 2 CFU/mL, indicating a substantial reduction in *E. coli* viability.

At 24 hours, the control and 45S5 groups maintained high bacterial viability, stabilizing around log 8 CFU/mL. In the Ga-treated groups, bacterial counts continued to decline in a dose-dependent manner. The 3% and 4% Ga groups showed bacterial reductions to log 3.5 and log 2 CFU/mL, respectively. Notably, the 5% Ga-doped BGs led to complete bacterial eradication, with CFU counts falling below the detection limit (log 0 CFU/mL).

The results confirm a dose-dependent antimicrobial effect of Ga-doped BGs, with the highest concentration (5%) demonstrating the most significant bactericidal activity. Statistical analysis revealed significant differences between the control and the 5% Ga group at 24 hours ($p < 0.01$).

5.4.2.2 Time-kill assay for S. aureus exposed to gallium-doped bioactive glass

The antimicrobial activity of Ga-doped BGs against *S. aureus* was assessed at concentrations of 10 and 20 mg/mL over 2, 6, and 24-hour intervals. Bacterial viability was measured as CFU counts and recorded as log CFU/mL (Figures 2, c and d).

At 0 hours, bacterial counts across all groups were comparable, averaging around log 4 CFU/mL. After 2 hours, bacterial growth remains at the baseline level across all groups, with CFU counts ~ log 5 CFU/mL.

By 6 hours, bacterial counts in the control and 45S5 groups increased further, approaching log ~8 CFU/mL. The 3% and 4% Ga groups showed moderate growth inhibition, while the 5% Ga group continued to exhibit the most significant inhibitory effect, maintaining counts closer to log 6 CFU/mL.

At 24 hours, bacterial growth plateaued in the control and 45S5 groups at approximately log 8 CFU/mL. In the Ga-treated groups, a dose-dependent trend was observed. The 3% and 4% Ga groups showed slightly reduced bacterial counts compared to the control (~log 7.5 CFU/mL). The 5% Ga group exhibited further inhibition, with bacterial counts stabilizing around log 7 CFU/mL.

The higher 20 mg/mL concentration had a more significant antimicrobial effect. After 2 hours, bacterial growth remained consistent with baseline levels in all groups, with CFU counts averaging around log 5 CFU/mL.

At 6 hours, bacterial growth continued in the control and 45S5 groups, with counts approaching just below log 8 CFU/mL. In contrast, the 3%, 4%, and 5% Ga groups displayed a dose-dependent reduction in bacterial counts. The 5% Ga group exhibited the strongest inhibition, with bacterial counts around log 4 CFU/mL.

By 24 hours, bacterial counts in the control and 45S5 groups stabilized at approximately log 8 CFU/mL. However, the Ga-treated groups continued to demonstrate growth inhibition. The 3% and 4% Ga groups exhibited moderate growth, with CFU counts near log 7 and 6.5 CFU/mL, respectively. The 5% Ga group showed the most significant effect, with bacterial counts around log 6 CFU/mL. By the 6-hour time point, *S. aureus* exhibited more significant suppression of bacterial growth, with CFU counts decreasing to approximately log 4. However, by 24 hours, bacterial growth resumed, reaching around log 6 CFU/mL.

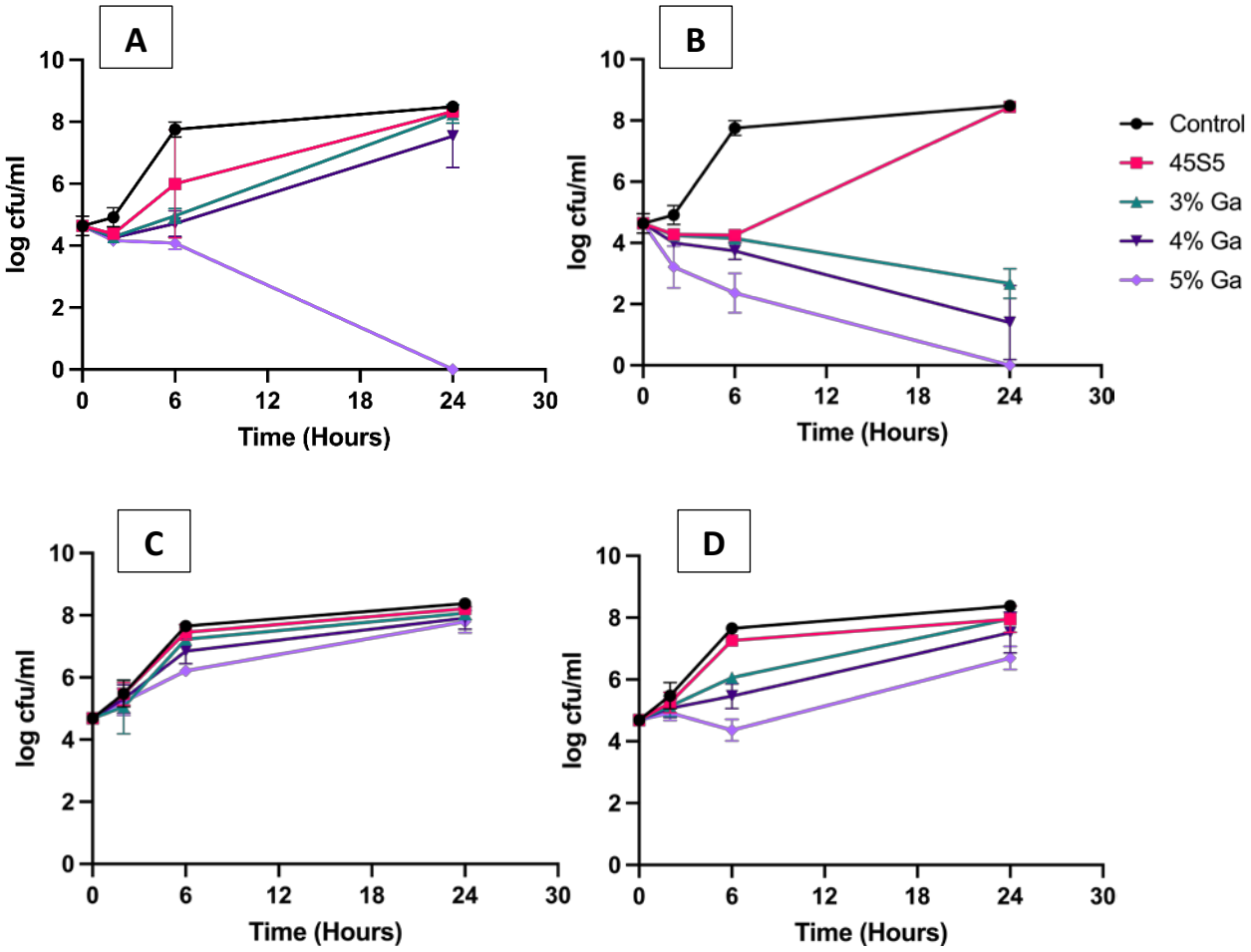

Figure 5.2. The effect of the dissolution products of Bioglass 45S5 and Ga doped silica-based BG (3-5 mol%) on the viability of *E. coli* **A,B)** and *S. aureus* **C,D)** was assessed at 2, 6, and 24-hour. Control (no bioactive glass) and 45S5 (Ga-free bioactive glass) groups were included for comparison. Data are presented as log CFU/mL (mean ± SD) from three independent experiments.

5.4.3 Live Dead assay

The viability of *E. coli* following exposure to Ga-doped bioactive glass was evaluated using the LIVE/DEAD BacLight™ Bacterial Viability Kit. This assay differentiates live and dead bacterial populations based on membrane integrity, with live cells emitting green fluorescence (SYTO 9) and dead cells emitting red fluorescence (propidium iodide).

Fluorescence microscopy images revealed a reduction in bacterial population with increasing concentrations of Ga-doped bioactive glass (Figure 5.3). In the control group (0% Ga), *E. coli* cells predominantly exhibited green fluorescence, indicating high bacterial viability and growth. Treatment with 3% and 4% Ga resulted in a noticeable reduction in the overall

number of bacterial cells, though the majority of the remaining cells still fluoresced green, suggesting intact membranes.

At 5% Ga concentration, a significant decrease in the total bacterial population was observed, with fewer cells present in the field of view. Although red fluorescence (indicative of membrane-compromised cells) was minimal, the overall reduction in bacterial density suggested a dose-dependent bactericidal effect, likely through inhibition of growth rather than direct membrane disruption. The qualitative fluorescence images illustrate this trend and align with results from the viability (turbidity) and time-kill assays.

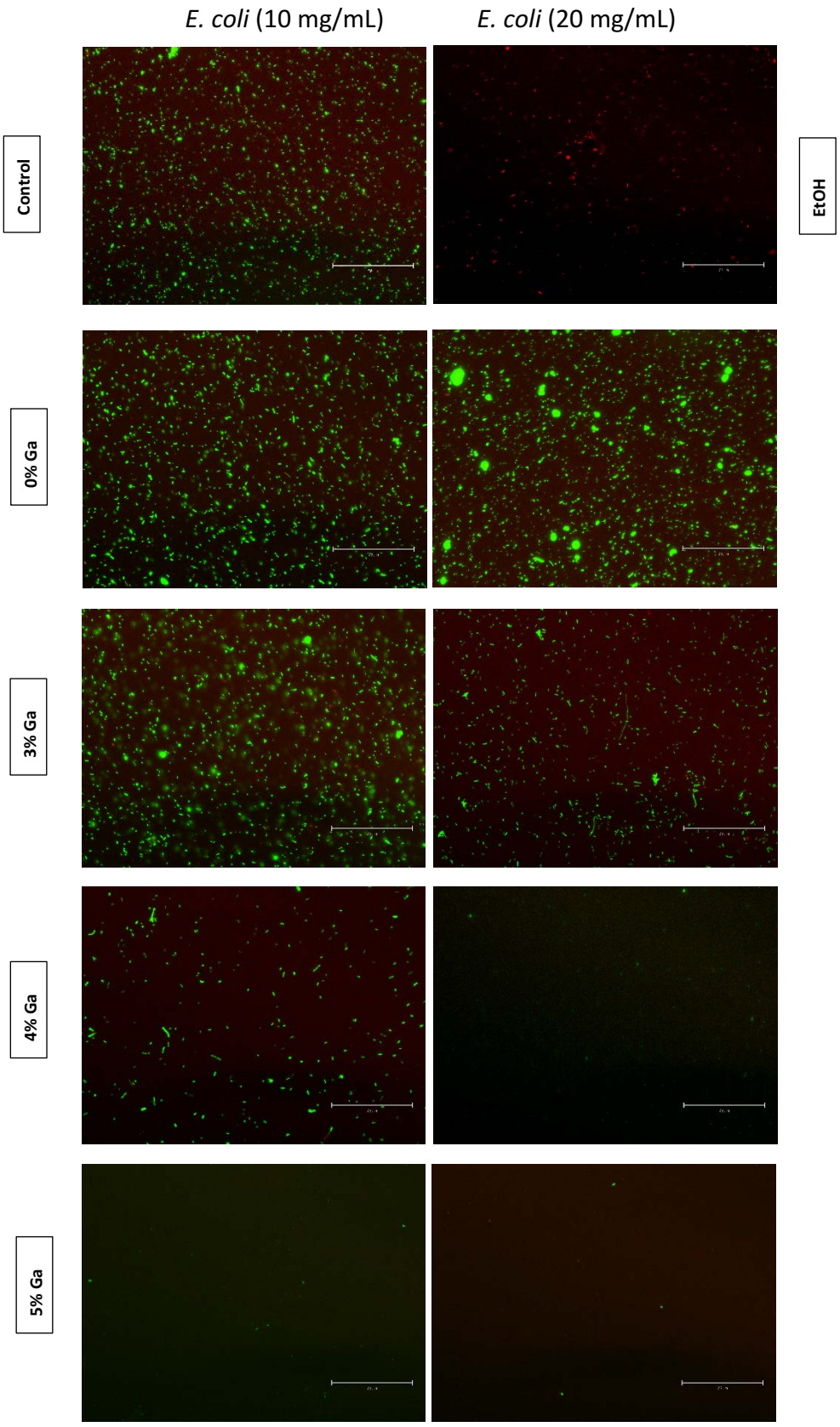

Figure 5.3. Fluorescence images of Live/Dead assay of *E. coli* treated with 10 and 20 mg/mL of Ga-doped glass dissolution product. Images were taken using a fluorescent microscope at 10x magnification. Live = green, and dead = red. The scale bar indicates 75 µm.

5.5 Discussion

The antimicrobial activity of Ga-doped BGs was assessed using viability assays, time-kill assays, and LIVE/DEAD bacterial staining. Ga-doped bioactive glass showed a strong dose-dependent reduction in *E. coli* viability, with the highest concentrations (4% and 5%) nearly eliminating bacterial populations. The 5% Ga-doped glass achieved over 95% and 99% bacterial reduction at 10 and 20 mg/ml concentrations, respectively, exhibiting the highest bactericidal activity. Furthermore, the 3% Ga-doped glass at 20 mg/ml had significant antibacterial activity, lowering the viability of *E. coli* by almost 75% compared to the control and Ga-free 45S5 glass. Equally, the results from the time-kill assay demonstrated the dose- and time-dependent antimicrobial efficacy of Ga-BGs against *E. coli* at 2, 6, and 24 hours. The samples treated with 5% Ga achieved near-complete bacterial eradication by 24 hours, 4% Ga showed significant reductions, and 3% Ga demonstrated moderate effects at both glass concentrations of 10 and 20 mg/mL.

However, *S. aureus* demonstrated higher resistance to Ga-doped BGs, with bacterial viability reductions remaining relatively stable (~60%) across all tested Ga compounds (3%, 4%, and 5%) at 10 and 20 mg/mL concentrations. Results from the time kill assay showed resistance in *S. aureus*, with only modest reductions in viability observed even at higher Ga concentrations.

The decreased effectiveness of Ga against Gram-positive bacteria is due to their structural defences rather than a shortcoming of the material itself. In addition, *S. aureus* showed remarkable adaptability in adverse conditions by employing mechanisms such as efflux pumps, biofilm formation, and other resistance strategies to counter antimicrobial agents. Its reduced sensitivity in comparison to *E. coli* is further explained by these biological adaptations. As a result, Ga's comparatively low efficacy against *S. aureus* emphasises how challenging it is to target Gram-positive bacteria without compromising the potential of Ga-doped BGs [10, 11].

To complement the quantitative data from viability and time-kill assays, Live/Dead bacterial staining was employed to visually assess the extent of bacterial killing. This approach was critical for verifying that the observed reduction in viable bacteria, particularly in *E. coli* treated with higher Ga concentrations, represented a true bactericidal effect rather than a shift to a viable but non-culturable (VBNC) state. While metabolic assays can indicate loss of

viability, they may not distinguish between cells that are dead and those that are metabolically inactive but still alive. The Live/Dead fluorescence assay provides a more direct indication of membrane integrity and cell death, confirming that Ga-treated cells were non-viable and not simply dormant [12, 13].

After 24 hours of exposure, it revealed a marked reduction in viable *E. coli* cells treated with 4% and 5% Ga-doped BG, with minimal red fluorescence indicative of non-viable cells. This absence of red fluorescence corresponds to a complete inhibition of bacterial growth at higher Ga concentrations and eliminating the likelihood of VBNC cells being overlooked in standard culture-based assays. Interestingly, this suggests that Ga's antimicrobial activity is predominantly bacteriostatic at lower doses and transitions to bactericidal at higher concentrations [14, 15].

In contrast, lower Ga concentrations (3% Ga) produced a mixed population of viable and non-viable *E. coli* cells. At the same time, control samples and Ga-free BG (45S5) displayed predominantly green fluorescence, indicating high bacterial viability. The fluorescence microscopy findings visually corroborate the quantitative results from bacterial viability and time-kill assays, providing robust evidence for the potent bactericidal effects of higher Ga concentrations against *E. coli*. These findings reinforce the dose-dependent efficacy of Ga-doped BG and highlight its potential for targeted antimicrobial action with minimal off-target cytotoxicity, paving the way for its use in preventing implant-associated infections [15].

The difference in susceptibility of *E. coli* and *S. aureus* to Ga can be explained by their structural variations. As a Gram-positive bacterium, *S. aureus* possesses a dense peptidoglycan layer that provides a strong physical defence, hindering the penetration of agents like Ga ions. On the other hand, Gram-negative bacteria such as *E. coli* have a thinner peptidoglycan layer and an outer membrane that may facilitate Ga's uptake, a key factor in its antimicrobial effectiveness [16]. The observed antimicrobial efficacy of Ga-doped BGs against *E. coli* aligns with Ga's mechanism of disrupting bacterial iron metabolism. This effect is likely driven by Ga's ability to disrupt bacterial iron by mimicking iron, called the "Trojan Horse" strategy and interfering with vital enzymatic functions [17]. As a Gram-negative bacterium with a thinner peptidoglycan layer, *E. coli* more readily takes up Ga. This uptake allows Ga to mimic iron, interfering with vital cellular processes such as DNA synthesis and respiration, ultimately causing bacterial death [18, 19].

In addition to Ga's well-established role in disrupting bacterial iron metabolism, the pronounced bactericidal effect observed against *E. coli* may also involve a contact-mediated mechanism of membrane disruption. This concept is reminiscent of copper-induced "punching holes", where copper ions interact directly with the bacterial membrane, leading to structural damage, leakage of intracellular contents, and rapid cell death [20]. It is possible that Ga^{3+} ions could interact electrostatically with the cell surface, destabilising membrane integrity, given the outer membrane composition of Gram-negative bacteria like *E. coli*, which is rich in negatively charged lipopolysaccharides. This interaction could compromise membrane potential and permeability, increasing Ga uptake and speeding up bacterial killing. While this membrane-targeting action of Ga has yet to be fully elucidated, our data, supported by fluorescence microscopy and Live/Dead staining, suggest that Ga may exhibit dual antimicrobial functionality: disrupting internal metabolic pathways and compromising the bacterial envelope through direct contact-mediated effects. Further studies are warranted to confirm this hypothesis and to determine whether Ga mimics copper in inducing membrane lesions in Gram-negative pathogens [21].

While earlier studies have suggested that Ga lacks intrinsic antimicrobial properties and that observed bactericidal effects may be attributed solely to pH changes in the surrounding medium, our findings challenge this interpretation. If the antimicrobial activity were primarily due to pH alterations, one would expect a similar bactericidal effect across all samples exhibiting comparable pH conditions. However, the absence of significant antibacterial activity in the Ga-free 45S5 glass, despite similar pH changes, strongly indicates that Ga itself contributes directly to the antimicrobial effect [22].

The potent antimicrobial activity of Ga-doped BGs against *E. coli* highlights their potential for addressing Gram-negative bacterial infections, particularly in orthopaedic and implant-related applications.

This efficacy can be attributed to the regulated release of Ga ions, which minimises systemic toxicity while concentrating antibacterial activity at the target location and ensuring therapeutic levels in the most infection-prone region [23]. However, the relatively moderate effect observed against *S. aureus* underscores the need for optimisation to broaden its antimicrobial spectrum. Particularly with this localised delivery, strategies like raising Ga concentrations, using synergistic combinations with other antimicrobial drugs, or adjusting ion release kinetics should improve its effectiveness against more resistant Gram-positive

pathogens [8]. The opposing reactions between *E. coli* and *S. aureus* further highlight the significance of tailoring Ga-doped materials according to the unique vulnerabilities of various bacterial species; this idea is backed by research demonstrating Ga's increased effectiveness against Gram-negative bacteria because of their structural characteristics [24]. The pronounced bactericidal activity of Ga-doped BG against *E. coli* highlights its potential as a material for managing Gram-negative infections, particularly in clinical contexts involving orthopaedic implants and post-surgical wounds. By targeting *E. coli*, a common pathogen in implant-associated infections, Ga-doped BG addresses a critical need for localised, targeted antimicrobial solutions in healthcare [14, 25]. Future research could focus on improving Ga uptake in Gram-positive bacteria, possibly by modifying ion release dynamics or incorporating complementary antimicrobial compounds. For example, integrating Ga-doped BG with antibiotics or peptides that are particularly effective against *S. aureus* could create a comprehensive solution for combating implant-associated infections [8].

5.6 Conclusion

Gallium-doped bioactive glasses (BG) have great promise as antibacterial materials, especially for infections linked to implants, as this study shows. Dissolution products from Ga-BGs exhibited potent, dose- and time-dependent antimicrobial activity against *E. coli*, culminating in near-complete eradication at 24 h with 5% Ga (and marked inhibition with 4%), while activity against *S. aureus* was modest under the same conditions. LIVE/DEAD imaging corroborated the quantitative assays, showing substantial reductions in viable *E. coli* at higher Ga contents and supporting a transition from predominantly bacteriostatic effects at lower Ga to bactericidal effects at higher Ga. The lack of comparable killing by Ga-free 45S5, despite similar culture conditions, indicates that gallium ions directly contribute to antimicrobial efficacy rather than effects being attributable solely to medium changes.

From a translational perspective, Ga content and glass loading (10–20 mg/mL) are practical levers to tune antimicrobial performance, with 5% Ga emerging as the lead for Gram-negative coverage. Despite its lower effectiveness against *S. aureus*, this difficulty is not a result of the material's limitations but rather of the structural defences of Gram-positive bacteria. The comparatively lower impact on *S. aureus* highlights a clear optimisation route: modulating ion-release kinetics and/or combining Ga-BGs with complementary agents (e.g., anti-Gram-positive antibiotics or antimicrobial peptides) to broaden spectrum and address biofilm-associated persistence. Future work should include biofilm and mixed-species models, pH-controlled tests, and *in vivo* infection scenarios proximal to implant materials to confirm therapeutic windows and durability of effect.

Overall, Ga-BGs deliver sustained, composition-dependent antibacterial activity with strong efficacy against *E. coli* and limited but measurable suppression of *S. aureus*, supporting their further development for preventing or managing implant-associated Gram-negative infections and motivating formulation strategies to enhance Gram-positive coverage.

5.7 References

[1] M. A. Azad and R. Patel, “Practical Guidance for Clinical Microbiology Laboratories: Microbiologic diagnosis of implant-associated infections,” Jun. 01, 2024, *American Society for Microbiology*. doi: 10.1128/cmr.00104-23.

[2] L. Drago, M. Toscano, and M. Bottagisio, “Recent evidence on bioactive glass antimicrobial and antibiofilm activity: A mini-review,” Feb. 24, 2018, *MDPI AG*. doi: 10.3390/ma11020326.

[3] M. B. Taye, “Biomedical applications of ion-doped bioactive glass: a review,” Dec. 01, 2022, *Springer Science and Business Media Deutschland GmbH*. doi: 10.1007/s13204-022-02672-7.

[4] M. N. Rahaman, B. S. Bal, and W. Huang, “Review: Emerging developments in the use of bioactive glasses for treating infected prosthetic joints,” Aug. 01, 2014, *Elsevier Ltd*. doi: 10.1016/j.msec.2014.04.055.

[5] H. R. Fernandes, A. Gaddam, A. Rebelo, D. Brazete, G. E. Stan, and J. M. F. Ferreira, “Bioactive glasses and glass-ceramics for healthcare applications in bone regeneration and tissue engineering,” *Materials*, vol. 11, no. 12, pp. 1–54, 2018, doi: 10.3390/ma11122530.

[6] A. Hoppe, N. S. Güldal, and A. R. Boccaccini, “A review of the biological response to ionic dissolution products from bioactive glasses and glass-ceramics,” *Biomaterials*, vol. 32, no. 11, pp. 2757–2774, 2011, doi: 10.1016/j.biomaterials.2011.01.004.

[7] U. Kadiyala, N. A. Kotov, and J. S. VanEpps, “Antibacterial Metal Oxide Nanoparticles: Challenges in Interpreting the Literature,” *Curr Pharm Des*, vol. 24, no. 8, pp. 896–903, May 2018, doi: 10.2174/1381612824666180219130659.

[8] F. Li, F. Liu, K. Huang, and S. Yang, “Advancement of Gallium and Gallium-Based Compounds as Antimicrobial Agents,” Feb. 04, 2022, *Frontiers Media S.A.* doi: 10.3389/fbioe.2022.827960.

[9] S. P. Valappil *et al.*, “Antimicrobial Gallium-Doped Phosphate-Based Glasses,” *Adv Funct Mater*, vol. 18, no. 5, pp. 732–741, Mar. 2008, doi: 10.1002/adfm.200700931.

[10] L. A. Onyango and M. M. Alreshidi, “Adaptive Metabolism in Staphylococci: Survival and Persistence in Environmental and Clinical Settings,” *J Pathog*, vol. 2018, pp. 1–11, Sep. 2018, doi: 10.1155/2018/1092632.

[11] S. Sinha, S. Aggarwal, and D. V. Singh, “Efflux pumps: gatekeepers of antibiotic resistance in Staphylococcus aureus biofilms,” 2024, *Shared Science Publishers OG*. doi: 10.15698/mic2024.11.839.

[12] C. Robben, S. Fister, A. K. Witte, D. Schoder, P. Rossmanith, and P. Mester, “Induction of the viable but non-culturable state in bacterial pathogens by household cleaners and inorganic salts,” *Sci Rep*, vol. 8, no. 1, p. 15132, Oct. 2018, doi: 10.1038/s41598-018-33595-5.

[13] M. L. Papa, A. Wasit, J. Pecora, T. M. Bergholz, and J. Yi, “Detection of Viable but Nonculturable E. coli Induced by Low-Level Antimicrobials Using AI-Enabled Hyperspectral

Microscopy," *J Food Prot*, vol. 88, no. 1, p. 100430, Jan. 2025, doi: 10.1016/J.JFP.2024.100430.

[14] J. Liu, F. Shi, S. Ma, J. Sun, S. Liu, and W. Ye, "Magnesium alloy with superhydrophilic magnesium/gallium-layered double hydroxides coating with antibacterial property as implant material," *Journal of Nanoparticle Research*, vol. 27, no. 1, Jan. 2025, doi: 10.1007/s11051-024-06210-0.

[15] F. Li, F. Liu, K. Huang, and S. Yang, "Advancement of Gallium and Gallium-Based Compounds as Antimicrobial Agents," Feb. 04, 2022, *Frontiers Media S.A.* doi: 10.3389/fbioe.2022.827960.

[16] W. Vollmer, D. Blanot, and M. A. De Pedro, "Peptidoglycan structure and architecture," Mar. 2008. doi: 10.1111/j.1574-6976.2007.00094.x.

[17] F. Shi *et al.*, "A novel antimicrobial strategy for bacterial infections: Gallium-based materials," Sep. 01, 2023, *Elsevier B.V.* doi: 10.1016/j.colcom.2023.100735.

[18] S. C. Andrews, A. K. Robinson, and F. Rodríguez-Quiñones, "Bacterial iron homeostasis," 2003, *Elsevier*. doi: 10.1016/S0168-6445(03)00055-X.

[19] A. B. Kelson, M. Carnevali, and V. Truong-Le, "Gallium-based anti-infectives: Targeting microbial iron-uptake mechanisms," 2013, *Elsevier Ltd*. doi: 10.1016/j.coph.2013.07.001.

[20] F. N. S. Raja, T. Worthington, and R. A. Martin, "The antimicrobial efficacy of copper, cobalt, zinc and silver nanoparticles: alone and in combination," *Biomedical Materials*, vol. 18, no. 4, p. 045003, Jul. 2023, doi: 10.1088/1748-605X/acd03f.

[21] X. Zhang, C. Yang, T. Xi, J. Zhao, and K. Yang, "Surface Roughness of Cu-Bearing Stainless Steel Affects Its Contact-Killing Efficiency by Mediating the Interfacial Interaction with Bacteria," *ACS Appl Mater Interfaces*, vol. 13, no. 2, pp. 2303–2315, Jan. 2021, doi: 10.1021/acsami.0c19655.

[22] S. Begum, W. E. Johnson, T. Worthington, and R. A. Martin, "The influence of pH and fluid dynamics on the antibacterial efficacy of 45S5 Bioglass," *Biomedical Materials*, vol. 11, no. 1, p. 015006, Feb. 2016, doi: 10.1088/1748-6041/11/1/015006.

[23] L. Yao *et al.*, "Osseointegration and anti-infection of dental implant under osteoporotic conditions promoted by gallium oxide nano-layer coated titanium dioxide nanotube arrays," *Ceram Int*, vol. 49, no. 14, pp. 22961–22969, Jul. 2023, doi: 10.1016/j.ceramint.2023.04.121.

[24] Y. Endo, E. Giunta, J. Mroueh, W. McCarthy, and N. Graf, "Editorial: The application of bioactive materials in bone repair," 2024, *Frontiers Media SA*. doi: 10.3389/fbioe.2024.1539142.

[25] F. Hong *et al.*, "NIR-II Photoresponsive Antibacterial Coatings on Titanium Implants Using Strontium Titanate Metastructures," *Ceram Int*, Jan. 2025, doi: 10.1016/j.ceramint.2025.01.366.

Chapter 6

Conclusion and Future Work

6.1. Conclusion

Osteosarcoma (OS) is the most prevalent primary bone malignancy, typically originating from osteoblasts responsible for new bone formation. It typically presents in young adults as well as adults over 40 years of age, with males affected more than females [1]. The current therapeutic approaches for OS are primarily based on surgery, radiotherapy, and chemotherapy with generic cytotoxic drugs, including cisplatin, doxorubicin, and methotrexate, continued with tumour resection and chemotherapy. In almost all cases, surgery is a must with the aim to remove the primary tumour completely, with wide margins [2]. Neoadjuvant chemotherapy is a standard approach for treating OS as it helps shrink the primary tumour and allows for histological assessment of treatment response, enabling personalised therapy [3]. However, chemotherapy is associated with significant side effects, including nausea, vomiting, neurotoxicity, nephrotoxicity, hypersensitivity reactions, and cardiomyopathy[4, 5]. Moreover, metastatic OS often exhibits resistance to standard chemotherapy, rendering it ineffective in over 30% of metastatic cases [6, 7]. Hence, the discovery and development of new approaches for tumour diagnosis and treatment are required to decrease the mortality rate of OS patients. The objective of this study was to develop innovative anticancer bioactive glass formulations for the treatment and management of OS.

The objectives of chapter 2 were to manufacture and characterise the physicals properties of the bioactive glasses including, the glasses amorphous nature and the ion release profile of un-doped and gallium doped bioactive glasses. The results can be summarised as follows:

- Gallium oxide was successfully incorporate into sodium-calcium phospho-silicate-based bioactive glasses across a broad concentration range (0-5 mol%).
- Evaluation of the controlled release behaviour of the gallium doped bioactive glass (Ga-BG) ions using inductively coupled plasma (ICP) analysis.
- Bioactivity assessment of the glasses by examining surface reactions in simulated body fluid (SBF).
- Formation of calcium and phosphate-rich layers via energy-dispersive X-ray spectroscopy (EDS) indicating bioactivity in the form of an amorphous calcium phosphate/hydroxyapatite layer.

- Identify the presence of phosphate (PO_4^{3-}) and carbonate (CO_3^{2-}) species indicating hydroxyapatite and carbonated apatite formation using Fourier-Transform Infrared Spectroscopy (FTIR).

The objectives of chapter 3 were to demonstrate that Ga-BG (0–5% Ga) effectively inhibited the growth of OS (Saos-2) cells in a dose-dependent manner, with up to 99% cell death observed at 5% Ga after 10 days. Importantly, these compositions exhibited minimal cytotoxic effects on healthy human osteoblasts (NHOst), indicating selective anticancer activity. The results confirm that the suppression of OS cells was primarily due to the cytotoxic action of gallium (Ga) ions released from the glass network. The results can be summarised as follows:

- Evaluation of cytotoxicity induced by 1-5% Ga-BGs in Saos-2 cells.
- Assess the biocompatibility of Ga-BGs on NHOst.
- Further analysis of cell viability, proliferation, and migration using MTT, Live/Dead staining, PicoGreen, and IncuCyte live-cell imaging.
- Selective targeting of cancerous cells, while sparing healthy ones, is central to the objective of this study.
- Determining the dose-dependent response of OS cells to Ga ion release from the BG.

The objectives of chapter 4 were to evaluate the effects of 45S5 and Ga-BGs (3–5%) on various OS cell lines (HOS, U2) and healthy human mesenchymal stem cells (hMSCs). The results demonstrated a significant, dose-dependent inhibition of OS cell growth, with the highest cytotoxicity observed in the 5% Ga composition. Importantly, Ga-BGs showed minimal impact on hMSC proliferation, confirming selective anticancer activity. Flow cytometry revealed elevated transferrin receptor (TfR) expression in OS cells, likely due to their increased iron demand. Caspase-3 and -7 activation, as confirmed by apoptosis assays, indicated that Ga induces cancer cell death via apoptotic pathways. The objectives of this chapter were as following:

- Investigate the cytotoxic effects of 45S5 and Ga-BGs (3–5%) on OS cell lines (HOS, U2).
- Biocompatibility confirmation of Ga-BGs on hMSCs.

- Cell viability assessment using MTT and Live/Dead assays after exposure to bioactive glass dissolution products.
- Investigate TfR expression in cancerous and non-cancerous cells using flow cytometry.
- To determine whether Ga induces apoptosis in OS cells via caspase-3 and -7 activation.

The objectives of chapter 5 were to demonstrates potential of Ga-BG as effective antibacterial materials for managing implant-associated infections. Ga's strong bactericidal activity, particularly against *Escherichia coli*, stems from its ability to disrupt bacterial iron metabolism, leading to a dose- and time-dependent reduction in bacterial viability. The controlled release of Ga ions ensures localised antibacterial effects while minimising systemic toxicity, making Ga-BG highly suitable for orthopaedic applications. The objectives of this chapter were as following:

- Assess the antibacterial activity of Ga-BGs against *E. coli* and *S. aureus*.
- To investigate the mechanism of Ga's bactericidal effect through its interference with bacterial iron metabolism.
- Evaluating the dose- and time-dependent impact of Ga ion release on bacterial viability.
- To explore the challenges associated with reduced efficacy against Gram-positive bacteria like *S. aureus*.

6.2. Future Work

The given study demonstrates that Ga ions incorporated into BG structure induce a significant cytotoxic effect on OS cells with minimum toxicity on non-cancerous cells. Although in vitro experiments have demonstrated the potential of the synthesized glasses as bone graft materials for osteosarcoma treatment, further investigations are necessary before their application in human subjects can be considered. These include, but are not limited to:

6.2.1. Patient-Derived *In Vitro* Models:

To bridge the gap between in vitro findings and clinical application, it is essential to evaluate the efficacy of Ga-BG using biopsy-derived samples from osteosarcoma (OS) patients. While established OS cell lines have provided valuable insights into the cytotoxic and antimicrobial properties of Ga-BG, they fail to fully replicate the complex tumour microenvironment, including cellular heterogeneity and drug resistance. Patient-derived biopsy models offer a more physiologically relevant platform, preserving the architectural and molecular features of native tumour tissue. These models enable realistic assessment of Ga ion interactions with tumour cells, including penetration, ion release kinetics, and apoptotic effects. Integrating such models into Ga-BG research is a critical step toward translational validation, enhancing clinical relevance and supporting progression toward preclinical and eventual clinical trials [8, 9].

6.2.2. Animal Studies:

Up to this point, all experiments have been conducted in vitro. To replicate the physiological conditions of the human body more accurately, in vivo studies are essential. Implantation of the synthesized bioactive glass particles into animal models would provide valuable insight into their biological performance. These studies would allow for the evaluation of the material's ability to inhibit bacterial growth, support bone regeneration, and potentially suppress cancer cell proliferation within a living system. Small animal models, such as rats or rabbits, are well-suited for this purpose. A surgical procedure could be performed to create cavitary defects in both proximal femurs. One defect would be filled with the synthesized bioactive glass granules, while

the other would receive autologous bone harvested from the contralateral side. After a 14-day post-operative period, the animals would be humanely euthanised to enable histological analysis and comparison of bone neoformation and osteoblast activity at both graft sites. To specifically assess the impact of the glasses on osteosarcoma in vivo, osteosarcoma can be induced in the femur, followed by grafting with the bioactive glass. Subsequent euthanasia and histological examination would allow for evaluation of the material's effect on tumour progression and bone tissue response [10, 11].

6.2.3. Antimicrobial Studies:

Bioactive glasses have been previously engineered to deliver controlled release of antimicrobial metallic ions, such as silver (Ag), copper (Cu), and strontium (Sr) for various soft and hard tissue applications. Although the current study has established a proof of concept and the antimicrobial analysis showed a strong toxicity toward Gram negative bacteria, *E. coli* but the cytotoxic effect toward Gram positive was minimum. Therefore, it is important to build upon this approach, and incorporate additional antimicrobial ions. The newly developed glasses should be evaluated *in vitro* against a panel of clinically relevant Gram-positive and Gram-negative microorganisms to validate the efficacy of the BGs [12-14].

In conclusion, this thesis has demonstrated that gallium-doped bioactive glasses hold significant potential as a novel approach to addressing the dual challenge of preventing osteosarcoma recurrence and promoting tissue regeneration. The multifaceted benefits of Ga-BGs, combined with their potential for further optimisation and clinical application, pave the way for new strategies in the development of implantable medical devices. Future research, particularly translational and clinical studies, will be essential to fully realise the therapeutic potential of this innovative material.

6.3. References

[1] A. J. Saraf, J. M. Fenger, and R. D. Roberts, 'Osteosarcoma: Accelerating progress makes for a hopeful future', *Front Oncol*, vol. 8, no. JAN, pp. 1–7, 2018, doi: 10.3389/fonc.2018.00004.

[2] A. Abarrategi *et al.*, 'Osteosarcoma: Cells-of-Origin, Cancer stem cells, and targeted therapies', *Stem Cells Int*, vol. 2016, 2016, doi: 10.1155/2016/3631764.

[3] C. Gerrand *et al.*, 'UK guidelines for the management of bone sarcomas', *Clin Sarcoma Res*, vol. 6, no. 1, p. 7, Dec. 2016, doi: 10.1186/s13569-016-0047-1.

[4] L. Tattersall and U. Kingdom, 'Osteosarcoma', pp. 1–17, 2019, doi: 10.1016/B978-0-12-801238-3.62259-6.

[5] B. A. Lindsey, J. E. Markel, and E. S. Kleinerman, 'Osteosarcoma Overview', *Rheumatol Ther*, vol. 4, no. 1, pp. 25–43, 2017, doi: 10.1007/s40744-016-0050-2.

[6] D. P. M. Hughes, 'How the NOTCH Pathway Contributes to the Ability of Osteosarcoma Cells to Metastasize', 2009, pp. 479–496. doi: 10.1007/978-1-4419-0284-9_28.

[7] S. S. Bielack *et al.*, 'Second and Subsequent Recurrences of Osteosarcoma: Presentation, Treatment, and Outcomes of 249 Consecutive Cooperative Osteosarcoma Study Group Patients', *Journal of Clinical Oncology*, vol. 27, no. 4, pp. 557–565, Feb. 2009, doi: 10.1200/JCO.2008.16.2305.

[8] T. Kondo, 'Current status and future outlook for patient-derived cancer models from a rare cancer research perspective', *Cancer Sci*, vol. 112, no. 3, pp. 953–961, Mar. 2021, doi: 10.1111/cas.14669.

[9] K. F. Idrisova, H.-U. Simon, and M. O. Gomzikova, 'Role of Patient-Derived Models of Cancer in Translational Oncology', *Cancers (Basel)*, vol. 15, no. 1, p. 139, Dec. 2022, doi: 10.3390/cancers15010139.

[10] W. Liang *et al.*, '*In vivo* behavior of bioactive glass-based composites in animal models for bone regeneration', *Biomater Sci*, vol. 9, no. 6, pp. 1924–1944, 2021, doi: 10.1039/D0BM01663B.

[11] R. N. Granito *et al.*, '*In vivo* biological performance of a novel highly bioactive glass-ceramic (Biosilicate®): A biomechanical and histomorphometric study in rat tibial defects', *J Biomed Mater Res B Appl Biomater*, vol. 97B, no. 1, pp. 139–147, Apr. 2011, doi: 10.1002/jbm.b.31795.

[12] S. Hijazi, D. Visaggio, M. Pirolo, E. Frangipani, L. Bernstein, and P. Visca, 'Antimicrobial activity of gallium compounds on ESKAPE pathogens', *Front Cell Infect Microbiol*, vol. 8, no. SEP, Sep. 2018, doi: 10.3389/fcimb.2018.00316.

[13] L. Drago, M. Toscano, and M. Bottagisio, 'materials Recent Evidence on Bioactive Glass Antimicrobial and Antibiofilm Activity: A Mini-Review', doi: 10.3390/ma11020326.

[14] F. N. S. Raja, T. Worthington, and R. A. Martin, 'The antimicrobial efficacy of copper, cobalt, zinc and silver nanoparticles: alone and in combination', *Biomedical Materials*, vol. 18, no. 4, p. 045003, Jul. 2023, doi: 10.1088/1748-605X/acd03f.

Appendix

Table A.1. Ions accumulation of Ga(NO3)3 in diH_2O at the range of concentration. The data are represented as ppm.

Ga(NO3)3 in µg/mL	**Ga^{3+}**
7.81	0.79
15.62	1.92
31.25	2.55
62.5	6.59
125	13.24
250	27.44
500	56.40
1000	114.24

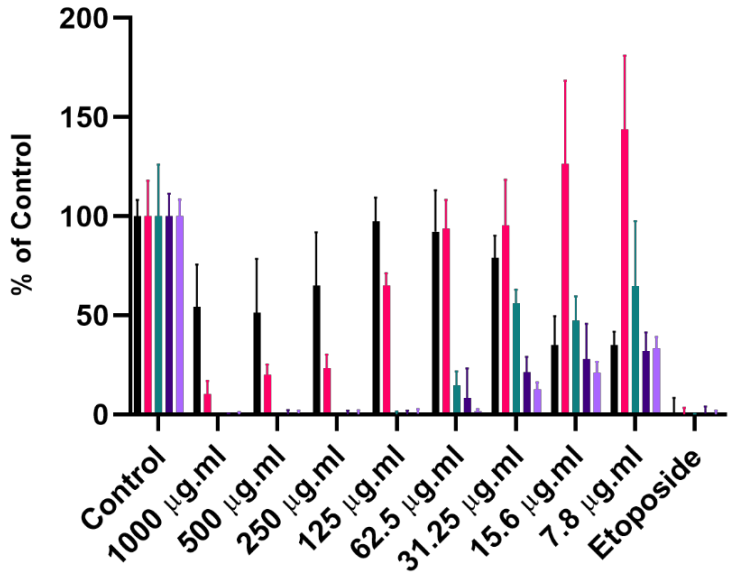

3 and Day 7

Figure A.1. The effect of the conditioned medium containing different concentrations of $Ga(NO_2)_3$ was investigated on Saos-2 cells.

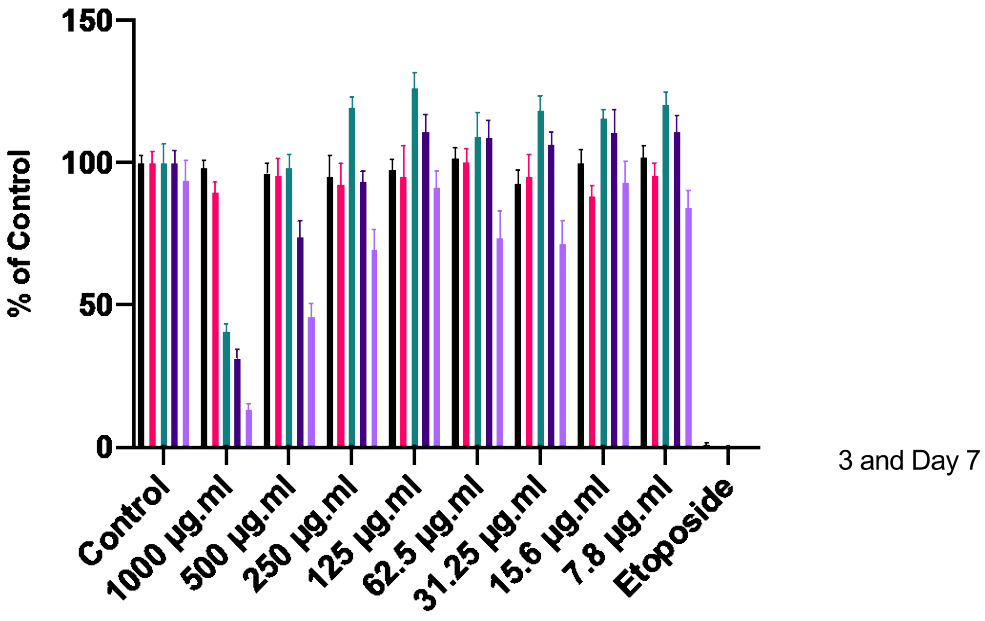

Figure A.2. The effect of the conditioned medium containing different concentrations of Ga(NO2)3 was investigated on Saos-2 cells.

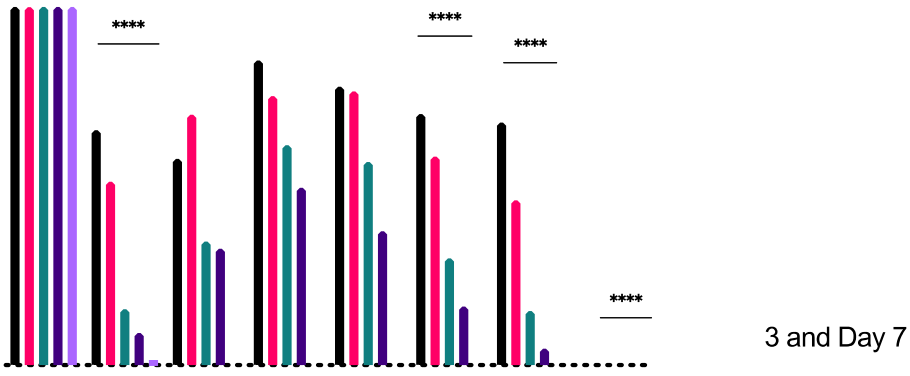

Figure A.3. The effect of the dissolution products of Bioglass 45S5 and Ga doped silica based bioactive glasses (1-5 mol%) **on Saos-2 at the concentration of 40 mg/mL** using MTT viability assay. The data is represented as Mean ± SD (N=5).

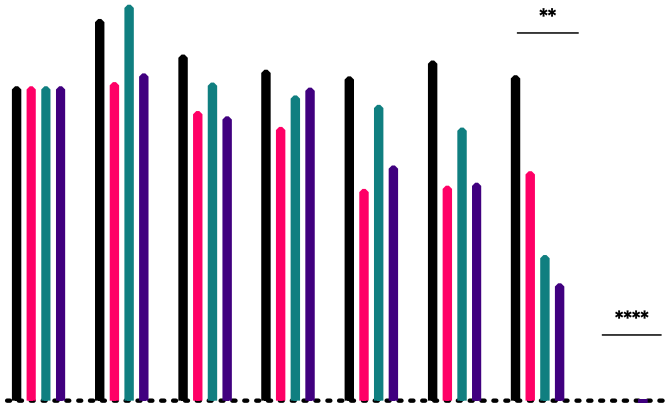

Figure A.4. The effect of the dissolution products of Bioglass 45S5 and Ga doped silica based bioactive glasses (1-5 mol%) on NHOst at the concentration of 40 mg/mL using MTT viability assay. The data is represented as Mean ± SD (N=5).

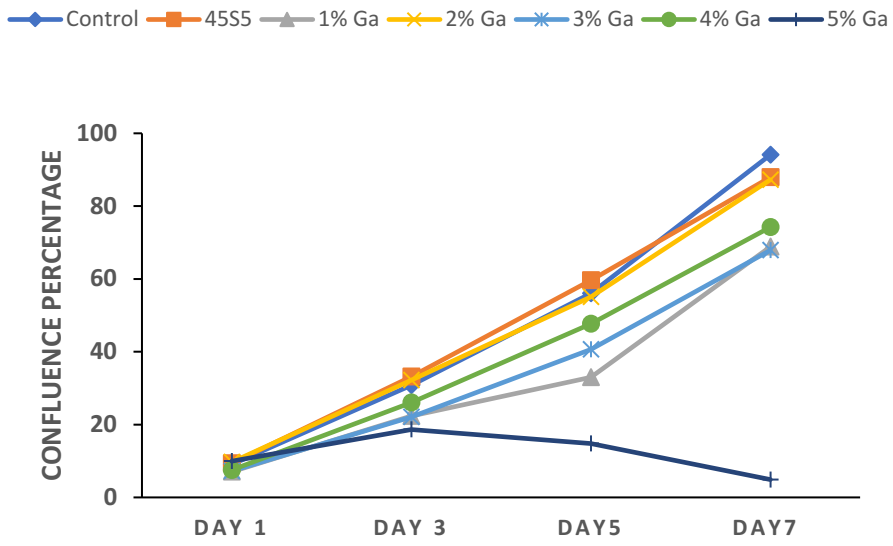

Figure A.5. Effect of Ga doped bioactive glass composition on Saos-2 cell proliferation at 10 mg/mL for a period of 7 days. Cell proliferation was monitored in real time using IncuCyte image analyser with the continuous presence of indicated treatments until the end of each experiment.

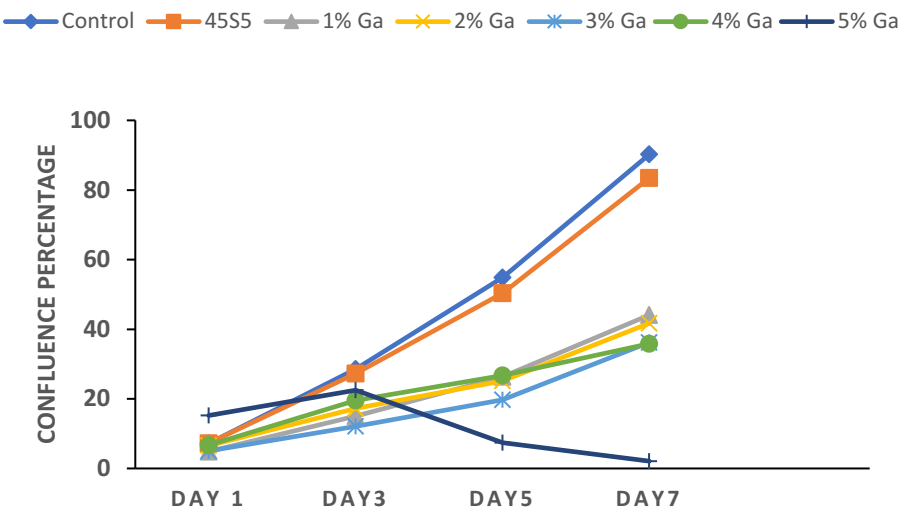

Figure A.6. Effect of Ga doped bioactive glass composition on Saos-2 cell proliferation at 20 mg/mL for a period of 7 days. Cell proliferation was monitored in real time using IncuCyte image analyser with the continuous presence of indicated treatments until the end of each experiment.

Presentations and Professional Activities

Oral Presentations

- Hanaei S. Development and characterisation of gallium doped bioactive glasses (2022). Sarcoma UK Postgraduate Research Day, London, U.K.
- Hanaei S. The impact of gallium ions on cancer therapy (2021). Sarcoma UK Postgraduate Research Day, London, U.K.

Poster Presentations

- Hanaei S. Development and characterisation of gallium doped bioactive glasses for cancer treatment (2024). Sarcoma UK Postgraduate Research Day, London, U.K.
- Hanaei S. (2023). Multifunctional Gallium Doped Bioactive Glasses: A Targeted Delivery for Antineoplastic Agents and Tissue Repair Against Osteosarcoma. Tissue Engineering and Regenerative Medicine International Society (TERMIS), Manchester.
- Hanaei S. (2022). Multifunctional Gallium Doped Bioactive Glasses: A Targeted Delivery for Antineoplastic Agents and Tissue Repair Against Osteosarcoma. Engineering for Health Research, Aston University, Birmingham, U.K.

Publications

- Gallium-Doped Bioactive Glass: A Novel Biomaterial for Bone Cancer Treatment with Antimicrobial Properties (In progress).
- Multifunctional gallium doped bioactive glasses: a targeted delivery for antineoplastic agents and tissue repair against osteosarcoma (Published).
- Synergistic Antimicrobial Metal Oxide-Doped Phosphate Glasses; a Potential Strategy to Reduce Antimicrobial Resistance and Host Cell Toxicity (Published).